



**Type 2 diabetes and breast cancer - the role of hyperinsulinaemia in breast cancer development and mortality**

**Emily Jane Gallagher MB BCh BAO MRCPI**

**Department of Physiology and Medical Physics**

**RCSI**

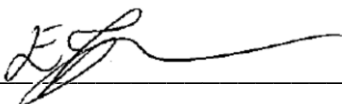
**A thesis submitted to the School of Postgraduate Studies, Faculty of  
Medicine and Health Sciences, Royal College of Surgeons in Ireland, in  
fulfillment of the degree of Doctor of Philosophy**

**Supervisors: Professor Jochen Prehn**

**Professor Derek LeRoith**

**February 2016**

I declare that this thesis, which I submit to RCSI for examination in consideration of the award of a higher degree of Doctor of Philosophy is my own personal effort. Where any of the content presented is the result of input or data from a related collaborative research programme this is duly acknowledged in the text such that it is possible to ascertain how much of the work is my own. I have not already obtained a degree in RCSI or elsewhere on the basis of this work. Furthermore, I took reasonable care to ensure that the work is original, and, to the best of my knowledge, does not breach copyright law, and has not been taken from other sources except where such work has been cited and acknowledged within the text.

Signed  \_\_\_\_\_

Student Number 12117072

Date 27<sup>th</sup> February 2016

# Table of Contents

List of Abbreviations .....	5
List of Figures .....	7
List of Tables.....	11
Summary .....	12
Acknowledgements .....	13
Insulin Resistance and Hyperinsulinaemia in Obesity and Type 2 Diabetes .....	15
Historical Context.....	18
Epidemiology .....	19
Obesity and Cancer.....	19
Diabetes and Cancer.....	21
Hyperinsulinaemia and Breast Cancer .....	22
A Non-Obese Mouse Model of Hyperinsulinaemia and Breast Cancer.....	28
Challenges with Inhibiting the IR/IGF-1R Signaling Pathway .....	30
Controversies Regarding Insulin Analogues and Breast Cancer .....	35
Insulin Resistance, Hyperinsulinaemia and Racial Disparities in Breast Cancer Mortality .....	37
Hypothesis .....	39
2. Materials and Methods .....	40
Cell Culture .....	40
Animal Studies.....	43
Genetically Engineered Mouse Models .....	43
In Vivo Tumour Studies .....	48
Metabolic Studies .....	49
Insulin Analogues .....	50
Histological Analysis.....	51
Mammary Epithelial Cell Isolation.....	52
Protein Isolation and Analysis .....	53
RNA Isolation and Analysis .....	54

Statistical Analysis For In Vitro and Pre-Clinical Studies .....	57
Hyperinsulinaemia and IR Signaling in Breast Cancer Survival Disparities Between Black and White Women .....	57
3. Results .....	62
Chapter 1. Hyperinsulinaemia and Breast Cancer Metastasis in a Transgenic NeuNT model. ....	62
Chapter 2. Human Tumour Xenografts in an Immunodeficient Mouse Model of Hyperinsulinaemia .....	71
Chapter 3. Vimentin in Hyperinsulinaemia-mediated Breast Cancer Metastasis. ....	80
Chapter 4. The role of the Insulin Receptor in Mammary Gland Development and Breast Cancer Growth in the Setting of Hyperinsulinaemia.....	92
Chapter 5. The effects of insulin analogues on breast cancer progression in an animal model .....	101
Chapter 6. Human Breast Cancer, Hyperinsulinaemia and IR Splicing. ...	117
4. Discussion.....	126
References.....	137
Appendix I. Publications From the Work in This Thesis .....	148
Published Papers.....	148



## List of Abbreviations

A21Gly,DiD	Insulin analogue with glycine substitution at position 21 of
-Arg	A chain and 2 D-arginines at position 31 and 32 of B chain
AspB10	Insulin analogue with aspartate substitution at position 10 of B chain of insulin
ATCC	American Type Culture Collection
BKM120	Pan-class I PI3K inhibitor
BMI	Body Mass Index
BSA	Bovine serum albumin
BSL2	Biosafety Level 2
CI	Confidence interval
CPS II	Cancer Prevention Study II
Cre	Cre recombinase
DMEM	Dulbecco's Modified Eagles Medium
EGFR	Epidermal growth factor receptor
EMT	Epithelial to mesenchymal transition
EPIC	European Prospective Investigation into Cancer and Nutrition
ER	Oestrogen Receptor
Erk1/2	Extracellular signal-regulated kinase
FBS	Foetal bovine serum
FFPE	Formalin fixed paraffin embedded
FVB/n	Friend Virus B/National Institutes of Health
GFP	Green fluorescent protein
GTT	Glucose tolerance test
HEAL	Healthy Eating, Activity and Lifestyle
HER2	Human Epidermal Growth Factor Receptor 2
HOMA-IR	Homeostasis model assessment of insulin resistance
HR	Hazard Ratio
i.p.	Intraperitoneal
IGF-1	Insulin-like growth factor 1
IGF-1R	Insulin-like growth factor 1 receptor
IGF-2	Insulin-like growth factor 2
IGFBP	Insulin-like growth factor binding protein
IL	Interleukin
IMEM	Improved Minimal Essential Medium
IR	Insulin receptor
ITT	Insulin tolerance test
MAPK	Mitogen-activated protein kinase
MBNL2	Muscle blind like splicing regulator 2
MCK	Muscle creatinine kinase
Met1	Murine breast cancer cell line derived from MMTV-polyoma middle T antigen cell line
	Muscle lysine to arginine substitution in IGF-1R mouse model
MKR	
MMTV-LTR	Mouse mammary tumour virus-long terminal repeat
MRI	Magnetic resonance imaging
MTB/TAN	Transgenic mouse line expressing activated Neu under the

	control of tetracycline
MVT1	Metastatic murine breast cancer cell line derived from mmtv c-myc / vegf mice
Neu	Ortholog of human epidermal growth factor receptor 2, HER2
NPI	Nottingham prognostic index
PCR	Polymerase chain reaction
PI3K	Phosphatidylinositol 3-kinase
PR	Progesterone receptor
Rag1	V(D)J recombination activation gene 1
rhIGF-1	Recombinant human IGF-1
RR	Relative Risk
sc	Subcutaneous
SEM	Standard error of the mean
SRSF3	Serine /arginine splicing factor 3
TG	Triglycerides
TNF	Tumour necrosis factor
Triple negative	ER negative / PR negative / Her2 negative
US	United States
VEGF	Vascular endothelial growth factor
WT	Wild type

## List of Figures

Figure 1 Hallmarks of Cancer .....	14
Figure 2 Biological Mechanisms Linking Obesity Diabetes and Cancer .....	15
Figure 3 Insulin Resistance and Hyperinsulinaemia Precede the Development of Hyperglycaemia in Type 2 Diabetes. ....	16
Figure 4 Risk of Cancer with diabetes .....	17
Figure 5 Fasting Insulin and Breast Cancer Survival .....	24
Figure 6 The Insulin-Like Growth Factor System .....	25
Figure 7 Insulin Receptor Isoforms .....	27
Figure 8 The Progressive Development of Type 2 diabetes in the Male MKR mice. .....	29
Figure 9 Inhibiting PI3K Reduced Tumour Growth in the MKR Mice .....	32
Figure 10 BKM120 Inhibited Akt phosphorylation in the tumours of the MKR mice .....	33
Figure 11 The Effects of PI3K Inhibition on Metabolic Parameters in the MKR mice .....	34
Figure 12 Epithelial to Mesenchymal Transition.....	35
Figure 13 Amino Acid Sequences of Human Insulin and Insulin Analogs.....	36
Figure 14 Clinical and Biological Factors Potentially Contributing to the Racial Disparities in Breast Cancer Prognosis in Black and White Women.....	38
Figure 15 Generation of the Hyperinsulinaemic Transgenic Inducible Activated Neu Mouse Model of Breast Cancer .....	45
Figure 16 Generation of Immunodeficient Hyperinsulinaemic mice .....	46
Figure 17 Generation of the MMTV Cre IR floxed mice. ....	47
Figure 18 Nanostring mRNA Gene Expression Analysis .....	56

Figure 19 Study Design for Study Examining Disparities in Breast Cancer Mortality .....	58
Figure 20 Metabolic Characterization of the MTB/TAN/MKR mice. ....	63
Figure 21 Effects of Hyperinsulinaemia on NeuNT-mediated Mammary Gland Hyperplasia.....	64
Figure 22 Tumour growth, IR $\beta$ /IGF-IR $\beta$ and Akt signaling are enhanced in tumours from MTB/TAN/MKR mice compared to MTB/TAN controls. ....	66
Figure 23 Lung Metastases in MTB/TAN and MTB/TAN/MKR mice .....	68
Figure 24 Vimentin expression is enhanced in NeuNT Tumours from MTB/TAN/MKR mice. ....	69
Figure 25 Metabolic Characteristics of Rag/MKR mice.....	72
Figure 26 MDA-MB-231 Tumours in Hyperinsulinaemic Mice.....	74
Figure 27 Insulin Receptor Signaling in MDA-MB-231 Tumours from Rag/WT and Rag/MKR Mice.....	75
Figure 28 Vimentin and Zeb-1 expression in MDA-MB-231 tumours from Rag/WT and Rag/MKR mice.....	76
Figure 29 Changes in EMT-related proteins in MDA-MB-231 Tumours from Rag/WT and Rag/MKR mice.....	77
Figure 30 Invasion of MDA-MB-231 cells in response to insulin in vitro.....	78
Figure 31 MVT1 Tumours have increased growth and metastasis in the MKR mice, associated with increased vimentin expression.....	81
Figure 32 Vimentin expression in MVT1 Tumours by Immunofluorescent Staining. ....	82
Figure 33 GFP and Vimentin co-Staining of MVT1 Tumours. ....	83
Figure 34 Insulin Stimulation Increases Vimentin Protein Expression in Vivo.....	84
Figure 35 Amino acid sequence and modifications of vimentin bands as determined by LC-MS.....	85

Figure 36 Silencing vimentin in MVT1 cells did not alter insulin-mediated activation of Akt and Erk in vitro.....	89
Figure 37 Proliferation, migration and invasion assays in MVT1 cells with vimentin knockdown.....	90
Figure 38 Vimentin knockdown reduced pulmonary metastases in the MKR mice .....	91
Figure 39 IR expression in the mammary epithelial cells of MMTV Cre IR floxed mice. ....	93
Figure 40 Whole mount and immunofluorescence analysis of the mammary epithelial cells of the MMTV Cre IR floxed mice.....	95
Figure 41 LCC6 tumour xenograft volume and weight in cells with normal and shRNA mediated silencing of the IR .....	97
Figure 42 Protein expression in LCC6 xenografts with normal and reduced IR expression. ....	98
Figure 43 Silencing the IR led to decreased c-myc expression in the MCF7 cells. ....	100
Figure 44 Insulin and AspB10 led to IR phosphorylation but not IGF-1R phosphorylation in vitro.....	102
Figure 45 IGF-1 increased orthotopic MVT1 and Met1 tumour growth in the hyperinsulinaemic MKR mice by increasing IGF-1R phosphorylation.....	104
Figure 46 Chronic activation of the IR by the insulin analog AspB10, increased orthotopic Met1 and MVT1 tumour growth.....	107
Figure 47 Endogenous hyperinsulinaemia and AspB10 treatment led to increased IR phosphorylation in MVT1 and Met1 tumours.....	108
Figure 48 Chronic administration of IGF-1 and AspB10 led to increased phosphorylation of Akt, but no change in Erk1/2 phosphorylation. ....	109
Figure 49 The effect of insulin analogs on MVT1 tumour growth .....	111

Figure 50 Western blot analysis revealed that all of the insulin analogs led to IR phosphorylation. ....	112
Figure 51 Insulin tolerance and metabolism with insulin glargine and A21Gly,DiD-Arg .....	114
Figure 52 MVT1 Tumour growth in response to A21Gly, DiD-Arg .....	115
Figure 53 Relative Expression of IR and IGF-1R in Human Breast Cancer.....	119
Figure 54 Insulin Receptor Isoform Expression in Human Breast Cancer Specimens. ....	120
Figure 55 Heatmap of clustered genes and cases from FFPE breast cancer samples .....	121
Figure 56 Insulin Receptor and IGF-1R expression in human breast cancer cell lines. ....	123
Figure 57 Insulin Receptor A and B expression in human breast cell lines.....	124
Figure 58 Heatmap of clustered genes and human breast cell lines.....	125

## **List of Tables**

Table 1 Primers for Mouse Genotype Determination .....	48
Table 2 Characteristics of Patients .....	117

## Summary

Obesity, type 2 diabetes and the metabolic syndrome are associated with an increased risk of developing breast cancer. In addition, these conditions are associated with more aggressive forms of breast cancer and greater breast cancer mortality. All three conditions are associated with insulin resistance and endogenous hyperinsulinemia. Breast cancers express the insulin receptor (IR), therefore we hypothesize that endogenous hyperinsulinaemia promotes breast cancer growth and metastases by acting directly on the IR on the tumour cells, and by causing epithelial to mesenchymal transition in the tumour. We found that hyperinsulinaemia led to increased growth and metastasis of both murine and human breast cancers in an animal model of hyperinsulinaemia. We found that the increase in tumour metastasis was associated with increased vimentin expression in the primary tumours. We found that silencing the IR reduced the growth of human breast cancer xenografts in the animals, associated with a decrease in vimentin expression. Silencing vimentin in breast cancer cells reduced their ability to invade in vitro and decreased their metastatic capabilities in the hyperinsulinaemic mice. Examining human breast cancer cell lines, we found that triple negative breast cancer cell lines had higher IR expression than oestrogen receptor positive breast cancer cell lines, and that the main isoform of the IR in both human breast cancer specimens and cell lines was the IR-A isoform. Higher levels of IR-A and lower levels of IR-B correlated with changes in the expression of splicing factors, SRSF3 and MBNL2 in both the breast cancer cell lines and the human breast cancer specimens. We found that none of the insulin analogues in clinical use increased tumour growth, but a mitogenic analogue AspB10 stimulated tumour growth by activating the IR. These data show that endogenous hyperinsulinaemia and IR signaling are important regulators of breast cancer growth and progression.



## **Acknowledgements**

Supervisors for this thesis were Professor Jochen Prehn and Professor Derek LeRoith.

The work described in this thesis was performed at the Icahn School of Medicine at Mount Sinai, Mount Sinai, New York, NY in the laboratory of Dr. Derek LeRoith, Division of Endocrinology, Department of Medicine.

Support for Dr. Emily J. Gallagher was provided by:

The Lucy G. Moses Fund,  
Department of Medicine, Mount Sinai School of Medicine  
NIH/NCI 1K08CA190770

Support for this research was provided to Dr. Derek LeRoith by the following grants and granting agencies:

NIH/NCI 5R01 CA171558  
NIH/NCI 2R01CA128799  
American Diabetes Association ADA 1-13-BS-108  
Sanofi

Members of Dr. LeRoith's lab who participated in the work described in this thesis were Dr. Yvonne Fierz (PI3K inhibitor study), Dr. Rosalyn Ferguson (MTB/TAN study), Dr. Ran Rostoker (GFP and IR shRNA studies), Zara Zelenko (Vimentin, Rag and Insulin analogue studies), Aviva Tobin-Hess (Insulin analogue studies), Jeffrey Blank (Insulin analogue studies), Marilyn Stasinopoulos (MCF7 cell studies), Rebeca Franco (Human breast cancer study)

Other Collaborators and Advisors:

Dr. Shoshana Yakar, NYU, New York, NY, USA.

Dr. Maria Byrne, Mater Misericordiae University Hospital, Dublin.

Professor Teresa Wood, Rutgers, UMDJ, Newark, NJ, USA

Professor Nina Bickell, Mount Sinai, New York, NY, USA.

Professor Ramon Parsons, Mount Sinai, New York, NY, USA.

## 1. Introduction

Cancer cells are not independent of their host. While there are specific hallmarks of cancer cells, they require nutrients, hormones and growth factors, and signals provided by the circulation and surrounding cells of their host, in a similar manner to any other cell of the human body. These factors influence their survival, growth and spread. The characteristics of cancer cells and the metabolic abnormalities of their host may influence how they survive, proliferate and spread (Figure 1).

An increased incidence of many cancers and cancer mortality has been observed in individuals with obesity and type 2 diabetes. While there are many metabolic factors that may contribute to cancer progression in these conditions (Figure 2), the focus of the work in this thesis is the role of hyperinsulinaemia.

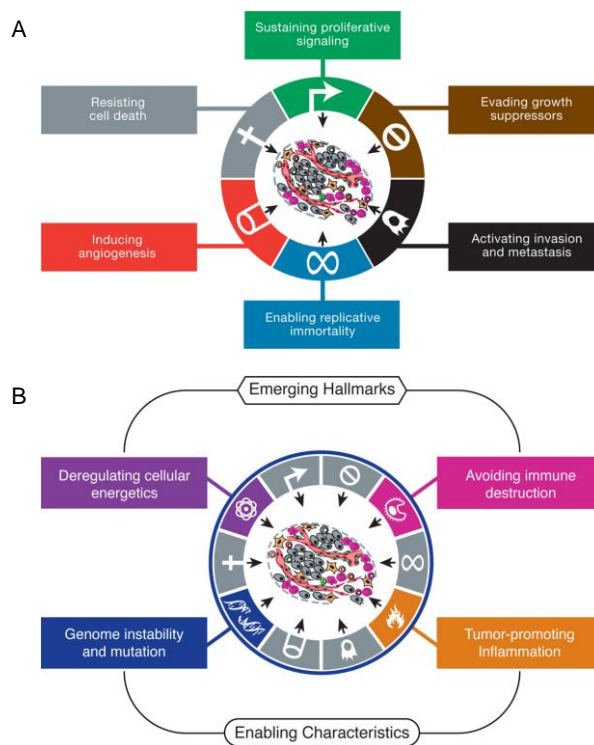


**Figure 1 Hallmarks of Cancer**

This illustration encompasses the six hallmark capabilities of cancer originally proposed in the year 2000 by Hanahan and Weinberg (A). (B) The hallmarks of cancer that have emerged in recent years and are the subject of ongoing investigation, and the characteristics of cancers that enable the core and emerging hallmarks. Hanahan D, Weinberg R. Cell 2001; 144(5): 646-674 (63). Reproduced with permission.

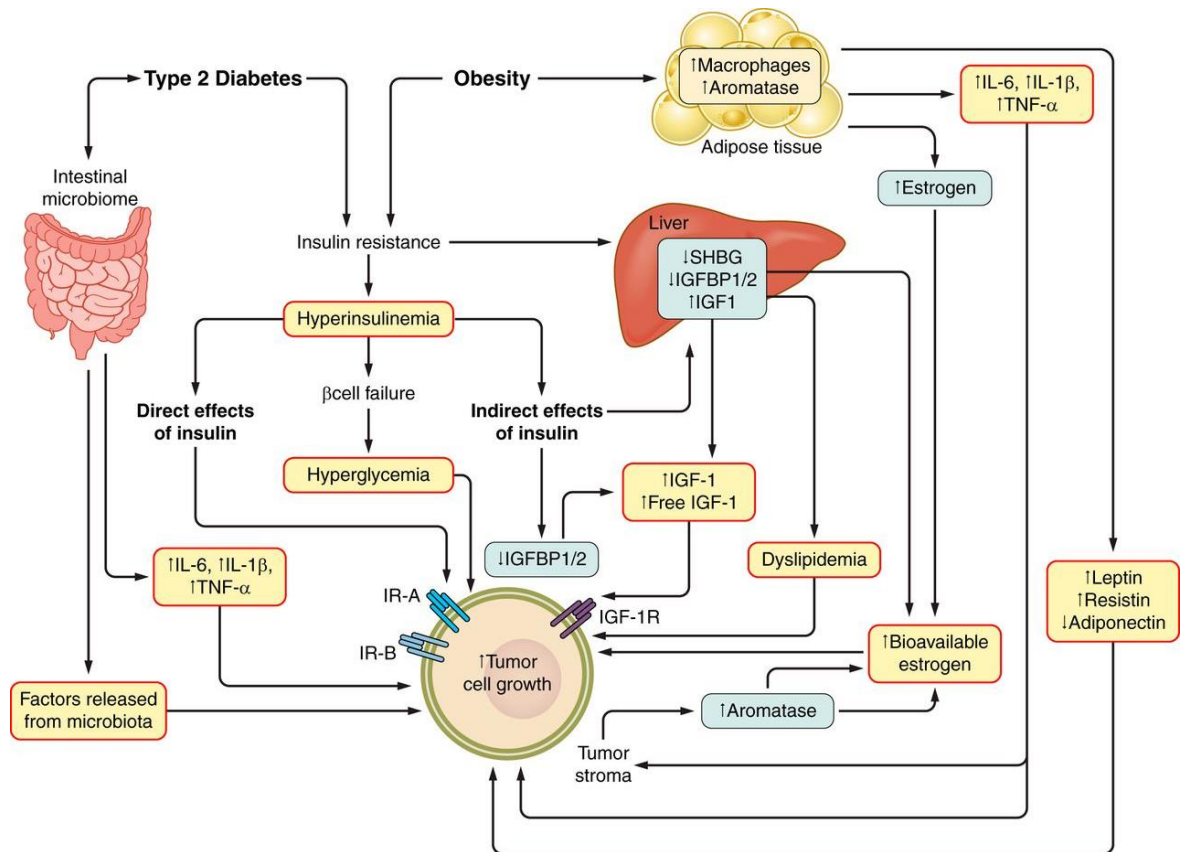


**Figure 2 Biological Mechanisms Linking Obesity Diabetes and Cancer**

Biological abnormalities associated with obesity and type 2 diabetes that may contribute to cancer growth and progression. From Gallagher EJ and LeRoith D *Physiol Rev* 2015; 95(3):727-748. Reproduced with Permission.

### Insulin Resistance and Hyperinsulinaemia in Obesity and Type 2 Diabetes

Obesity, specifically abdominal obesity, and type 2 diabetes are associated with multiple metabolic abnormalities (Figure 2). Abdominal obesity is associated with increased adipose tissue inflammation with the production of cytokines and changes in the circulating concentrations of adipokines. These changes can contribute to insulin resistance in metabolic tissues, necessitating an increase in the production of insulin from the pancreatic beta cells to maintain normal glucose levels, leading to circulating hyperinsulinaemia. Eventually, the beta cell failure occurs, and hyperglycaemia develops, sometime after which diabetes is diagnosed (Figure 3).

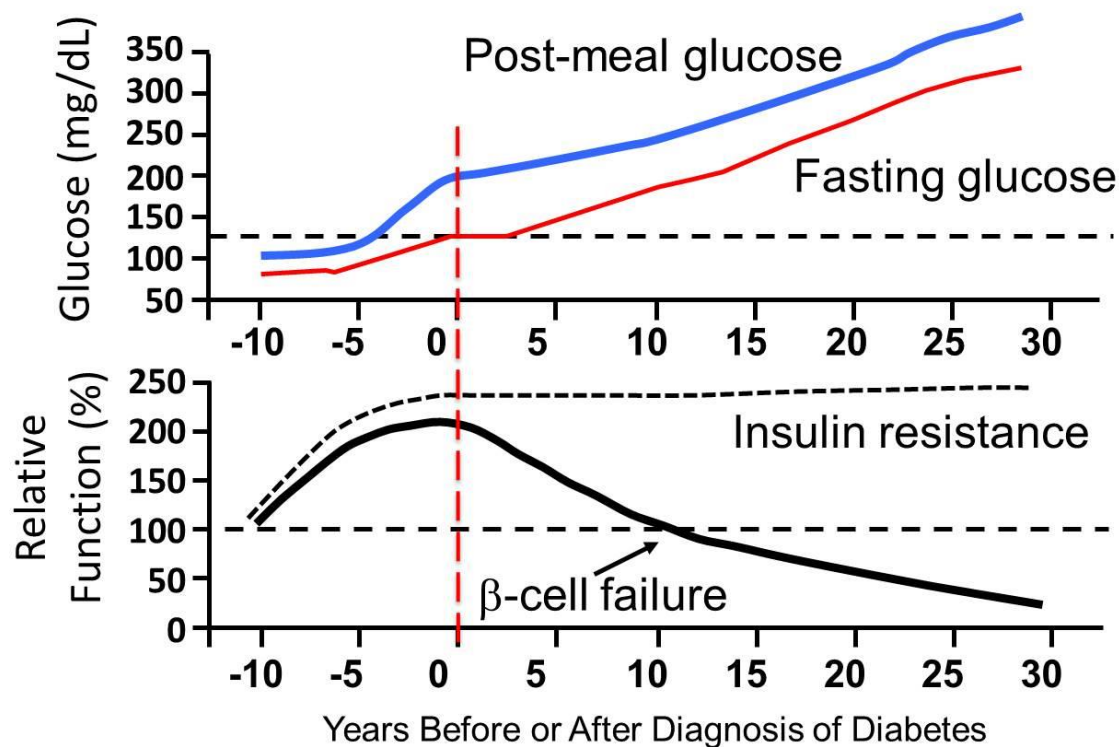


**Figure 3 Insulin Resistance and Hyperinsulinaemia Precede the Development of Hyperglycaemia in Type 2 Diabetes.**

These two graphs illustrate the insulin resistance and hyperinsulinaemia that are present for many years prior to the diagnosis of type 2 diabetes. The upper graph represents the initial development of impaired glucose tolerance, with an increase in post-meal glucose (blue line) followed by the increase in fasting glucose (red line). The horizontal dotted line indicates the threshold fasting glucose level for the diagnosis of diabetes. The vertical dotted red line represents the time of diabetes diagnosis. The y-axis indicates glucose levels in mg/dL. Equivalent values in mmol/L are 2.8mmol/L (50mg/dL), 5.5mmol/L (100mg/dL), 8.3mmol/L (150mg/dL), 11.1mmol/L (200mg/dL), 13.9mmol/L (250mg/dL), 16.7mmol/L (300mg/dL), 19.3mmol/L (350mg/dL). The x-axis on the upper and lower graphs represents the years before, or after the development of glucose levels that define diabetes. The lower graph indicates the development of insulin resistance (dotted black line) and hyperinsulinaemia (solid black line) many years before the development of hyperglycaemia. The y-axis indicates beta cell function. Figure provided by Dr. Derek LeRoith, Mount Sinai, New York, NY.

Insulin resistance is frequently calculated using the HOMA-IR ((homeostasis model assessment of insulin resistance) [fasting plasma glucose (mmol/L) x fasting serum insulin (μU/ml)]/22.5) (143), HOMA-IR positively correlates with abdominal obesity (141). Of individuals with type 2 diabetes (who comprise 90% of all diabetes cases worldwide), almost all patients are insulin resistant (124). High circulating insulin levels correlate strongly with insulin resistance, and have been found to do so in women with breast cancer (61).

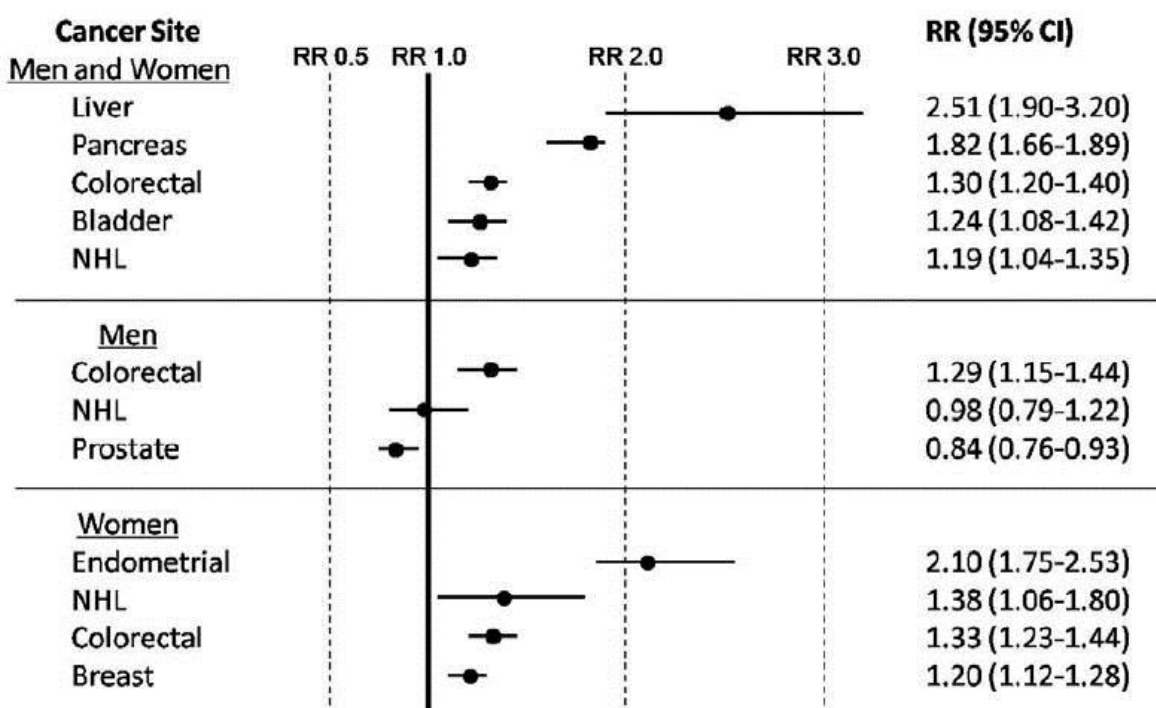


**Figure 4 Risk of Cancer with diabetes**

Results from meta-analyses examining the relative risk (RR) of cancers at specific sites in individuals with diabetes. Breast cancer risk is highlighted by the red arrow, and has a 20% increased risk in women with diabetes. From Gallagher EJ et al. Endocrine Practice 2010; 16(5): 864-873 (52). Reproduced with Permission.

The association between obesity, diabetes and cancer has recently received much attention due to the alarming increases in the prevalence of obesity and type 2 diabetes worldwide. There is a large body of evidence linking obesity, type 2 diabetes and the risk and mortality from many cancers (Figure 4). In the next sections I will discuss the historical studies that tied obesity and diabetes to

cancer, and the more recent population studies. I will then discuss the previously published human and animal studies linking hyperinsulinaemia and cancer progression.

### **Historical Context**

The first reported case of diabetes associated with cancer has been attributed to the 19<sup>th</sup> century English physician, Dr. Richard Bright. In 1832, he reported the case of a patient with polyuria, polydipsia, sweet urine and carcinoma of the pancreas. This case was described years before the identification of the Islets of Langerhans as the source of insulin secretion. In 1910, the South African epidemiologist Mr. George Darell Maynard reported that diabetes was associated with an increased risk of many cancers. His findings were controversial, and disputed by many epidemiology and diabetes experts following his publication (107). By 1957 Dr. E.T. Bell, the renowned pathologist from the University of Minnesota stated that it was “well known” that carcinoma of the pancreas was frequently associated with glycosuria and hyperglycaemia; however, it was not known whether there was an increased incidence of “true” diabetes in subjects with pancreatic carcinoma, or if subjects with “true” diabetes demonstrated an increased incidence of carcinoma of the pancreas; a question that was debated subsequently for many years (15).

In 1926, Otto Warburg and colleagues reported that cancer cells have the ability to obtain energy both from aerobic respiration and anaerobic glycolysis with the formation of lactic acid, in the presence of oxygen, (a characteristic known as the Warburg phenomenon) (144). He reported that this ability to produce energy from aerobic respiration and glycolysis enhanced the survival of cancer cells in glucose- or oxygen-deprived conditions. In recent years, a greater understanding has developed of the mechanisms that lead to the Warburg phenomenon. In addition, it has emerged that changes in glucose uptake and metabolism are not the only metabolic idiosyncrasy of cancer cells. In fact, cancer cells are influenced by the nutrients in the environment in which they reside, and the hormonal signals to which they are subjected. It is these interactions between an individual's metabolic status and the distinct characteristics of tumours that are believed to underlie the associations between obesity, diabetes and cancer.

Obesity, calorie restriction and cancer links have been explored in animal studies since the 1940's. An increase in toxin-induced cancers was found in obese animals, and a decrease in calorie restricted animals (145). In the 1960's it was recognised that obese women had a greater incidence of endometrial cancer than their lean counterparts. This association was attributed to an increase in oestrogen synthesis from adipose tissue in overweight / obese women (149), and weight loss was proposed by the authors as the most practical preventative measure for endometrial cancer.

Since the time of these groundbreaking clinical observations and research studies, much work has been done to understand the links between obesity, diabetes and cancer. As type 2 diabetes and obesity are a global epidemic, an urgent need to understand the interactions between these metabolic conditions and cancer has emerged.

### **Epidemiology**

The initial clinical observations and studies discussed above, paved the way for the many recent large cohort studies examining the links between obesity, diabetes and cancer incidence and mortality.

#### *Obesity and Cancer*

The large cohort studies that have provided much of our knowledge today on the links between obesity and cancer have been performed since the 1990's. The Cancer Prevention Study II (CPS II) was one such study that followed patients from 1982 to 1996 and included over 1 million adults in the United States. The study examined the association between body mass index (BMI), calculated from patients self-reported height and weight, and cancer mortality. The authors found that the most obese men and women had a 40-80% increased risk of dying from cancer (29). The same group subsequently published a more detailed analysis of the CPS II cohort and the association between BMI and mortality from cancer at specific sites after 16 years of follow up. They found a linear trend of increased overall cancer mortality with increasing BMI for multiple cancers, one of which was breast cancer in women (28). Multiple subsequent studies and meta-analyses have been performed that have confirmed these findings that obesity is associated with greater mortality from breast cancers.

The incidence of certain cancers is also higher in obese individuals. A comprehensive meta-analysis was performed in 2007, including 221 datasets from different populations. The authors of this study found that in men and women, for every 5kg/m<sup>2</sup> increase in BMI, there was an increased risk of many cancers, with an increased risk of postmenopausal breast cancer in this cohort (126).

Although BMI is most frequently used as a measure of obesity, it is well recognised in the field of endocrinology that when obesity is measured by BMI, a number of individuals who are metabolically unhealthy are classified as not obese. Waist circumference is preferred over BMI as measure of obesity, as it correlates better with visceral adiposity and insulin resistance, as well as other markers of metabolic “unhealthiness” including dyslipidemia, glucose intolerance and hypertension, which are all associated with the metabolic syndrome and the risk of developing of type 2 diabetes (6). Furthermore, specific populations including South-East Asian populations frequently have these metabolic abnormalities despite the fact that their BMI falls into the normal range (6).

Few studies have specifically examined the contribution of waist circumference to cancer risk and mortality, compared with the number of studies that used BMI as a marker of obesity. In the CPS II study of predominantly white women in the United States, waist circumference did correlate with post-menopausal breast cancer risk, but did not offer a greater predictive power than BMI in this population (56). However, in the Nurses’ Health Study population, it was found that waist circumference was associated with post-menopausal breast cancer risk, specifically in women who had never received post-menopausal hormone replacement therapy (72). A meta-analysis of studies found that adjusting for BMI actually revealed that waist circumference may be specifically associated with breast cancer risk in pre-menopausal women while BMI was not (66). These studies suggest that it is not simply obesity, but abdominal obesity that is associated with insulin resistance, is specifically linked to the increased risk of breast cancer.

If obesity is associated with increased cancer incidence and mortality, then can intentional weight loss reduce the risk of cancer and cancer mortality? When evaluating the effect of weight loss on cancer risk and mortality, it is important to distinguish between intentional and unintentional weight loss, as cancer cachexia,



associated with anorexia and weight loss is associated with significant mortality (69). A recent review of 34 published articles covering this field was published by Birks and colleagues in 2012 (19). They separately examined the effects of intentional surgical weight loss, intentional non-surgical weight loss, and weight loss that was unintentional, or undefined, on cancer incidence and mortality. The three studies examining the effect of surgical weight loss on cancer incidence found that there was a 24-78% reduction in overall cancer incidence in the bariatric surgery population compared to the obese control group (1, 33, 132). After further analysis the Swedish Obesity Study (132) and a study from Utah in the United States (1) found that the decreased risk was only apparent in women. The Utah study also specifically examined the risk of obesity-related cancers and found a significant 38% risk reduction in the bariatric surgery group. The authors of this study also examined cancer mortality and found a 46% decrease in cancer mortality in the group who had undergone bariatric surgery (1). Birks and colleagues examined 3 cohort studies investigating the effect of non-surgical weight loss on the incidence and mortality from cancer. In these studies, 17-19% of the study populations achieved intentional weight loss and the results were examined based on the degree of weight loss (148). The prospective cohort from the Iowa Women's Health Study reported a decrease in the incidence of all cancers, breast cancer and obesity-related cancer in the population that lost  $\geq 9$ kg (121). Overall, these studies support the association between obesity, and breast cancer incidence and mortality, and suggest that intentional weight loss may reduce the risk of certain cancers, particularly in women.

### *Diabetes and Cancer*

Along with the increasing prevalence of obesity worldwide, there is an increasing prevalence of Type 2 diabetes. Large prospective cohort studies to re-explore Maynard's initial observations on the association between diabetes and cancer were not performed until relatively recently. The Nurses' Health Study was one such study. In this study they enrolled women in 1976 and followed them biennially to determine potential risk factors for cancer, amongst other diseases. In 2003, the investigators reported a 17% increased risk of breast cancer incidence (HR 1.17, CI 1.01-1.35) in women with diabetes, compared to women without diabetes. This association remained after adjustment for multiple factors, and was found to be independent of age, and obesity. The researchers reported that the association

was predominant among postmenopausal women, and women with oestrogen receptor (ER)-positive breast cancer (109). One of the largest cohorts with the longest duration of follow up is the CPS II cohort (30). After following these patients for 26 years, an increased risk of death from multiple cancers was seen, including breast, which was observed in diabetic women and men (30). Many other studies and meta-analyses have been performed to examine breast cancer incidence and mortality in diabetic patients, compared to the general population. Overall, a consistent increase in the risk of breast cancer has been reported in women with diabetes (48, 89). Furthermore, studies on cancer mortality have revealed that patients with diabetes have greater cancer mortality compared to their non-diabetic counterparts (12, 30).

Type 2 diabetes is preceded by many years by pre-diabetes, which is defined as an elevated fasting glucose level or abnormal glucose tolerance, but without blood glucose levels in the diabetic range (Figure 3). It has been reported in some studies that the incidence of cancer is greatest within the first months to years following diabetes diagnosis. This observation was reported in a retrospective study of breast cancer incidence from Australia (118), and in a study from Canada that reported that 9.7% of 24,976 patients diagnosed with breast cancer were diagnosed with diabetes within 5.5 years of follow up (93). The authors of these studies suggest that the increased incidence of breast cancer around the time of diabetes diagnosis is because of the risk of cancer being greatest in the prediabetes (hyperinsulinaemic) phase (93, 118). These results suggest that the metabolic abnormalities associated with pre-diabetes, which include insulin resistance and endogenous hyperinsulinaemia may contribute to breast cancer development.

#### *Hyperinsulinaemia and Breast Cancer*

As discussed previously, insulin resistance and hyperinsulinaemia are common in individuals with obesity and type 2 diabetes. Large cohort studies have examined whether endogenous hyperinsulinaemia is associated with cancer risk and mortality. These studies have examined serum insulin or C-peptide levels as markers of insulin secretion. C-peptide is co-secreted with insulin and has a longer half-life than insulin, as unlike insulin, it is not extracted by the liver (104). C-peptide is therefore a more stable marker of insulin secretion than insulin. The

Nurses' Health Study cohort found an association between C-peptide and invasive breast cancer, particularly oestrogen receptor alpha (ER $\alpha$ )-negative disease (4). In the Healthy Eating, Activity and Lifestyle (HEAL) Study, C-peptide was associated with a 35% increased risk of breast cancer death, particularly in women with ER $\alpha$ -positive tumours (76). The European Prospective Investigation into Cancer and Nutrition (EPIC) study found a 2 fold increased risk of breast cancer in women over the age of 60 years with elevated C-peptide levels (140). Furthermore, in women with newly diagnosed early stage breast cancer, having a fasting insulin level in the highest quartile of the population was associated with the greatest disease recurrence and mortality over 7 years of follow up (Figure 5). Therefore, the epidemiological studies support the role of endogenous hyperinsulinaemia, in promoting tumour growth and progression.

#### *Insulin and Insulin-Like Growth Factor Signaling*

The insulin-like growth factor system consists of the insulin receptor (IR), insulin-like growth factor-1 receptor (IGF-1R), the insulin-related receptor and the IGF-2R, along with the ligands insulin, IGF-1 and IGF-2, and the insulin like growth factor binding proteins (IGFBP's, 1-6) that bind IGF-1 and IGF-2, but not insulin (Figure 6).

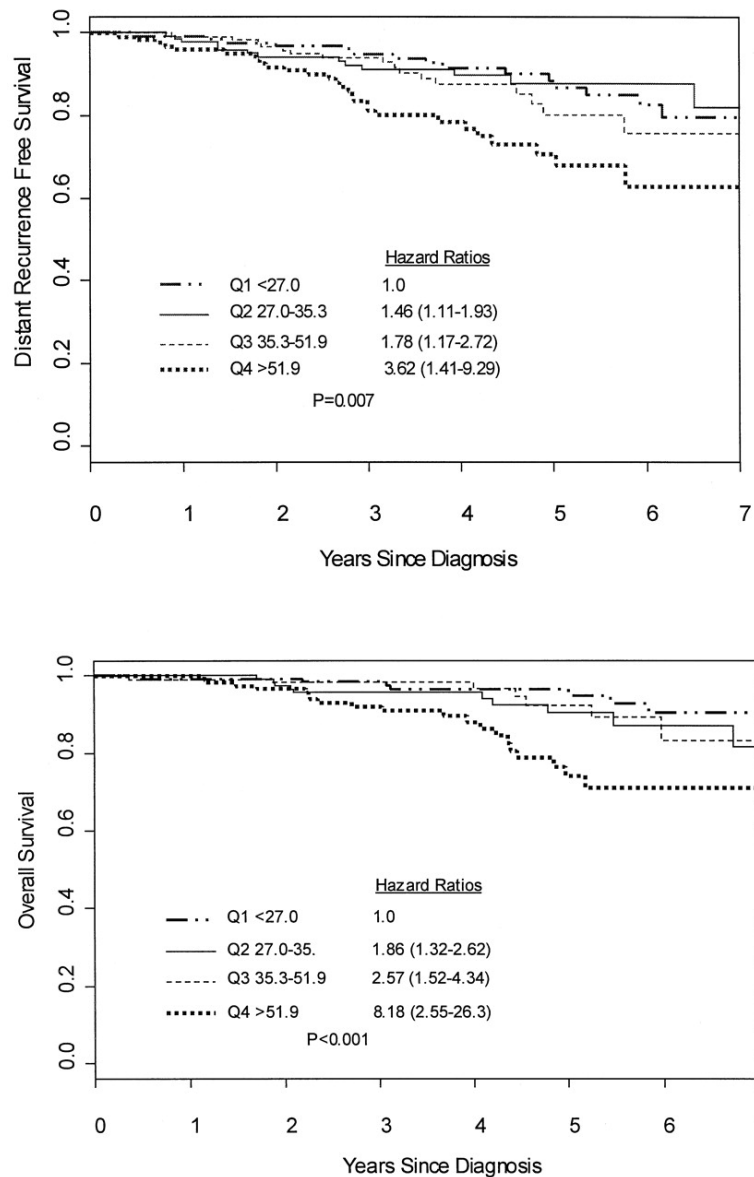


**Figure 5 Fasting Insulin and Breast Cancer Survival**

Kaplan-Meier estimates of distant recurrence-free survival (upper panel) and OS (lower panel) according to quartiles (Q) of fasting insulin (ng/L). Hazard ratio and P values are taken from Cox models of DDFS and OS, in which insulin was treated as a continuous variable. Pamela J. Goodwin et al. JCO 2002;20:42-51. Reproduced with permission.

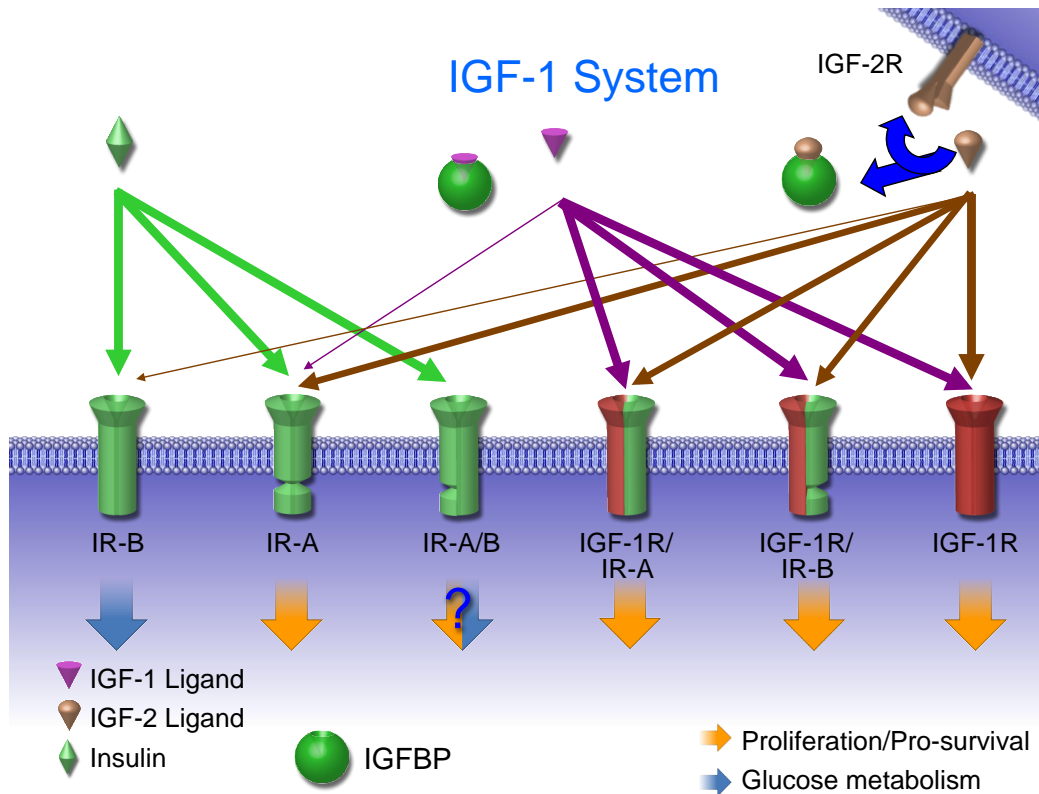


**Figure 6 The Insulin-Like Growth Factor System**

The ligands, receptors and binding proteins of the insulin-like growth factor system. Figure provided by Dr. Paul Haluska, Mayo Clinic, Rochester, MN.

The IGF-1R was initially found to be overexpressed in a number of childhood cancers, such as Wilms' Tumour, osteosarcoma and rhabdomyosarcoma (91), and subsequently found to be overexpressed in a number of other cancers including breast cancers. In addition, many tumours overexpress IGF-2 due to loss of imprinting, which signals through the IGF-1R and the mitogenic form of the IR (152). In addition, many tumours express IGF-1, which is the main ligand for the IGF-1R. The loss of tumour suppressor genes BRCA1, p53 and PTEN were found to lead to an increase in IGF-1R expression (151, 152, 154), and similarly IGF-1 stimulation of tumour cells was found to down-regulate tumour suppressor genes such as WT1 (17). In animal models, high doses of exogenous IGF-1 have been found to increase tumour growth and metastases. Reduced tumour growth was seen in mice with liver-specific IGF-1 deletion (LID) mice and low circulating IGF-1 levels, and in the lit/lit mice that have low circulating IGF-1 due to decreased growth hormone production (151). A number of epidemiological studies reported

that circulating IGF-1 levels in the upper quartile of the normal population range were associated with an increased risk of cancer. In addition in a population of individuals from Ecuador with growth hormone receptor mutations, who have very low circulating IGF-1 levels appear to be protected from cancer development compared to the normal population (62). These human and animal data suggested that blocking the IGF-1R would be an effective target for anti-cancer therapy. However, clinical trials that targeted the IGF-1R have not been successful (153). The postulated reasons for their failure are numerous. Firstly, the trials didn't specifically target people with tumours that overexpressed the IGF-1R. In addition, inhibiting the IGF-1R leads to elevated circulating levels of IGF-1, which from in vitro and in vivo studies is known to be capable of activating the IR. Furthermore, inhibiting the IGF-1R leads to impaired feedback on GH secretion, causing elevated circulating levels of GH, which causes insulin resistance and hyperinsulinaemia. Hyperinsulinaemia through activation of the IR on tumour cells may also contribute to tumour growth and progression (153).

The insulin receptor (IR) is expressed in many tissues, not only metabolic tissues. It is also expressed in the foetus, where insulin is important for growth, and hyperinsulinaemia, secondary to maternal gestational diabetes, leads to macrosomia (81). Many tumours, including breast cancers overexpress the IR (14, 34). Insulin receptors are not downregulated in the foetus in response to hyperinsulinaemia, nor are they downregulated in breast cancers of hyperinsulinaemic women (81, 113). Although the IGF-1R has traditionally been thought of as a mediator of mitogenic signaling, and the IR as an activator of metabolic signaling, IR phosphorylation actually activates both metabolic and mitogenic signaling pathways (14).

There are two splice variants of the IR, IR-A and IR-B (Figure 7). IR-A lacks exon 11 and is predominantly expressed in foetal and cancer tissues, while IR-B is predominantly expressed in the liver, skeletal muscle, adipose tissue and kidney. The expression of certain splicing factors in cells determines the ratio of IR-A to IR-B in the cell (14). Recent studies have found that activation of the EGFR/mitogen-activated protein kinase (MAPK) pathway increases the IR-A / IR-B ratio in hepatocellular carcinoma cell lines by upregulating expression of certain splicing factors in the tumour cells, but not in regenerating normal liver (31). Decreased expression of some splicing factors such as serine /arginine splicing

factor 3 (SRSF3), led to increased expression of IR-A, and promoted the growth of hepatocellular carcinoma (130).

Studies in different cell lines have revealed that the different IR isoforms have different affinity for insulin, IGF-1 and IGF-2. IR-A has a 1.7 fold greater affinity for insulin than IR-B (112). IR-A binds IGF-2 with approximately 40 times greater affinity than IR-B, and IGF-1 with approximately 10 times higher affinity than IR-B (14). Signal transduction after ligand binding to IR-A or IR-B differs greatly, and differs depending on the ligand that is bound to the receptor isoform. In murine 32D haematopoietic cells, IR-A has been shown to activate mitogenic, anti-apoptotic signaling, while IR-B activation leads to cell differentiation. Therefore, in tumours aberrant signaling, leads to changes in the expression of splicing factors, leading to an increase in IR-A expression, and this is hypothesized to be responsible for the effects of hyperinsulinaemia on tumour growth (14).

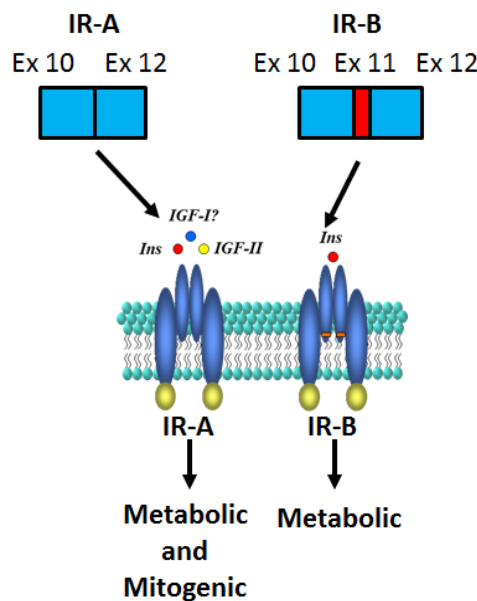


**Figure 7 Insulin Receptor Isoforms**

Splice variants of the insulin receptor, insulin receptor isoform A (IR-A) and insulin receptor isoform B (IR-B). The red bar represents exon 11, encoded by 36 base pairs, that is located in the transmembrane domain of the IR isoform B, but not IR-A.

### **A Non-Obese Mouse Model of Hyperinsulinaemia and Breast Cancer**

A common method of inducing insulin resistance and hyperinsulinaemia in mice is through diet-induced obesity. High-fat diet feeding of mice induces obesity, and elevations in circulating cytokines, including TNF- $\alpha$ , IL-1 $\beta$ , and IL-6 (96). It is also associated with increased circulating IGF-1, decreased IGFBP-3, glucose intolerance, increased leptin, resistin and decreased adiponectin in mice (117). An increase in growth of breast cancer has been found in diet-induced obesity models (57, 82, 92, 96). However, in these models, it is difficult to tease apart which abnormality, or if all of the abnormalities resulting from high fat diet feeding, contribute to the cancer.

A mouse model of hyperinsulinaemia and Type 2 diabetes was previously developed in the LeRoith lab using a transgenic approach (45). By overexpressing a dominant-negative insulin-like growth factor-1 receptor (IGF-1R) specifically in skeletal muscle (named MKR for muscle (M) lysine (K) to arginine (R) substitution in the tyrosine kinase motif of the IGF-1R), the mice developed severe muscle insulin resistance, leading to beta cell compensation and hyperinsulinaemia two weeks after birth. Insulin resistance developed in fat and liver by 3-4 weeks of age. At 6 to 8 weeks of age, the male mice demonstrated a beta cell defect (loss of first phase insulin release) and the male mice became hyperglycaemic and hyperlipidemic, but were not obese (Figure 8) (45).

The female MKR mice developed a similar degree of insulin resistance and hyperinsulinaemia (2-3 fold higher insulin concentration than normal) as the male mice, but did not develop hyperglycaemia or hyperlipidemia. The female MKR mouse has normal circulating lipids, IGF-1, and levels of the inflammatory cytokines, interleukin-6 (IL-6) and tumour necrosis factor-alpha (TNF $\alpha$ ) (46, 115). Therefore, the female MKR mice have allowed for the study of the effect of hyperinsulinaemia on breast cancer development and progression, independent of hyperglycaemia, dyslipidemia and increased circulating inflammatory cytokines (115).



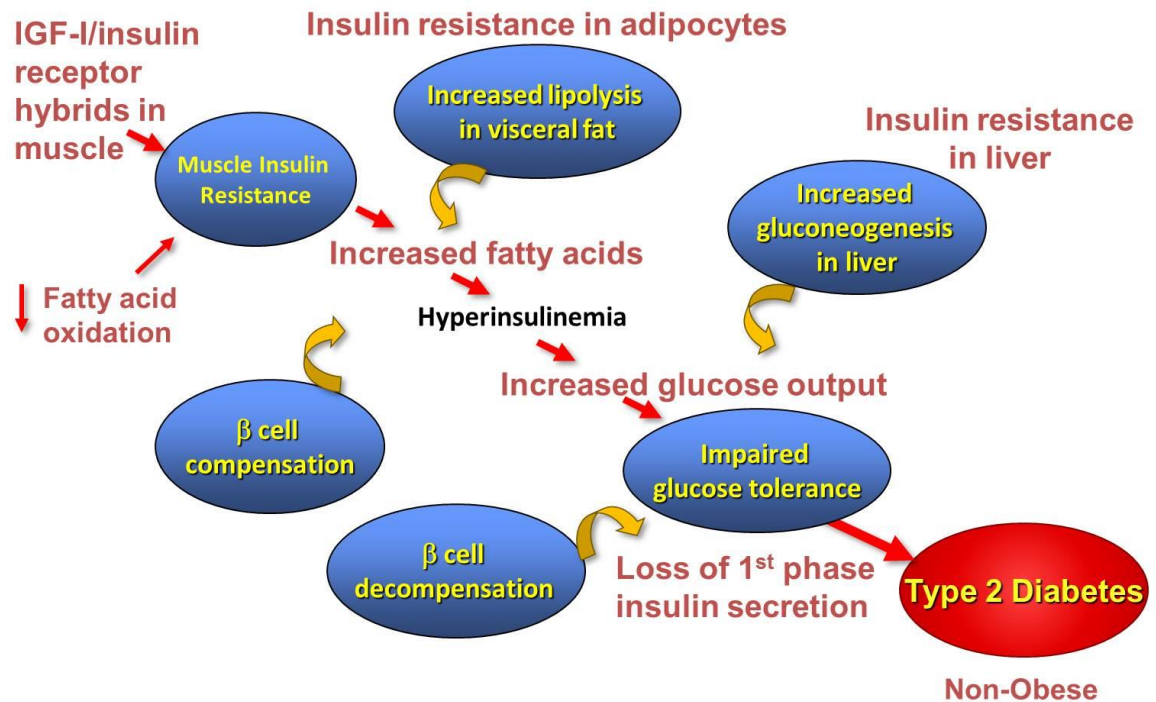


**Figure 8 The Progressive Development of Type 2 diabetes in the Male MKR mice.**

The graphic represents (from left to right) the initial genetic defect in the MKR mouse that leads to progressive insulin resistance in other organs, initially leading to beta cell compensation, but subsequently leading to beta cell decompensation, with impaired glucose tolerance, and eventually fasting hyperglycaemia indicative of type 2 diabetes.

When mammary tumours were induced in the female MKR mice, by crossing them with mice expressing the polyoma virus middle T antigen (PyVmT) oncogene in mammary epithelium (a mouse model of luminal B type human breast cancer (25)), the MKR mice developed larger tumours (115). Similarly, when cells overexpressing the Neu (ortholog of human epidermal growth factor receptor 2, HER2) or c-myc/vegf oncogenes were injected orthotopically into mammary glands the tumours grew more rapidly in the hyperinsulinaemic female MKR mice (44, 115). In all of the models we found that the tumours from the hyperinsulinaemic mice had increased activation of PI3K / Akt signaling, compared to WT mice. Reducing insulin levels in the MKR mice using a  $\beta$ -3 adrenergic receptor agonist (CL-316,243) or blocking the IR and IGF-1R using a tyrosine kinase inhibitor, reduced the growth of the primary tumours in the female MKR

mice (44, 46, 51, 115). The female MKR mice develop more numerous lung metastases than wild-type mice after orthotopic injection of c-myc/vegf overexpressing (MVT1) cells (44). Reducing the insulin levels using the  $\beta$ -3 adrenergic agonist CL-316,243 reduced the number of metastases to the number seen in the wild-type mice (28). These results support the hypothesis that endogenous hyperinsulinaemia enhances primary breast cancer growth by activation of the IR and/or IGF-1R. However, these studies were all performed in mouse tumours, therefore, we aimed to expand the studies to other transgenic models, and to tumours derived from human breast cancer cell lines.

### **Challenges with Inhibiting the IR/IGF-1R Signaling Pathway**

Although lowering circulating insulin levels in the MKR mice was a successful strategy to reducing breast cancer growth and metastases, the use of the compound CL-316,243 does successfully improve insulin resistance and reduce hyperinsulinaemia in humans in the same way. Therefore, this compound is not in clinical use for insulin resistance. However another insulin sensitizing agent metformin has been reported to reduce mortality from cancer in epidemiological studies in individuals with type 2 diabetes (42). Prospective clinical trials are ongoing to determine if metformin has beneficial effects as an adjuvant therapy in patients with breast cancer.

Another method of blocking insulin signaling is by targeting the IGF-1R / IR or downstream signaling proteins. Prior to starting the work described in this thesis, I investigated the effect of inhibiting phosphatidylinositol 3-kinase (PI3K) signaling on primary breast tumour growth in the hyperinsulinaemic mice, using a pan Class I PI3K inhibitor, BKM120 (53). In that study, we found that systemic administration of the PI3K inhibitor led to a significant reduction in the growth of Met1 and MCNeuA tumours in the MKR mice (Figure 9), with reduction in Akt phosphorylation (Figure 10). However, there was significant worsening of the hyperinsulinaemia, with the development of frank hyperglycaemia in the MKR mice treated with BKM120 (Figure 11) (53).

Clinical studies with this compound found similar results, with frequent development of hyperglycaemia in those treated with BKM120 (16). These results prompted us to investigate whether there were downstream changes in proteins or

gene expression in the tumours, as a result of hyperinsulinaemia, that could be targeted without worsening the metabolic status of the animal.

As we had observed an increase in breast cancer metastases, along with an increase in PI3K / Akt signaling, we hypothesized that hyperinsulinaemia may increase tumour progression by promoting epithelial to mesenchymal transition (EMT) in the tumours from the MKR mice. EMT is the process through which cells lose their epithelial markers and gain mesenchymal markers, as shown in Figure 12. EMT is believed to be a key feature of invading and metastasizing cancer cells. Recent studies have reported that PI3K / Akt activation may promote EMT, therefore, we aimed to study if hyperinsulinaemia led to an increase in mesenchymal characteristics of the tumours in the MKR mice (150).

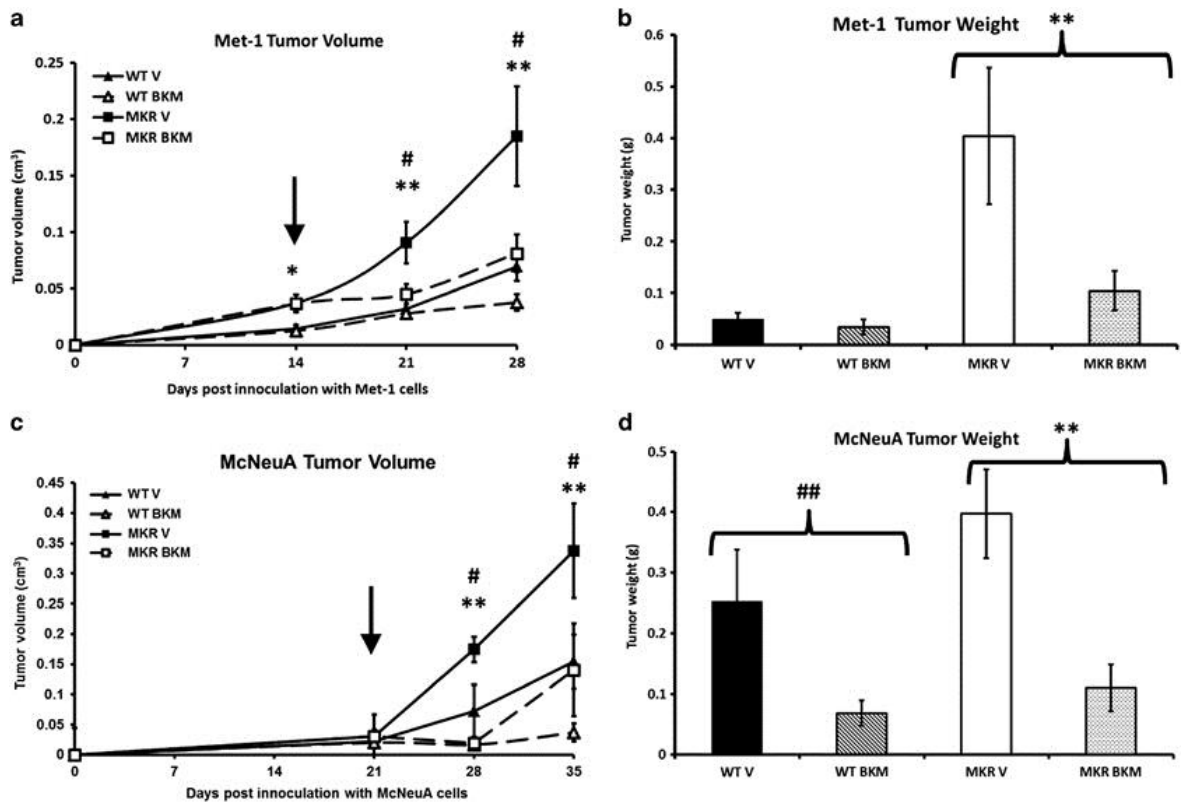


### Figure 9 Inhibiting PI3K Reduced Tumour Growth in the MKR Mice

Treatment with NVP-BKM120 reduced the accelerated tumour growth in the MKR mice. (a, c): Met-1 cells ( $0.5 \times 10^6$ ) and MCNeuA cells ( $1 \times 10^6$ ) were injected into the 4th mammary fat pad of 8–10-weeks old virgin WT and MKR mice on day 0. Treatment with NVP-BKM120 (BKM) or vehicle (V) began 2 weeks after Met-1 cell injection and 3 weeks after MCNeuA cell injection (arrows). Tumour volume was measured during the 2 weeks of treatment with NVP-BKM120 or vehicle. (b, d): Tumour weight was measured at necropsy. All data are expressed as mean $\pm$ SEM. \*P value <0.05 between WT and MKR groups. \*\*P<0.05 between MKR NVP-BKM120 and MKR vehicle groups. #P<0.05 between the MKR vehicle group and the WT vehicle group. ##P<0.05 between the WT NVP-BKM120 and WT vehicle-treated groups. n=8–9 mice per group. Reproduced with permission from Gallagher EJ et al. *Oncogene* 2012;31:3213-3222 (53).

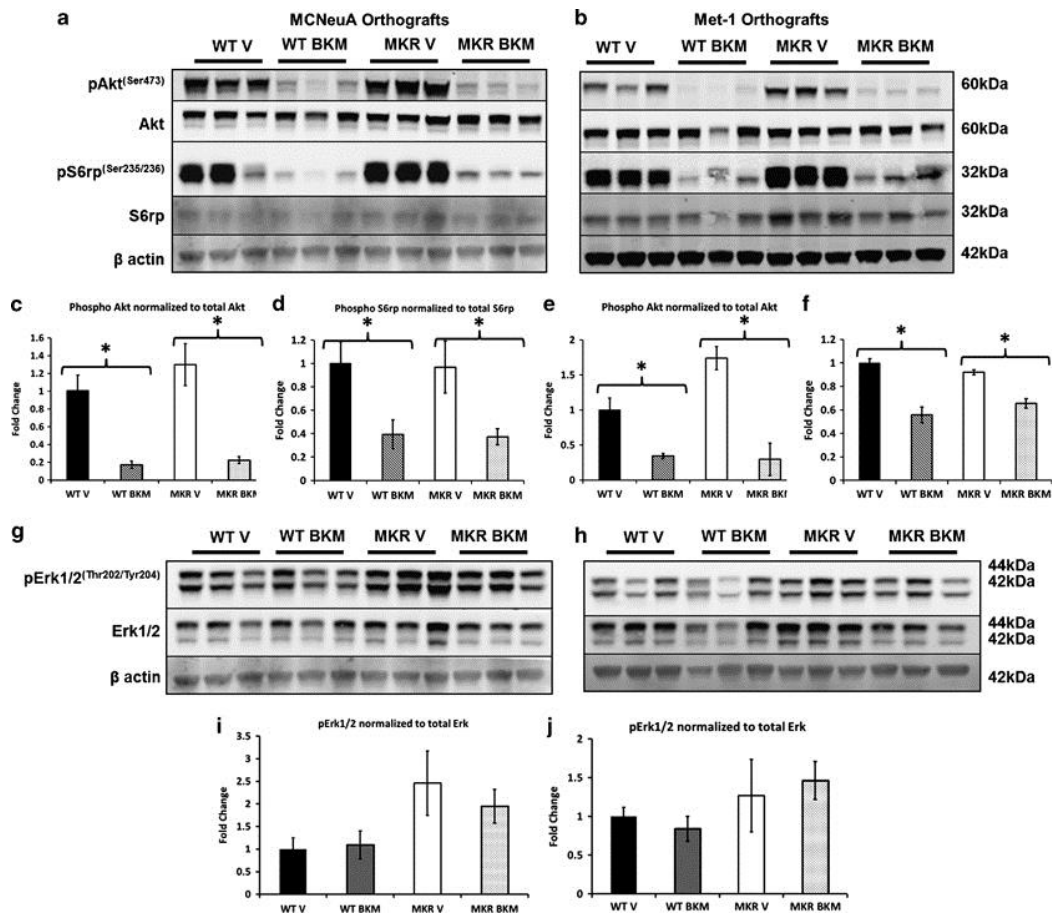


**Figure 10 BKM120 Inhibited Akt phosphorylation in the tumours of the MKR mice**

Treatment with NVP-BKM120 reduced phosphorylation of Akt and S6 ribosomal protein (S6rp) in MCNeuA and Met-1 tumours. Protein extracts from MCNeuA and Met-1 tumours from WT and MKR mice were immunoblotted against phospho(Ser473) and total Akt, phospho(Ser235/236) and total S6rp, and phospho(Thr202/Tyr204) and total Erk1/2 (a, b, g, h). Representative western blots are displayed for MCNeuA tumours (a, g) and Met-1 tumours (b, h). c–f, i, j Densitometric analyses of phosphorylated Akt normalised to total Akt, phosphorylated S6rp normalised to total S6rp levels and phosphorylated Erk1/2 normalised to total Erk1/2 for MCNeuA and Met-1 tumours. Data in (c–f, i, j) are presented as a fold change in the mean ( $\pm$ SEM) of each group compared with the WT vehicle-treated group. \* $P < 0.05$  between groups. BKM, NVP-BKM120 treated; V, vehicle treated. Reproduced with permission from Gallagher EJ et al. *Oncogene* 2012;31:3213–3222 (53).

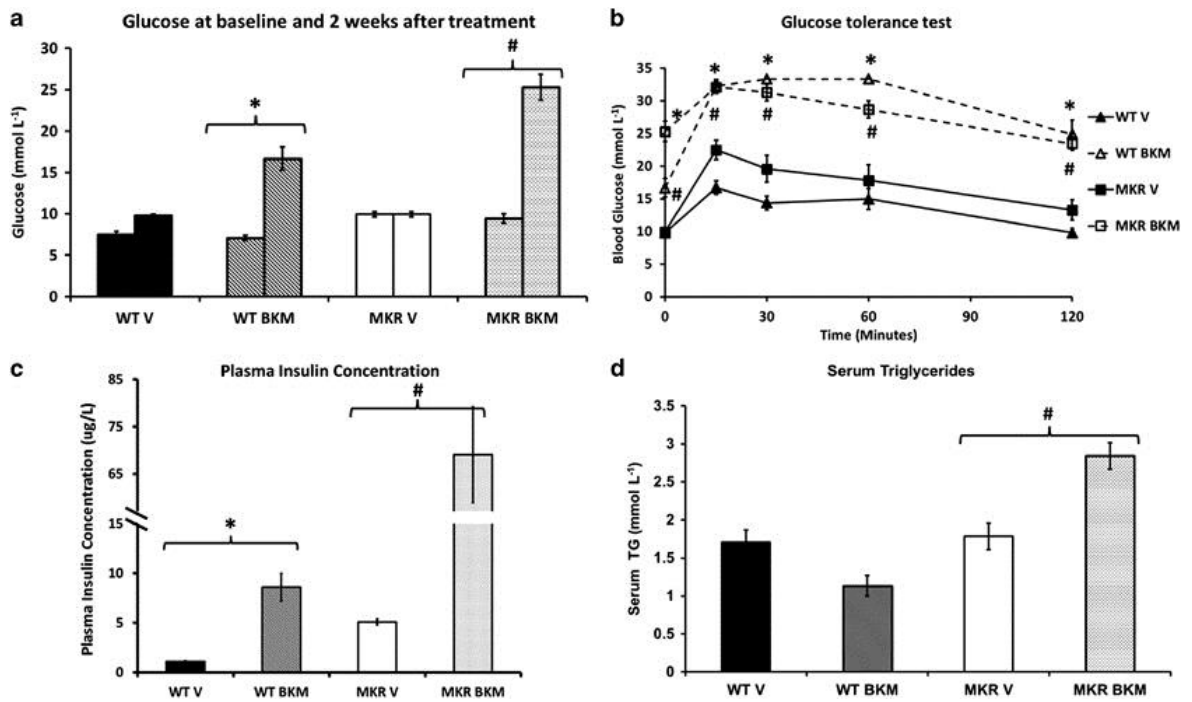


**Figure 11 The Effects of PI3K Inhibition on Metabolic Parameters in the MKR mice**

NVP-BKM120 treatment led to hyperglycaemia, hypertriglyceridaemia and exacerbated hyperinsulinaemia in MKR mice. (a) Mean random glucose levels at the start of treatment with NVP-BKM120 or vehicle and after 2 weeks of treatment. (b) Results of the 1.5 g/kg glucose tolerance test. Glucose was injected at time 0 and glucose measurements were taken at 0, 15, 30, 60 and 120 min. (c) Plasma insulin concentrations of the WT and MKR mice after 2 weeks of treatment with NVP-BKM120 or vehicle. The y-axis is broken at the parallel lines to aid visualization of the groups. (d) Serum triglyceride concentration in WT and MKR mice after 2 weeks of treatment with NVP-BKM120 or vehicle. All data are presented as the mean $\pm$ SEM., \* $P$ <0.05 between the WT NVP-BKM120 treated mice and WT vehicle group. # $P$ <0.05 between MKR NVP-BKM120-treated mice and MKR vehicle-treated group. BKM, NVP-BKM120 treated; TG, serum triglyceride; V, vehicle treated. Reproduced with permission from Gallagher EJ et al. *Oncogene* 2012;31:3213-3222 (53).

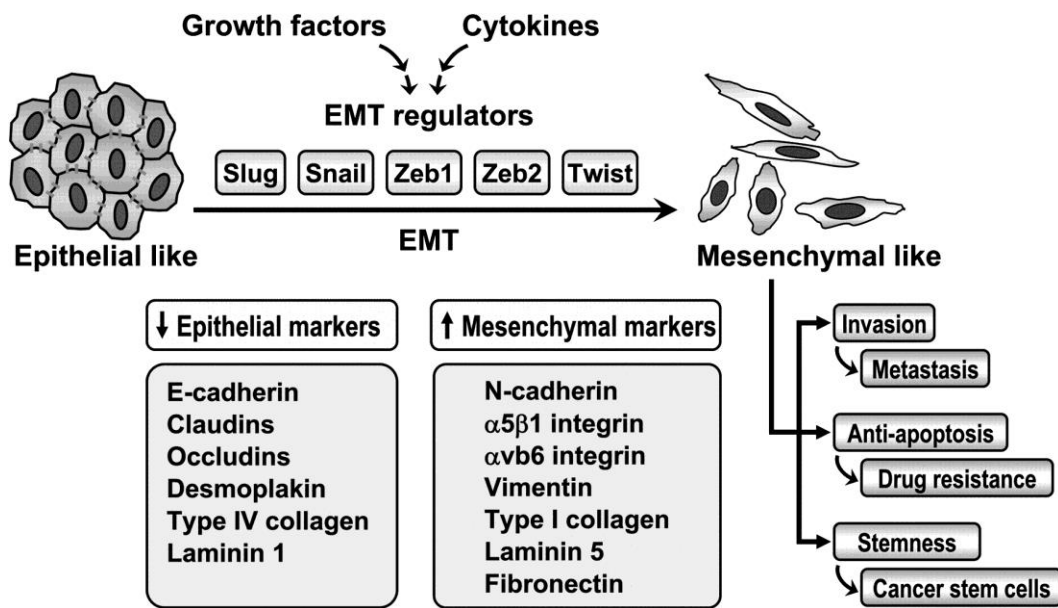


**Figure 12 Epithelial to Mesenchymal Transition**

EMT involves the change of polarised epithelial cells into mobile mesenchymal cells. On the left is a list of the markers expressed by epithelial cells, and on the right are proteins commonly studied for their expression by mesenchymal cells.

### Controversies Regarding Insulin Analogues and Breast Cancer

All individuals with Type 1 diabetes, and many individuals with Type 2 diabetes require exogenous insulin therapy to prevent and treat hyperglycaemia. The advent of recombinant DNA technology allowed for the production of recombinant human insulin, which largely replaced porcine and beef insulin in clinical use in the 1980's (54). A number of insulin analogues were developed to create a more physiological meal-related insulin profile and to reduce hypoglycaemia (43, 80). In broad terms these insulin analogues fall into two categories, those with a more rapid onset of action and peak effect than human insulin, and those with a longer duration of action. A number of such analogues are in clinical use today (Figure 13). One such analogue that is not in clinical use is known as AspB10, as it has an amino acid substitution of aspartic acid in place of histidine at position 10 on the B chain of insulin. This insulin analogue was found to induce spontaneous mammary tumours in rats, and has subsequently been shown to be mitogenic in human breast cancer cells in vitro (110).

		AA Number	1	2	3	4	5	6	7	8	9	10	11	12	13	14	15	16	17	18	19	20	21	22	23	24	25	26	27	28	29	30	31	32
Human Insulin	A Chain		G	I	V	E	Q	C	C	T	S	I	C	S	L	Y	Q	L	E	N	Y	C	N											
	B Chain		F	V	N	Q	H	L	C	G	S	H	L	V	E	A	L	Y	L	V	C	G	E	R	G	F	F	Y	T	P	K	T		
Insulin Glargine	A Chain		G	I	V	E	Q	C	C	T	S	I	C	S	L	Y	Q	L	E	N	Y	C	G											
	B Chain		F	V	N	Q	H	L	C	G	S	H	L	V	E	A	L	Y	L	V	C	G	E	R	G	F	F	Y	T	P	K	T	R	R
M1	A Chain		G	I	V	E	Q	C	C	T	S	I	C	S	L	Y	Q	L	E	N	Y	C	G											
	B Chain		F	V	N	Q	H	L	C	G	S	H	L	V	E	A	L	Y	L	V	C	G	E	R	G	F	F	Y	T	P	K	T		
A21Gly,DiD-Arg	A Chain		G	I	V	E	Q	C	C	T	S	I	C	S	L	Y	Q	L	E	N	Y	C	G											
	B Chain		F	V	N	Q	H	L	C	G	S	H	L	V	E	A	L	Y	L	V	C	G	E	R	G	F	F	Y	T	P	K	T	R	R
AspB10	A Chain		G	I	V	E	Q	C	C	T	S	I	C	S	L	Y	Q	L	E	N	Y	C	N											
	B Chain		F	V	N	Q	H	L	C	G	S	D	L	V	E	A	L	Y	L	V	C	G	E	R	G	F	F	Y	T	P	K	T		
Insulin Degludec	A Chain		G	I	V	E	Q	C	C	T	S	I	C	S	L	Y	Q	L	E	N	Y	C	N											
	B Chain		F	V	N	Q	H	L	C	G	S	H	L	V	E	A	L	Y	L	V	C	G	E	R	G	F	F	Y	T	P	K <sup>+</sup>			
Insulin Detemir	A Chain		G	I	V	E	Q	C	C	T	S	I	C	S	L	Y	Q	L	E	N	Y	C	N											
	B Chain		F	V	N	Q	H	L	C	G	S	H	L	V	E	A	L	Y	L	V	C	G	E	R	G	F	F	Y	T	P	K <sup>+</sup>			

**Figure 13 Amino Acid Sequences of Human Insulin and Insulin Analogues**

The amino acid sequences of human insulin and the analogues used in this study. Mature human insulin is comprised of an A chain with 21 amino acids, and a B chain with 30 amino acids. The modification to each amino acid in the respective analogue that is different from human insulin is highlighted by a box around the altered, removed or added amino acid. K<sup>+</sup> at position 29 on the B chain of insulin degludec and insulin detemir indicate the addition of a fatty acid to the lysine. In the case of insulin degludec it is a hexadecanedioic acid. For insulin detemir, it is a tetradecanoic acid. In vivo insulin glargine is metabolised by carboxypeptidases that remove one of the C-terminal arginines on the B chain, yielding the M1 metabolite. The insulin analogue A21Gly,DiD-Arg has the same amino acid sequence as insulin glargine. The C-terminal arginines are italicised to distinguish that they are D-isomers, rather than L-isomers or arginine, as in insulin glargine. It is not metabolised by carboxypeptidases in vivo.



Human registry studies and retrospective cohort studies published in 2011-2012 reported that other insulin analogues may increase the risk of certain cancers, including breast cancer (67, 127, 139). However, a number of methodological flaws have been found in these studies (125). A follow up publication to one of the studies that initially reported an increased risk of cancer with insulin glargine use during the three year follow up study found that in the four year follow up study no increase in breast cancer was found with subsequent follow up (97). Furthermore, in the only prospective study to date of insulin glargine, no increase in the risk of developing cancer was found in those being treated with insulin glargine compared to the standard treatment group (22). These studies raised an important question: why is AspB10 more mitogenic than human insulin, while other insulin analogues are not?

New insulin analogues are currently in development, and understanding the mitogenic activity of AspB10 is important so that other analogues that come into clinical use do not have this effect. In this thesis, I undertook to determine whether high doses of insulin analogues would increase tumour growth in the MKR mouse model.

### **Insulin Resistance, Hyperinsulinaemia and Racial Disparities in Breast Cancer Mortality**

Although breast cancer mortality has been declining overall, there is an increasing disparity in the mortality between Black and White women (73). A number of biologic and socio-economic factors may contribute to greater mortality in Black women with breast cancer (Figure 14) (18). Mortality in breast cancer is primarily predicted by the characteristics of the cancer, including stage at presentation, and histological findings including ER and progesterone receptor (PR) and HER2 status (40, 41). Patient characteristics including advanced age at the time of diagnosis, overweight or obesity and the presence of co-morbidities, including diabetes, also impact survival (12, 26, 28, 122). Traditional breast cancer risk factors as well as access to breast cancer screening and treatment contribute to some of the survival disparities, but do not provide a complete explanation (75, 86). Compared to White women with breast cancer, Black women are more likely to have tumour characteristics associated with poor prognosis (as summarised in Figure 14), including more advanced stage at presentation and ER and PR

negative cancers (75). In addition, there are greater rates of obesity and Type 2 diabetes in the Black population, compared with the White population (95).

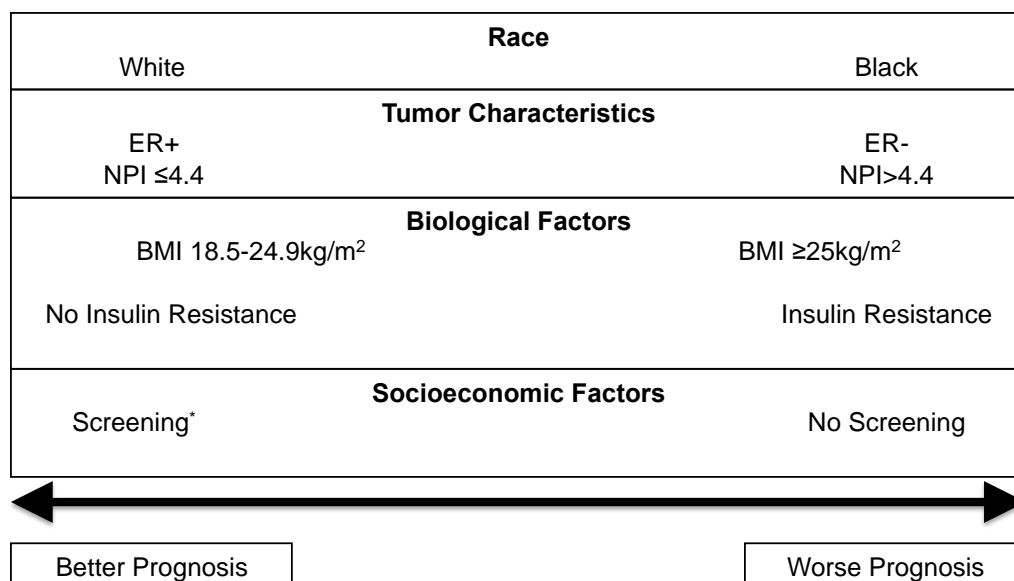


**Figure 14 Clinical and Biological Factors Potentially Contributing to the Racial Disparities in Breast Cancer Prognosis in Black and White Women.**

The Healthy Eating And Lifestyle (HEAL) study found that Black women with breast cancer had higher insulin resistance scores than White women when measured by the HOMA-IR (76). The prevalence of insulin resistance and endogenous hyperinsulinaemia is greater in Black than White women; however the studies examining circulating insulin levels and breast cancer incidence and recurrence have largely been performed in White populations. Increased IR expression in pathological breast cancer tissues and increased phosphorylation of the IR/ IGF-1R has been associated with a worse prognosis in some studies (90). Certain breast cancer cell lines derived from Black women express higher levels of the IR (3), but it is unknown whether there is higher IR expression in pathological specimens from Black women compared to White women. Therefore, it is important to understand whether endogenous hyperinsulinaemia and IR signaling are key factors contributing to the racial disparity in breast cancer mortality between Black and White women. If insulin resistance and hyperinsulinaemia are important factors, then strategies to improve the metabolic health of these women

and reduce endogenous hyperinsulinaemia or the use of adjuvant therapies to target hyperinsulinaemia and the IR signaling pathway may improve survival.

## **Hypothesis**

We hypothesize that endogenous hyperinsulinaemia promotes breast cancer growth and metastases by acting directly on the insulin receptor on the tumour cell, and by causing epithelial to mesenchymal transition in the tumour.

## **Aims**

1. To determine if hyperinsulinaemia promotes the growth and metastasis of a transgenic HER2 model of breast cancer
2. To explore if hyperinsulinaemia increases the metastases of human triple negative breast cancer xenografts.
3. To detect downstream changes associated with epithelial to mesenchymal transition, caused by hyperinsulinaemia, and establish their importance in cancer metastasis.
4. To examine the importance of the IR in mediating the effects of hyperinsulinaemia on the murine mammary gland and human breast cancer.
5. To understand if insulin analogues in clinical use increase breast cancer growth.
6. To determine if insulin resistance, endogenous hyperinsulinemia and IR signaling play a role in the breast cancer survival disparities between Black and White women.

## 2. Materials and Methods

### Cell Culture

The mouse MVT1 cells were a donation from K. Hunter at the Center for Cancer Research in the National Institute of Health. The MVT1 cells were derived from MMTV c-Myc/Vegf transgenic female mice (123). Met1 murine mammary tumour cells were derived from MMTV-Polyoma virus middle T antigen (PyVmT) transgenic mice (23). The human MDA-MB-231 cells were purchased from the American Type Culture Collection (ATCC, Manassas, VA). The human MDA-MB-468 cells were a donation from Dr. Ramon Parsons at the Department of Oncology at the Icahn School of Medicine at Mount Sinai (New York, NY). The LCC6 parental, LCC6 noncoding control and LCC6 insulin receptor knockdown (IRKD) cells were a donation from Dr. Douglas Yee at Department of Medicine at the University of Minnesota (Minneapolis, MN). Met1, MVT1, MDA-MB-231, LCC6 and MDA-MB-468 cells were grown in Dulbecco's Modified Eagles Medium (DMEM) supplemented with 10% Foetal Bovine Serum (FBS) (Invitrogen Life Technologies, Grand Island, NY), 100 U/ml penicillin and 100µg/ml streptomycin (Mediatech, Manassas, VA). MCF-7 human mammary carcinoma cell lines were obtained from ATCC (Rockville, MD, USA) and were cultured in Improved Minimal Essential Medium (IMEM) supplemented with 10% FBS, 100 units/mL penicillin and 100 µg/ml streptomycin (1% penicillin / streptomycin). All cells were grown at 37C in 5% CO<sub>2</sub> atmosphere. All cell culture work was performed using Biosafety Level 2 (BSL2) protocols, as approved by Mount Sinai Environmental Health and Safety.

### Lentiviral-mediated shRNA Gene Silencing

Vectors (GIPZ) encoding the following microRNA-adapted short hairpin RNAs (shRNA) 5'-TGAAGTGTGAAATCTTCGGC-3' (human IGF-1R), 5'-CTTACCAAGGCCTGTCTAA-3' (human IR) packed in high titer lentiviral particles were purchased from Open Biosystems (Huntsville, AL, USA). These vectors or a vector containing a noncoding shRNA sequence (control shRNA; Open Biosystems) were transfected in the presence of 8mg/ml polybrene (Sigma-Aldrich, Rehovot, Israel) into MCF7 cells. All 3 vectors contained a GFP marker and puromycin resistance gene.

Glycerol stocks of lentiviral shRNA targeting vimentin were obtained from Sigma-Aldrich (St. Louis, MO). A non-coding shRNA was 5'-

CAACAAGATGAAGAGCACCAA-3'. The sequence of the vimentin RNA of clone TRC 317673 was 5'-GCTTCAAGACTCGGTGGACTT-3', and of vimentin RNA of clone TRC 317676 was 5'- GCGCAAGATAGATTGGAATA-3'. The shRNA of the vimentin targets and the non-coding control were struck out onto lysogeny broth (LB) agar plates with 100µg/ml carbenicillin. Colonies were picked and inoculated in 5mL LB and carbenicillin medium. 3.5mL of the culture was used with the QIAprep Spin Miniprep kit (Qiagen, Valencia, CA) to obtain plasmid DNA following the manufacturer's protocol. After the DNA concentration of the plasmid DNA was measured using spectrophotometry (NanoDrop ND-1000 Spectrophotometer, Thermo Scientific; Wilmington), 500ng-1µg of the sample was used with EcoRI and NcoI restriction enzymes to verify the correct fragment sizes of the plasmid DNA by separation on a 0.8% agarose gel. Once the insert was confirmed to contain the correct plasmid DNA, the 1mL culture was used to obtain a larger quantity of the plasmid DNA by overnight culture in LB and carbenicillin medium, and DNA isolation using the Qiagen Plasmid Maxi Kit (Qiagen, Valencia, CA) following the manufacturer's protocol. HEK293FT cells were transfected with 20µg of lentiviral DNA and 10µg of each helper plasmid (gag/pol and env). The virus was concentrated by centrifugation and the target cells were infected in duplicate with lentiviral non-coding control or vimentin shRNA lentivirus.

To generate the GFP expressing cell line, a construct containing GFP (NV-SV-40-puro-linker-Ins-PGK-eGFP) was received as a gift from Dr. Neufeld, Technion, Haifa, Israel. The plasmid DNA was transfected into the Lentiviral packaging cell line HEK293FT together with ViraPower packaging mix (Invitrogen, Carlsbad, CA) by using the Lipofectamine 2000 reagent (Invitrogen, Carlsbad, CA). The virus was concentrated and the target MVT1 cells were infected.

Stable selection of cells was obtained by puromycin selection. After the infection, 2 weeks of 2.5µg/ml puromycin (Sigma-Aldrich, St. Louis, MO) was used for selection and to ensure stable knockdown of the target gene. Successful gene and protein knockdown was confirmed by Real Time qPCR and Western Blot analysis. After 2 weeks cells were maintained in DMEM with 10% FBS, 1% penicillin/streptomycin with 1µg/ml puromycin.

## Cell Stimulations

Prior to stimulation, cells were grown in full medium to 70-80% confluency, then serum-starved overnight in media (DMEM or IMEM) supplemented with 0.1% Bovine Serum Albumin (BSA) (Sigma Aldrich, St Louis, MO, USA) and 1% penicillin / streptomycin. Cells were stimulated with vehicle (PBS+0.1% BSA), 10nM of insulin (Humulin R, Lilly, Indianapolis, IN, USA), or one of the insulin analogues, as described below in the “Insulin Analogues” section of the Materials and Methods.

## Cell Proliferation

Cell proliferation was performed using two methods. As indicated, for some studies, the Cell Counting Kit-8 (CCK-8) was used (Dojindo Molecular Technologies Inc, Rockville, MD). A cell number to absorbance curve was generated per the manufacturer’s protocol, by plating cells in triplicates in serial dilutions from 125,000 to 1953 cells. Where no difference was found in the absorbance between cell lines, this method was used for cell proliferation assays. 5,000 cells were plated in 96-well plates in phenol free DMEM with 10% FBS, 100 U/ml penicillin and 100µg/ml streptomycin. The cells analyzed for cell proliferation at 24, 48, and 72h, taking the absorbance readings 3 hours after the addition of CCK-8 reagent.

As CCK-8 measures cell proliferation by measuring NADH production, certain cell lines had significant differences in CCK-8 readings for the same cell number. For cell lines that had significant differences in absorbance or in those stimulated with insulin analogues, cells were seeded in 24-well plates and grown in standard growth medium overnight and then changed to DMEM with 1% FBS, 1% penicillin/streptomycin. Cells were stimulated as indicated in the experimental results. After 72 hours, cells were then trypsinised, diluted in trypan blue (1:1) and counted using a hemocytometer, or with the BioRad TC20 cell counter.

## Cell Migration and Invasion

For the migration assay, transwell permeable inserts with 8µm sized-pores were used (Corning Inc., Corning, NY). 500µL of DMEM supplemented with 10% FBS, 1% penicillin/streptomycin was added to the lower chamber. 150,000 MVT1 cells were seeded in 300µl of DMEM with 10% FBS, 1% penicillin/streptomycin in the

insert. For the invasion assay, 24 well Corning BioCoat Tumour Invasion System with 8µm pore inserts was used. Similar to the migration assay, 500µL of DMEM with 10% FBS or when appropriate 0.1% BSA (with or without 10nM insulin) was added to the lower chamber. The insert was seeded with 400,000 cells in 300µl of DMEM with 10% FBS or in serum free medium with 0.1% BSA and 1% penicillin / streptomycin. For the insulin stimulation studies, the standard DMEM was exchanged for serum-free DMEM contained 0.1% BSA, 1% penicillin / streptomycin. 400,000 cells treated with 10nM insulin diluted in PBS with 0.1% BSA or vehicle. For both assays cells were allowed to invade for 24 hours. For the migration and invasion assays, the number of cells migrated and invaded was analyzed as previously described (105), with the modification of measuring the absorbance of the eluted crystal violet dye at 595nm on a plate spectrophotometer. For both the migration and invasion assays, cell number was extrapolated by performing serial dilutions from 64,000 to 250 cells in a 96-well plate following previously described methods (105). The absorbance versus cell number standard curve was generated to calculate the number of invaded cells.

## **Animal Studies**

### **Animal Care and Housing**

All animal study protocols were approved by the Mount Sinai School of Medicine Institutional Animal Care and Use Committee (IACUC). Mice were housed in The Icahn School of Medicine at Mount Sinai Center for Comparative Medicine and Surgery, Association for Assessment and Accreditation of Laboratory Animal Care International and Office of Laboratory Animal Welfare (OLAW) accredited facility, where animal care and maintenance were provided. Mice were kept on a 12-h light/dark cycle, had free access to standard mouse chow (Picolab rodent diet #5053; LabDiet, St. Louis, MO, USA) and fresh water. Immunodeficient Rag1<sup>-/-</sup> and Rag1<sup>-/-</sup>/MKR mice were maintained on trimethoprim / sulfamethoxazole impregnated regular lab diet from LabDiets.

### ***Genetically Engineered Mouse Models***

All mice used for tumour studies were female, on the Friend Virus B/National Institutes of Health (FVB/N) background and were 8-12 weeks old when studies began.

## MKR Mouse Model

We used a previously described mouse model of insulin resistance for these studies, the MKR mouse (Figure 8). The generation and characteristics of the MKR mouse have been previously described in detail (45, 115). Briefly, the muscle (M)-IGF-1R-lysine (K)-arginine (R) mice (MKR) transgenically express a human dominant negative (dn)IGF-1R with a lysine to arginine point mutation in the ATP binding site in the tyrosine kinase domain (45). The dnIGF-1R is expressed in skeletal muscle under the muscle creatine kinase (MCK) promoter. The dnIGF-1R forms hybrids with the IR, leading to skeletal muscle insulin resistance, with subsequent whole body insulin resistance, as described in the Introduction Section of this thesis, and illustrated in Figure 8 (45). Homozygous female MKR mice are insulin resistant and hyperinsulinaemic (46, 115). Mouse genotype was confirmed as described below.

## Neu-NT Mouse Model

The Neu-NT mice were a gift from Dr. Louis Chodosh, Perelman School of Medicine, University of Pennsylvania (111). The generation of the NeuNT mice has been previously described (111). The NeuNT is constitutively active due to a point mutation in the transmembrane domain of the Neu receptor (rodent ortholog of HER2). These mice express constitutively active Neu (NeuNT) under the control of a tetracycline and were generated by cloning the NeuNT coding sequence downstream of the minimal tet operator (TetO) to generate TetO Activated Neu (TAN) mice. The TAN mice were crossed with mice carrying the mouse mammary tumour virus-long terminal repeat (MMTV-LTR) to drive expression of the reverse tetracycline-dependent transactivator (rtTA) to generate MTB/TAN mice (111). We then generated the hyperinsulinaemic MKR/MMTV-rtTA/TetO-NeuNT (MTB/TAN/MKR) mice by crossing the MMTV-rtTA/TetO-NeuNT (MTB/TAN) mice with MKR mice to generate MTB/TAN/MKR mice, and control MTB/TAN mice (Figure 15).



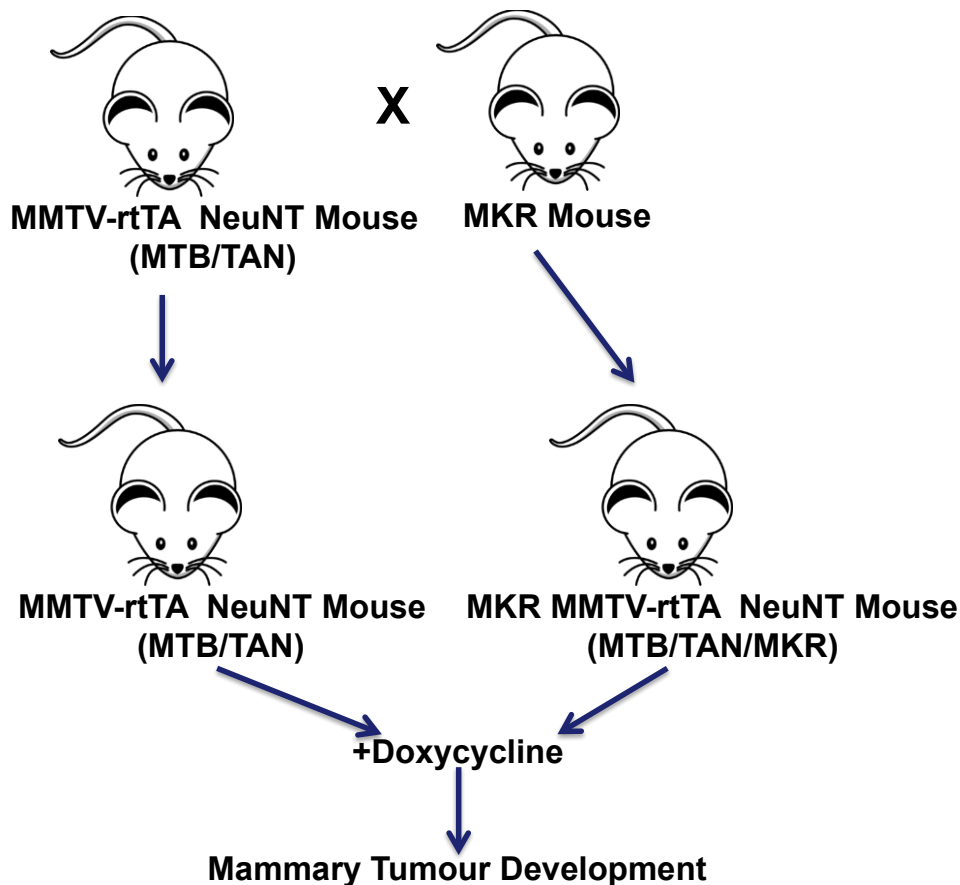


**Figure 15 Generation of the Hyperinsulinaemic Transgenic Inducible Activated Neu Mouse Model of Breast Cancer**

Illustration of the generation of the MKR MMTV-rtTA (MTB) Tetracycline operator (TetO) activated Neu (NeuNT) (TAN) mice. Tumours were generated by treating the mice with doxycycline in their drinking water from 8 weeks of age.

#### Immunodeficient Rag1<sup>-/-</sup> Mouse Model

The V(D)J recombination activation gene 1 (Rag1) knockout (Rag1<sup>-/-</sup>) mice on an Friend Virus B (FVB) background were a gift from Dr. Lisa Coussens, Oregon Health and Science University, Portland, Oregon. Rag1<sup>-/-</sup> mice lack mature T and B lymphocytes and were used to study the role of hyperinsulinaemia in the growth and metastasis of tumours derived from human breast cancer cell lines. The Rag1<sup>-/-</sup> mice were crossed with the MKR<sup>+/+</sup> mice to generate a homozygous line (Rag1<sup>-/-</sup> MKR<sup>+/+</sup>), Rag1<sup>-/-</sup> mice were used as controls (Figure 16).

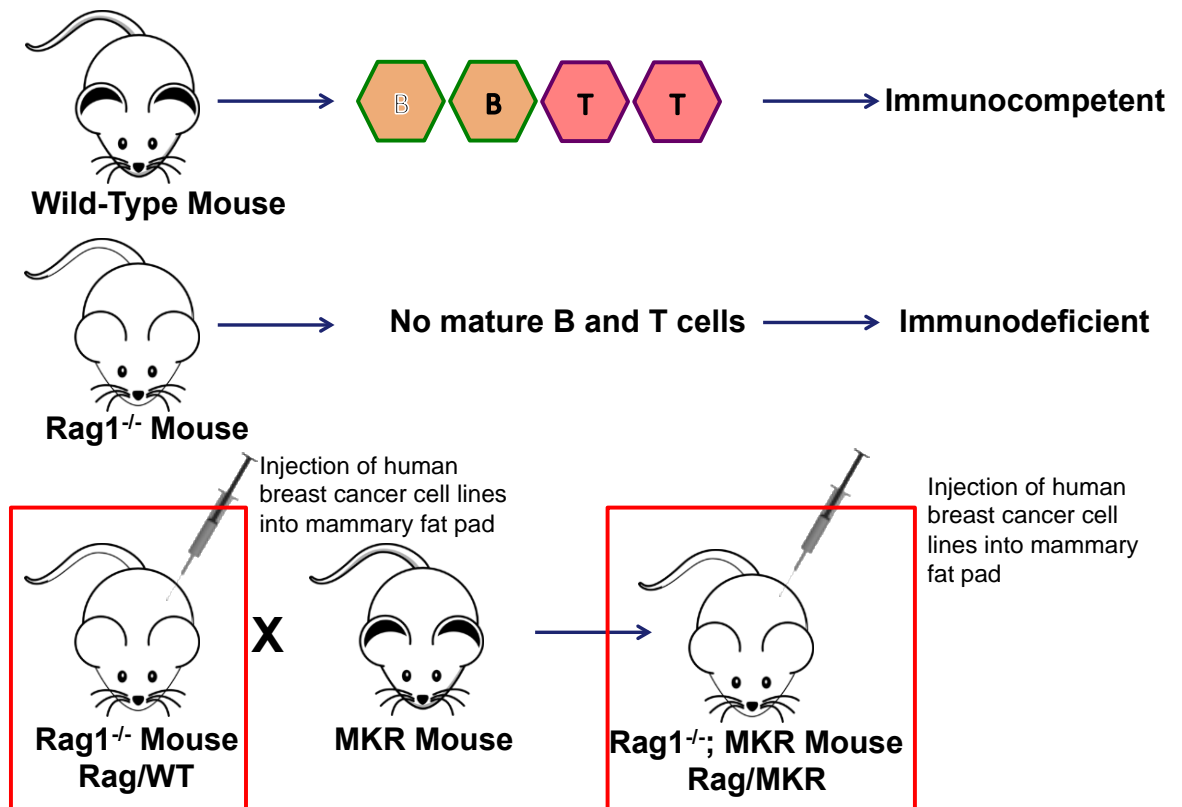


**Figure 16 Generation of Immunodeficient Hyperinsulinaemic mice**

The figure depicts the generation of the Rag1<sup>-/-</sup> / MKR<sup>+/+</sup> mice and the induction of tumour xenografts in these mice by injection of human breast cancer cells into the 4<sup>th</sup> mammary fat pad of the mice.

#### MMTV Cre Insulin Receptor floxed mice

The MMTV Cre Line A mice were obtained from Dr. Lothar Hennighausen and Dr. K.U. Wagner, NIH, Bethesda, MD (142). The IR floxed mice were obtained from Dr. Ronald Kahn, Joslin Diabetes Center, Boston, MA (24) and were backcrossed for 8 generations to an FVB/n background. After backcrossing the IR floxed (IRLL) mice, they were crossed with the MMTV-Cre Line A (MMTV-Cre) and MKR mice. As described by K.U Wagner, a breeding strategy was employed as shown in Figure 17A to maintain the line, and as shown in Figure 17B to produce mice with the IR deleted in the mammary epithelial cells. The primer design strategy for detecting the floxed alleles and recombined “null” allele are shown in Figure 17C.

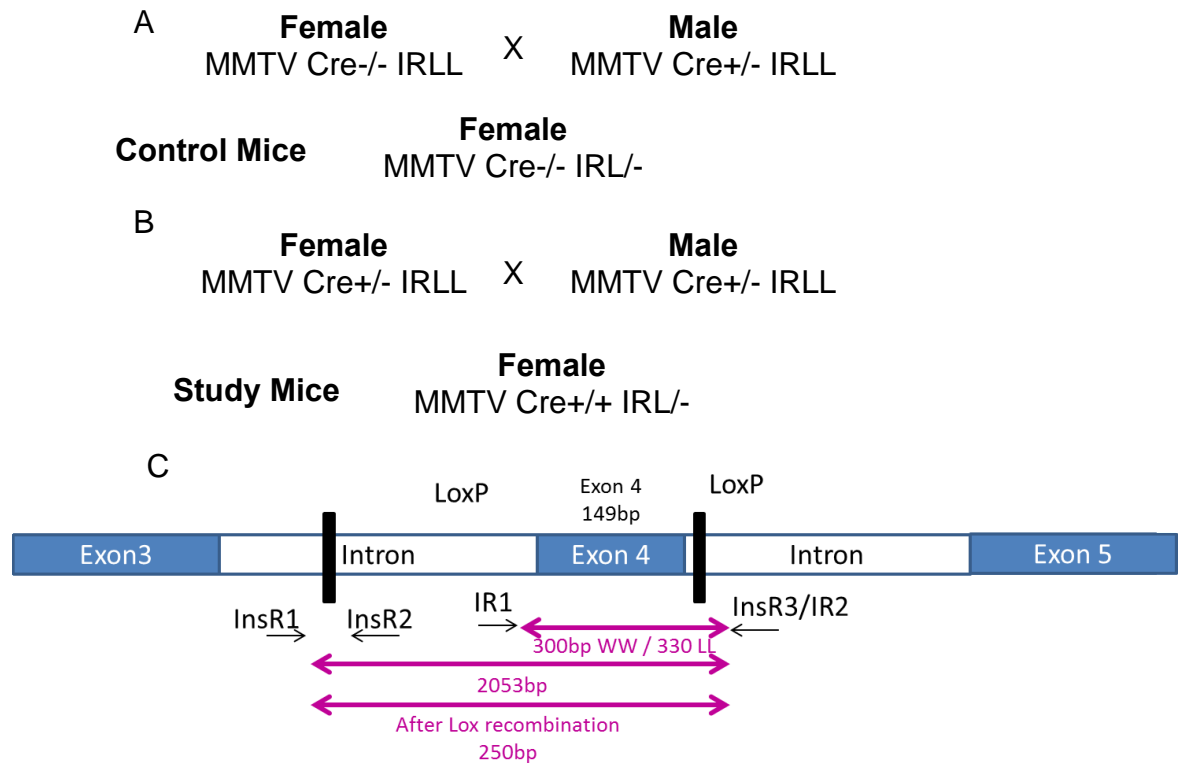


**Figure 17 Generation of the MMTV Cre IR floxed mice.**

K.U. Wagner and colleagues described that MMTV Cre leads to recombination of the gene of interest in the germline, of the female mice. As total body knockout of the IR is fatal to mice, in order to maintain the line and generate control mice MMTV Cre negative females were crossed with MMTV Cre<sup>+/-</sup> male mice (A). To generate study mice with loxP site recombination and excision of exon 4 of the IR, MMTV Cre<sup>+/-</sup> IRL<sup>L</sup> females were crossed with MMTV Cre<sup>+/-</sup> IRL<sup>L</sup> male mice (B). 50% of female pups would receive a recombined “null” allele from the mother, however this was not detected by usual genotyping with the IR1 / InsR3/IR2 genotyping primers, as shown in the schematic (C). Using the InsR1/IR2 primers we could detect the null allele in the female pups.

### Mouse Genotyping

At or before 3 weeks of age mouse genotype was analyzed by isolating DNA from a 3mm snip of tail. DNA was isolating by overnight digestion in Proteinase K at a concentration of 2mg/ml in 100mMTris-HCl, 5mM EdTA, 200mM Sodium Chloride with 0.2% SDS buffer (pH8.0) at 56C in a horizontal shaker. The digest was

centrifuged at 13000rpm for 15 minutes in a benchtop microcentrifuge, isopropanol was added at a 1:1 ratio to the supernatant, and DNA was precipitated by microcentrifugation for 5 minutes, and washed once with 70% ethanol, air-dried and resuspended in 100µl of molecular grade water for subsequent PCR.

The PCR primers for mouse genotype determination are shown in Table 1. The PCR products were run on 1-1.5% agarose gels with 10µg/µL ethidium bromide.

**Table 1 Primers for Mouse Genotype Determination**

	Forward Primer	Reverse Primer
NeuNT	TTTCCTGCAGCAGCCTACGC	CGGAACCCACATCAGGCC
rtTA	CGCTGTGGGGCATTCTTACTTTAG	CATGTCCAGATCGAAATCGTC
MKR	GTCTGAACCCGGTCTGCTCGC	CAGCAATCACCGTGCAGTT
RAG1	AGACACCAAGGCTTGCAACACAG	TGCCGAGAAAGTCCTTCTGCCAG GTGGAATGAGTGCGAGGCCAGA
Cre	AATGCTTCTGTCCGTTTGCCGGT	CAGGCTAAGTGCCTTCTCTACA
IR	IR1: TCTTTGCCTGTGCTCCACTCTCA  InsR1: CACACACACACGCCTACAC	IR2: CTGAATAGCTGAGACCACAG

### *In Vivo Tumour Studies*

#### MKR/MTB/TAN Model

For induction of *NeuNT*, mice were administered 1.5mg/ml doxycycline (Sigma-Aldrich, St Louis, MO, USA) in drinking water for the duration of the period of tumour growth from two weeks up to twelve weeks. Doxycycline water was changed twice per week. Mice were followed on a daily basis and body score conditions were recorded. To determine tumour mass, each animal was euthanised and mammary tumours from all thoracic and inguinal glands were carefully dissected and weighed.

## Orthotopic / Xenograft / Intravenous Tumour Models

When the mice were 8-12 weeks of age, 100,000 MVT1 or 250,000 Met1 cells resuspended in 100µL of sterile PBS were injected into the 4<sup>th</sup> mammary fat pad of mice anaesthetised with isoflurane. 1,000,000 MDA-MB-231 cells resuspended in 100µl of 1:1 sterile PBS and Matrigel (Trevigen, Gaithersburg, MD) or 5,000,000 LCC6 noncoding control or LCC6 insulin receptor knockdown cells resuspended in 100µl of DMEM were injected into the 4<sup>th</sup> mammary fat pad. To determine the effect of cell manipulations on pulmonary metastases independent of the primary tumour, we performed tail vein injections of 10,000 MVT1 cells that had lentiviral mediated transduction of vimentin shRNA or a noncoding control shRNA.

## Mouse Monitoring and Tumour Measurement

For all studies, body weight was monitored weekly, body condition was monitored twice weekly and tumour size was measured twice weekly with calipers. The formula used for the calculating tumour volume was:  $Vol = 4/3 \times \pi \times (length/2 \times width/2 \times depth/2)$ . For intravenous tumour studies, the mice were monitored for signs of loss of body condition or body weight. All mice were euthanised as soon as body weights reduced by 10% of baseline.

## Pulmonary Metastases

In order to analyze the pulmonary metastasis, post mortem lungs were inflated with 10% formalin, removed and surface macrometastasis were counted.

## *Metabolic Studies*

Body weights were measured weekly during all studies. Body composition analysis was performed using the EchoMRI 3-in-1 NMR system (Echo Medical Systems, Houston, TX, USA), before tumour cell injection and at the end of treatment. Nonfasted blood glucose measurements were performed on tail vein blood during tumour studies using a Bayer Contour Glucometer (Bayer Healthcare, Mishawaka, IN, USA), prior to commencing treatment and weekly thereafter. Plasma insulin levels were measured at the end of the studies using the Sensitive Rat Insulin radioimmunoassay (RIA) kit (Millipore, St. Charles, MO, USA). Serum IGF-1 levels were measured by RIA (ALPCO, Salem, NH, USA). All radioimmunoassays were performed in compliance with the Radiation Safety Protocols at Mount Sinai.

For the insulin tolerance test (ITT), mice were fasted of food, but had free access to water for two hours prior to the test, blood glucose was measured from the tail vein using a Bayer Contour Glucometer (Bayer Healthcare, Mishawaka, IN, USA) at time 0, immediately before PBS, human insulin (Humulin R, Eli Lilly, Indianapolis, IN), or insulin analogue injection, and at the times indicated after injection, after which time the mice were refed.

WT FVB/n mice were injected with 1 unit / kg of human insulin, insulin glargine or A21Gly,DiD-Arg insulin by i.p. injection. MKR mice were injected with 1 unit / kg or 12.5 units / kg of each insulin analogue, as indicated in the Results section.

### *Insulin Analogues*

All insulin analogues were provided by Sanofi R&D Diabetes Division, Frankfurt am Main, Germany, except where indicated. Recombinant human insulin (Insuman Rapid), insulin degludec, insulin glargine and A21Gly,DiD-Arg insulin were produced by recombinant DNA techniques or enzymatic semi-synthesis, purified homogeneity and made available by Process Development Biotechnology (Sanofi, Frankfurt, Germany). Insulin detemir (Levemir) was produced by NovoNordisk A/S, Denmark, and obtained commercially. The details of the amino acid sequences of these insulin analogues compared to human insulin are shown in Figure 13. Insulin degludec was generated by the addition of a fatty acid (hexadecanedioic acid) by a  $\gamma$ -L-glutamic acid linker acylated to lysine at B29 of the truncated form of insulin, lacking the C-terminal threonine of the B chain (79). Insulin glargine has two arginine residues added to the C-terminal of the B chain and an amino acid substitution of glycine (instead of asparagine) at position 21 of the A chain (8). A21Gly-DiD-Arg insulin has the same amino acid sequence as insulin glargine but with D-arginine residues at B31 and B32 instead of L-arginine residues (147). Insulin detemir is also a truncated form of human insulin, lacking threonine at position 30 of the B chain, and with the addition of a tetradecanoic (myristic) acid, acylated to lysine at B29 (87). Prior to injection into the mice, insulin analogues were diluted in phosphate buffered saline (human insulin, AspB10, IGF-1, insulin degludec insulin detemir), or in a placebo solution containing water, glycerol and adjusted to pH4 with HCl and NaOH (insulin glargine, or A21Gly,DiD-Arg). For in vitro studies recombinant human insulin Humulin R (Lilly, Indianapolis, IN).

## Insulin Glargine and A21Gly-DiD-Arg Metabolite Measurements

Plasma was isolated from mice 60 minutes after insulin glargine, or A21Gly-DiD-Arg insulin injection. The plasma concentrations of insulin glargine and its M1 and M2 metabolites were determined by liquid chromatography-tandem mass spectrometry (LC/MS) using methods previously described (20).

## Histological Analysis

### *Mammary gland whole mount analysis*

Inguinal mammary glands were removed, placed on a glass slide and fixed for four hours in Carnoy's fixative (60% ethanol 30% chloroform and 10% glacial acetic acid). Glands were serially rehydrated in 100%, 95%, 70%, 50% and 30% ethanol for 15 minutes each, rinsed in water for 5 minutes and stained overnight with carmine alum stain. Glands were then serially dehydrated in 30%, 50%, 70%, 95%, and 100% ethanol for 15 minutes each and cleared overnight in xylenes. Glands were then covered by Mount-Quick mounting medium (Daido Sangyo, Japan), before a glass cover slip was placed on top. Photographs were carried out using a stereomicroscope (Zeiss, Thornwood, NY, USA) at 4X magnification. Quantification of the relative area of end buds was performed using Image J by measuring the mean end bud area of four random images at 4X objective taken from each whole mount.

### Immunofluorescence and Immunohistochemistry

For immunofluorescence studies, mammary tumours were cut in cross section at time of sacrifice, fixed in 10% formalin before being embedded in paraffin and sectioned at the Mount Sinai Histology Shared Resource Facility, or the Columbia University Diabetes Education and Research Center histology core facility. Sections were deparaffinised with xylenes and rehydrated through serial ethanol washes. Tissues were subjected to antigen retrieval by heating in a microwave for 20 minutes in sodium citrate buffer (pH 6.0). Tissues were then blocked with TGB superblock [10% BSA, 0.05% NaN<sub>3</sub>, 10% goat serum (Dako North America, Carpinteria, CA) and 0.5M Tris (pH 7.6)], incubated with primary antibody overnight at 4°C. Primary antibodies used for immunofluorescence were anti c-Myc antibody, anti- Vimentin antibody, anti-GFP antibody (Cell Signaling Cell Signaling Technologies, Danvers, MA, USA) and anti-Neu antibody (Abcam, Cambridge,

MA, USA. Secondary antibodies used were AlexaFluor568-conjugated goat anti-rabbit IgG and Alexa-Fluor488 conjugated goat anti-mouse IgG (Invitrogen, Molecular Probes, Eugene, OR, USA) at 1:500 dilution for 2 hours. Nuclei were counterstained with 0.2 µg/ml 4',6-diamidino-2-phenylindole (DAPI), (Sigma-Aldrich, St Louis, MO, USA). Sections were then mounted using Fluorogel mounting medium (Electron Microscopy Sciences, Hatfield, PA). Stained slides were photographed using the Olympus AX70 fluorescent microscope at 40X objective, and quantified using CellSens software (Olympus).

For immunocytochemistry, 5000 cells were seeded in usual medium as described above on sterilised glass coverslips in a 24 well plate for 24 hours. They were then serum starved in DMEM with 0.1% BSA overnight and stimulated with 10nM insulin for 1 hour. After stimulation, cells were washed with PBS, fixed in 4% paraformaldehyde and blocked with TBG superbloc, incubated with primary and secondary antibodies as above, and nuclei were counterstained with DAPI as above. Coverslips were mounted on slides using Fluorogel and imaged as above.

For immunohistochemistry (IHC) staining, slides were processed and subjected to antigen retrieval, as described in the immunofluorescence protocol. Slides were stained using the ABC Elite Universal Kit and protocol (Vector Labs, Burlingame, CA). After antigen retrieval, slides were blocked for an hour in dilute horse serum, and the incubated overnight with anti-IRβ antibody at 4C. Slides were then washed, and incubated with secondary antibody, avidin-biotin complex (ABC) reagent and stained with 3,3'-diaminobenzidine (DAB), counterstained with haematoxylin, and dehydrated through increasing concentrations of ethanol. Slides were then washed with xylenes and mounted with Eukitt Mounting Medium (EMS, Hatfield, PA). Stained slides were photographed by brightfield microscopy using the Olympus AX70 microscope.

### **Mammary Epithelial Cell Isolation**

At 12 weeks of age, MMTV Cre+/- IRL/- and MMTV Cre-/- IRL mice were anaesthetised with isoflurane, and after careful removal of the lymph nodes, the mammary glands were removed, minced and digested in collagenase solution (300U/ml) for 2-4 hours until glands were visibly digested, and the epithelial cells were separated by differential centrifugation and washed with PBS (115, 156). Protein and DNA were isolated from the fresh cell pellets.



## Protein Isolation and Analysis

### Protein Extraction from cells

After stimulation, medium was removed from the plates, the cells were washed with ice-cold PBS, and cells were subsequently lysed in freshly-made lysis buffer (pH 7.4; 50 mM Tris, 150 mM NaCl, 1 mM EDTA, 1.25% CHAPS [3-[(3-cholamidopropyl) dimethylammonium-1-propanesulfonate](Roche, Indianapolis, IN, USA), supplemented with phosphatase inhibitors 2mM sodium fluoride, 1 mM sodium orthovanadate, 10 mM sodium pyrophosphate, 8 mM  $\beta$ -glycerophosphate and Complete EDTA-free Protease Inhibitor Cocktail (Roche, Indianapolis, IN, USA).

### Protein Extraction from Tumours

At the time of sacrifice of the mice, the tumours were flash frozen in liquid nitrogen. Protein was isolated from the tumours by lysis in freshly made lysis buffer, as described above. Tumour tissue was placed in 1ml of ice cold lysis buffer, and homogenized on ice.

The protein concentration of the cells and tumours was measured using the BCA protein assay kit (Thermo Scientific, Rockford, IL).

### SDS Page and Western Blotting

20-25 $\mu$ g of protein was prepared for SDS-PAGE in SDS loading buffer and dithiothreitol (DTT) (Cell Signaling Technologies, Danvers, MA, USA) and boiled for 5 minutes. Samples were then run on 8% or 8-12% Tris-Glycine gels, (Invitrogen, Carlsbad, CA, USA) and then transferred to a nitrocellulose membrane (Bio-Rad, Hercules, CA, USA) at 100V for one hour on ice. Membranes were blocked in 5% nonfat milk or LICOR blocking buffer (LICOR Biosciences, Lincoln, NE, USA), incubated overnight with primary antibodies for anti-phospho IGF-1R- $\beta^{(Tyr1135/1136)}$ /IR- $\beta^{(Tyr1150/1151)}$ , anti-total IGF-1R- $\beta$ , anti-cMyc, anti-phospho AKT<sup>(Ser473)</sup>, anti-total Akt at manufacturers recommended dilutions (Cell Signaling Technology, Danvers, MA, USA), anti-total IR- $\beta$  at 1:200 dilution (Santa Cruz Biotechnology, Santa Cruz, CA, USA), anti- $\beta$ -actin (Sigma Aldrich, St Louis, MO, USA) and then with Odyssey anti-mouse or anti-rabbit secondary antibodies (LICOR Biosciences, Lincoln, NE, USA), before exposure and detection with the LI-COR Biosciences infrared detection system. The western bands were quantified

using open source Image J software (National Institutes of Health, Bethesda, MD) or Licor Image Studio Software.

### Immunoprecipitation and Proteomic Analysis

Immunoprecipitation of proteins was performed following the manufacturer's protocol using magnetic Dynabeads Protein G (Invitrogen Life Technologies, Grand Island, NY). The protocol was modified by utilizing 1000µg of protein lysate with 10µg of antibody incubated at 4°C overnight with rotation. The samples were incubated with the magnetic beads for 4 hours at 4°C with rotation and then washed with ice-cold tris buffer (pH 7.4). Then, the antigen was eluted in 3X loading buffer supplemented with dithiothreitol (DTT). The samples were denatured at 96°C for 5 minutes and loaded on an 8% Tris-Glycine gel. For total IRβ and total IGF-1Rβ immunoprecipitation, the proteins were transferred to a nitrocellulose membrane, and the gel was probed for phospho IGF-1Rβ<sup>(Tyr1135/1136)</sup>/IRβ<sup>(Tyr1150/1151)</sup>, total IRβ and total IGF-1Rβ. For vimentin, the membrane was probed with mouse monoclonal anti-Vimentin (Santa Cruz Biotechnology, Dallas, TX) after transfer. Secondary antibodies and imaging techniques were performed as described in the SDS Page and Western Blotting section of the Materials and Methods.

For proteomic analysis of vimentin, the gel was stained in 0.025% Coomassie G-250 blue dye (Amresco, Solon, OH), 10% acetic acid and 50% methanol for 1 hour, destained in 10% acetic acid and 50% methanol and stored in ddH<sub>2</sub>O. The Mount Sinai Proteomics Shared Resource Facility then analyzed the bands of interest. The vimentin double band was excised from the gel, reduced with tris(2-carboxyethyl)phosphine (TCEP) and alkylated with iodoacetamide and analyzed by mass spectrometry after trypsin digestion. The analysis was performed using reversed-phase liquid chromatography (LC) over a Waters BEH130 C18 column (100 µm × 100 mm, 1.7 µm particle size) in a Waters NanoAcquity UPLC system (Waters, Milford, MA) interfaced to a Thermo LTQ-Orbitrap mass spectrometer (Thermo Scientific, San Jose, CA).

### RNA Isolation and Analysis

For RNA isolation from formalin fixed paraffin embedded (FFPE) tissues, four 5µm sections were cut from FFPE tissue blocks at the Mount Sinai Histology Core Facility, and RNA was isolated from the samples using the RNeasy FFPE Kit

(Qiagen, Valencia, CA), as per the manufacturer's protocol. RNA concentrations were measured using the Nanodrop ND-1000 (Thermo Scientific, Wilmington, DE). Gene expression was performed using the digital mRNA profiling technology, Nanostring (Nanostring Technologies, Seattle, WA). The principle of Nanostring mRNA analysis is shown in Figure 18, and its comparison to SyBr Green and TaqMan qPCR have been validated previously (47, 59). We designed a Custom CodeSet of genes which included the IR, the IR-A and IR-B isoforms, and a number of splicing factors that have been previously described in the literature to regulate IR splicing, or have been previously correlated with IR slicing in gene expression studies. Gene target sequences were designed from the NCBI accession numbers in collaboration with the Nanostring technicians, and were generated by Nanostring Technologies (Seattle, WA). In addition to the IR isoforms, and splicing factors, we included probes for expression of IGF-1R and IGF-2 and Ki67 to determine if IR-A or IR-B expression correlated with Ki67 expression. 150ng of RNA from each sample was subjected to gene expression analysis using Nanostring nCounter at the Mount Sinai qPCR Core Facility. The results were normalised to negative controls and housekeeping genes and analyzed using the nSolver Analysis Software 2.5 (Nanostring, Seattle, WA). Differences in the expression of IR and the expression ratio of IR-A and IR-B were compared between the patients' samples, and correlated with laboratory and anthropometric measurements of obesity, the metabolic syndrome, insulin resistance and pre-diabetes (described below in the Materials and Methods section entitled, Hyperinsulinaemia and IR Signaling in Breast Cancer Survival Disparities Between Black and White Women).

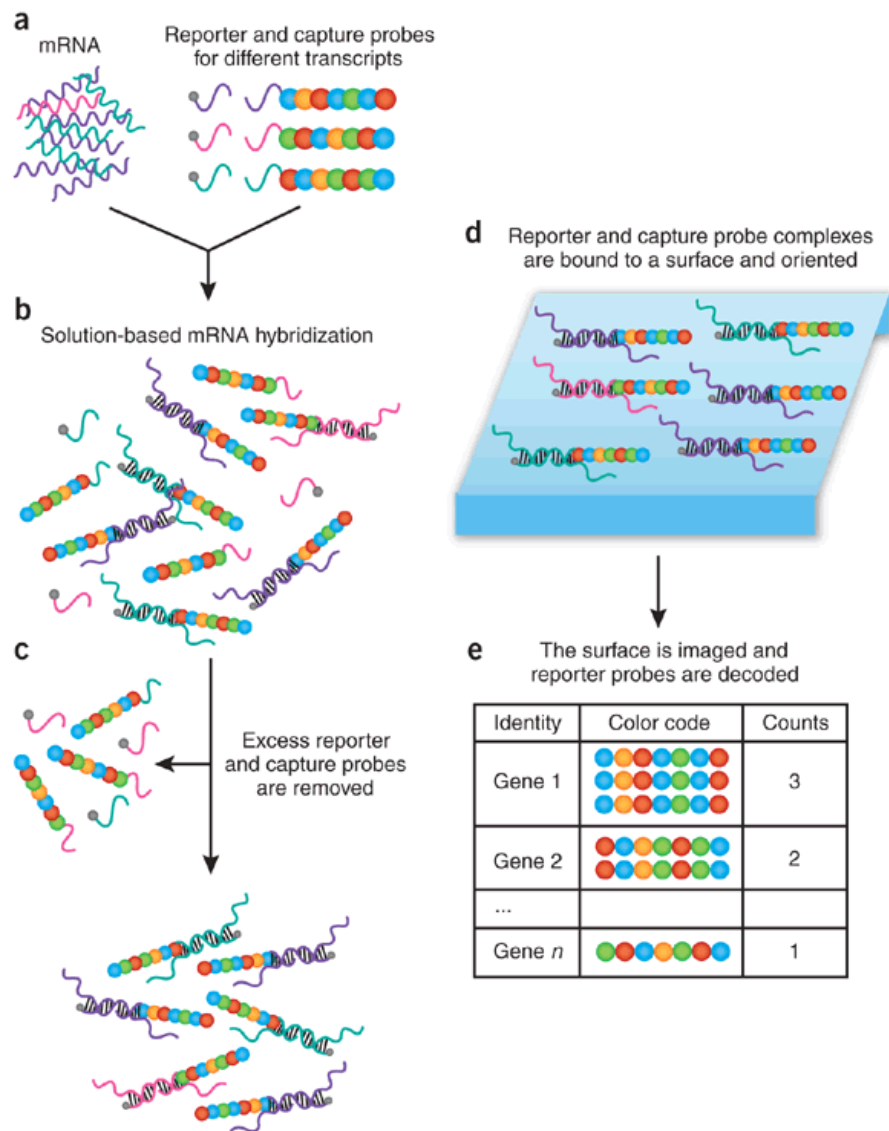


### Figure 18 Nanostring mRNA Gene Expression Analysis

This schematic explains the analysis of mRNA gene expression using Nanostring. (a) Total RNA is mixed directly with nCounter reporter and capture probes. No cDNA synthesis or amplification of the target is required. (b–d) After hybridization (b), excess reporters and capture probes are removed (c) and the purified ternary complexes are bound to the imaging surface, elongated and immobilised (d). (e) Reporter probes, representing individual copies of mRNA, are tabulated for each gene. Figure from Fortina P, Surrey S. *Nature biotechnology* 2008; 26(3):293-294. Reproduced with permission.

## **Statistical Analysis For In Vitro and Pre-Clinical Studies**

All data are expressed as mean  $\pm$  SEM, unless otherwise noted. Student's t-test was performed to compare two groups with equal variance. Welch's t-test was used to compare two groups with unequal variance. A one-way ANOVA followed by Holm-Sidak post-hoc test was used for comparing more than 2 groups. A p value  $\leq 0.05$  was considered significant. Analysis was performed using the statistics software package SPSS Statistics (IBM, Armonk, NY).

## **Hyperinsulinaemia and IR Signaling in Breast Cancer Survival Disparities Between Black and White Women**

This study was approved by the Institutional Review Board of the Icahn School of Medicine at Mount Sinai. This study is ongoing and the protocol details are currently under review for publication in Diabetes/Metabolism Research and Reviews (DMRR). The manuscript for the protocol is attached in Appendix I. It was designed by Dr. Derek LeRoith, Dr. Nina Bickell and myself and is funded by the NIH. Dr. Nina Bickell is recruiting the patients at multiple US hospital sites. Research co-ordinators are collecting the anthropometric data and blood. The pathologists at the patients' hospitals will assess ER, PR and Her2 status of the tumours. The blood tests are being performed at Mount Sinai Hospital clinical laboratory. We, at the LeRoith lab, are receiving de-identified tissue sections cut from the FFPE tumour blocks for IHC staining and RNA isolation and analysis using Nanostring, as described in the RNA Isolation and Analysis section of the Materials and Methods, and are performing IHC and RNA analysis.

In this thesis, the initial clinical data is presented from the first 101 recruited patients. In addition, we present the results from the RNA analysis of the first 47 deidentified FFPE breast cancer samples that were analyzed for IR isoform and splicing factor expression.

The complete details of the recruitment of patients, anthropometric data, lab measurements, and determination of prognosis are described in the DMRR manuscript that is under review. In the following sections are the details relevant to the data presented in the Results section, Chapter 6.

### **Patient Accrual**

The study aims to recruit 350 Black women and 936 White women (see Statistical Analysis section below for power calculations). At each participating site, all women over the age of 21 years with a primary diagnosis of breast cancer will be identified from the surgery schedule or diagnostic biopsy and contacted by letter and telephone, to ascertain their willingness to participate. Bloods will be drawn with intravenous catheter insertion at surgery, prior to medication and fluid administration. Patients' demographic characteristics, access to care, factors affecting breast cancer prognosis, overall health status and prognosis and factors affecting insulin resistance will be assessed using a validated questionnaire. Women who have undergone bariatric surgery for weight loss, organ transplantation, have Type 1 diabetes or medically treated Type 2 diabetes, have been taking oral glucocorticoid treatment within two weeks of blood draw and tumour resection, have taken neoadjuvant therapies, have end stage renal disease or hepatic cirrhosis, or are receiving neoadjuvant therapy will be excluded as these conditions can affect insulin levels. The study design is summarised in Figure 19.

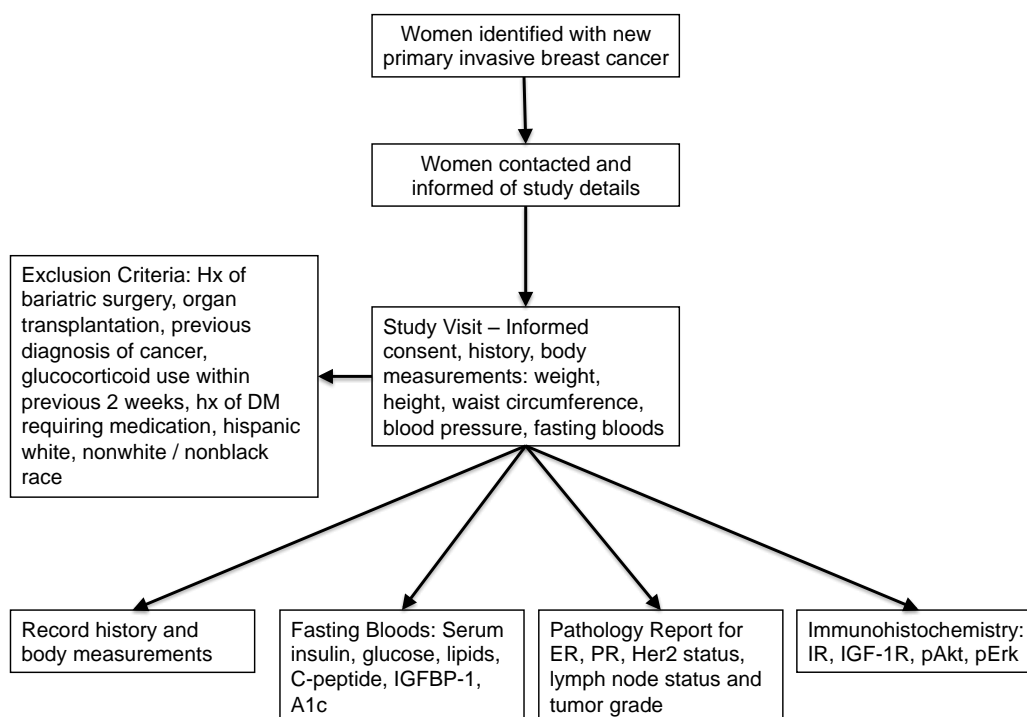


**Figure 19 Study Design for Study Examining Disparities in Breast Cancer Mortality**

Schematic of the study design.

## Anthropometric Data

Participant's height and weight are recorded using a stadiometer. Body mass index (BMI) is calculated from weight (kg)/height<sup>2</sup> (m<sup>2</sup>). Waist circumference is measured at the umbilical level and blood pressure will be recorded using standard National Health and Nutrition Examination Study (NHANES) procedures.

## Determining Prognosis

The final pathology report will be obtained which contains the tumour size, histological grade, nodal status, ER $\alpha$ , PR and HER2 status. Where available, Oncotype Dx reports will be recorded. Pathological data is used to calculate the Nottingham Prognostic Index (NPI). The NPI score is calculated as  $[0.2 \times \text{tumour size (cm)} + \text{lymph-node stage (1, node negative; 2, 1-3 positive lymph nodes; 3, } \geq 4 \text{ positive lymph nodes)} + \text{histological grade (1, well differentiated; 2, moderately differentiated; 3, poorly differentiated)}]$  (50). Tumour grade will be defined by the Nottingham combined histological grade (NCHG), as recommended by the American Joint Committee on Cancer (AJCC) (41). Based on a recent U.S. study that dichotomised NPI at 4.4 (poor prognosis  $>4.4$  and good prognosis  $\leq 4.4$ ) and showed significant differences in biomarkers (e.g., hormone receptor, Her2) in these groups (11, 120), we will define good prognosis as those women with an NPI score of  $\leq 4.4$ , and poor prognosis as an NPI score  $>4.4$ . Therefore, we will determine whether insulin resistance is associated with a poor prognosis, defined primarily by NPI  $>4.4$ .

## Laboratory Measurements

Blood was drawn after an overnight fast on the morning of surgery for preserved plasma glucose, serum lipids (total cholesterol, low-density lipoprotein (LDL) cholesterol, high-density lipoprotein (HDL) cholesterol, triglycerides (TG)), hemoglobin A1c (HbA1c), serum insulin, C-peptide, IGF-1, insulin-like growth factor binding protein-1 (IGFBP-1). Insulin resistance will be calculated from the HOMA-IR  $[(\text{fasting plasma glucose (mg/dL)} \times \text{fasting serum insulin (uU/ml)})/405]$  (143), a widely used and validated measure of insulin resistance (21). Insulin resistance is defined as a HOMA-IR  $>2.8$ , the upper quartile of insulin resistance in the U.S. population, reported by the NHANES (10). We will assess the presence of the metabolic syndrome, defined by the 2009 International Diabetes Federation

(IDF), National Heart, Lung and Blood Institute (NHLBI), American Heart Association (AHA), World Heart Federation (WHF), International Atherosclerosis Society (IAS) and International Association for the Study of Obesity (IASO) joint position statement, as the presence of 3 or more of the following features: waist circumference  $\geq 88\text{cm}$ ; triglycerides (TG)  $\geq 150\text{mg/dL}$ ; high density lipoprotein (HDL) cholesterol  $< 50\text{mg/dL}$ ; systolic blood pressure  $\geq 130\text{mmHg}$  or diastolic blood pressure  $\geq 85\text{mmHg}$ ; fasting glucose  $\geq 100\text{mg/dL}$  or the use of medication to treat elevated TG, low HDL or blood pressure (6).

#### Immunohistochemical and RNA Analysis of Formalin Fixed Paraffin Embedded Tissue Sections

All recruitment sites will fix tissue specimens in 10% formalin for 48-72 hours before processing and embedding in paraffin. 5 $\mu\text{m}$  thick sections will be obtained for each patient's tumour paraffin block that was used by the hospital's pathology department to determine tumour ER/PR/HER2 status to maximise the sample's tumour tissue. Immunohistochemistry staining will be performed as described in the Histological Analysis section of the Materials and Methods to detect the presence of the total IR $\beta$ , IGF-1R $\beta$ , phosphorylation Akt(Ser473) and phosphorylation of ERK1/2(Thr202/Tyr204) in the tumour. RNA will be isolated and analyzed as described in the RNA Isolation and Analysis section of the Materials and Methods.

#### Outcomes and Statistical Analysis

We will use the NPI rather than cancer stage at presentation to determine prognosis at the time of tumour resection, as the NPI is less affected by health care access than tumour stage and has been validated in several different countries (5, 11, 13).

Descriptive analyses will be performed to profile Black and White women separately including examination of proportions, means, and medians, as well as estimates of variability including standard errors, ranges, and confidence intervals. Continuous data distributions will be evaluated for appropriateness of scale, and transformations will be used where appropriate. For each racial group, we will compute appropriate summary statistics for women who have good prognosis ( $\text{NPI} \leq 4.4$ ;  $\text{iNPI} \leq 5.4$ ) and poor prognosis ( $\text{NPI} > 4.4$ ;  $\text{iNPI} > 5.4$ ). For each population



(White and Black), we will compare good and poor prognosis patients with respect to age at diagnosis, year of diagnosis, income, education, access to care, stage at diagnosis family history of breast cancer, smoking status, BMI, waist circumference, blood pressure, lipid profile, medications, use of oestrogen, fasting serum insulin, plasma glucose, HbA1c, C-peptide, IGFBP-1, tumour IR $\beta$ , tumour IGF-1R $\beta$ , pAkt, pErk.

Multivariable analyses for each racial group will be performed to examine the association between insulin resistance (HOMA-IR>2.8) and poor tumour prognosis (NPI>4.4) using logistic regression, adjusting for potential confounding factors and assessing mediating factors for each group.

This study is powered to detect a significant interaction by race of the association between insulin resistance (HOMA-IR) and poor prognosis breast cancer (NPI >4.4). Based on the power analysis, 936 White women and 350 Black women would need to be recruited over 4 years to detect a significant interaction between insulin resistance and poor prognosis in breast cancer by race. A prior study examining the relationship between insulin resistance and mortality among a sample of predominantly White women with breast cancer found a hazard ratio=1.6 among women with HOMA-IR scores >2.7 (39). With a sample size of 936 White women, we will have adequate power to detect a main effect OR>1.6 in White women. Under the specified assumptions, this study will have >80% power to detect a significant interaction ratio of  $\geq 1.5$ , comparing the effect size in Black women to the effect size in White women (Type I error =0.05).

### 3. Results

#### Chapter 1. Hyperinsulinaemia and Breast Cancer Metastasis in a Transgenic NeuNT model.

##### *Generation and Characterization of the MTB/TAN/MKR mouse model.*

The generation of the tetracycline-inducible NeuNT mouse model (MTB/TAN) and MTB/TAN/MKR is described in the Materials and Methods section.

After generation of the MTB/TAN/MKR line, we characterized the metabolic phenotype of the mice, to determine if the mice maintained the pre-diabetic phenotype observed in the female MKR mice (115). Female MTB/TAN/MKR mice demonstrated decreased body weight compared to the MTB/TAN control females, consistent with the MKR mice (Figure 20A). In addition, they demonstrated increased plasma insulin concentrations (Figure 20C), and severe insulin resistance to a 0.75U/kg insulin tolerance test (Figure 20D).

MTB/TAN/MKR mice show augmented NeuNT-induced abnormalities of the mammary gland at eight weeks compared to MTB/TAN control mice.

The Chodosh Lab has shown that doxycycline-induced *NeuNT* expression results in noticeable hyperplastic abnormalities in the mouse mammary gland such as the presence of cellular masses along the length of ducts, as well as terminal end bud enlargement due to the presence of acinar-like structures (111). We investigated whether or not hyperinsulinaemia would have an additive effect on these early *NeuNT*-mediated hyperplastic abnormalities. We induced *NeuNT* expression for three days in eight week-old MTB/TAN/MKR and MTB/TAN mice, at which point we euthanized the animals and compared mammary gland morphology by whole mount analysis. Since MKR mice have precocious mammary gland growth and differentiation compared to control mice at both three and fifteen weeks (115), we also performed whole mount analysis and H&E staining of mammary glands from eight week-old MTB/TAN/MKR and MTB/TAN mice which had not been administered doxycycline (Figure 21A and Figure 21B, upper panels). In MTB/TAN/MKR mice, we found *NeuNT* mediated abnormalities to be enhanced compared to MTB/TAN controls, with larger cellular masses growing on ducts, greater terminal end bud enlargement and precocious lobular development (Figure 21A, Figure 21C). This finding was further confirmed by histological evaluation of

H&E stained sections of the mammary gland (Figure 21B) where we observed advanced ductal hyperplasia in MTB/TAN/MKR mice compared to MTB/TAN controls.

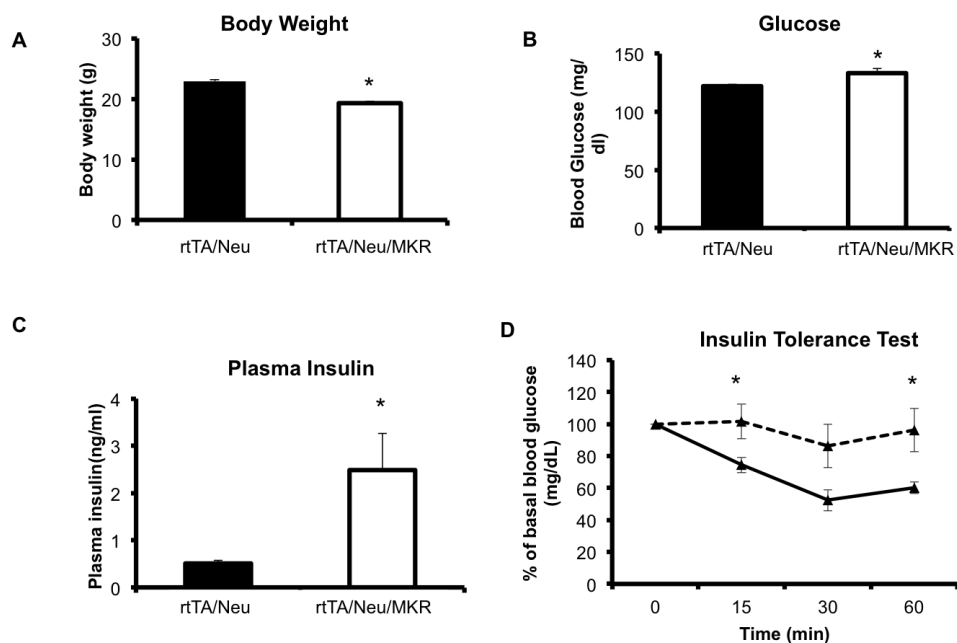


**Figure 20 Metabolic Characterization of the MTB/TAN/MKR mice.**

(A) Body weight (MTB/TAN, n=14; MTB/TAN/MKR<sup>+/+</sup>, n=10), (B) blood glucose (MTB/TAN, n=30; MTB/TAN/MKR<sup>+/+</sup>, n=22), and (C) serum insulin (MTB/TAN, n=13; MTB/TAN/MKR<sup>+/+</sup>, n=20) of MTB/TAN and MTB/TAN/MKR<sup>+/+</sup> mice at 8 weeks of age. (D) An ITT was performed on 8 week-old MTB/TAN/MKR<sup>+/+</sup> (n=5) and MTB/TAN mice (n=5) after intraperitoneal injection of insulin (0.75 Units/kg). Blood samples were obtained from the tail vein and glucose concentrations were determined at the indicated time points. Graphs represent mean values of each group, error bars represent the SEM. \*P value <0.05.

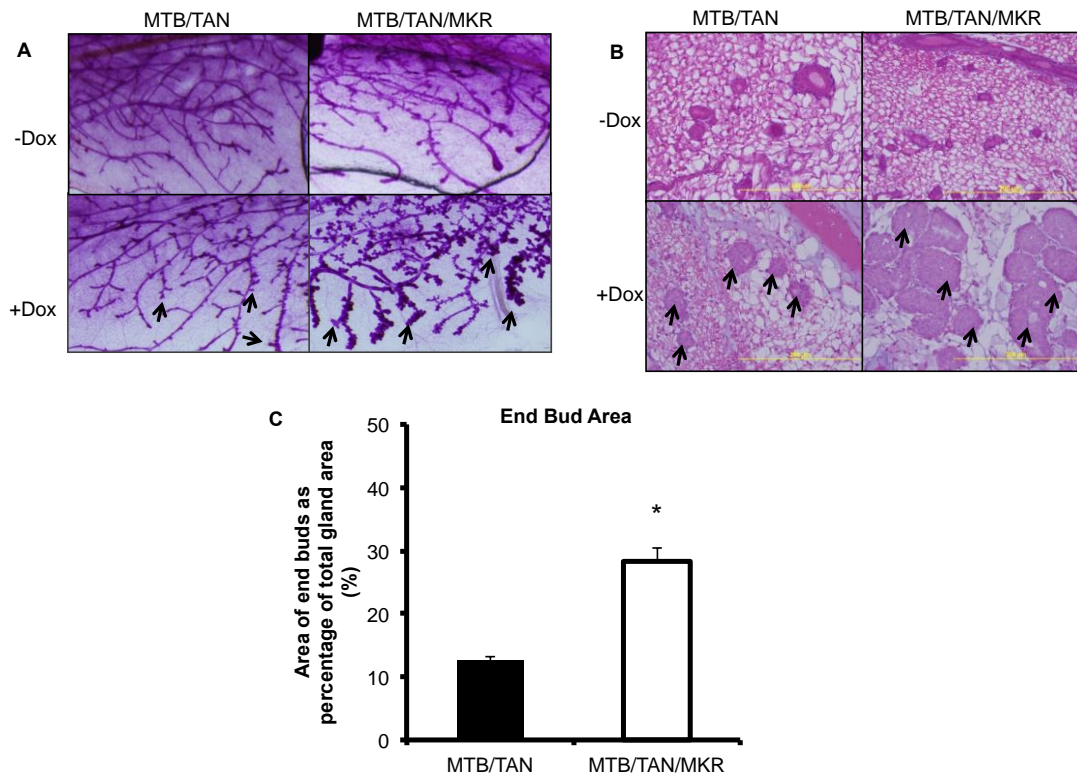


**Figure 21 Effects of Hyperinsulinaemia on NeuNT-mediated Mammary Gland Hyperplasia**

(A) Whole mount analysis of mammary glands obtained from eight week-old female MTB/TAN and MTB/TAN/MKR<sup>+/+</sup> mice without doxycycline (-Dox) and after three days of doxycycline treatment (+Dox). (B) Histological analysis (H & E staining) of mammary glands after three days of doxycycline treatment. (C) Quantification of percentage area of mammary gland whole mounts composed of end buds (MTB/TAN, n=3; MTB/TAN/MKR, n=3. Arrows, End buds (A) and ductal hyperplasia (C) At least five animals per group were analyzed and the representative images are shown. Original magnification, x 4 (A) and x 40 (B). Graph represents mean for each group, error bars represent SEM. \* P value <0.05.

NeuNT-induced mammary tumour burden is greater in MTB/TAN/MKR mice than MTB/TAN mice, and is regulated through IR/IGF-IR signaling pathways.

When administered doxycycline for several weeks, MTB/TAN mice developed multiple invasive mammary adenocarcinomas with tumours arising in all inguinal and thoracic glands (111). We administered doxycycline to eight-week-old MTB/TAN and MTB/TAN/MKR mice for two, four, six or twelve weeks. Mice were euthanised at each time-point and the combined tumour weight from all inguinal and thoracic glands from each mouse was recorded. As shown in Figure 22A, MTB/TAN/MKR mice exhibited significantly higher total tumour mass than MTB/TAN controls at all time-points with the exception of the twelve week time-point, suggesting that hyperinsulinaemia augments *NeuNT*-driven mammary tumour growth. We extracted proteins from tumour tissues to examine whether IR/IGF-IR activation was upregulated in MTB/TAN/MKR mice compared to MTB/TAN controls. As shown in Figure 22B and Figure 22C, mammary tumour tissues from MTB/TAN/MKR mice demonstrated higher levels of phosphorylated insulin receptor/insulin-like growth factor receptor (IR $\beta$ /IGF-IR $\beta$ ) after two, four and six weeks of *NeuNT* upregulation, suggesting that these receptors are involved in mediating the additional tumour growth present in MTB/TAN/MKR mice. In MTB/TAN/MKR and MTB/TAN mice, which had been administered doxycycline for a period of 12 weeks, we observed an increase in IR/IGF-IR phosphorylation in mammary tissues of MTB/TAN/MKR mice which was not statistically significant (Figure 22B and Figure 22C). There was no significant difference in tumour weights after 12 weeks of doxycycline administration, possibly due to tumours reaching their physiologically maximal size after this time period (Figure 22A). We also compared Ser473 phosphorylation of Akt, which lies downstream in the signaling pathway of both the IR/IGF-IR and Her2 and found that at 2 weeks there was a significant upregulation of phosphorylated Akt in tumours from MTB/TAN/MKR mice compared to MTB/TAN mice (Figure 22D and Figure 22E). At later stages of tumour development, levels of Akt phosphorylation in the tumours appeared to be similar in the two groups.

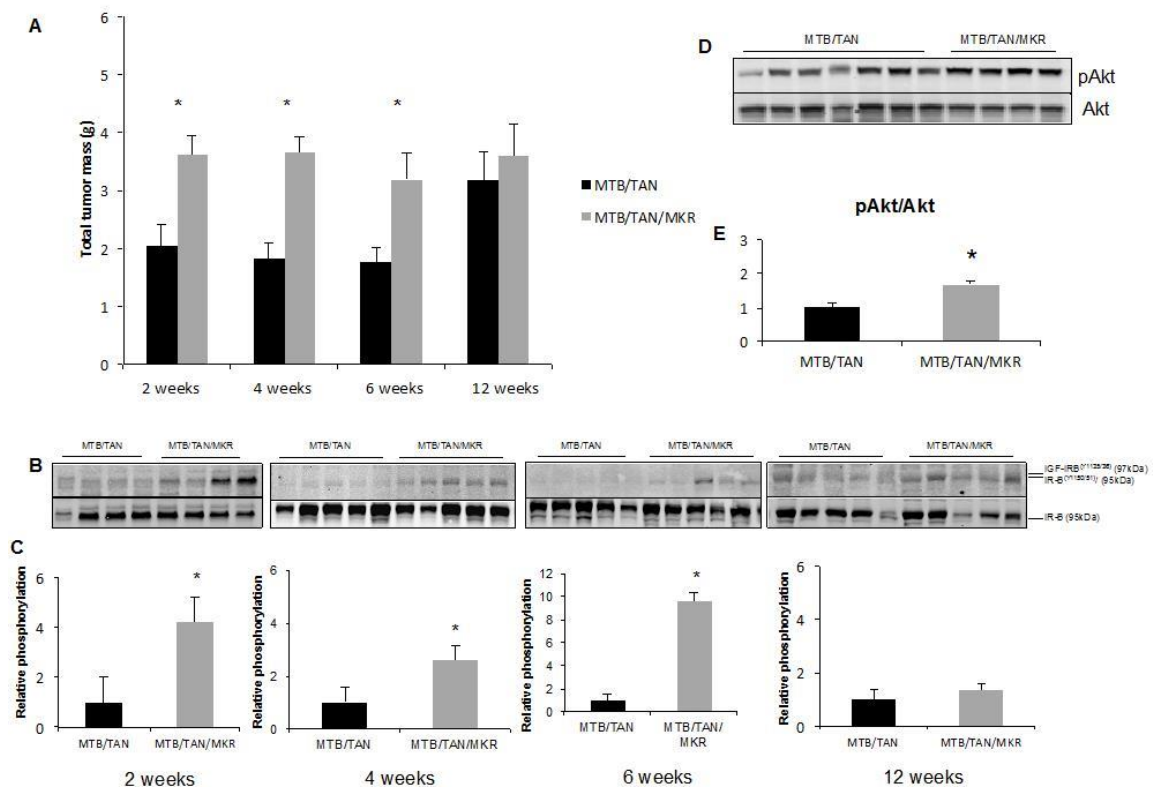


**Figure 22 Tumour growth, IRβ/IGF-IRβ and Akt signaling are enhanced in tumours from MTB/TAN/MKR mice compared to MTB/TAN controls.**

(A) MTB/TAN and MTB/TAN/MKR mice were maintained on doxycycline for two, four, six or twelve weeks. Mice were euthanised and the combined tumour mass from all mammary glands was quantified. At two week time-point, MTB/TAN, n=11; MTB/TAN/MKR, n=4. At four week time-point, MTB/TAN, n=11; MTB/TAN/MKR, n=7. At six week time-point, MTB/TAN, n=16; MTB/TAN/MKR, n=6. At twelve week time-point, MTB/TAN, n=12; MTB/TAN/MKR, n=11. (B) Western blot analysis of tumour tissue, probed with antibodies to pIRβ<sup>(Y1150/51)</sup>/pIGF-IRβ<sup>(Y1135/36)</sup>, IRβ. (D) Western blot analysis of tumour tissue from mice on doxycycline for 2 weeks probed with antibodies to pAkt<sup>Ser473</sup> and total Akt. Using densitometry, protein expression was quantified (C, E). Error bars represent SEM \*, P<0.05. At two week time-point, Western blot is representative of MTB/TAN, n=9; MTB/TAN/MKR, n=4 samples. At four and six week time-points, MTB/TAN, n=7; MTB/TAN/MKR, n=7 samples. At twelve week time-point MTB/TAN, n=10; MTB/TAN/MKR<sup>+/+</sup>, n=10.

*NeuNT-induced spontaneous lung macrometastases is enhanced in MTB/TAN/MKR<sup>+/+</sup> mice after 12 weeks of tumour growth.*

MTB/TAN mice were reported to harbor *NeuNT*-dependent spontaneous lung macrometastases (111). We removed the lungs of euthanized MTB/TAN/MKR and MTB/TAN mice after two, four, six or twelve weeks of doxycycline induced *NeuNT* expression in mammary epithelium and recorded the numbers of visible macrometastases. We also examined H&E stained sections of lung at all time-points for both micrometastases and macrometastases. After two, four or six weeks of *NeuNT* expression and mammary tumour growth, no visible macrometastases were observed in either MTB/TAN/MKR or MTB/TAN mice. However, H&E staining revealed the presence of micrometastases in lungs of both groups of mice after six weeks of *NeuNT* expression. Although there was a trend for the number of micrometastases to be increased in MTB/TAN/MKR mice (0.3 micromets/lung section in MTB/TAN vs 0.8 micromets/lung section in MTB/TAN/MKR) this did not reach statistical significance. In contrast, after 12 weeks of *NeuNT* expression in mammary tissue, macrometastases could be clearly observed in the lungs, and these were significantly increased in MTB/TAN/MKR compared to MTB/TAN mice (Figure 23A and Figure 23B) suggesting that hyperinsulinaemia increases the metastatic potential of *NeuNT*-driven mammary cancer.

*Increased expression of vimentin was found in the NeuNT-induced mammary tumours in hyperinsulinaemic MTB/TAN/MKR mice*

To determine whether hyperinsulinaemia enhances the progression of *NeuNT*-mediated primary tumours to lung metastases by increasing EMT, we analyzed tumour tissue for the expression of vimentin protein, a marker of mesenchymal cells. As shown in Figure 24A and Figure 24B, western blot analysis of tumour lysates demonstrated increased vimentin expression in tumours from 6 week old MTB/TAN/MKR mice, compared to MTB/TAN mice. We additionally, analyzed vimentin expression in six-week tumour tissues by immunofluorescent staining of paraffin-embedded sections. As shown in Figure 24B and Figure 24C, vimentin levels as measured by immunofluorescence were significantly elevated, indicating that more mesenchymal cells were present in MTB/TAN/MKR mice at this time

point. The vimentin positive cells generally did not stain positive for NeuNT, indicating that these were either cells that had undergone EMT and lost Neu expression, or were cancer associated fibroblasts.

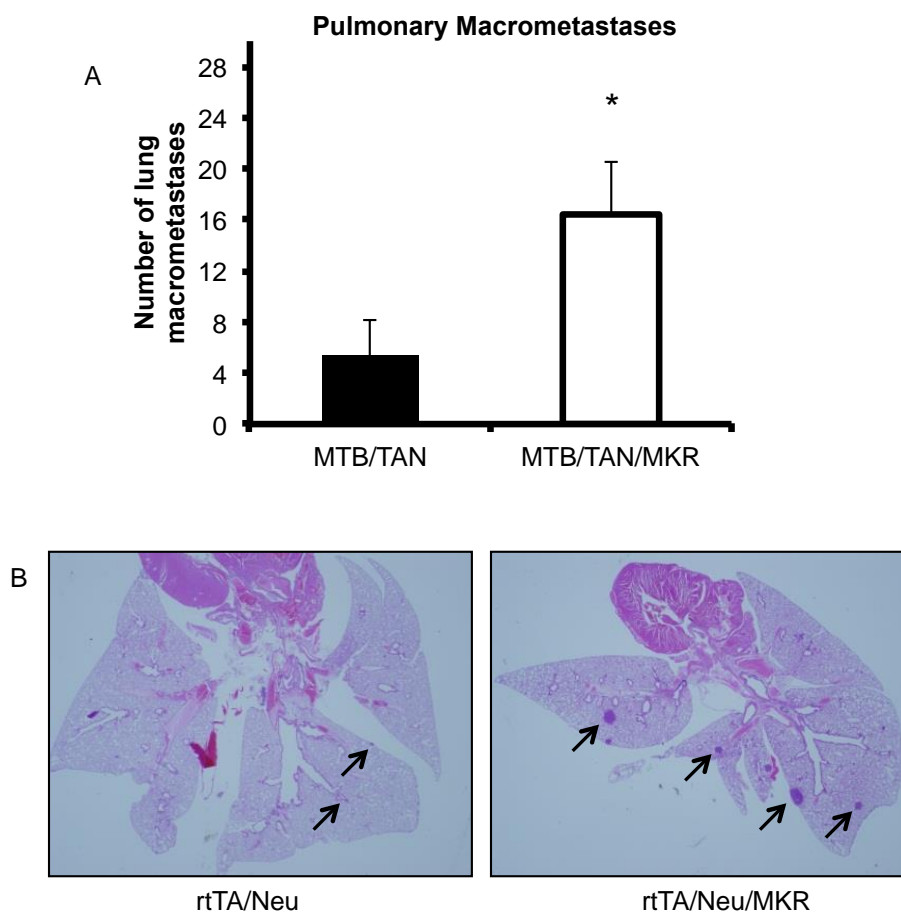


### Figure 23 Lung Metastases in MTB/TAN and MTB/TAN/MKR mice

After 12 weeks on doxycycline, MTB/TAN and MTB/TAN/MKR<sup>+/+</sup> mice were euthanised, lungs removed and inflated and (A) number of lung macrometastases were recorded. (B) Lungs were paraffin-embedded, sectioned and stained with H&E to reveal macrometastases. Original magnification 4X. Arrows indicate metastatic cells.



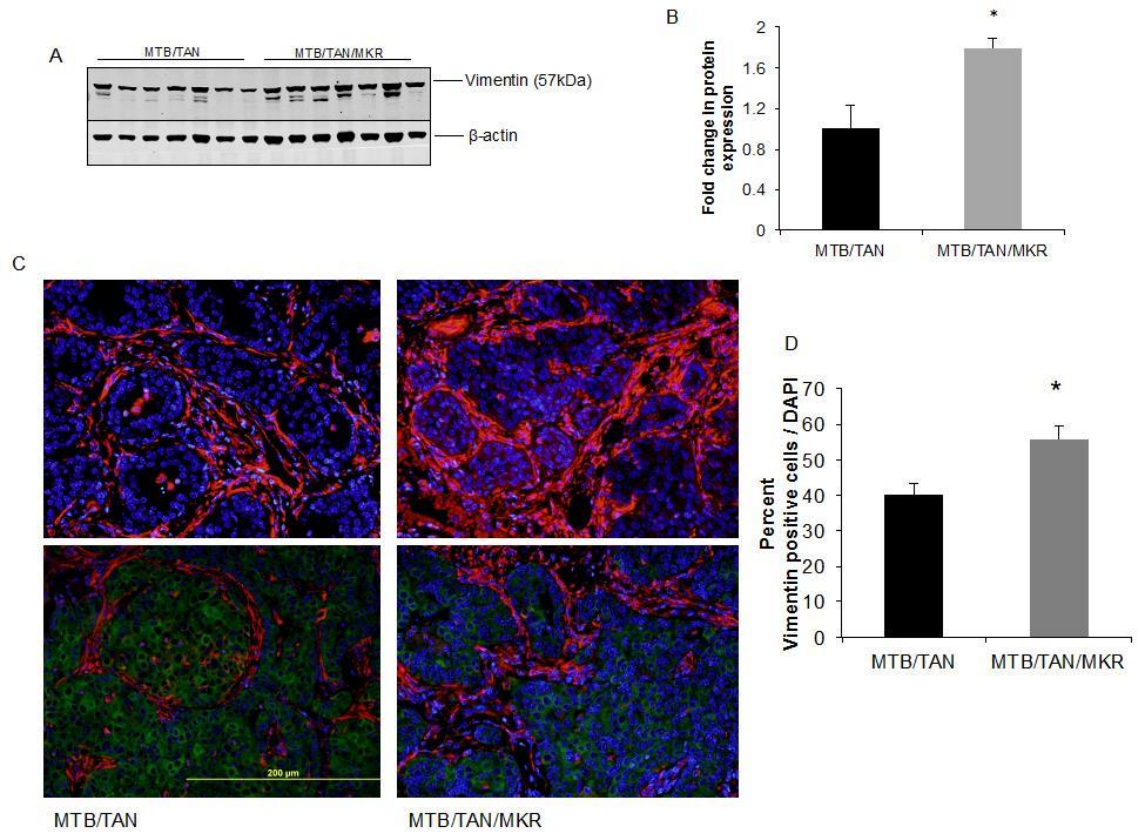


**Figure 24 Vimentin expression is enhanced in NeuNT Tumours from MTB/TAN/MKR mice.**

(A). After six weeks *Neu-NT* upregulation, mammary tumours were removed from MTB/TAN and MTB/TAN/MKR<sup>+/+</sup> mice, tumour lysates were subjected to western blot analysis and probed with anti-vimentin antibodies. Using densitometry, vimentin protein expression / beta actin was quantified (B). Tumour tissue was paraffin embedded, sectioned and analyzed by immunofluorescence microscopy for the expression of vimentin (red) and Neu (green) proteins, nuclei were stained with DAPI (blue) (C). Vimentin expression was analyzed using 'Image J' program to quantify expression of vimentin protein in six-week tumours from MTB/TAN and MTB/TAN/MKR<sup>+/+</sup> mice (D). Photographs are representative of at least four mice from each group. Five high power fields were photographed on every slide and each image was quantified. Original magnification 40X. Graphs represent the mean for each group, error bars represent SEM. \* P value <0.05.

In summary, these data show that hyperinsulinaemia promotes mammary gland hyperplasia, primary tumour growth and lung metastasis in a Her2/Neu model of breast cancer. These results demonstrate that hyperinsulinaemia increases the growth of the MTB/TAN tumors particularly at early timepoints by increased activation of Akt above that of activated Neu. However, at later timepoints it is possible that the transgenic activation of Neu leads to maximal activation of Akt, leading to catchup growth of the tumors in the MTB/TAN mice to the MTB/TAM/MKR mice by 12 weeks.

However, our results also raised certain questions. In this study we do not demonstrate that it is a direct effect of insulin on the IR of the tumours that is promoting tumour growth and progression. Under conditions of hyperinsulinaemia, IGF binding proteins (IGFBP)-1 and -2 are repressed (27) which may lead to an increase in circulating or local “free” IGF-1. In the MTB/TAN/MKR mouse model, increased IGF-1 levels at the level of the target tissue could lead to increased activation of the IGF-IR, thus directly increasing tumour growth. The *Neu* receptor tyrosine kinase has no known ligand, depending for its activation upon dimerization with either ErbB3 or ErbB1 (32, 55). Interestingly, *Neu* also dimerises with the IGF-IR, an occurrence which provides a significant source of resistance to Her2-mediated therapies in humans (98). Thus, in our MTB/TAN/MKR mouse model, it is possible that elevations of either insulin or “free” IGF-1 could promote tumour growth through increased activation of *Neu*/IGF-IR hybrids (98).

Our finding of greater numbers of lung metastases in MTB/TAN/MKR mice suggests that as well as promoting primary tumour growth, insulin may also enhance primary tumour progression and/or circulating tumour cell survival in the lung. The EMT permits tumour cells to gain the plasticity required to extravasate from the primary tumour site. During extravasation cells become increasingly mesenchymal in nature due to numerous changes in cytoskeletal scaffolding protein structures. Vimentin belongs to the intermediate filament (IF) family of proteins and has recently been shown to be an important marker of the EMT in epithelial cells, which normally express only cytokeratin-type IFs (129). However, vimentin is not specific for EMT, and is also a marker of cancer-associated fibroblasts (135, 138).

Therefore, this study raised the following questions:

1. Does hyperinsulinaemia increase tumour growth by directly activating the IR?
2. Does hyperinsulinaemia increase vimentin expression in tumour cells, or increase tumour-associated fibroblasts?

These questions are addressed in subsequent chapters.

## **Chapter 2. Human Tumour Xenografts in an Immunodeficient Mouse Model of Hyperinsulinaemia**

### *Generation and Metabolic Phenotyping of the Rag/MKR mice*

We developed the Rag1<sup>-/-</sup>/MKR<sup>+/+</sup> (Rag/MKR) mouse line to facilitate our studies on the role of hyperinsulinaemia on the progression of human breast cancer xenografts. As the immune system may play a role in the development of insulin resistance, we characterised the metabolic phenotype of the Rag/MKR and Rag1<sup>-/-</sup> (Rag/WT) male and female mice.

Male and female Rag/MKR mice demonstrated lower body weight, of approximately 3-4 g, compared to age and gender matched Rag/WT control mice from 3-8 weeks of age; characteristic of MKR mice (Figure 25A). NMR body composition analysis revealed that the Rag/MKR mice had decreased body fat compared to Rag/WT control mice, again characteristic of the MKR mice (Figure 25B). Insulin tolerance tests were performed in all four groups and Rag/MKR male and female mice demonstrated severe insulin resistance, with no glucose reduction in response to the 0.75IU/kg insulin injection over 60 minutes, while in Rag/WT control mice blood glucose levels rapidly fell to less than 50% of baseline, 60 minutes after the insulin injection (Figure 25C). The presence of endogenous hyperinsulinaemia was confirmed by the measurement of non-fasting plasma insulin levels;  $4.64 \pm 0.69$  in x week old female Rag/MKR mice compared with  $0.61 \pm 0.08$  in Rag/WT mice ( $p < 0.01$ ) (Figure 25D). Glucose levels were higher in the Rag/MKR male mice than Rag/WT male mice after an 8 hour fast (Figure 25E), however female Rag/MKR mice did not demonstrate frank hyperglycaemia. The GTT demonstrated that the Rag/MKR male mice had severe glucose intolerance, while Rag/WT female mice had mild glucose intolerance, compared to control Rag/WT mice (Figure 25E).

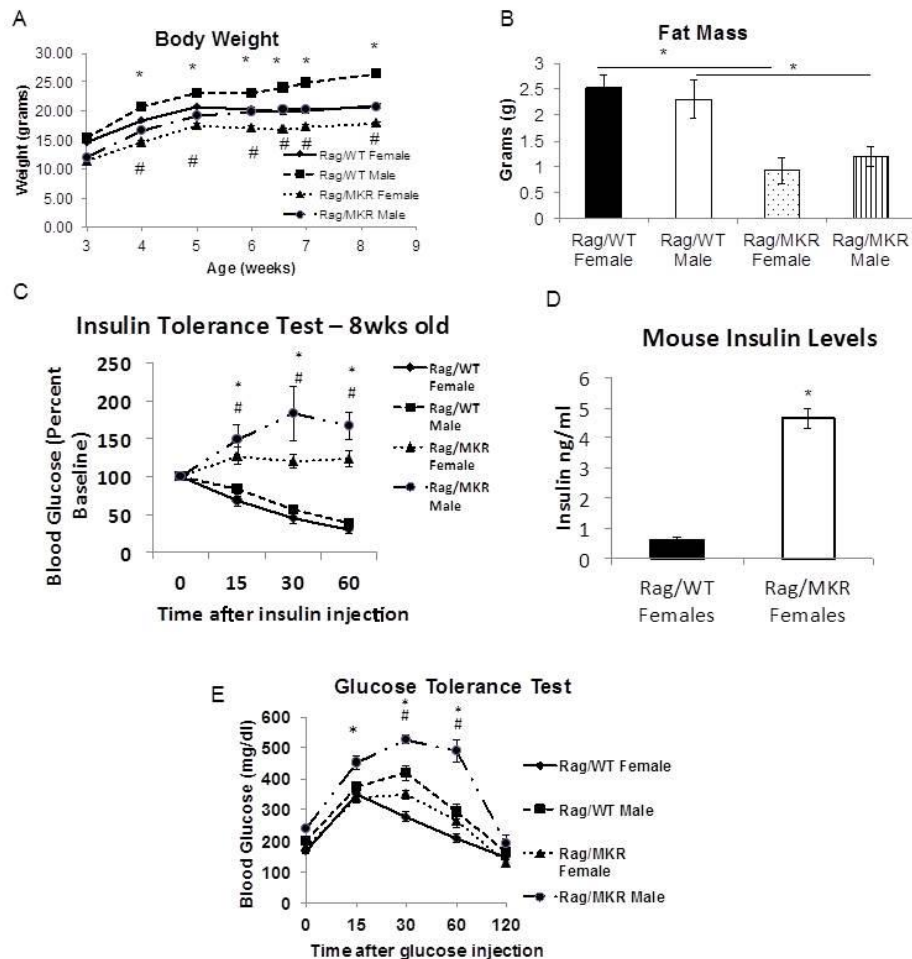


**Figure 25 Metabolic Characteristics of Rag/MKR mice**

(A) Body weight Rag/MKR and Rag/WT male and female mice (n=5-8 per group). (B) Body fat mass, measured by NMR (n=5 per group). (C) An ITT was performed on 8 week-old Rag/MKR and Rag/WT male and female mice (n=5 per group) after intraperitoneal injection of insulin (0.75 Units/kg). Blood samples were obtained from the tail vein and glucose concentrations were determined at the indicated time points. (D) Plasma insulin in the Rag/WT and Rag/MKR mice measured at 8 weeks of age (n=5 per group). (E) A glucose tolerance test was performed after 8 h of fasting using a glucose bolus of 2g/kg body weight administered by intraperitoneal injection. Blood glucose was measured from the tail vein immediately before (Time 0) and 15, 30, 60, and 120 minutes after glucose injection (n=5 per group). Graphs represent mean values of each group, error bars represent the SEM. \*P value <0.05.

*Human triple negative breast cancer xenografts grow larger and develop more pulmonary metastases in the hyperinsulinaemic Rag/MKR mice.*

1 x 10<sup>6</sup> MDA-MB-231 human triple negative breast cancer cells were injected into the 4<sup>th</sup> mammary fat pad of female Rag/MKR and control Rag/WT mice. Tumour size was measured twice weekly until tumours reached a size no greater than 10% of the mouse's body weight (as determined by our previous studies), and as per our animal protocols. At the time of euthanasia tumour weights were measured, lungs were inflated with formalin for subsequent quantification of lung macrometastases.

MDA-MB-231 tumours grew more rapidly in Rag/MKR mice compared to Rag/WT controls, measuring 748.9mm<sup>3</sup> ± 39.6 and 393.9mm<sup>3</sup> ± 19.37, respectively, p<0.05 (Figure 26A). Tumour weights were significantly greater in the Rag/MKR mice compared to Rag/WT mice, weighing 0.49±0.03g and 0.33±0.02g respectively, p<0.05 (Figure 26B). An increase in lung metastases (Figure 26C) was found in the Rag/MKR mice 13.2 ±2.22 surface macrometastases per mouse, compared with 7.38 ±1.38 surface metastases per mouse in Rag/WT mice (p<0.05). Each study was performed with 8-10 mice in each group.

*Increased activation of the IR/IGF-1R signaling pathway was found in the tumours from the Rag/MKR mice.*

Compared to tumours from the Rag/WT mice, an increase in Akt(Ser473) phosphorylation was observed in the tumours from the Rag/MKR mice (Figure 27A, Figure 27B), consistent with our previous studies showing increased PI3K / Akt activation in tumours from the hyperinsulinaemic mice. was observed in the tumours from the Rag/MKR mice, compared to the Rag/WT mice. In addition, we found an increase in the expression of total IRβ and total IGF-1Rβ in the tumours from the Rag/MKR mice, compared with Rag/WT mice (Figure 27C, D, E). These data demonstrate the human triple negative breast cancer xenografts grow larger and develop more metastases in an immunodeficient hyperinsulinaemic mouse model. This increase in tumour growth was associated with increased activation of the IR/IGF-1R signaling pathway.

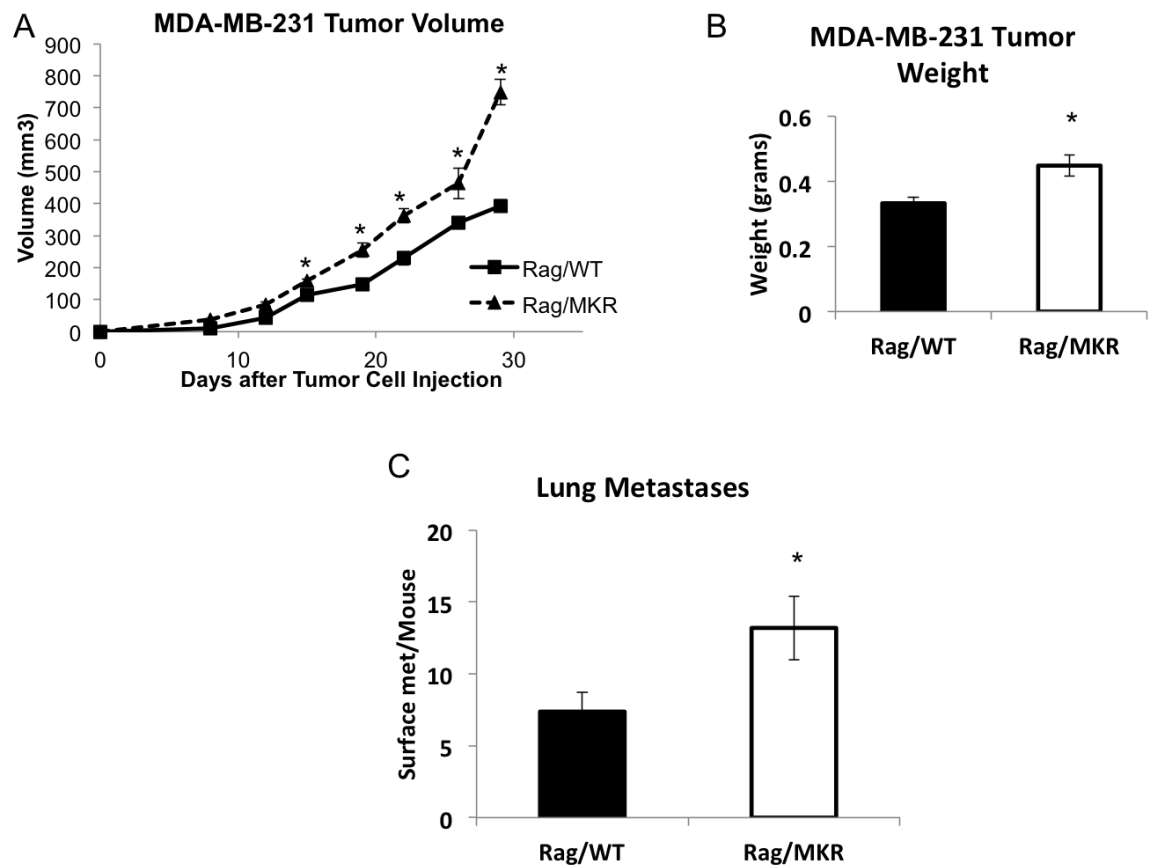


**Figure 26 MDA-MB-231 Tumours in Hyperinsulinaemic Mice**

(A) Rag/MKR and Rag/WT mice were injected with MDA-MB-231 tumour cells at day 0 and tumours were measured twice weekly thereafter until tumours reached a volume of 1cm<sup>3</sup>. (B) Tumour weight was measured at the end of the study. (C) Lung macrometastases were quantified in the lungs of Rag/WT and Rag/MKR mice after inflation with 10% formalin. Graphs represent the mean of each group and error bars indicate the SEM. \*P value <0.05 between groups.

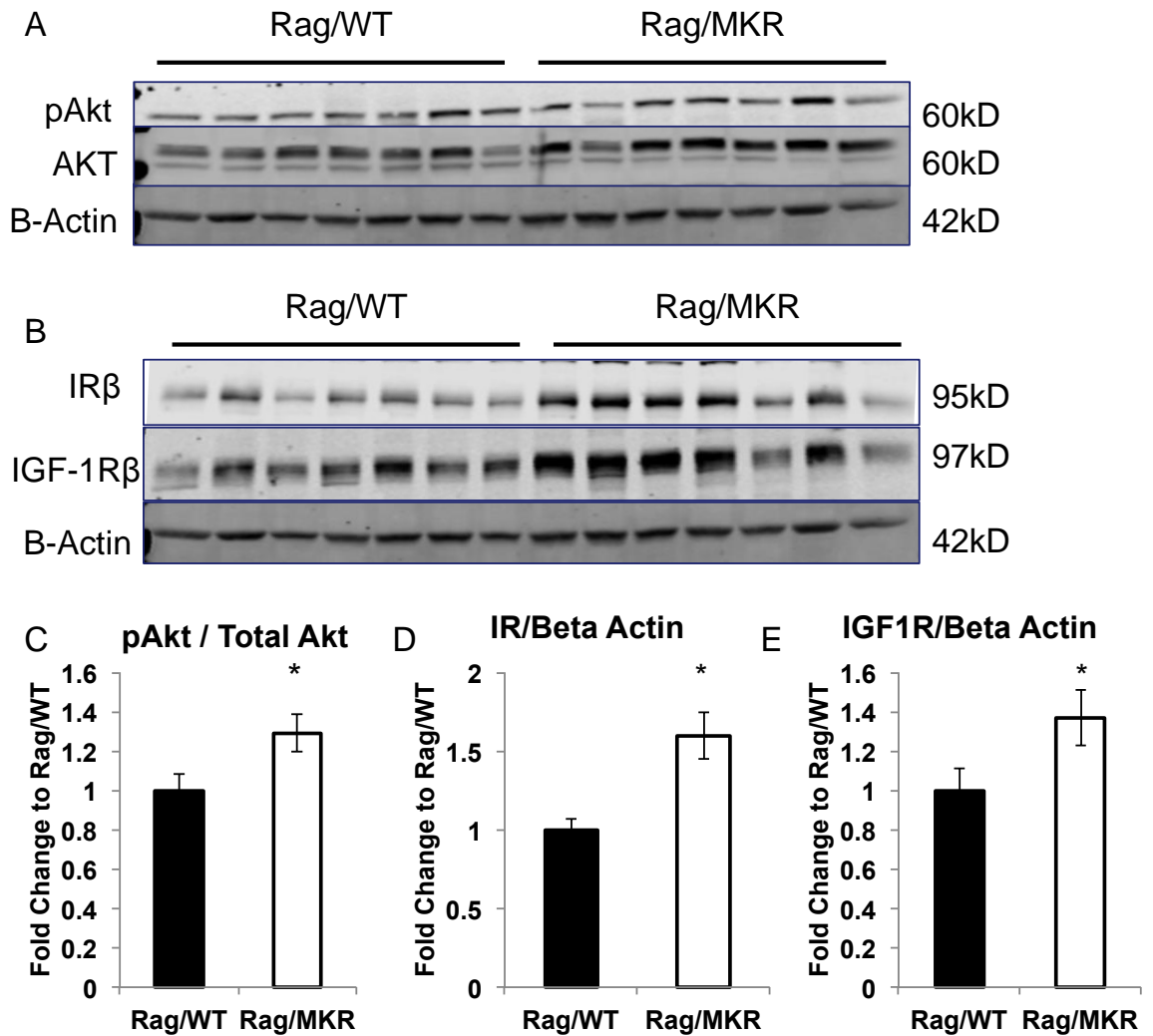


**Figure 27 Insulin Receptor Signaling in MDA-MB-231 Tumours from Rag/WT and Rag/MKR Mice**

(A) Western blot analysis of tumour lysates from MDA-MB-231 tumours from Rag/WT and Rag/MKR mice immunoblotted for (A) pAkt(Ser472), total Akt and beta actin, (B) total IR $\beta$ , total IGF-1R $\beta$  and beta actin. (C) Densitometric quantification of pAkt(Ser473)/Total Akt, total IR $\beta$ /beta actin, and total IGF-1R $\beta$ /beta actin. n=7 per group. Graphs represent mean of each group and error bars indicate SEM. \*P value <0.05 between groups.

*Increased expression of EMT markers were found in the human tumour xenografts from the Rag/MKR mice, compared with Rag/WT mice.*

We examined protein expression of known EMT proteins in the tumours of the Rag/MKR and Rag/WT mice. Similar to our findings in the MTB/TAN/MKR

tumours, we again found an increase in vimentin protein expression in the tumours from the Rag/MKR mice (Figure 28B, D). In addition, an increase in other EMT markers, including Zeb1 (Figure 28A, C) and MMP-9 (Figure 29A, C) were observed. Consistent with our previously published studies on MVT1 tumours in MKR mice (44), increases in c-myc and VEGF-A were observed in the MDA-MB-231 tumours from Rag/MKR mice compared with Rag/WT mice (Figure 29A, D, E). We also found increased protein expression of Foxo3a (Figure 29A, B) in the tumours from the Rag/MKR mice.

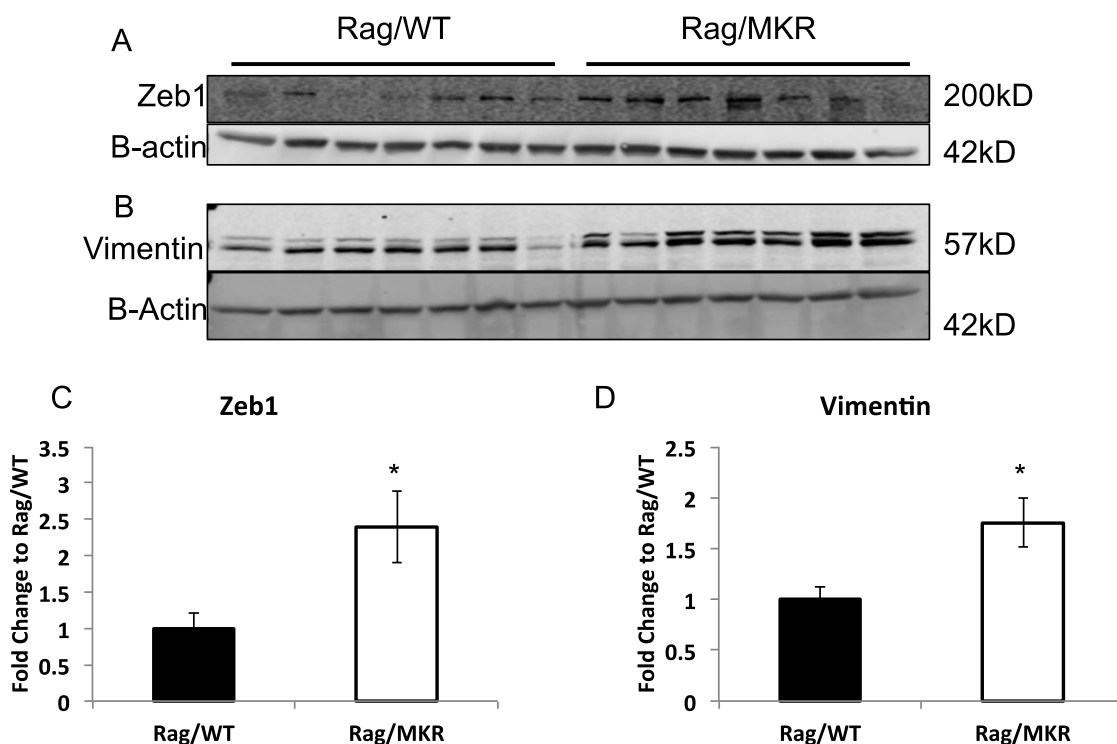


**Figure 28 Vimentin and Zeb-1 expression in MDA-MB-231 tumours from Rag/WT and Rag/MKR mice**

(A) Western blot analysis of tumour lysates from MDA-MB-231 tumours from Rag/WT and Rag/MKR mice immunoblotted for (A) Zeb-1 and beta actin, (B) vimentin and beta actin. (C) Densitometric quantification of Zeb-1/beta actin, and (D) vimentin/beta actin. n=7 per group. Graphs represent mean of each group and error bars indicate SEM. \*P value <0.05 between groups.



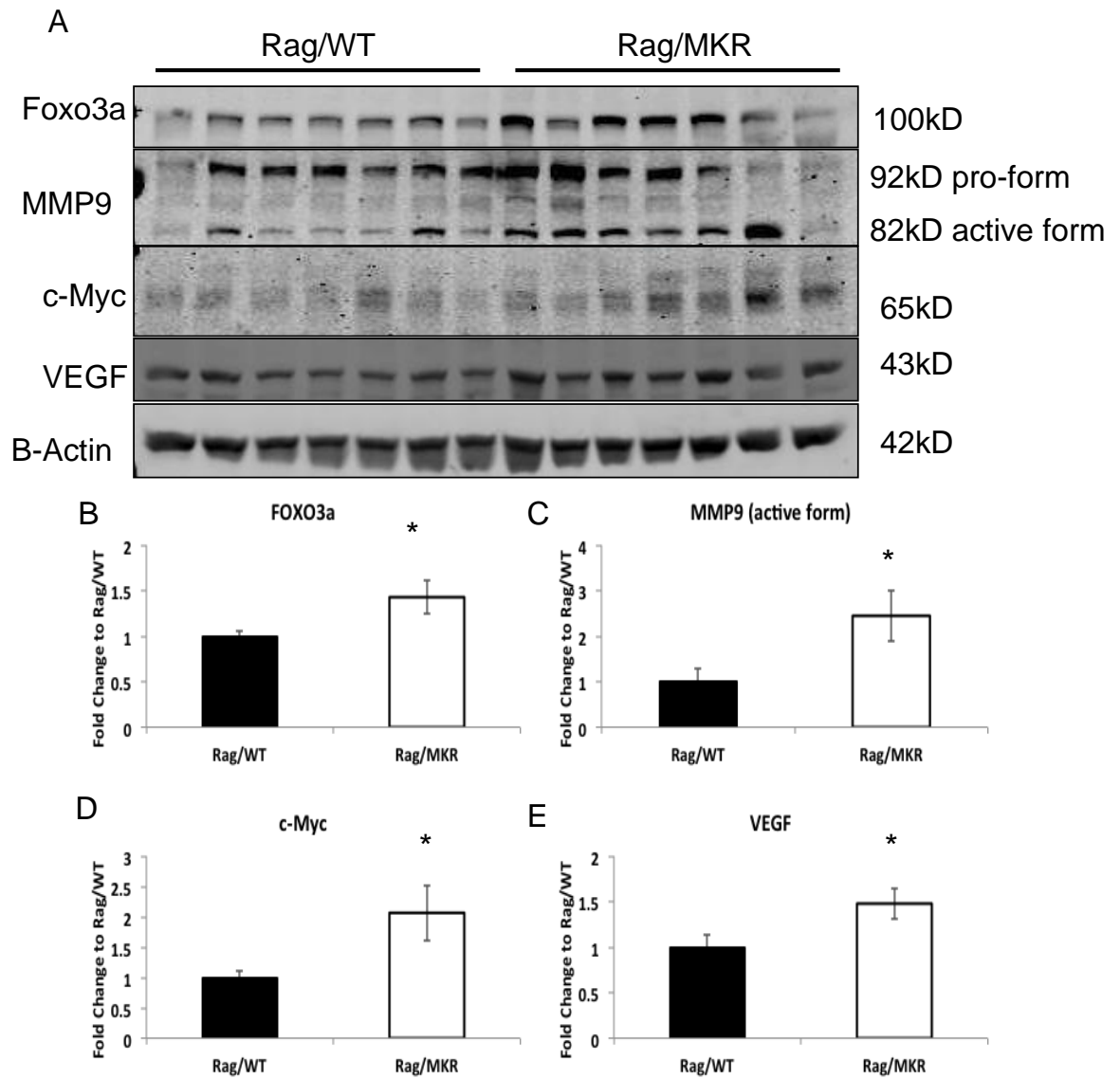


**Figure 29 Changes in EMT-related proteins in MDA-MB-231 Tumours from Rag/WT and Rag/MKR mice.**

(A) Western blot analysis of tumour lysates from MDA-MB-231 tumours from Rag/WT and Rag/MKR mice immunoblotted for (A) Foxo3a, MMP9, c-myc, VEGF and beta actin, (C-E) Densitometric quantification of (B) Foxo3a/beta actin, (C) MMP9/beta actin, (D)c-myc/beta actin, (E) VEGF/beta actin. n=7 per group. Graphs represent mean of each group and error bars indicate SEM. \*P value <0.05 between groups.

*Insulin increases the invasion of MDA-MB-231 cells in vitro.*

To examine if insulin directly increased the invasion of human triple negative breast cancer cell lines in vivo, we performed a transwell migration assay. As described in the Materials and Methods section, 400,000 MDA-MB-231 cells were seeded in the upper chamber of a transwell plate in serum free DMEM with 0.1% BSA, with and without supplementation with 10nM insulin in the lower chamber. An increase in the invasion of MDA-MB-231 cells was observed in response to insulin (Figure 30).

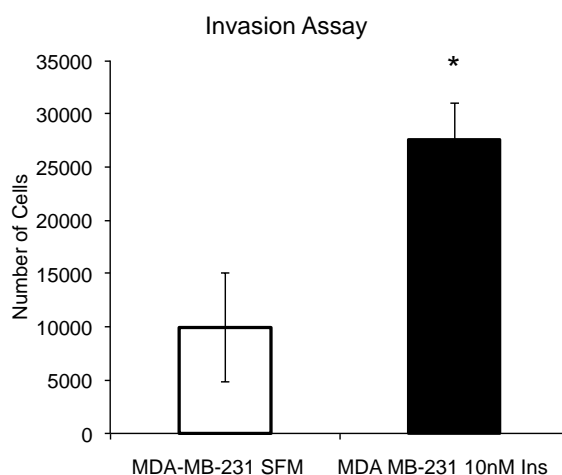


**Figure 30 Invasion of MDA-MB-231 cells in response to insulin in vitro**

Number of cells that invaded through matrigel invasion chamber after 24 hours. Cells were stained with crystal violet and the cell number was calculated from a standard curve of crystal violet absorbance to cell number in a 96 well plate. The graph represents a mean of 3 plates per group, and error bars represent SEM. The assay was performed on two separate occasions with consistent results.

Overall, these data demonstrate that the tumour xenografts from the human triple negative breast cancer cell line, MDA-MB-231 grow larger and form more metastases in hyperinsulinaemic mice. The increase in metastases was associated with protein expression changes in the primary tumour, including an increase in vimentin and c-myc protein expression, consistent with our previous findings of increased vimentin in the NeuNT tumours, as described in Chapter 1, and the increase in c-myc previously found in our published studies (44).

Therefore, we next aimed to determine whether insulin directly regulates vimentin and c-myc expression, and if vimentin is merely a marker of EMT or has a functional role in mediating breast cancer metastasis in setting of hyperinsulinaemia.

### **Chapter 3. Vimentin in Hyperinsulinaemia-mediated Breast Cancer Metastasis.**

As described in Results Chapters 1 and 2, we found an increase in vimentin protein expression in the transgenic NeuNT tumours in the MTB/TAN/MKR mice, and in the MDA-MB-231 tumours of the Rag/MKR mice compared with their respective controls. However, the immunofluorescent co-staining with anti-vimentin and anti-Neu antibodies in the MTB/TAN/MKR and MTB/TAN mice demonstrated that most of the vimentin-positive cells in the tumours did not stain for Neu, and conversely, the Neu-positive cells did not stain for vimentin. This raised the possibility that the vimentin-positive cells were tumour invading fibroblasts, rather than tumour cells that had undergone EMT. We therefore wished to determine if hyperinsulinaemia led to increased vimentin expression within the tumour cells, and if silencing vimentin affected tumour metastasis in the setting of hyperinsulinaemia.

#### *MVT1 Tumours from Hyperinsulinaemic Mice have Increased Vimentin Protein Expression*

For these studies we used the MVT1 breast cancer cell line, this cell line, as described in the Materials and Methods section was derived from explant culture from mammary tumours from the MMTV-c-myc/vegf mouse model. The LeRoith lab has previously found that these tumours grow more rapidly in the hyperinsulinaemic MKR mice, and develop more numerous pulmonary metastases after orthotopic or intravenous injection (44).

We first aimed to determine if the MVT1 tumours from the MKR mice expressed increased vimentin, compared to tumours from WT mice. For this study we used immunocompetent female MKR mice and at 8 weeks of age mice were injected with 100,000 MVT1 cells into the 4<sup>th</sup> mammary fat pad, as previously described (46, 115). Consistent with our previous studies, there was a significant increase in tumour size in MKR mice when compared to the tumours from the WT mice (Figure 31A) (44). We also observed significant an increase in average number of pulmonary macrometastasis per mouse in the MKR mice compared to WT mice (Figure 31B). At the end of the study, the primary tumours from WT and MKR mice were flash frozen and protein was extracted, and fixed in formalin for paraffin embedding, processing and subsequent immunofluorescence analysis. We found

an increase in vimentin protein expression in the MVT1 tumours from the MKR mice compared with tumours from WT mice by western blot (Figure 31C, D) and immunofluorescent staining of FFPE tumours (Figure 32A, B).

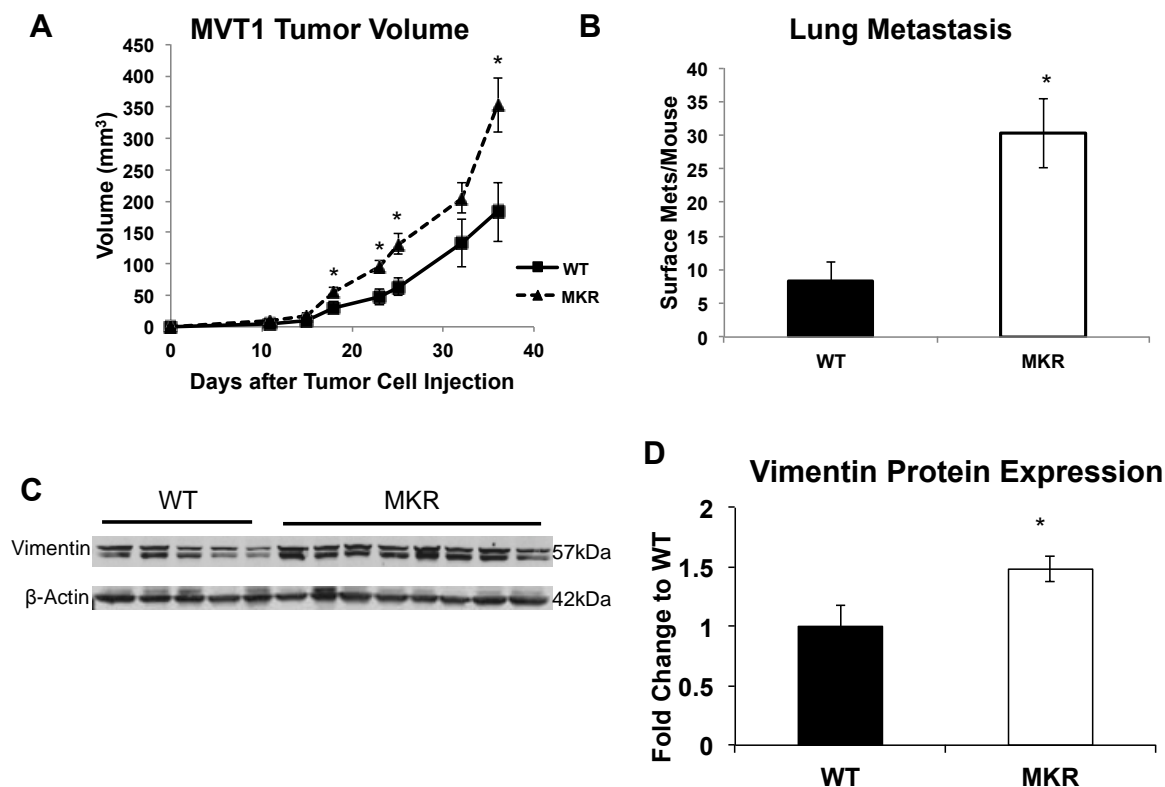


**Figure 31 MVT1 Tumours have increased growth and metastasis in the MKR mice, associated with increased vimentin expression.**

(A) 100,000 MVT1 tumour cells were injected at Day 0 into the 4<sup>th</sup> mammary fat pad of WT and MKR mice. The tumour was measured twice weekly thereafter until termination of the study. (B) Pulmonary macrometastases were greater in the MKR compared to WT mice. (C) Representative western blot of vimentin expression in the WT and MKR mice. (D) Densitometric analysis of vimentin / beta actin protein expression in MVT1 tumours from WT and MKR mice (n=8-11 per group). Graphs represent the mean of each group and error bars are SEM. \* P value <0.05.

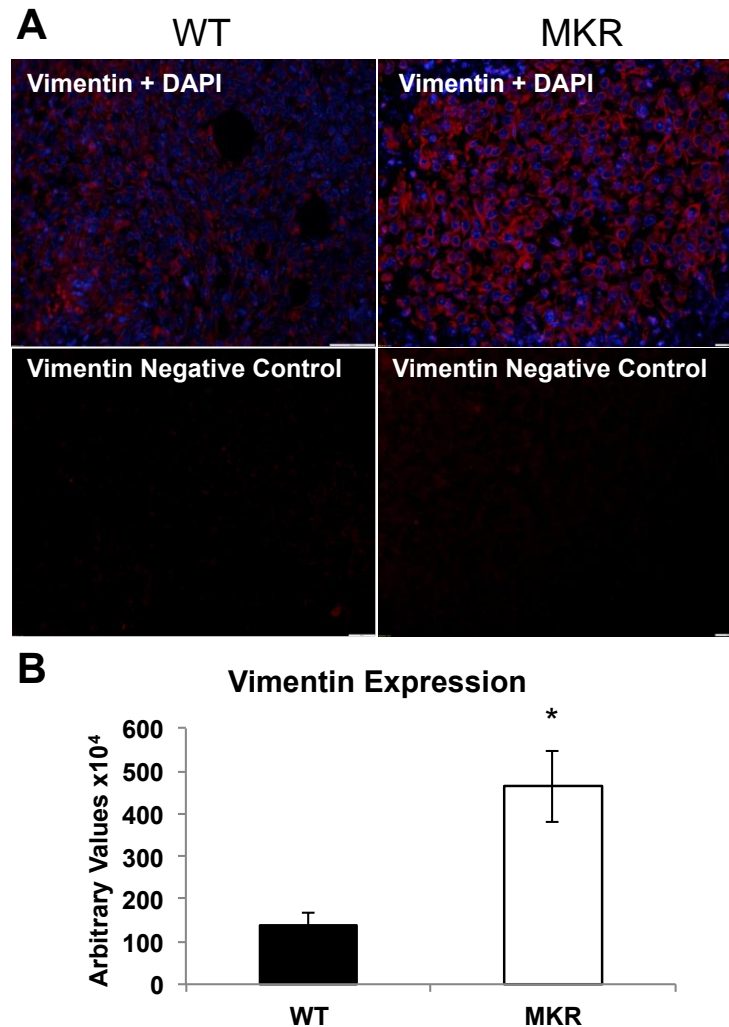


**Figure 32 Vimentin expression in MVT1 Tumours by Immunofluorescent Staining.**

(A) Representative images of MVT1 tumour sections stained with anti-vimentin primary antibody (Red) and counterstained with DAPI (blue) (upper panels) and vimentin negative controls (lower panels). (B) Quantification of vimentin expression in the tumours (n=10 per group). \* P value <0.05. Graphs represent mean per group and error bars are SEM.

As previously discussed in Chapter 1, tumours may be invaded by tumour associated fibroblasts that also are vimentin positive. Therefore, we aimed to determine that it was the tumour cells that expressed vimentin, and had increased vimentin expression in the MKR mice, rather than infiltrating cells. To do this, we introduced an EGFP expression vector into the MVT1 cells by lentiviral

transduction, and after puromycin selection, we injected the EGFP expressing MVT1 cells into the MKR and WT mice. Tumours were allowed to grow in both WT and MKR mice, and at the end of the study, tumours were fixed in formalin, processed embedded in paraffin, and sectioned for immunofluorescence staining with anti-GFP antibody and anti-vimentin antibody. Immunofluorescence staining of these sections showed that the GFP positive cells also stained for vimentin, demonstrating that increase in vimentin in the MVT1 tumours is from increased expression in the primary tumour cells and not from invading fibroblasts (Figure 33).

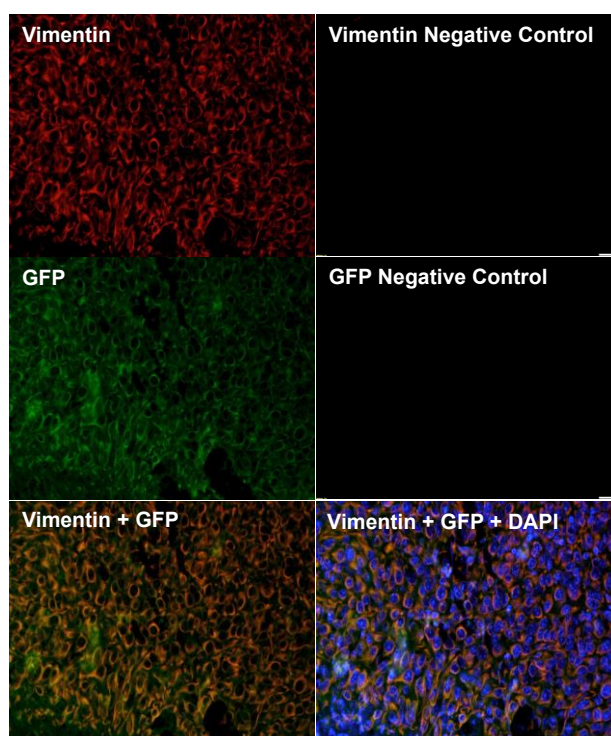


**Figure 33 GFP and Vimentin co-Staining of MVT1 Tumours.**

Representative images of anti-vimentin (red) and anti-GFP (green) antibody immunofluorescence staining of MVT1 tumours with respective negative controls and DAPI (blue) nuclear counterstaining.

#### *Insulin Increases Vimentin Protein Expression in Vitro*

To determine whether the increase in vimentin expression was a direct effect of insulin on the tumour cells, we examined the effect of insulin on vimentin protein expression in vitro. We plated MVT1 cells to 70% confluency in 10cm plates. The cells were serum starved overnight and stimulated with 10nM of insulin for 48

hours. We observed a significant increase in vimentin protein expression following the insulin stimulation (Figure 34).

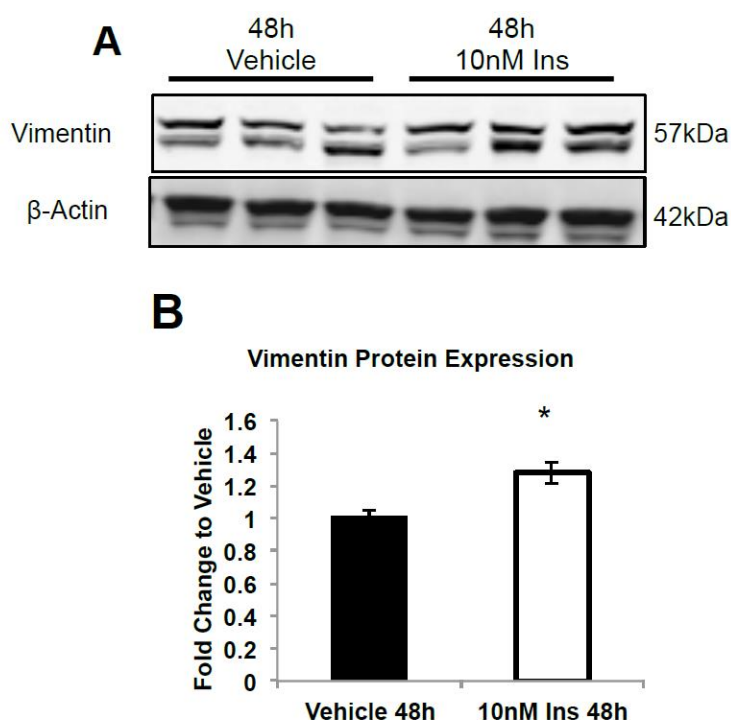


**Figure 34 Insulin Stimulation Increases Vimentin Protein Expression in Vivo**

(A) Representative western blot demonstrating insulin stimulation increasing vimentin expression at 48 hours. (B) Densitometric quantification of vimentin / beta actin on western blot. \* P value <0.05 between groups. Graph represents the mean of each group, and error bars are SEM. n=3 per group per experiment. Experiment was performed on three occasions with consistent results.

*Vimentin Protein Bands Displayed Multiple Different Post-Translational Modifications and Co-Immunoprecipitated with ATP Synthase.*

As we consistently observed two bands of different molecular weights on the western blots upon immunoblotting with anti-vimentin antibody, and found an increase in the band of higher molecular weight consistently in our in vivo tumour studies. We aimed to determine if these bands represented different isoforms of vimentin, or if there were different post-translational amino acid modifications in the two vimentin bands, causing an increase in the molecular weight of the protein.



We therefore immunoprecipitated vimentin from MVT1 cell protein lysate and analyzed the bands by LC-MS at the Mount Sinai proteomics core facility. As shown in Figure 35, the vimentin band of higher molecular weight had two phosphorylation sites at Thr417 and Ser420, not present on the lower band. In addition, there were multiple asparagine (N) and glutamine (Q) deamidation sites, histidine (H) and glutamine (Q) oxidation sites, and a single glutamine to pyroglutamate transformation on the higher molecular weight band, not found on the lower molecular weight band. In addition, vimentin co-immunoprecipitated with the ATP synthase alpha and beta subunits.

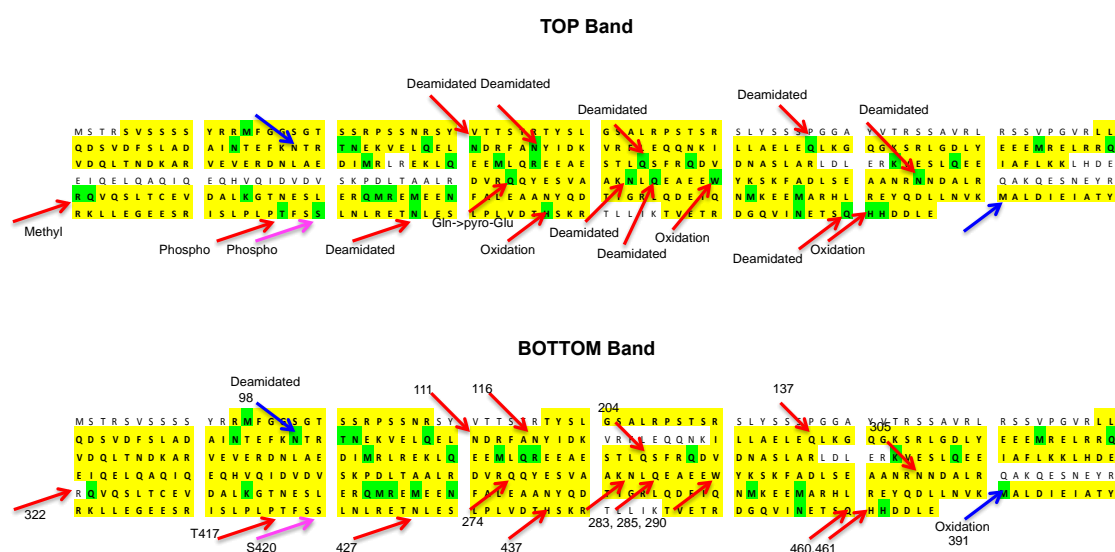


**Figure 35 Amino acid sequence and modifications of vimentin bands as determine by LC-MS.**

The green highlighted amino acids are the amino acids that were modified in one or other of the vimentin bands. The red and pink arrows indicate amino acids that are modified on the top (higher molecular weight) band and not on the bottom (lower molecular weight) band, and the blue arrows indicate amino acids that are modified on the bottom band but not the top band. The numbers on the bottom indicate the number of the amino acid in the mouse vimentin protein and the modification is denoted on the top or bottom band, depending on where it was observed. (Glu →pyro-Glu indicates a glutamine to pyroglutamate modification).

### *Silencing Vimentin in MVT1 Cells Decreased Cell Invasion But Did Not Alter Insulin Signaling or Cell Proliferation*

To determine if vimentin was a marker of EMT, or had a functional role in insulin-mediated cell migration, MVT1 cells were transduced with lentiviral plasmid DNA with non-coding shRNA sequence or vimentin shRNA sequences, as described in the Materials and Methods section. After puromycin selection, the cells were analyzed for the degree of vimentin knockdown by protein and RNA analysis. The vimentin protein from the non-coding control showed no difference when compared to the parental (non-transduced) MVT1 cells line (Figure 36). Two vimentin shRNA sequences led to significant decrease in vimentin protein expression. We observed a 60% knockdown of vimentin protein expression in clone Vimentin-317673 and a 77% knockdown of vimentin protein expression in clone Vimentin-317676 (Figure 36A). Quantitative Real Time PCR analysis showed a 60% and a 90% decrease in vimentin gene expression in the clones Vimentin-317673 and Vimentin-317676, respectively (Figure 36B).

As vimentin has been reported to be involved in signal transduction (128, 155), we next determined if silencing vimentin affected the insulin-signaling pathway. The MVT1 control and MVT1 vimentin knockdown cells were plated in 6cm plates, serum starved overnight and stimulated with 10nM insulin for 15min. Following the insulin stimulation we observed an increase in AKT (Ser473) and ERK (Thr202/Tyr204) phosphorylation in both the MVT1 control and MVT1 vimentin knockdown cells (Figure 36C and D). This indicated that the vimentin knockdown did not alter the insulin-mediated activation of the PI3K/Akt and MAPK pathways.

The MVT1 control and vimentin knockdown cells were analyzed for proliferation, migration and invasion. 5,000 MVT1 control and vimentin knockdown cells were plated in 96-well plates and analyzed for cell proliferation at 24, 48, and 72h. There was no difference in calculated cell number between the MVT1 control and MVT1 vimentin knockdown cells at each time point using the CCK8 cell proliferation assay (Figure 37A). There was no difference in the MVT1 control or vimentin knockdown migration capacity through an 8 $\mu$ m pore (Figure 37B). Interestingly, we did observe a significant decrease in the invasion capacity of the MVT1 vimentin knockdown cells compared to the MVT1 control cells in full serum

(Figure 37C). Stimulation with insulin in serum free conditions led to an increase in invasion of MVT1 control cells, but did not significantly increase the invasion of MVT1 vimentin knockdown cells (Figure 37D). Our data demonstrate that vimentin is important for mediating insulin's effect on cell invasion, but is not a key mediator of insulin receptor signal transduction, or cellular proliferation.

*Knockdown of vimentin in MVT1 tumours led to a decreased number of pulmonary metastases in the hyperinsulinaemic MKR mice*

In order to study the effects of knocking down vimentin on tumour growth and lung metastases, WT and MKR mice were split into 4 groups and orthotopically injected with 100,000 MVT1 control cells (8-10 mice per group) and 100,000 MVT1 vimentin knockdown (Vimentin-317676 clone) cells (10-13 mice per group). The four groups were the WT-noncoding control, WT-vimentin knockdown, MKR-noncoding control, and MKR-vimentin knockdown. A significant increase in primary tumour size was found in the MKR-noncoding control mice compared with the WT-noncoding control mice (Figure 38). However, no significant difference was observed between the tumour volume of the vimentin knockdown and noncoding control tumours in MKR or WT mice (Figure 38A).

We observed a significant increase in average number of surface pulmonary metastases per mouse from the MVT1 noncoding control tumours in the MKR group compared to WT group, consistent with our previous studies on non-transduced MVT1 tumours (Figure 38B). There was a significant decrease in pulmonary macrometastases in the MKR-vimentin knockdown group compared to the MKR-noncoding control group (Figure 38B).

Western blot of the protein lysates from the primary tumours of the four groups revealed an increase in vimentin protein expression in the MKR-noncoding control group compared to the WT-noncoding control group. We also confirmed that the primary tumours derived from the MVT1 vimentin knockdown cells, showed a significant decrease in vimentin protein expression at the end of the in vivo study (Figure 38C).

To evaluate the importance of vimentin in the extravasation of tumour cells from the circulation into lungs, we performed tail vein injections on the WT and MKR mice, again with four groups of mice: WT-noncoding control, WT-vimentin

knockdown, MKR-noncoding control, and MKR-vimentin knockdown. We observed a similar, but not statistically significant, decrease in lung macrometastases in the vimentin knockdown groups, compared to the control groups (Figure 38D).

Overall, these results demonstrate that insulin increases vimentin protein expression in vitro and in vivo, and that vimentin is an important regulator of pulmonary metastases in this c-myc / vegf driven breast cancer model in the setting of hyperinsulinaemia. Interestingly, silencing vimentin led to decreased pulmonary metastases to a similar extent in both the WT and MKR mice after tail vein injection, but led to a greater relative reduction in metastases in the MKR mice after orthotopic tumour cell injection. This suggests that in the setting of hyperinsulinaemia, the higher vimentin expression, promotes the invasion of the primary tumour cells and/or migration toward blood vessels, rather than increasing the extravasation of tumour cells into distant organs. However, the reduction of metastases in both WT and MKR mice after tail vein injection suggests that vimentin also plays a role in extravasation into metastatic sites. In the primary tumours of the MKR mice, an increase in vimentin expression was found in the tumours with the vimentin knockdown, compared to WT mice. This increase may be due to hyperinsulinaemia stimulating vimentin expression, even in the presence of shRNA gene silencing, due to incomplete silencing. Alternatively, it may be due to the presence of other vimentin positive cells within the tumours that are more prevalent in the tumours of the MKR mice. Despite this increase, there were less pulmonary metastases in the MKR mice with vimentin silencing, implying that an incomplete reduction of vimentin levels is sufficient to reduce metastases. Future studies are required to determine the precise mechanisms by which insulin increases vimentin expression. In addition, further studies should be performed on different breast cancer cell lines to determine if silencing vimentin leads to decreased metastases in all cell lines, or only in c-myc driven tumours. In this study, we did not explore the effect of insulin on the post-translational modifications of vimentin discovered by LC-MS, or the importance of the interaction between vimentin and ATP-synthase. These results will be the subject of further investigation. Finally, pharmacological agents that target vimentin should be explored in pre-clinical studies to determine the value of reducing vimentin expression is an important strategy to reduce lung metastases in individuals with hyperinsulinaemia and breast cancer.

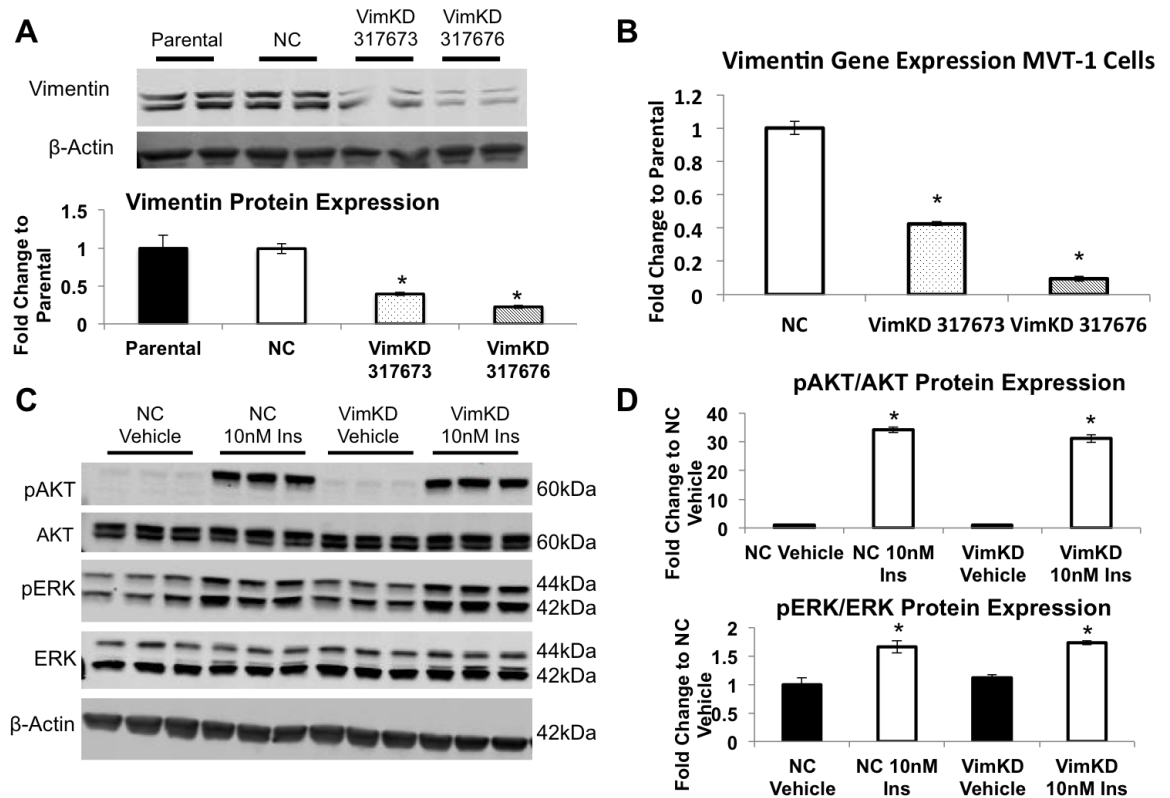


**Figure 36 Silencing vimentin in MVT1 cells did not alter insulin-mediated activation of Akt and Erk in vitro.**

(A.) Lentiviral shRNA for vimentin and control non-coding (NC) sequences was used to generate MVT1 cells with a knockdown of vimentin protein expression, and control cell lines (A) Western blot analysis of vimentin expression in MVT1 cell lines after lentiviral transduction compared to the non-transduced (parental) cell line (upper panel) and densitometry analysis of protein expression of the parental, noncoding control, Vimentin 317673 clone, and Vimentin 317676 clone (lower panel). (B) Real Time PCR gene expression analysis by SyBr from transduced MVT1 cell lines. (C) Western blot analysis of cell lysates from MVT1 non coding and 317676 clone after fifteen minute stimulation with insulin (10nM Ins) after overnight serum starvation. (D) Densitometry analysis of western blot of pAKT/AKT and pERK/ERK. \*  $p < 0.05$  between the vimentin knockdown (VimKD) cells and the noncoding shRNA transduced control (NC) cells (B) or between the insulin stimulated group and their respective unstimulated control (D) Graphs represent mean per group and error bars are SEM.

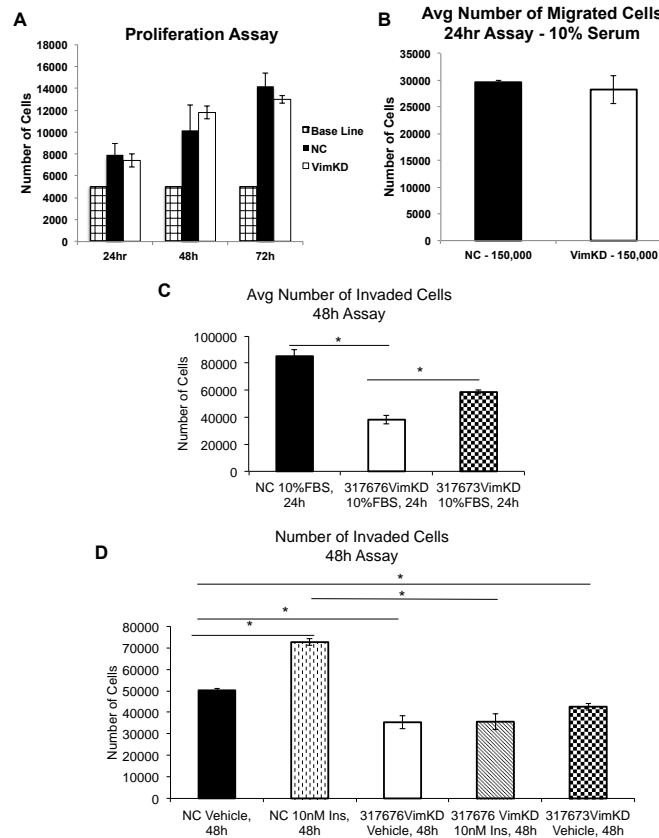


**Figure 37 Proliferation, migration and invasion assays in MVT1 cells with vimentin knockdown.**

(A) CCK-8 was used to assess cell proliferation in MVT1 non-coding control (NC) and MVT1 vimentin knockdown (VimKD) cells. 5,000 cells were plated and analyzed for cell proliferation at 24, 48 and 72 hours. (B) 150,000 MVT1 NC and MVT1 VimKD cells were plated in 0.8 $\mu$ m inserts. The number of cells that migrated through the insert after 24 hours was quantified by crystal violet staining. (C) 400,000 MVT1 NC and MVT1 VimKD cells were plated into 0.8 $\mu$ m inserts coated with matrigel in DMEM with 10% FPS and 1% penicillin streptomycin, or (D) in serum free medium stimulated with PBS+0.1% BSA (vehicle) or 10nM insulin. The number of cells that invaded through the matrigel-coated insert after 48 hours was quantified by crystal violet staining. Graphs represent the mean of each group, error bars are SEM. \*P value <0.05 between groups. Each experiment was performed 2-3 times with consistent results.

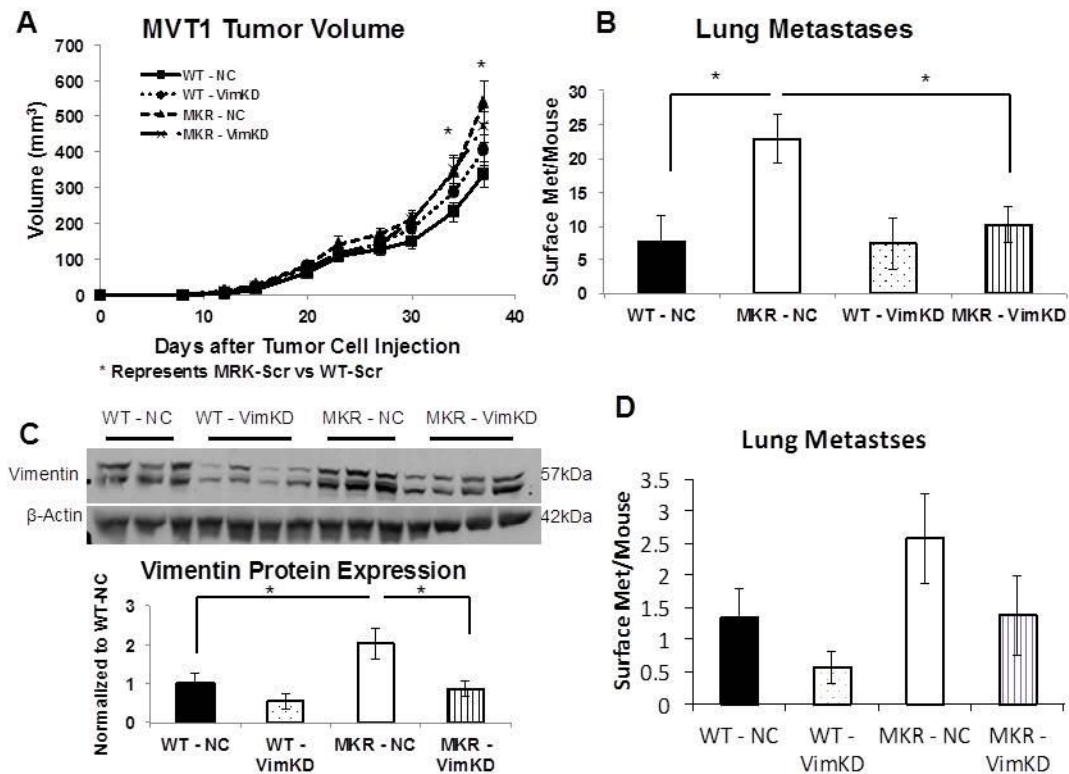


**Figure 38 Vimentin knockdown reduced pulmonary metastases in the MKR mice**

Wild type (10 per group) and MKR (13 per group) mice were injected with 100,000 of MVT1 noncoding control (NC) and 100,000 of MVT1 vimentin KD (VimKD) into the 4<sup>th</sup> mammary fat pad. (A) Tumour volumes were measured with calipers. Significant difference between the tumour sizes of MKR-NC and WT-NC group was observed. (B) Numbers of surface pulmonary macrometastases in WT and MKR mice. (C) Tumour tissue was extracted and analyzed for Western Blot for vimentin antibody. Representative blot is shown. Densitometry of vimentin/beta actin of representative blot n=3 WT-NC, n=4 WT-VimKD, n=3 MKR-NC, and n=4 MKR-VimKD. (D) Number of pulmonary metastases after intravenous tail vein injection of 10,000 MVT1 cells. Graphs represent mean per group and error bars are SEM. \* P value <0.05.

## **Chapter 4. The role of the Insulin Receptor in Mammary Gland Development and Breast Cancer Growth in the Setting of Hyperinsulinaemia**

As discussed in Chapter 1, while we have found that hyperinsulinaemia increases the growth of many different orthotopic and xenograft tumours, as well as transgenic tumours in our animal model, we have not demonstrated that the effects of insulin are directly mediated through the IR, rather than indirectly by changes in IGFBP's and bioavailable IGF-1. Therefore, in this Chapter we aimed to determine some of the in vitro and in vivo effects of silencing the IR on the growth and characteristics of mammary epithelial cells and cancer cells.

*MMTV-Cre mediated deletion of the IR leads to decreased side-branching of the mammary epithelium in WT and MKR mice.*

The LeRoith lab had previously described that the MKR mice had increased terminal end bud formation and increased branching of the mammary epithelium, when compared to WT mice. This was associated with an increase in IR mRNA expression (115). The role of the IR in mammary gland development has not been previously explored because whole body knockout of the IR in mice is fatal shortly after birth (83). One recent mouse study using a Blg-Cre to delete the IR in mouse mammary epithelial cells demonstrated that the IR is important for lactation (114). We generated the MMTV-Cre<sup>+/+</sup> IRL<sup>-</sup> and MMTV-Cre<sup>-/-</sup> IRL<sup>LL</sup> mice as described in the Materials and Methods section and Figure 17. In order to identify mice with a single floxed allele and a null allele (indicating Cre-mediated recombination of the IR), we analyzed tail DNA and selected MMTV-Cre positive mice with one floxed and one null allele as study mice, and used MMTV-Cre negative IRL<sup>LL</sup> mice as controls.

To validate the IR deletion in the mammary epithelial cells, we digested the mammary glands from 8-12 week old MMTV-Cre<sup>+/+</sup> IRL<sup>-</sup> and MMTV-Cre<sup>-/-</sup> IRL<sup>LL</sup>, and separated the mammary epithelial cells from the adipose tissue and fibroblasts by serial centrifugation. DNA and protein were isolated from the mammary epithelial cells to confirm Cre-mediated IR loxP recombination (Figure 39A), and a loss of the IR $\beta$  protein expression in the mammary epithelial cells (Figure 39B). In addition immunohistochemistry staining for IR $\beta$  was performed on FFPE mammary glands from the MMTV-Cre<sup>-/-</sup> IR<sup>fl/fl</sup> and MMTV-Cre<sup>+/+</sup> IR<sup>fl/-</sup> mice



(Figure 39C). In MMTV-Cre<sup>+/+</sup> IRL<sup>-/-</sup> mice, a decrease in IR $\beta$  protein was found on both western blotting and IHC staining, compared to control mice (Figure 39C).

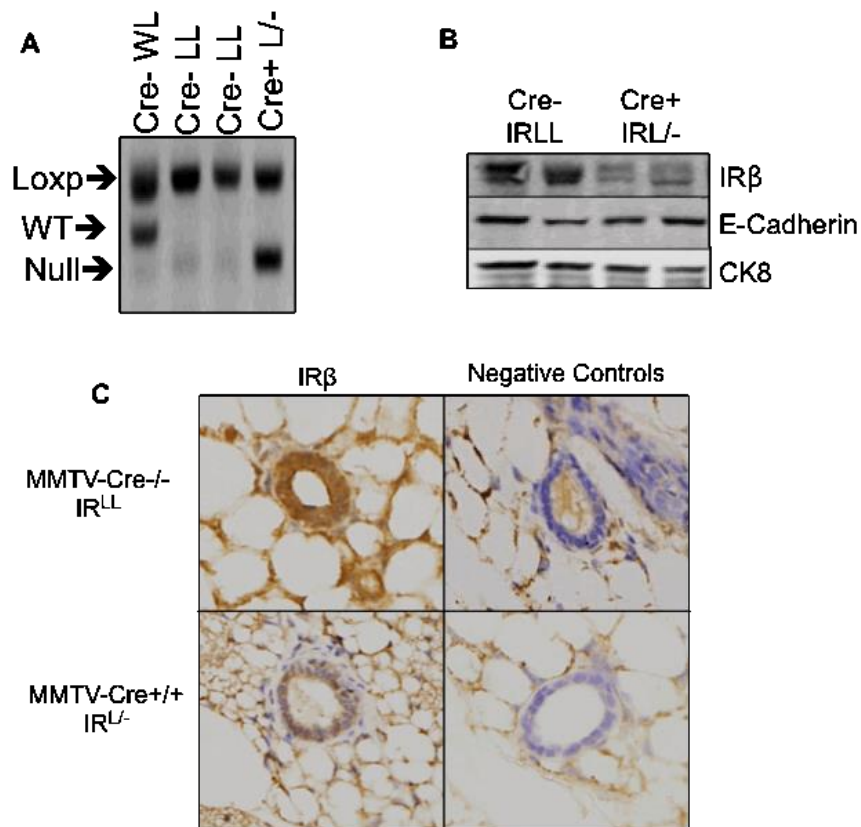


**Figure 39 IR expression in the mammary epithelial cells of MMTV Cre IR floxed mice.**

(A) DNA was isolated from the mammary epithelial cells of MMTV Cre negative (Cre<sup>-</sup>) IR heterozygous WT/Loxp, homozygous IRL<sup>LL</sup>, and MMTV Cre<sup>+/+</sup> (Cre<sup>+</sup>) IR Loxp/null (L<sup>-</sup>) mice, subjected to PCR using the primers in Table 1, and run on an agarose gel. The LoxP band is 334bp, the WT band is 300bp and the Null band is 284bp. (B) Western blot of mammary epithelial cells immunoblotted for IR $\beta$ , E-cadherin (a marker of epithelial cells) and cytokeratin 8 (CK8). (C) Immunohistochemistry staining for IR $\beta$  in the mammary epithelial cells from control (MMTV-Cre<sup>-/-</sup> IRL<sup>LL</sup>) and mammary epithelial cell specific knockout (MMTV-Cre<sup>+/+</sup> IRL<sup>-/-</sup>) mice. Pictures were taken at 40X magnification, and cropped to display comparable representative transverse sections of similar ducts.

Whole mount analysis was performed on 12 week old female MMTV-Cre<sup>-/-</sup> IR<sup>fl/fl</sup>, MMTV-Cre<sup>+/+</sup> IR<sup>fl/-</sup> and MKR/MMTV-Cre<sup>-/-</sup> IR<sup>fl/fl</sup> and MKR/MMTV-Cre<sup>+/+</sup> IR<sup>fl/-</sup> mice 48 hours after estradiol and progesterone injection and revealed that MMTV-Cre<sup>+/+</sup> IR<sup>fl/-</sup> and MKR/MMTV-Cre<sup>+/+</sup> IR<sup>fl/-</sup> mice had decreased side branching, compared to their respective MMTV-Cre<sup>-/-</sup> controls (Figure 39A). IR knockout in the mammary epithelial cells of the MKR mice, partially reversed the hyperbranching mammary epithelial phenotype. As the progesterone receptor (PR) is important for mammary epithelial side branching (9), and as cross talk between IGF and PR signaling pathways have previously been described (35), we hypothesized that the decrease in mammary gland side branching was due to decreased PR expression in the mice with MMTV-Cre mediated IR deletion. However, immunofluorescence analysis of PR expression in the MMTV-Cre<sup>-/-</sup> IR<sup>fl/fl</sup>, MMTV-Cre<sup>+/+</sup> IR<sup>fl/-</sup> mice revealed no difference in PR expression between the mice (Figure 39B upper panels). Similarly, no changes were observed in the expression of cytokeratin 8 (CK8), a marker of luminal epithelial cells, or cytokeratin 5 (CK5), a marker of myoepithelial cells in the MMTV-Cre<sup>-/-</sup> IR<sup>fl/fl</sup>, MMTV-Cre<sup>+/+</sup> IR<sup>fl/-</sup> mice (Figure 39B lower panels). These data indicate that the IR is important for excess mammary epithelial side branching of the MKR mice, as the increased branching is partially reversed in the IR knockout mice. However the reduction in side branching is not mediated by a reduction in PR expression. Further, loss of the IR does not disrupt the luminal or myoepithelial cells in the normal mammary epithelial ducts.

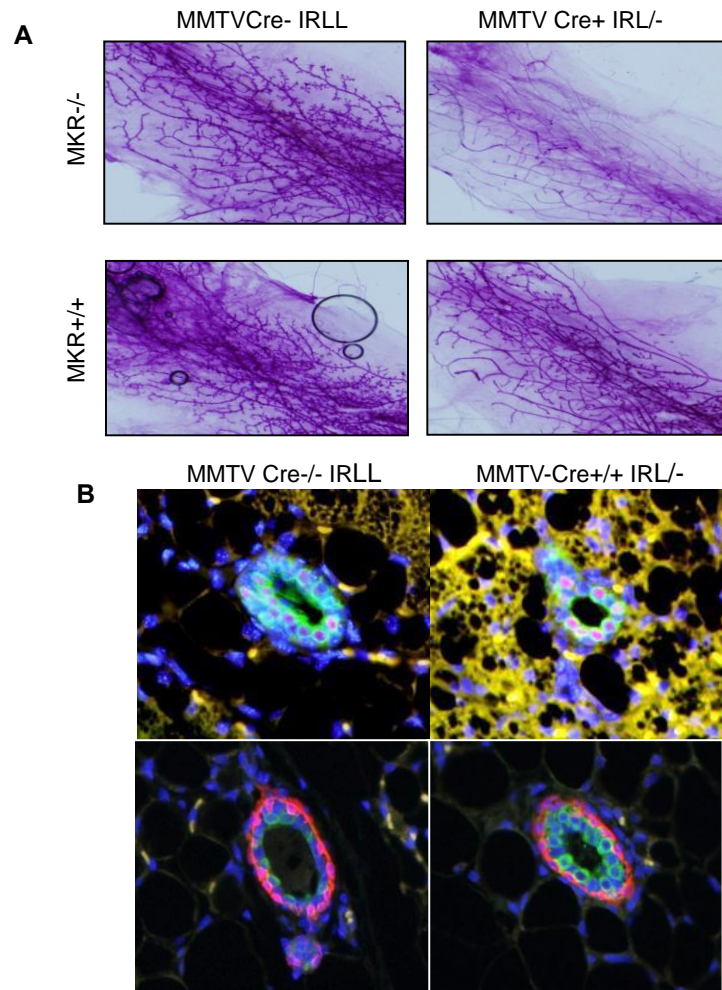


**Figure 40 Whole mount and immunofluorescence analysis of the mammary epithelial cells of the MMTV Cre IR floxed mice.**

(A) Whole mount analysis of the 4<sup>th</sup> mammary gland of MKR negative and positive mice with normal IR expression and with IR knocked out in the mammary epithelial cells. Photographs were taken at 2.5X magnification. (B) Immunofluorescence staining of progesterone receptor (red) and cytokeratin 8 (green) upper panels, and of cytokeratin 8 (green) and cytokeratin 5 (red) lower panels, both with nuclear DAPI (blue) counterstain. Pictures were taken at 40X magnification, and cropped to display comparable representative transverse sections of similar ducts.

*Silencing the IR attenuates the growth of human triple negative LCC6 breast cancer xenografts in the hyperinsulinaemic Rag/MKR mice.*

We examined the effect of hyperinsulinaemia and silencing the IR on the growth of a human triple negative breast cancer xenograft model, derived from the LCC6 cells. We injected  $5 \times 10^6$  LCC6 cells with normal IR expression (transduced with lentiviral particles with noncoding shRNA) and shRNA mediated IR knockdown into the 4<sup>th</sup> mammary fat pad of the Rag/WT and Rag/MKR mice. Similar to our findings in the MDA-MB-231 (as described in Results Chapter 2), we found a significant increase in the growth of the LCC6 tumours carrying the noncoding shRNA (NC) in the Rag/MKR mice, compared to Rag/WT mice (Figure 41). However, tumours derived from the LCC6 IR shRNA (IRKD) in the Rag/MKR mice were significantly smaller in volume than the LCC6-NC tumours, and were of similar size to tumours in the Rag/WT mice (Figure 41). At the end of the study tumour weights were also significantly smaller in the LCC6-IRKD xenografts in the MKR mice, compared to the LCC6-NC xenografts (Figure 41).

Western blot analysis of the tumour lysates revealed a decrease in pAkt signaling in the LCC6 IR-KD xenografts from both Rag/WT and Rag/MKR mice, compared to their respective LCC6-NC controls (Figure 42A, Figure 42B). No decrease in Erk1/2 phosphorylation was seen in the LCC6-IRKD tumours, but an increase in total Erk1/2 was observed in the LCC6-IRKD tumours in both Rag/WT and Rag/MKR mice. Decreased protein expression of c-myc and vimentin were observed in the LCC6-IRKD tumours compared to the LCC6-NC tumours (Figure 42). Therefore, silencing the IR in human triple negative breast cancer xenografts leads to reduced tumour growth in the hyperinsulinaemic mice and decreased expression of c-myc and vimentin, that we have previously found to be increased in a number of breast cancer subtypes in the setting of hyperinsulinaemia.

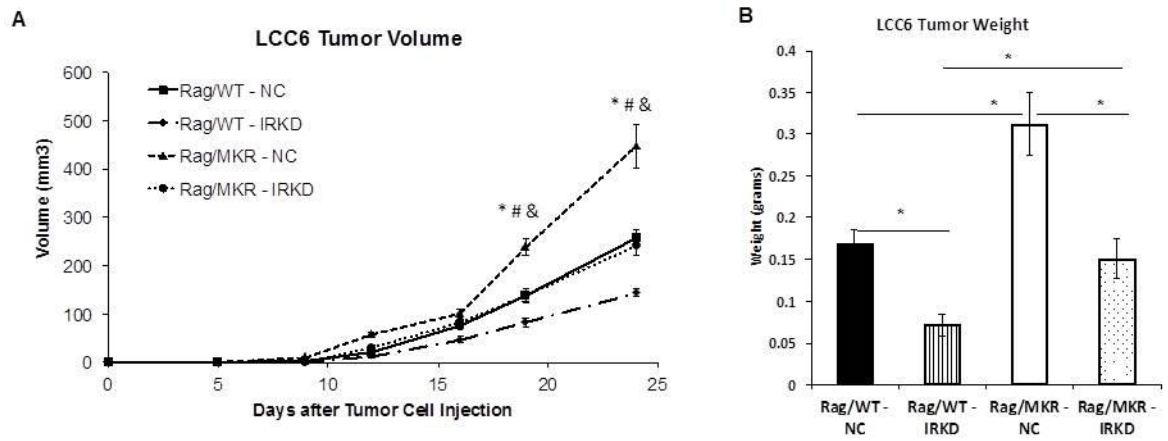


**Figure 41 LCC6 tumour xenograft volume and weight in cells with normal and shRNA mediated silencing of the IR**

(A) LCC6 tumour volumes after injection of cells on day 0. Rag/WT and Rag/MKR mice were divided into two groups that received either LCC6 cells transduced with lentiviral particles carrying non-coding shRNA (NC), or IR targeting shRNA (IRKD). \* P value <0.05 between Rag/MKR-NC and Rag/WT-NC, # P value <0.05 between Rag/MKR-NC and Rag/MKR-IRKD, & P <0.05 between Rag/WT-NC and Rag/WT-IRKD. (B) Tumour xenograft weights at euthanasia. \*P value <0.05 between the groups as indicated with the horizontal bars. Graphs represent the mean of each group and error bars are SEM. n=10 per group.

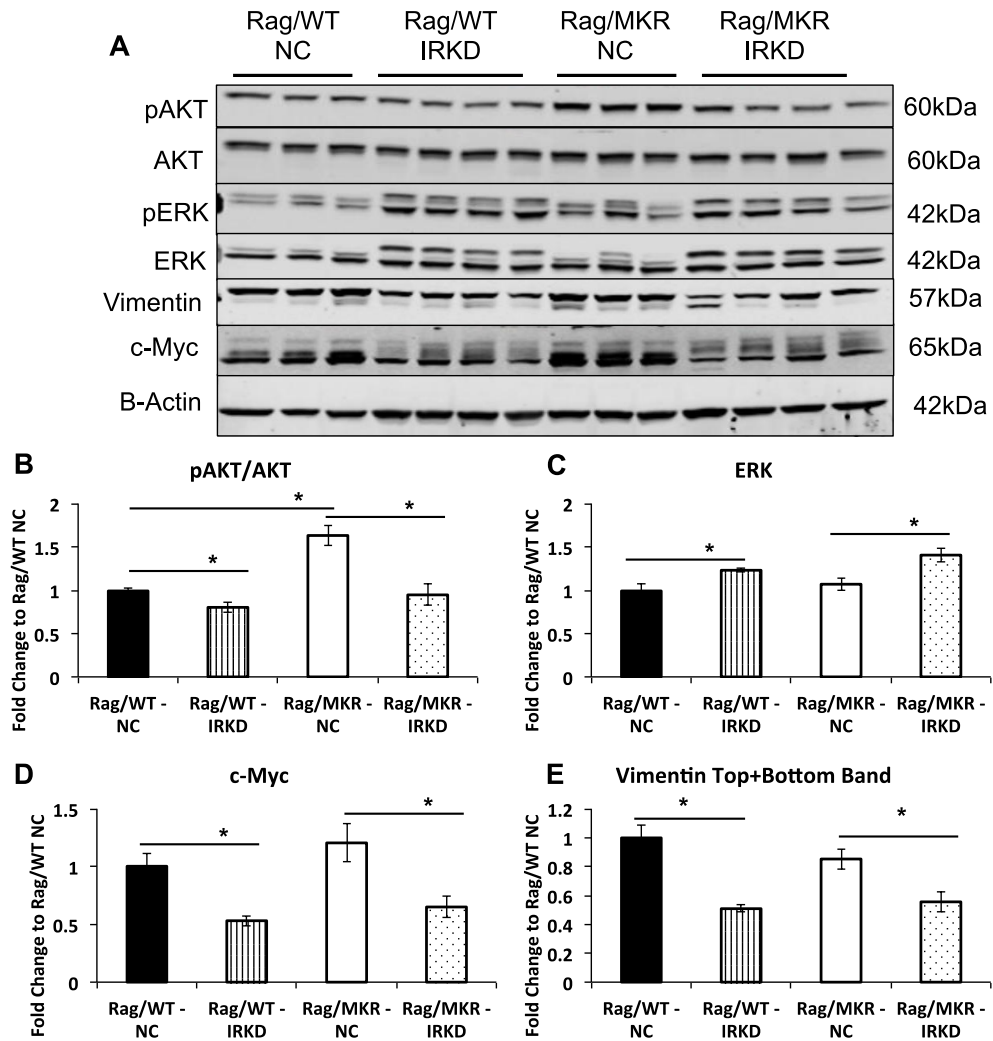


**Figure 42 Protein expression in LCC6 xenografts with normal and reduced IR expression.**

(A) Representative western blot analysis of protein lysates from LCC6 tumours from Rag/WT and Rag/MKR mice immunoblotted for pAkt (Ser473), total Akt, pErk1/2(Thr202/Tyr204), total Erk1/2, vimentin, c-myc and beta actin. (B-E) Densitometric analysis of pAkt / total Akt, total Erk1/2 / beta actin, c-myc / beta actin, vimentin / beta actin. Graphs represent mean of each group, error bars are SEM, \*P value <0.05 between groups as indicated (n=10 per group).

In the LCC6 cells in 2D culture, silencing the IR did not lead to a reductions in vimentin or c-myc protein expression in full medium (DMEM with 10% FBS) or in serum free conditions (DMEM+0.1% BSA) for 24 hours. This apparent discrepancy is likely a reflection of the known differences in gene expression that

exist between monolayer culture of cells, and tumour xenografts where an increase in the expression of certain proteins including vimentin and c-myc may occur (70).

*Silencing the IR in MCF-7 Cells leads to decreased c-myc expression in vitro and decreased proliferation.*

We then examined if silencing the IR would alter the expression of c-myc in a breast cancer cell line known to express high levels of c-myc. For these studies we used the human ER $\alpha$ -positive MCF-7 breast cancer cell line, as it has previously been shown to express high levels of c-myc protein compared to other human breast cancer cell lines (94). We silenced the IR in the MCF-7 cells using lentiviral mediated transduction of shRNA, and transduced a non-coding (Scr) sequence as a control cell line. We found that silencing the IR led to a reduction in c-myc expression in MCF-7 cells (Figure 43A, B), and this decrease in c-myc was associated with a decrease in cell proliferation (Figure 43C).

These data show that the IR plays an important role in normal development of the murine mammary gland, and in xenograft formation from human LCC6 breast cancer cells in the hyperinsulinaemic mice. Silencing the IR leads to decreased cell proliferation in vitro and decreased expression of c-myc and vimentin. Interestingly, in each of the models silencing or knocking out the IR led to changes in both the control and hyperinsulinaemic mice, suggesting that the IR plays an important role in mammary gland development and tumor growth in the setting of normal circulating insulin levels. In fact, the changes in WT and hyperinsulinaemic mice were similar in the setting of IR silencing, suggesting that in addition to signaling through the IR, hyperinsulinaemia may alter mammary gland development and tumor growth through indirect mechanisms.

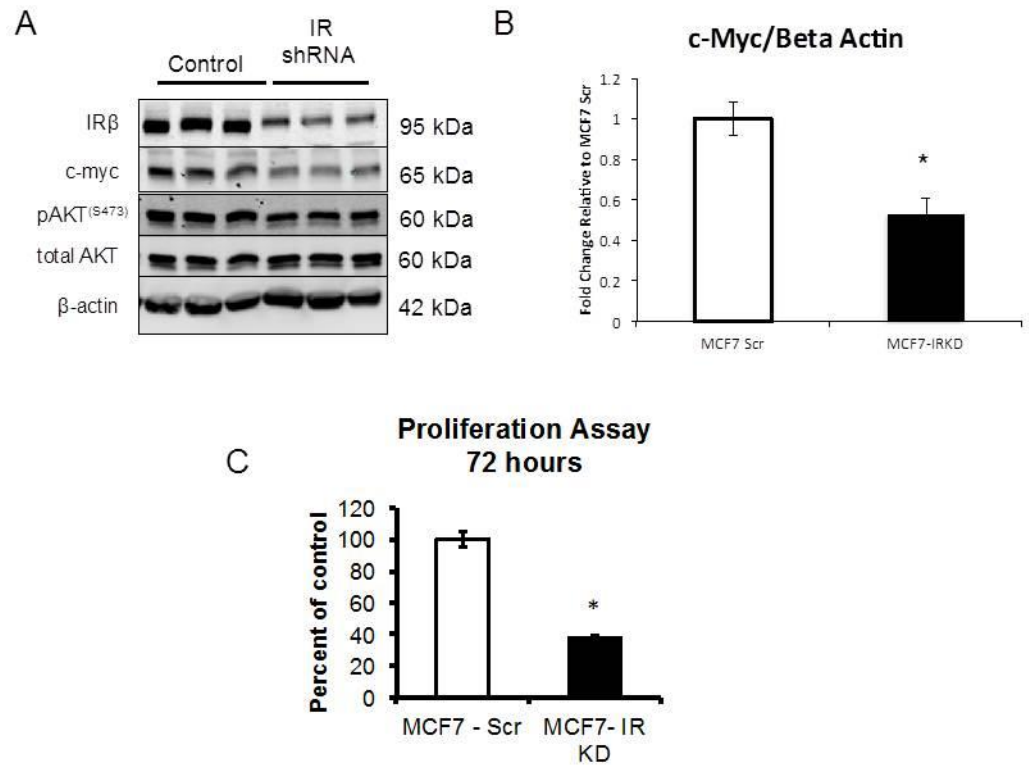


**Figure 43 Silencing the IR led to decreased c-myc expression in the MCF7 cells.**

(A) Western blot of protein lysates from MCF7 cells transduced with a non-coding shRNA (control) or IR targeted shRNA (IR shRNA) immunoblotted with antibodies to total IRβ, pAkt(Ser473), total Akt, c-myc and beta actin. (B) Densitometric analysis of c-myc/beta actin expression in control cells transduced with non-coding shRNA (MCF7-Scr) and those transduced with IR targeting shRNA (IRKD). (D) 72 hour proliferation assay demonstrating the number of cells as a percent of the control cells. These graphs represent the mean and error bars are SEM. n=3 per group. Each study was performed in triplicate, with consistent results.



## Chapter 5. The effects of insulin analogues on breast cancer progression in an animal model

Having found that the insulin receptor plays an important role in breast cancer xenograft growth in vivo, we next aimed to explore if stimulating the insulin receptor by administering insulin analogues would promote tumour growth in the MKR mice. We used the MKR mice for these studies because of their insulin resistance and tolerance to high dose insulin injections.

Human insulin and AspB10 lead to IR phosphorylation, while IGF-1 led to IGF-1R / hybrid receptor activation in vitro

We first aimed to determine if differences in IR and IGF-1R phosphorylation could be found in vitro in the MVT1 and Met1 cell lines after stimulation with recombinant human insulin, the mitogenic analogue AspB10 and rhIGF-1. MVT1 and Met1 cells were stimulated with PBS, or 10nM of insulin, AspB10 or IGF-1 for 10 minutes (Figure 44). Western blot analysis using the primary pIGF-1R $\beta$ <sup>(Tyr1135/1136)</sup>/pIR $\beta$ <sup>(Tyr1150/1151)</sup> antibody suggested that insulin and AspB10 stimulation led to IR $\beta$  phosphorylation, observed as a distinct band on the membrane at 95kDa (78). IGF-1 stimulation led to phosphorylation of the IGF-1R $\beta$  at 97kDa, as well as the IR $\beta$  at 95kDa (78). These findings suggested that in both MVT1 and Met1 cells, IGF-1 mediated phosphorylation of the IGF-1R $\beta$  and the IR $\beta$ , and probably the IR/IGF-1R hybrids. To confirm the western blot findings, we performed immunoprecipitation of the IR $\beta$  and IGF-1R $\beta$  from the Met1 cell lysates. We found that insulin and AspB10 were indeed phosphorylating the IR $\beta$ , but not the IGF-1R $\beta$  (Figure 44E, H), while IGF-1 stimulation led to phosphorylation of the IGF-1R $\beta$  and probable IGF-1R/IR hybrids (Figure 44E, H). Importantly, we noted that AspB10 stimulation led to greater IR $\beta$  phosphorylation than insulin in Met1 cells (Figure 44D). These results show that it is possible to distinguish differences in IR $\beta$  and IGF-1R $\beta$  phosphorylation in response to insulin, IGF-1 and AspB10 by western blot as confirmed by immunoprecipitation in Met1 and MVT1 cell lines in vitro.

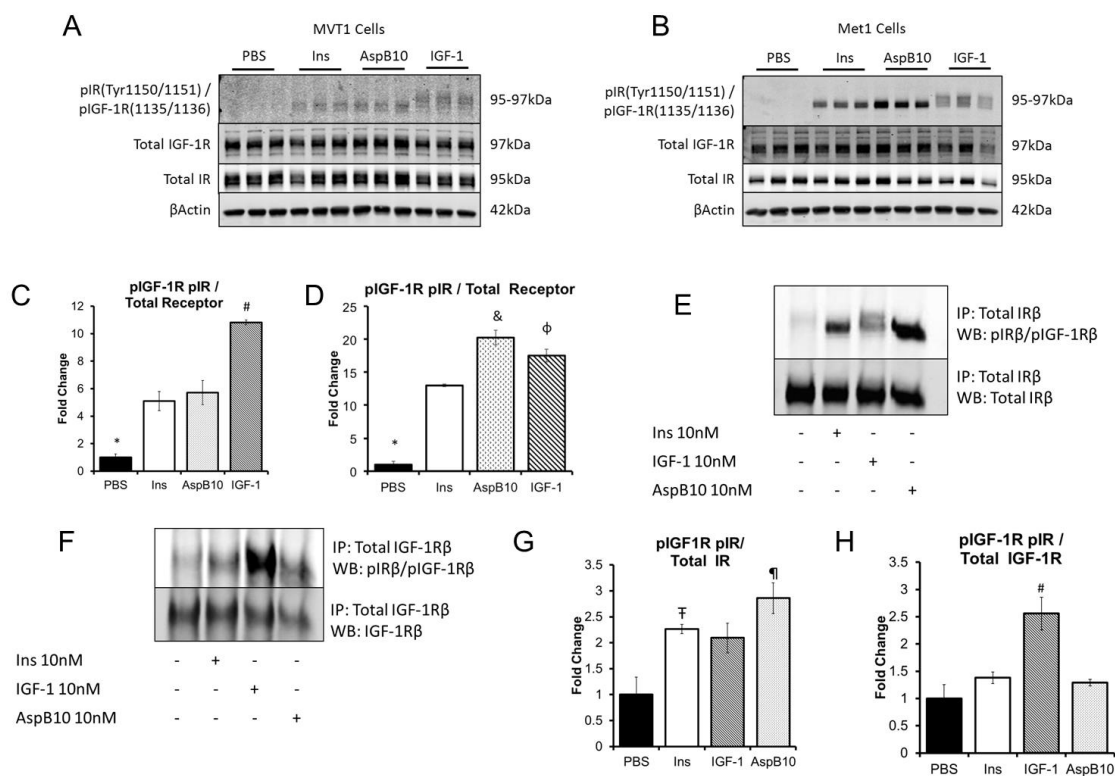


**Figure 44 Insulin and AspB10 led to IR phosphorylation but not IGF-1R phosphorylation in vitro.**

MVT1 and Met1 cells were stimulated with 10nM of insulin (Ins) the insulin analogue AspB10, rhIGF-1 (IGF-1) or PBS. Western blot of protein lysates and densitometry from MVT1 (A, C) and Met1 cells (B, D) demonstrated that insulin and AspB10 led to phosphorylation of IRβ<sup>(Tyr 1150/1151)</sup> at 95kDa, while IGF-1 stimulation led to phosphorylation of IGF-1Rβ<sup>(Tyr 1135/1136)</sup> at 97kDa and IRβ<sup>(Tyr 1150/1151)</sup> at 95kDa (A, B). Immunoprecipitation of IRβ in Met1 cell lysates after in vitro stimulation with PBS, 10nM of insulin (Ins), IGF-1 or AspB10 confirmed that insulin and AspB10 caused phosphorylation of IRβ<sup>(Tyr 1150/1151)</sup>, while IGF-1 led to phosphorylation of IGF-1Rβ<sup>(Tyr 1135/1136)</sup> and IRβ<sup>(Tyr 1150/1151)</sup> (E, F), with densitometry (G, H). Representative blots are shown. All experiments were performed 2-3 times. Bar graphs display means and SEM. \*PBS group lower than all other groups,  $p < 0.05$ ; # IGF-1 group higher than all other groups,  $p < 0.05$ ; & AspB10 group higher than insulin group,  $p < 0.05$ ; Φ IGF-1 group higher than insulin group,  $p < 0.05$ ; † human insulin greater than PBS,  $p < 0.05$ ; ‡ AspB10 greater than PBS,  $p < 0.05$ ; § IGF-1 group greater than PBS,  $p = 0.05$ .

*Endogenous hyperinsulinaemia leads to phosphorylation of the IR in vivo, and exogenous rhIGF-1 increase the growth of Met1 and MVT1 tumours with IR/IGF-1R phosphorylation*

We next aimed to determine whether endogenous hyperinsulinaemia stimulated Met1 and MVT1 tumour growth by acting directly on the IR in vivo, or by indirect mechanisms, namely through phosphorylation of the IGF-1R $\beta$ . To assess the effect of endogenous hyperinsulinaemia on tumour growth and receptor phosphorylation, compared to rhIGF-1 in vivo, we studied Met1 and MVT1 tumours from WT mice and MKR mice treated with rhIGF-1 or vehicle. WT and MKR mice were orthotopically injected with 100,000 MVT1 or 250,000 Met1 tumour cells. Consistent with our previous studies, MKR mice developed larger MVT1 and Met1 tumours than WT mice (Figure 45A, B). MVT1 and Met1 tumours were then induced in MKR mice, and when tumours were measurable, the MKR mice were divided into two groups with equal mean tumour size. From that time, rhIGF-1 (1mg/kg twice daily i.p). or vehicle were administered for 2 weeks. Serum IGF-1 levels were measured two hours after injection at the end of the study and were 2.6 times higher in the rhIGF-1 treated mice (806 $\pm$  59.05 ng/mL) than vehicle treated mice (302  $\pm$  8.75 ng/mL),  $p < 0.05$  (Figure 45C). rhIGF-1 treated MKR mice developed significantly larger tumours than the vehicle treated MKR mice (Figure 45D-E). Repeated studies demonstrated a non-significant increase in the number of MVT1-derived pulmonary macrometastases in the rhIGF-1 treated group compared to the MKR vehicle treated group (Figure 45F). Western blot analysis of tumour lysates demonstrated that rhIGF-1 treatment led to phosphorylation the IGF-1R $\beta$  at 97kDa and IR $\beta$  at 95kDa, in both Met1 and MVT1 tumours (Figure 45F, G). In contrast, tumours from vehicle treated MKR mice had only IR $\beta$  phosphorylation at 95kDa (Figure 45G-I). These results suggest that endogenous hyperinsulinaemia increases mammary tumour growth by directly acting on the IR of the tumours and not by indirectly activating the IGF-1R. IGF-1 in contrast leads to phosphorylation of the IGF-1R $\beta$  and IR $\beta$ , most likely through IGF-1R/IR hybrid receptors.

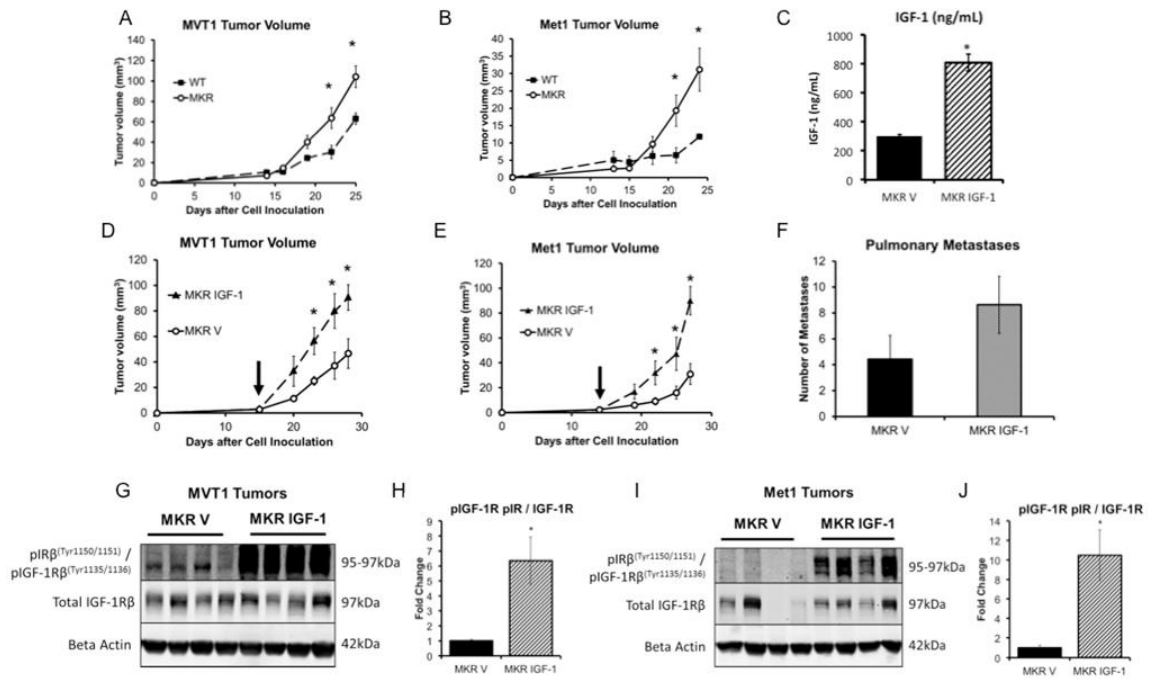


**Figure 45 IGF-1 increased orthotopic MVT1 and Met1 tumour growth in the hyperinsulinaemic MKR mice by increasing IGF-1R phosphorylation.**

(A, B) WT and MKR mice were injected with tumour cells on Day 0. MKR mice developed larger MVT1 and Met1 tumours than WT mice. (D, E) MVT1 and Met1 tumour cells were orthotopically injected into MKR mice, mice were divided into 2 groups with equal mean tumour size and mice were administered either rhIGF-1, or vehicle (vertical arrow indicates when treatment began). Administration of rhIGF-1 led to a further stimulation in tumour growth, over endogenous hyperinsulinaemia (D, E). (C) Serum IGF-1 concentration in the rhIGF-1 treatment group was 2.6 times the control group. (F) Mean number of pulmonary macrometastases. (G-J) Western blot analysis of tumour lysates demonstrated that MKR mice show IR $\beta$  phosphorylation at 95kDa, rhIGF-1 treatment led to increased IGF-1R $\beta$  and IR $\beta$  or hybrid receptor phosphorylation in MVT1 and Met1 tumours. Representative images from three repeated experiments of tumour volume and western blots are displayed. The graphs represent the average for each group; error bars indicate SEM. \* indicates statistically significant differences (P<0.05) between the groups. n=8-11 mice per group.

Chronic administration of the insulin analogue AspB10 increased Met1 and MVT1 tumour growth

Our in vitro studies had shown that AspB10 increased IR $\beta$  phosphorylation in both Met1 and MVT1 cells, without increasing IGF-1R $\beta$  phosphorylation (Figure 44). Therefore, to investigate whether IR activation could truly increase tumour growth independent of IGF-1R activation, we used the insulin analogue AspB10 to chronically activate the IR of the tumours in vivo. After orthotopic injection with MVT1 or Met1 tumour cells, mice were treated with AspB10 (12.5 IU/kg twice daily sc) or vehicle for approximately 2 weeks after the tumours became measurable. AspB10 treatment led to a significant increase in the size of both MVT1 and Met1 tumours (Figure 46A, B). The increased average number of surface pulmonary macrometastases in the AspB10 treated group did not reach statistical significance (Figure 46C). AspB10 treatment significantly increased plasma insulin concentrations to  $70.2 \pm 21.2 \mu\text{g/L}$ , compared to vehicle treated mice ( $1.08 \pm 0.3 \mu\text{g/L}$ ),  $p < 0.05$ , when measured two hours after insulin or vehicle injection. An insulin tolerance test revealed that AspB10 (12.5 units / kg sc) led to a reduction in blood glucose similar to human insulin from 30 minutes to four hours after injection that reached a nadir ( $43.9 \pm 6.1\%$  baseline) two hours after injection (Figure 46D). No differences in body weight was observed between the AspB10 and vehicle treated group before or after two weeks of treatment (Figure 46E). Although overall body weight was not different between the treatment groups, both vehicle and AspB10 treated mice showed a relative loss of lean mass and a relative gain in fat mass; however, the change in lean and fat mass did not differ between vehicle and AspB10 treated groups (Figure 46F-G).

Endogenous hyperinsulinaemia and AspB10 increased mammary tumour growth by directly activating the IR, but not the IGF-1R

To ascertain whether AspB10 stimulated tumour growth in vivo by acting directly on the IR, we examined IR $\beta$  and IGF-1R $\beta$  phosphorylation in Met1 and MVT1 tumours after 2 weeks of AspB10 or vehicle treatment. Western blot analysis of the tumour lysates revealed that AspB10 treatment led to phosphorylation of the IR $\beta$ , but not the IGF-1R $\beta$  in both MVT1 and Met1 tumours (Figure 47A-D). To confirm these findings, the tumour lysates of MVT1 and Met1 tumours from WT mice, vehicle treated MKR mice, IGF-1 treated MKR mice and AspB10 treated

MKR mice were subjected to immunoprecipitation of the IR $\beta$  and the IGF-1R $\beta$ , and immunoblotted for the phosphorylated IGF-1R $\beta$ /IR $\beta$ . Tumours from vehicle treated MKR mice demonstrated  $1.38 \pm 0.17$  fold increase in phosphorylation of the IR $\beta$  compared to tumours from WT mice (Figure 47E), but no increase in IGF-1R $\beta$  phosphorylation was seen in the vehicle treated MKR mice (Figure 47F). Similarly, AspB10 treatment led to  $1.81 \pm 0.17$  fold increased phosphorylation of the IR $\beta$  compared to WT mice, as demonstrated by immunoprecipitation (Figure 47E), but not the IGF-1R $\beta$  (Figure 47F). In contrast, rhIGF-1 administration led to phosphorylation of both the IGF-1R $\beta$  and IR $\beta$  (Figure 47E, F). Taken together, these data demonstrate that endogenous hyperinsulinaemia directly increases tumour growth by acting on the IR of the tumours, but not the IGF-1R and that stimulating the IR, independently of the IGF-1R, further exacerbates tumour growth.

AspB10-induced IR phosphorylation and rhIGF-1-induced IGF-1R / hybrid receptor phosphorylation led to increased Akt phosphorylation in tumours

In order to examine whether differences in receptor activation in vivo led to differences in downstream signaling, we examined Akt and Erk1/2 phosphorylation in the two tumour types from mice treated with AspB10 or IGF-1. Despite the differences in receptor phosphorylation resulting from AspB10 and rhIGF-1 administration, increased Akt phosphorylation was observed in MVT1 tumours after treatment with both AspB10 and rhIGF-1 (Figure 48A-D), although a greater fold change was observed in the rhIGF-1 treated group. In Met1 tumours, a 2.5 fold increase in Akt phosphorylation after rhIGF-1 treatment,  $p < 0.05$  and a 15% increase was observed after AspB10 treatment that did not reach statistical significance. No increase in Erk1/2 phosphorylation was found in MVT1 or Met1 tumours after either rhIGF-1 or AspB10 treatment (Figure 48A, B). These results show that in tumours with certain oncogenes, despite differences in IR and IGF-1R activation, both rhIGF-1 and AspB10 led to activation of the Akt signaling, rather than MAPK.

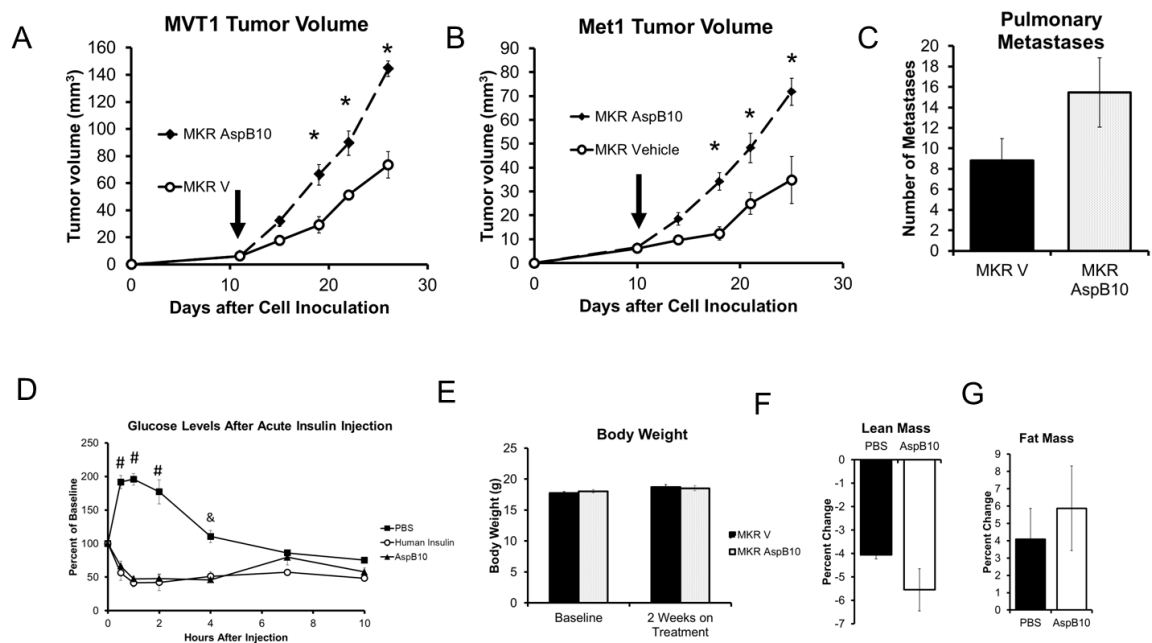


**Figure 46 Chronic activation of the IR by the insulin analogue AspB10, increased orthotopic Met1 and MVT1 tumour growth.**

(A, B) MKR mice were injected with MVT1 or Met1 tumour cells on Day 0. Treatment was started with AspB10 (12.5 IU/kg twice daily sc) or vehicle, indicated by vertical arrow. AspB10 led to increased growth of both MVT1 and Met1 tumours. (C) The number of pulmonary macrometastases showed a non-significant increase in the AspB10 treated group. An insulin tolerance was performed with AspB10 (12.5 IU/kg sc), regular human insulin (12.5 IU/kg sc) and PBS (vehicle). Blood glucose was measured at time 0.5, 1, 2, 4, 7 and 10 hours after injection. # p value <0.05 between PBS and AspB10 and human insulin groups, & p value <0.05 between PBS and AspB10 treated groups. n=4 per group. # PBS group significantly greater than other groups, p<0.05; & PBS significantly higher than AspB10 group, p<0.05. (F-H) No change in body weight, or difference in relative lean or fat mass was observed after 2 weeks of AspB10 administration. Graphs are representative of two studies. All graphs show the mean for each group and error bars represent the SEM. \*p value < 0.05 between groups. n=9-11 mice per group.

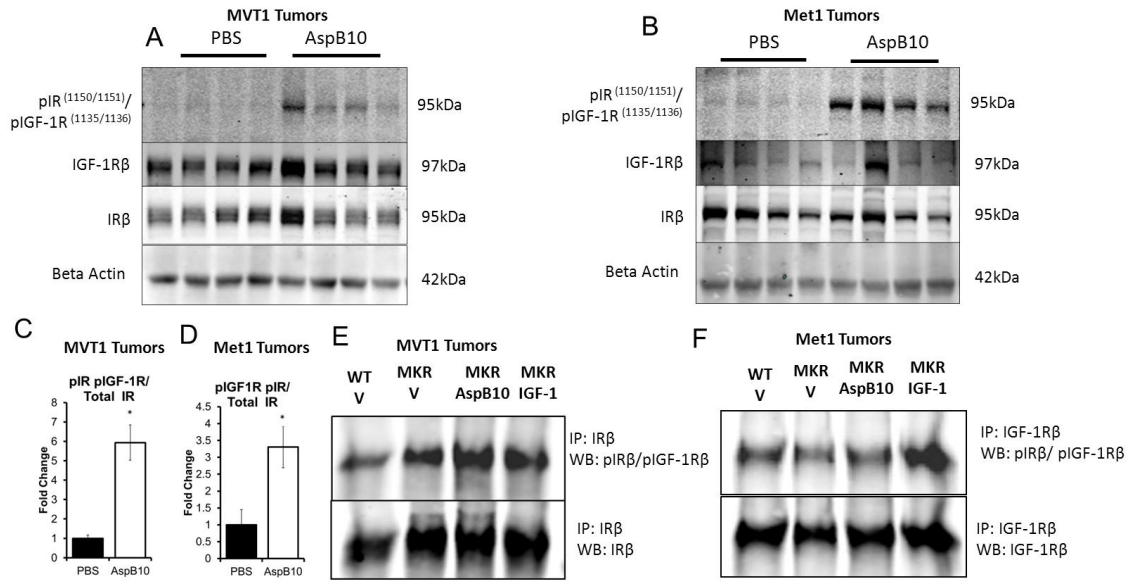


**Figure 47 Endogenous hyperinsulinaemia and AspB10 treatment led to increased IR phosphorylation in MVT1 and Met1 tumours.**

(A, B) Representative western blot analysis and (C, D) densitometry of MT1 and Met1 tumour lysates revealed that chronic AspB10 treatment led to increased IRβ phosphorylation at 95kDa. (E) Immunoprecipitation of the IRβ and (F) IGF-1Rβ was performed on MVT1 and Met1 tumour protein lysates. They were immunoblotted for the phosphorylated IGF-1Rβ/ IRβ. Endogenous hyperinsulinaemia (MKR V) and chronic AspB10 administration (MKR AspB10) led to increased IR phosphorylation (E). rhIGF-1 administration led to increased IGF-1Rβ and IRβ phosphorylation (F). Graphs are representative of two studies. All graphs show the mean for each group and error bars represent the SEM. \*P value < 0.05 between groups. n=9-11 mice per group.



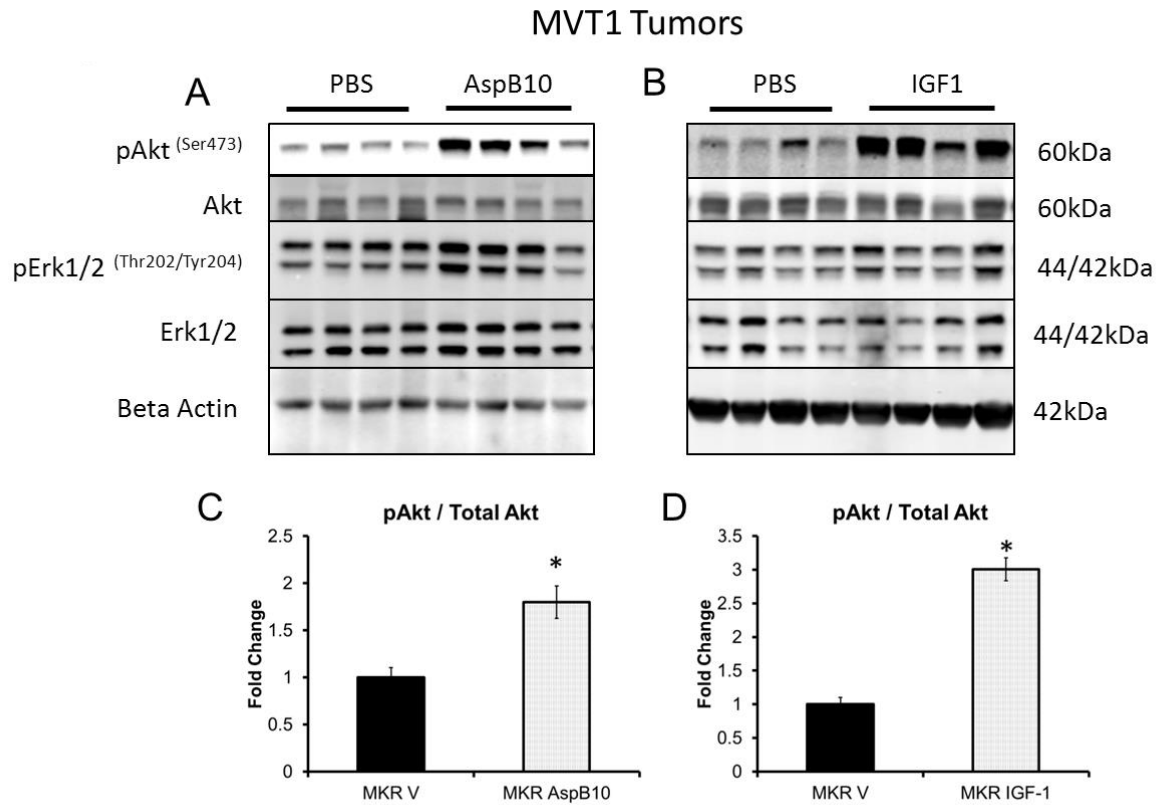


**Figure 48 Chronic administration of IGF-1 and AspB10 led to increased phosphorylation of Akt, but no change in Erk1/2 phosphorylation.**

(A-D) Western blot analysis and densitometry of MVT1 tumour lysates at the end of the treatment periods with (B) rhIGF-1 and (A) AspB10 revealed that rhIGF-1 and AspB10 treatment led to increased Akt phosphorylation and no change in Erk1/2 phosphorylation. Graphs are representative of two studies for AspB10 treatment and three studies for rhIGF-1 treatment. All graphs show the mean for each group and error bars represent the SEM. \*P value < 0.05 between groups. n=9-11 mice per group.

*No increase in primary MVT1 tumour growth was observed after treatment with insulin glargine, insulin detemir or insulin degludec*

We then proceeded to examine if other insulin analogues in clinical use would promote tumour growth in this model. We compared the in vivo effects of the long acting basal insulin analogues insulin glargine, insulin detemir and insulin degludec on breast cancer growth to determine if glargine would increase tumour growth in this model. AspB10 insulin and rhIGF-1 served as positive controls. Mice

were injected with 100,000 MVT1 cells, as described in the Materials and Methods. When tumours measured 2-3mm in diameter, mice were divided into groups with equal tumour sizes and treated with 12.5 units / kg twice daily of one of insulin glargine, insulin detemir, insulin degludec, or the mitogenic insulin analogue AspB10 (12.5units/kg twice daily), or IGF-1 (1mg/kg twice daily), or vehicle for 2 weeks. Compared to vehicle treated mice, no increase in MVT1 tumour growth was seen with insulin glargine, insulin detemir or insulin degludec. However, both AspB10 and IGF-1 administration stimulated MVT1 tumour growth to a similar extent, more than vehicle treatment with significantly larger volumes and greater weight at the end of the study (Figure 49A, B). Three separate tumours studies were performed in the MKR mice, using insulin glargine, insulin detemir and insulin degludec. None of the studies found any increase in MVT1 tumour growth over vehicle or human insulin, and no difference in tumour growth was found between the three analogues.

*Chronic administration of insulin glargine led to phosphorylation of the insulin receptor in tumours in the MKR mice.*

Previous in vitro studies have reported that insulin glargine has greater affinity for the IGF-1R than human insulin, and may mediate mitogenic effects in tumours that express the IGF-1R. MVT1 cells and tumours express both the IR and IGF-1R. After two weeks of treatment, mice were dissected one hour after the last insulin analogue, vehicle or IGF-1 injection, and tumours were flash frozen in liquid nitrogen for subsequent protein isolation. Protein lysates were analyzed by western blot (Figure 50). Consistent with our previous in vivo studies, chronic rhIGF-1 administration led to IGF-1R/IR phosphorylation (Figure 50A). In contrast, AspB10 insulin, insulin glargine, insulin detemir and insulin degludec all led to IR phosphorylation. Greater IR phosphorylation was observed in tumours from the AspB10 treated mice (Figure 50B), compared to the other insulin analogues. This finding is consistent with previous studies that report the mitogenic effects of AspB10 are mediated by sustained IR phosphorylation (64).

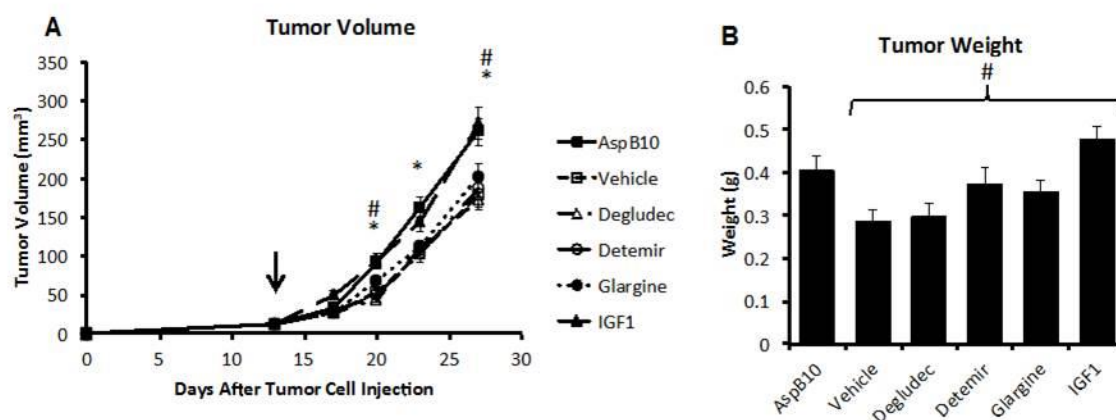


**Figure 49 The effect of insulin analogues on MVT1 tumour growth**

(A) No increase in tumour growth was observed over vehicle in MKR mice treated with insulin glargine, insulin detemir, or insulin degludec, while AspB10 and IGF-1 significantly increased tumour volume. 100,000 MVT1 cells were injected into the 4<sup>th</sup> mammary fat pad of MKR mice at day 0. Tumours were measured, and insulin injections were begun when tumours measured 2-3mm in diameter. Injections began as indicated by the vertical arrow. Injections continued until the largest tumour volumes reached 10mm in diameter. (B) Tumour weights were measured at the end of the study. The graphs represents the mean of each group and error bars represent the SEM. \* Indicates a statistically significant difference between the volume of the AspB10 and the vehicle group ( $p < 0.05$ ). # Indicates a statistically significant difference between the IGF-1 treated group and the vehicle treated group ( $p < 0.01$ ).  $n = 9-12$  mice per group.

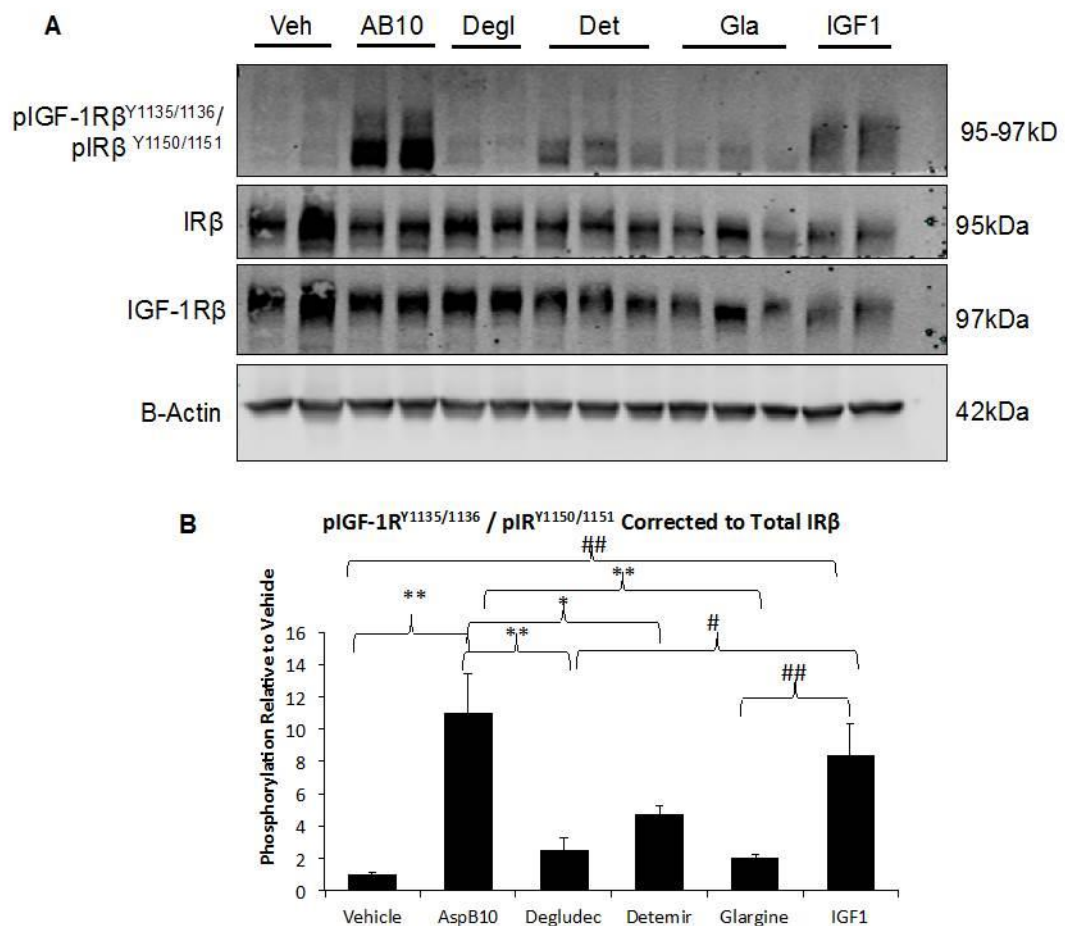


**Figure 50 Western blot analysis revealed that all of the insulin analogues led to IR phosphorylation.**

AspB10 led to significantly greater IR phosphorylation than the other analogues, while IGF-1 led to IGF-1R/IR phosphorylation. (A) Representative western blot of MVT1 tumour lysates from MKR mice treated with vehicle (Veh), AspB10 insulin (AB10), insulin degludec (Degl), insulin detemir (Det), insulin glargine (Gla) all at 12.5units/kg twice daily, and IGF1 (IGF1) 1mg/kg twice daily. (B) Densitometric analysis of western blots of receptor phosphorylation corrected to total IR $\beta$  expression in the tumours is expressed relative to vehicle treated mice, n=12 per group. \* indicates P value<0.05, \*\* indicates P<0.01, # p<0.05, ##p<0.01 between groups as indicated. No statistically significant differences in receptor phosphorylation were found between insulin degludec, insulin detemir, or insulin glargine. n=9-12 mice per group.

*Treatment with (A21Gly,DiD-Arg) insulin did not increase MVT1 tumour growth compared to insulin glargine or vehicle.*

Human studies in individuals with Type 2 diabetes have found that insulin glargine is rapidly metabolized by peptidases that cleave the carboxy terminal arginines of the B chain, yielding M1 and M2 metabolites (99). In vitro studies using human plasma and in vivo studies have found that there is inter-individual variability in the rate of conversion from glargine to the M1 metabolite (2, 99). Therefore, some individuals may have higher exposure to the parent glargine compound than others, particularly at high doses. It has been hypothesized that exposure to the parent compound may lead to mitogenic effects by IGF-1R activation in tumours expressing high levels of IGF-1R. As described in the Materials and Methods, a non-metabolizable form of insulin glargine was generated by replacing the L-arginine residues at position 31 and 32 on the B chain of insulin with D-arginine residues (A21Gly, DiD-Arg) (147). The differences in amino acid sequence between human insulin, insulin glargine, the M1 metabolite of glargine and A21Gly, DiD-Arg are shown in Figure 13.

To examine the biological activity of A21Gly, DiD-Arg on glucose lowering compared to insulin glargine, an insulin tolerance test was performed in wild type FVB/n mice (Figure 51A). An insulin tolerance test was performed using human insulin, insulin glargine and A21Gly, DiD-Arg using 1unit / kg. Glucose levels declined to  $29.3 \pm 5.4\%$  of baseline in the human insulin treated group,  $36.3 \pm 6.2\%$  in the glargine treated group, and to  $50.6 \pm 7.7\%$  in the A21Gly,DiD-Arg treated group at 60 minutes, with no statistically significant difference between the three groups at any time point (Figure 51A). To determine the concentrations of parent glargine and its M1 metabolite rats were subcutaneously injected with each 12.5 U/kg insulin glargine or A21, DiD-Arg the plasma levels of glargine parent compound and glargine metabolites M1 and M2 were measured by LC/MS 60 minutes after subcutaneous injection. After this time period there is only 7% of glargine parent compound left while 91% is converted to M1 (= A21Gly human insulin) with insulin glargine. In contrast after injection of A21, DiD-Arg almost all circulating insulin consists of the DiD-Arg glargine parent compound while no M1 is detectable in plasma. With both treatments only minor concentrations (3% and 1%) of the second metabolite M2 (=A21Gly,des-B30 human insulin) were detectable (Figure 51B).

To determine if this non-metabolizable form of insulin glargine would lead to mitogenic effects in vivo, MKR mice were orthotopically injected with MVT1 cells and divided into three treatment groups once tumours became 2-3mm in size. Mice were then treated with vehicle, insulin glargine or A21Gly, DiD-Arg for 2 weeks. Consistent with our previous studies, no difference in the growth of MVT1 tumours was found between vehicle and insulin glargine treated mice (Figure 52A). Furthermore, A21Gly, DiD-Arg treatment did not increase tumour MVT1 tumour growth in the MKR mice (Figure 52A). This experiment was repeated and compared to human insulin. No increase in MVT1 tumour growth was found with either analogue above that of human insulin. Western blot analysis revealed that insulin glargine and A21Gly, DiD-Arg both led to IR phosphorylation in tumours, rather than IGF-1R phosphorylation (Figure 52B). These results demonstrate that in vivo, a non-metabolizable form of insulin glargine, A21Gly, DiD-Arg does not promote tumour growth and does not lead to IGF-1R phosphorylation in murine breast tumours that express both the IR and IGF-1R.

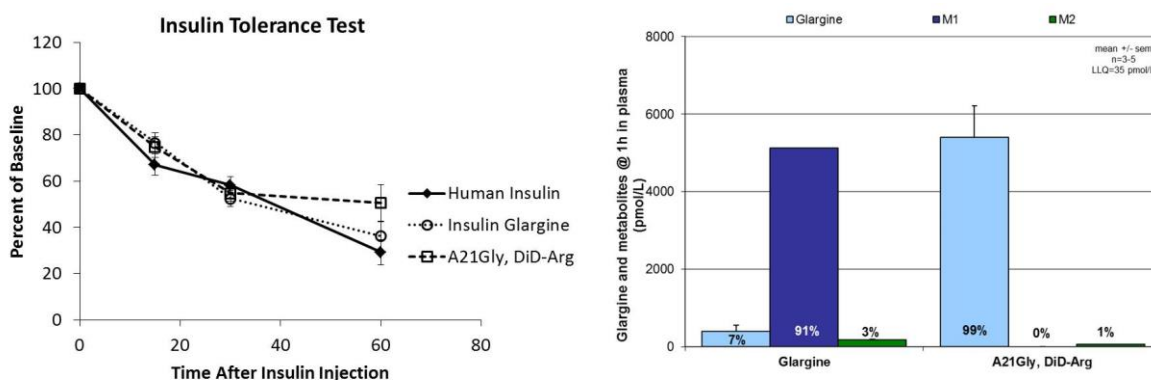


**Figure 51 Insulin tolerance and metabolism with insulin glargine and A21Gly,DiD-Arg**

(A) An insulin tolerance test was performed in wild type FVB/n mice using 1 unit / kg of each of the insulin analogues, as indicated. No statistically significant difference was found in the percent reduction in capillary glucose measurements between the groups. (B) The metabolites of insulin glargine found in mice 60 minutes after injection of insulin glargine and A21Gly, DiD-Arg insulin 12.5units/kg.

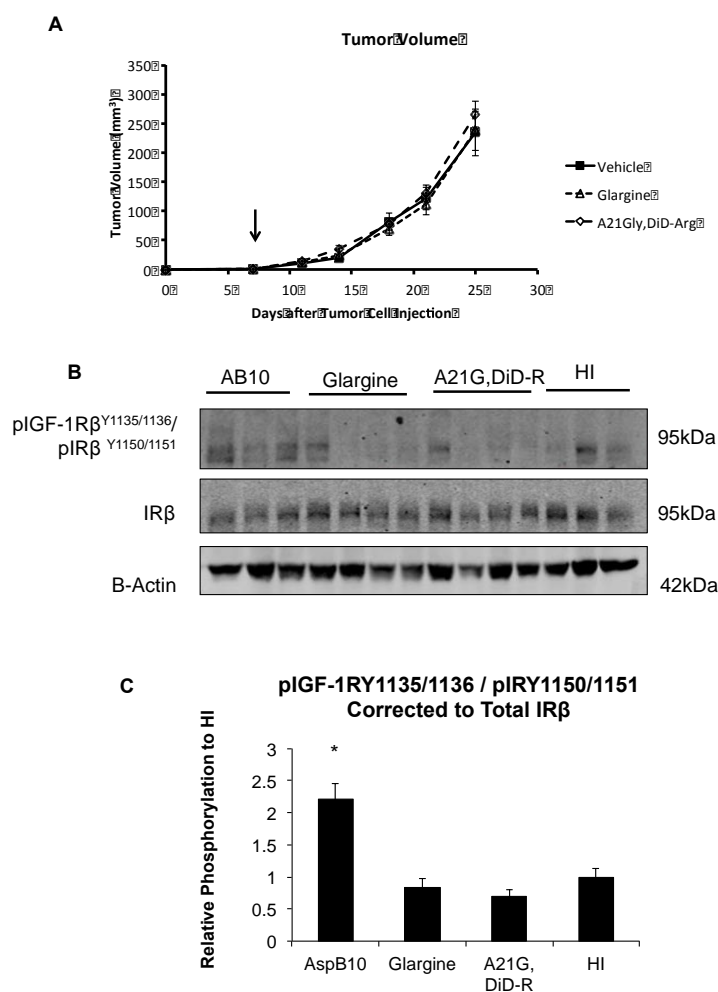


**Figure 52 MVT1 Tumour growth in response to A21Gly, DiD-Arg**

(A) No increase in MVT1 tumour volume was found after treatment with insulin glargine or A21Gly, DiD-Arg compared to vehicle treatment. (n=8 per group). The arrow indicates the time when insulin injections were started. 12.5units / kg of insulin glargine and A21Gly, DiD-Arg or vehicle were administered twice daily. (B) Representative western blot and (C) densitometry compared IR/IGF-1R $\beta$  phosphorylation of MVT1 tumours derived from MKR mice after chronic treatment with AspB10 (AB10), insulin glargine (Glargine), A21Gly, DiD-Arg (A21G, DiD-R) or human insulin (HI) 12.5 units /kg twice daily. All analogues were found to lead to IR $\beta$  rather than IGF-1R $\beta$  phosphorylation. \* P value <0.01 between AspB10 and other groups. No difference in IR/IGF-1R phosphorylation was found between insulin glargine, A21Gly, DiD-Arg or human insulin (n=8 per group).

The results of these studies do show that IGF-1 can drive primary MVT1 tumour growth in the setting of endogenous hyperinsulinaemia, by activating the IR and IGF-1R. AspB10, the mitogenic insulin analogue also leads to significant increase in tumour growth, but mediates its effects through the IR. None of the other insulin analogues increased tumour growth over endogenous hyperinsulinaemia in the MKR mice. These analogues caused significantly less IR phosphorylation in the MVT1 tumours than AspB10 an hour after injection, consistent with previous in vitro studies that have attributed the mitogenic effects of AspB10 to prolonged activation of the IR (37). In addition, in this in vivo model, neither glargine nor the non-metabolizable form of glargine activated the IGF-1R, or promoted tumour growth, demonstrating the limitations of in vitro assessments of the mitogenic potential of insulin analogues.



## Chapter 6. Human Breast Cancer, Hyperinsulinaemia and IR Splicing.

### *Is hyperinsulinaemia associated with a worse prognosis in breast cancer?*

The results presented for this study are preliminary data on a study that will continue over the next two years. The characteristics of the first 101 recruited patients are shown in Table 2. White and Black women recruited were of similar age at presentation. The Black women had a tendency to have more triple negative tumours, but the numbers were small in these groups (n=6 in White population and n=3 in Black population). Despite the small numbers, a significantly larger number of Black women were obese and the increase in insulin resistance approached statistical significance. Although there was a tendency of the Black women to present with more stage 2 and less stage 1 breast cancers, and to have a higher NPI, these trends did not reach statistical significance. The recruitment of patients for this study is ongoing. These patients were the source of the de-identified FFPE sections from which we isolated and analyzed RNA in the following sections.

**Table 2 Characteristics of Patients**

	<b>Total (N=101)</b>	<b>White (N=84, 83%)</b>	<b>Black (N=17, 17%)</b>	<b>P</b>
<b>Age, mean (SD) years</b>	59.9 (12.1)	60.0 (12.1)	59.1 (12.6)	0.77
<b>Tumour size, mean (SD) cm</b>	1.46 (0.95)	1.37 (0.8)	1.93 (1.3)	0.11
<b>Triple negative tumour *</b>	9 (9%)	6 (7%)	3 (19%)	0.14
<b>Obese (BMI≥30)*</b>	17 (17%)	9 (11%)	8 (47%)	0.002
<b>Waist Circumference Mean (SD) cm</b>	94.1 (11.7)	92.6 (11.8)	100.5 (8.8)	0.01
<b>Stage</b>				0.66
<b>I</b>	66 (65%)	56 (67%)	10 (59%)	
<b>II</b>	32 (32%)	25 (30%)	7 (41%)	
<b>III</b>	3 (3%)	3 (4%)	0	
<b>Insulin Resistant (HOMA &gt; 2.8)</b>	10 (10%)	6 (7%)	4 (24%)	0.06
<b>Poor prognosis (NPI &gt; 4.4)</b>	19 (19%)	15 (18%)	4 (24%)	0.73
<b>Inadequate Screening</b>	14 (15%)	11 (14%)	3 (19%)	0.70

### *Insulin Receptor Expression in Human Breast Cancers and Breast Cancer Cell Lines*

RNA was isolated from de-identified FFPE breast cancers from this study and subjected to Nanostring RNA analysis, as described in the Materials and Methods section. 47 individual patient RNA samples were analyzed using nSolver Analysis software. Data were normalised to beta actin, RPL19 and RPLP0 and to positive and negative controls. One sample was excluded due to an abnormality in normalization, and so further analysis was performed on 46 patient samples. The IR was expressed in all cases. To put into context the level of IR expression in these cases, we compared IR expression to IGF-1R expression (Figure 53). We found that in 32.6% of cases the IR expression was greater than the IGF-1R expression.

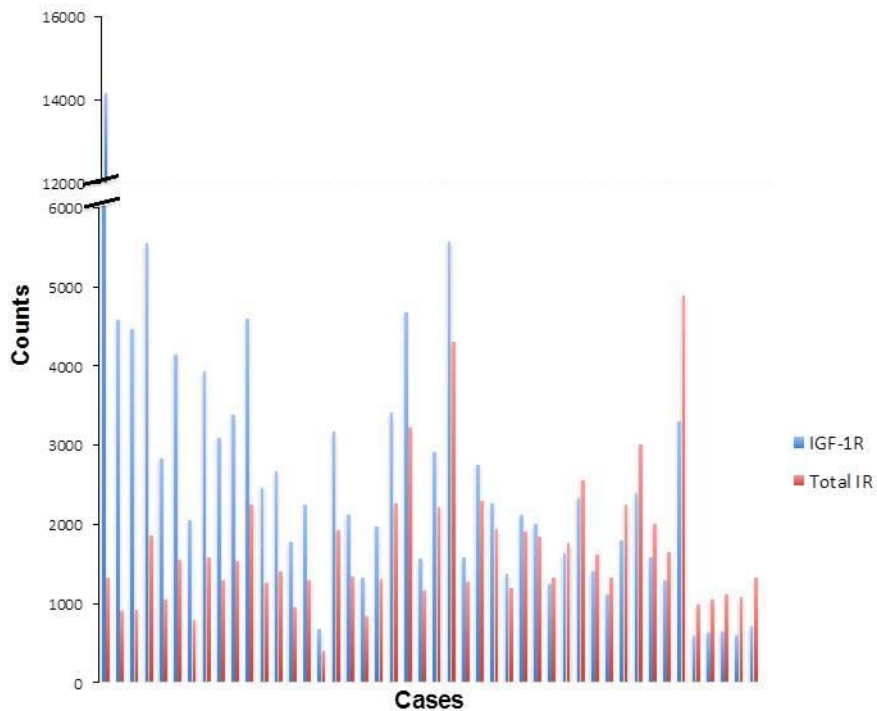


**Figure 53 Relative Expression of IR and IGF-1R in Human Breast Cancer**

The IR and IGF-1R expression patterns in individual patient breast cancer samples from which RNA was isolated. The individual bars represent the individual cases ranked in order of low to high of IR/IGF-1R expression ratio, with blue indicating IGF-1R expression and the red bars indicating IR expression. The y-axis is the total counts per gene as measured by the Nanostring nCounter. The bars breaking the y axis are to account for one sample that had 10 fold higher IGF-1R vs IR expression

*IR-A is the dominant IR isoform in all breast cancer cases.*

We then examined the IR-A and IR-B isoform expression across the different cases (Figure 54). In every case the IR-A was the predominant isoform observed in the cancers, and was detectable in all cases. IR-B had much lower expression across cases and in some cases was just above the limit of detection. A heatmap was generated by z-score transformation of genes, and calculated using Euclidean distance. Samples and genes were then clustered (Figure 55). The strongest correlation on initial analysis was between IR-A and total IR (correlation coefficient 0.65), which both correlated with IR-B and the splicing factors MBNL1, MBNL2,

SF3A1 and SRSF3 (Figure 55A). To remove the high correlation cluster between IR-A and the total IR, we regenerated the heatmap after removal of total IR (Figure 55B). After removal of total IR, IR-B no longer correlated with IR-A, but remained correlated with MBNL1, MBNL2, SF3A1 and SRSF3, while IR-A clustered with the IGF-1R and HNFNPA1. Neither IR-A nor IR-B isoforms, nor any of the splicing factors were correlated with Ki67 expression in the breast cancer specimens. During the course of this study, further samples will be analyzed for IR isoform and splicing factor expression, and will be correlated with breast cancer subtypes, race and prognosis to determine if the differential expression of the different IR isoforms plays an important role in this regard.

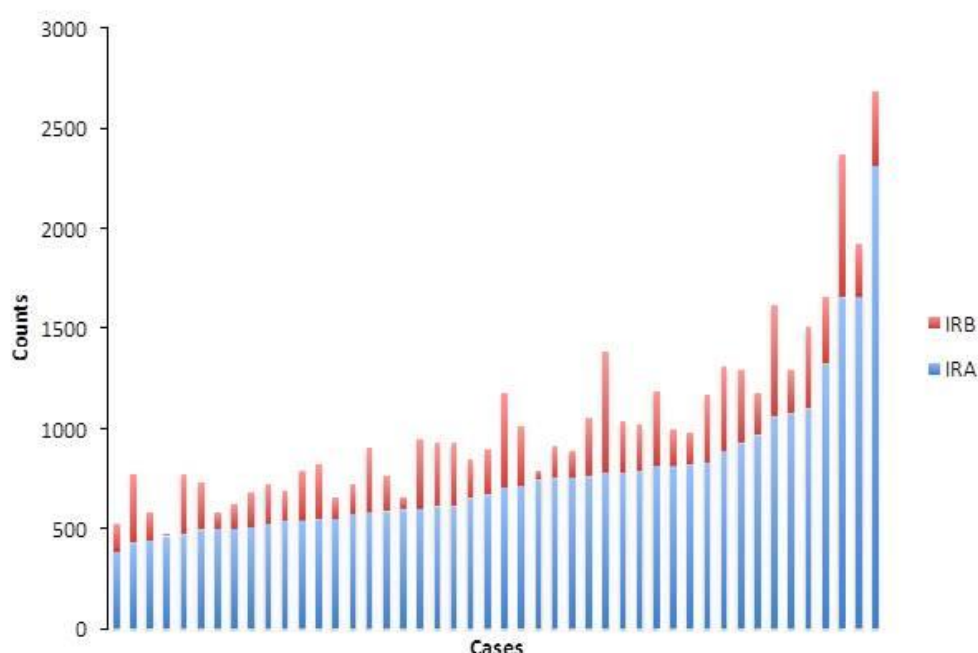


**Figure 54 Insulin Receptor Isoform Expression in Human Breast Cancer Specimens.**

The IR-A and IR-B expression patterns in individual patient breast cancer samples from which RNA was isolated. The individual bars represent the individual cases ranked in order of low to high IR-A expression, with blue indicating IR-A expression and the red bars indicating IR-B expression. The y-axis is the total counts per gene as measured by the Nanostring nCounter.

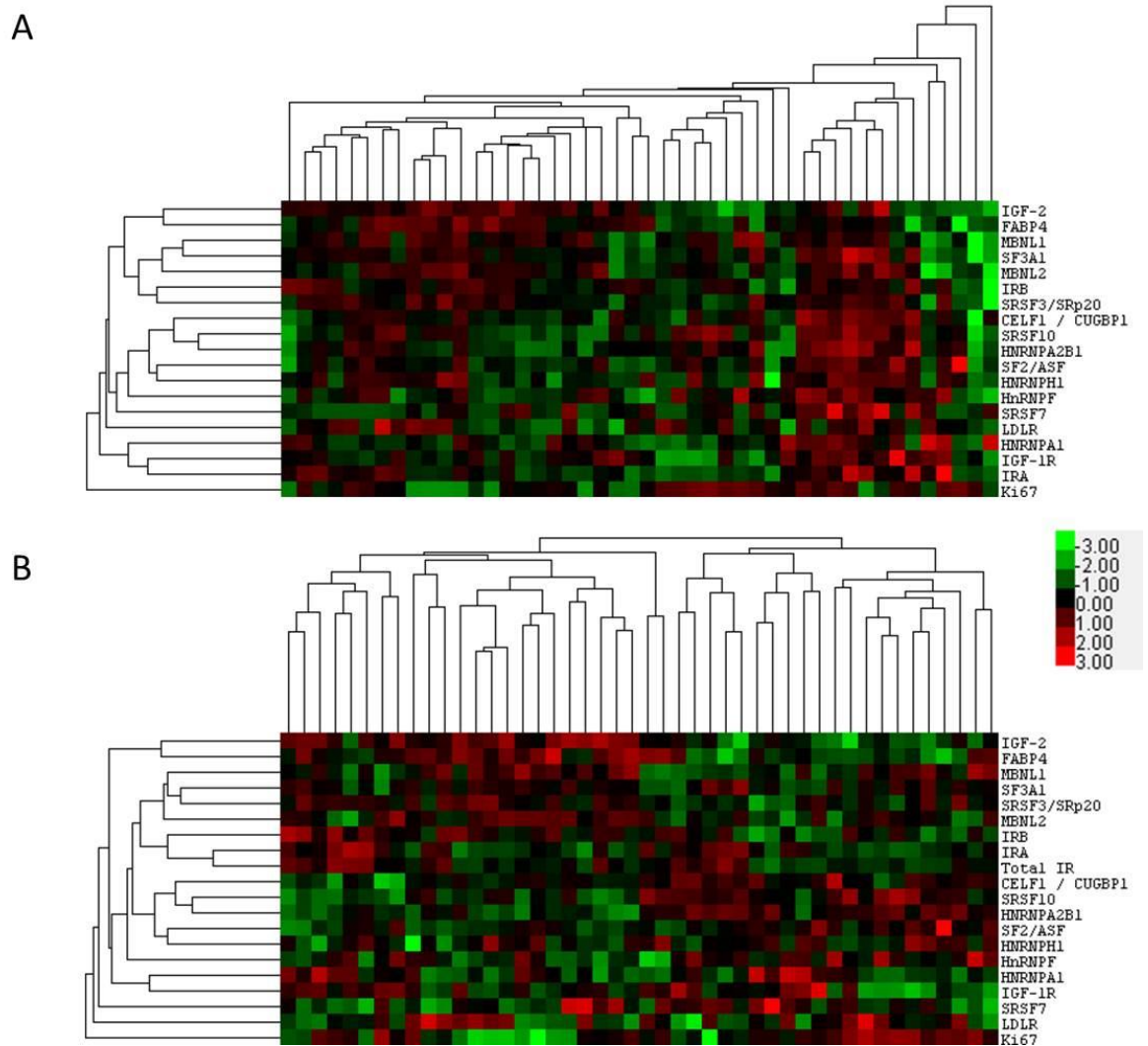


**Figure 55 Heatmap of clustered genes and cases from FFPE breast cancer samples**

Using the nSolver analysis software patient samples (x-axis) and genes (y-axis) were clustered together. (A) Heatmap of clustered genes and cases including all genes. The most highly correlated genes were total IR and IR-A (correlation 0.65), and they clustered with IR-B, and the splicing factors MBNL1, MBNL2, SF3A1, and SRSF3. (B) Analysis was repeated excluding the total IR to determine if specific genes clustered with the IR isoforms. IR-B correlated with SRSF3 (0.36) and clustered with MBNL1, MBNL2 and SF3A1. IR-A correlated with IGF-1R expression (0.32) and clustered with the splicing factor HNFNPA1. (n=46 cases).

In order to gain further insights into the role of the IR and these splicing factors in regulating IR-A and IR-B expression, we then analyzed the expression of the IR compared to the IGF-1R, and the IR isoforms in a number of human breast cancer cell lines, all grown in full medium with serum. We found that the non-tumourigenic MCF-10A cell line, expressed relatively low levels of both IGF-1R and IR, and expressed both receptors to a similar degree. The ER $\alpha$  positive cell lines (MCF7 and T47D) had higher IGF-1R than IR, while the triple negative breast cancer cell lines (SUM159, MDA-MB-231 and MDA-MB-468) had relatively more IR than IGF-1R (Figure 56). While the SUM149 breast cancer cell line is not traditionally considered to be ER $\alpha$  positive, it has recently been found to express an ER $\alpha$  variant (116). These data suggest that ER $\alpha$  expression or signaling plays a role in regulating IR expression.

We next analyzed the IR isoform expression in these human breast cancer cell lines. Similar to our findings with the human breast cancer cases, we found that the IR-A isoform was the predominant IR isoform in all breast cancer cell lines, and the expression of IR-A was lowest in the non-tumourigenic MCF10A epithelial cell line, and the next lowest ranking cell lines were the ER $\alpha$  positive cell lines (MCF7 and T47D) (Figure 57). Similar to the human samples, the expression of the IR-B was variable, in some samples the expression of IR-B was very low, being just above the lower threshold of detection in many of the cell lines. We further analyzed the gene expression profiles for clustering of genes and cell lines (Figure 58A), and found again that total IR correlated highly with IR-A (correlation coefficient 0.68) and less strongly with IR-B (correlation coefficient 0.54) and these genes clustered with splicing factors MBNL2 and SRSF3 (correlation coefficient 0.54). We then reanalyzed the data after removing total IR from the analysis and found that IR-A most closely correlated with SRSF3 expression (correlation coefficient 0.62) and IR-B correlated with MBNL2 (correlation coefficient 0.57). In the cell lines Ki67 weakly correlated with IR-A and IR-B expression and the expression of MBNL2 and SRSF3 (correlation coefficient 0.24).

From these human samples and human breast cancer cell lines it appears that the IR-A is highly expressed and is the dominant form of the IR in human breast cancer. The cell line data suggests that the oestrogen receptor may play a role in

suppressing IR-A expression. We will correlate the RNA data from the FFPE breast cancer samples with the pathological data to determine if the patient sample clusters correlate with breast cancer subtype splicing factors consistently correlated with IR-B expression is MBNL2 and the splicing factor consistently correlated with IR-A is SRSF3. The role of these splicing factors in breast cancer has not been well defined. Therefore, in future studies I aim to further understand the importance of IR-A and IR-B splicing and the expression of these splicing factors in human breast cancers.

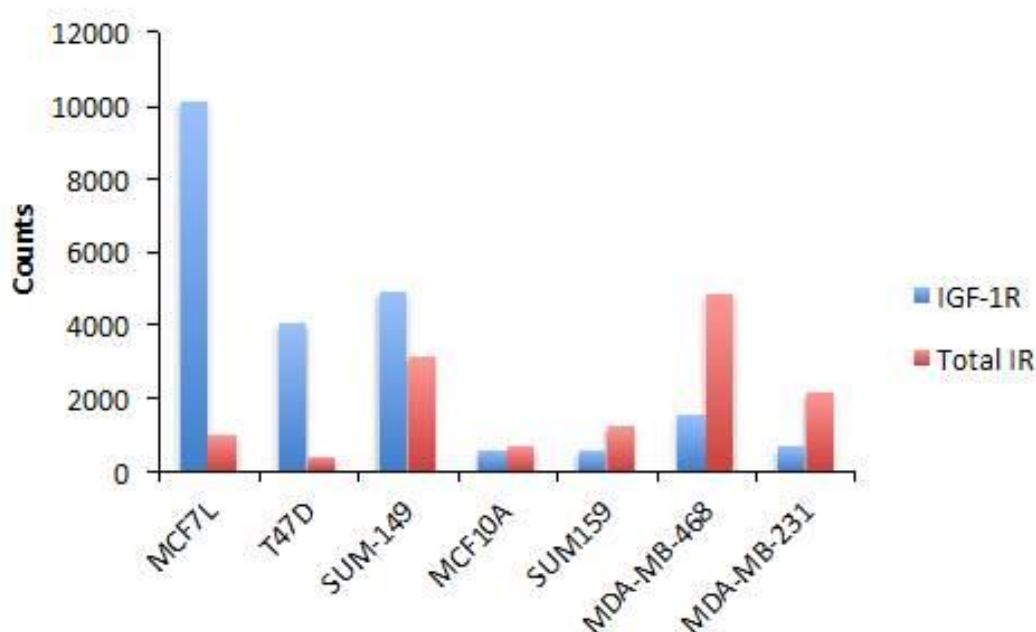


**Figure 56 Insulin Receptor and IGF-1R expression in human breast cancer cell lines.**

RNA expression of IR and IGF-1R in human breast cancer cell lines assessed by Nanostring and ordered from left to right based on the ratio of IGF-1R / IR expression. Blue bars represent the IGF-1R, red bars represent the IR expression. The y-axis is total counts per gene as measured by the Nanostring nCounter.

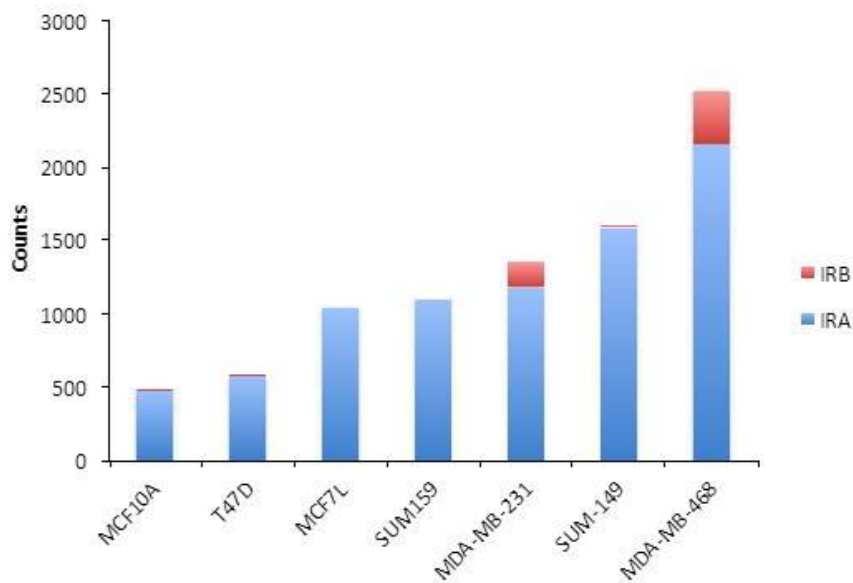


**Figure 57 Insulin Receptor A and B expression in human breast cell lines.**

The RNA expression of IR-A and IR-B in different human breast cell lines assessed by Nanostring, and ordered from left to right based on lowest to highest IR-A expression. The blue columns represent IR-A expression and the red columns are IR-B expression. The y-axis is the total counts per gene as measured by the Nanostring nCounter.



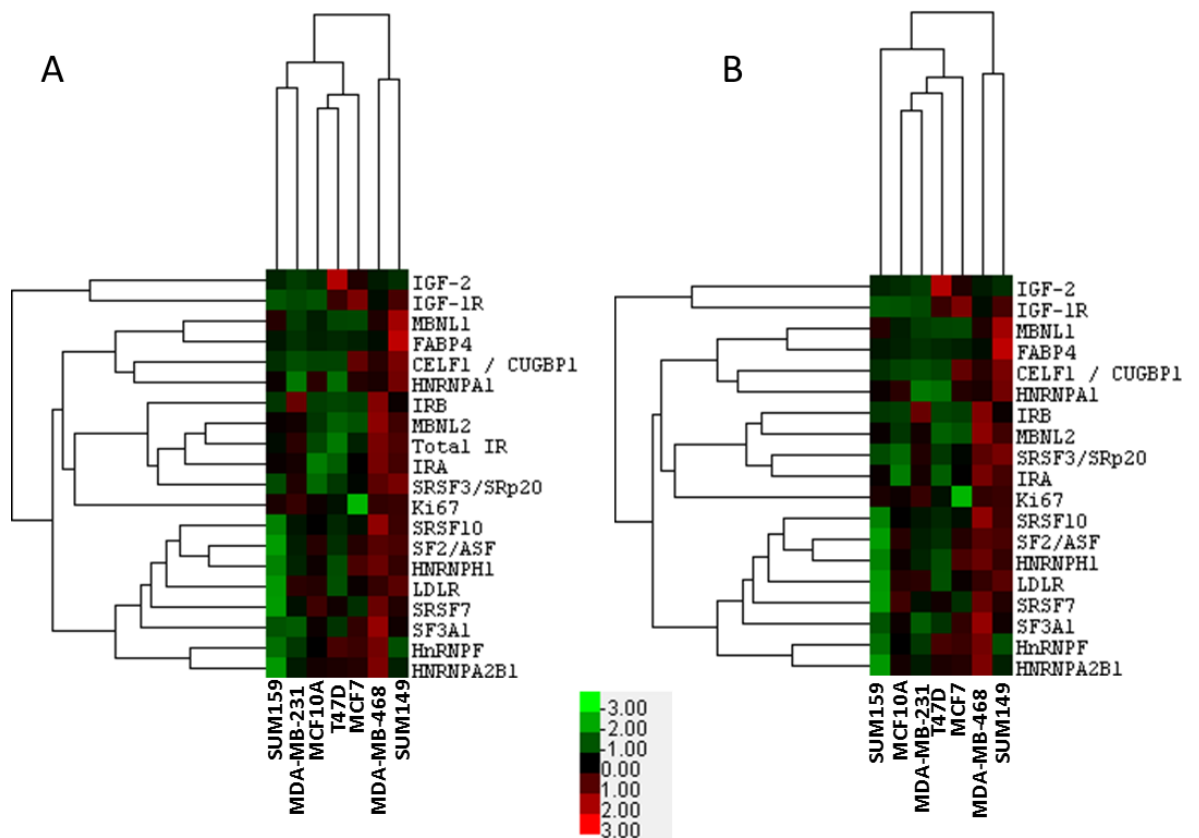


**Figure 58 Heatmap of clustered genes and human breast cell lines**

(A) Heatmap of clustered genes and cases including all genes. The most highly correlated genes were total IR and IR-A (correlation 0.65), and they clustered with IR-B, and the splicing factors MBNL1, MBNL2, SF3A1, and SRSF3. (B) Analysis was repeated excluding the total IR to determine if specific genes clustered with the IR isoforms. IR-B correlated with SRSF3 (0.36) and clustered with MBNL1, MBNL2 and SF3A1. IR-A correlated with IGF-1R expression (0.32) and clustered with the splicing factor HNFNPA1.

#### 4. Discussion

The results presented in this thesis demonstrate the importance of hyperinsulinaemia and IR activation in promoting the growth and metastasis of murine breast cancer orthografts and human breast cancer xenografts. This increase in growth and metastasis was consistently associated with an increase in Akt phosphorylation and an increase in c-myc and vimentin expression in different models. Deleting or reducing expression of the IR led to alterations in mammary gland development, most notably, a reduction in side branching. Silencing the IR in human triple negative breast cancers led to a decrease in tumour growth in the setting of hyperinsulinaemia, with decreased c-myc and vimentin expression in the xenografts. Silencing the IR in ER $\alpha$  positive human breast cancer cells, led to decreased proliferation and a decrease in c-myc expression. Conversely, activating the IR using the mitogenic insulin analogue (AspB10) increased the growth of orthotopic murine breast cancers. We have extended these studies into human breast cancers, and found that compared to the IGF-1R, the IR has higher expression in almost a third of cases. In all cases we found that the IR-A isoform of the IR is the predominant isoform. Further in the human breast cancer cell lines, we found that the ER $\alpha$  positive breast cancer cell lines had higher IGF-1R expression, while the ER $\alpha$  negative breast cancer cell lines had higher IR expression. These data suggest that endogenous hyperinsulinaemia is capable of driving breast cancer growth and metastasis.

These results support the epidemiological studies that suggest a causal relationship between type 2 diabetes and the incidence, recurrence and mortality from breast cancer. Hyperinsulinaemia has been identified as a specific factor that may drive breast cancer cell proliferation, but data in human patients which focuses on how specific subtypes of breast cancer respond to elevated circulating insulin are limited. In these studies we found that in ER $\alpha$  negative breast cancer subtypes of murine and human breast cancer, hyperinsulinaemia promoted tumour growth and metastasis. These data are the first time that this it has been shown in an animal model that endogenous hyperinsulinaemia significantly affects the rate of *Neu-NT*-mediated mammary tumour development as well as the progression of breast cancer metastasis to the lungs, and human triple negative breast cancer xenograft growth.

Previously we have employed the MKR mouse model to demonstrate that PyVmT-driven mammary gland hyperplasia at 3 and 15 weeks postnatal development is more advanced under conditions of hyperinsulinaemia (115). Hyperplasia of the mammary gland has previously been shown to occur rapidly (3-4 days) after conditionally-activated *Neu-NT*-expression (111). In MTB/TAN/MKR<sup>+/+</sup> mice, we observed that in the presence of elevated insulin, mammary gland hyperplasia was more advanced after 3 days, suggesting that hyperinsulinaemia can enhance the mitogenic effect of *Neu* oncogenic transformation on terminal end buds during mammary growth and development. The MMTV-c-Neu mouse model has been previously used to determine the effect of a high fat diet (HFD) on mammary gland hyperplasia. Although the c-Neu is a different model from ours (NeuNT), having a much longer tumour latency, it is interesting to note that either 5 or 10 weeks of HFD treatment in FVB/N mice had no effect upon mammary gland hyperplasia in MMTV-c-Neu mice compared to controls suggesting that at very early stages of tumour development, insulin may have a more potent effect than dietary fat in promoting terminal end bud hyperplasia. In the same model it was shown that a HFD based on corn oil resulted in shorter tumour latency than a HFD based on fish oils. Fish oil has been shown to lead to improved insulin sensitivity in some studies, when compared to corn oil, suggesting that hyperinsulinaemia may have played a role in the different tumour latency described in this study (100).

The role of hyperinsulinaemia in promoting the growth and metastasis of human triple negative breast cancers has been less clear from the literature. Previous studies linked obesity and type 2 diabetes with post-menopausal ER $\alpha$ -positive breast cancers, however more recent studies have found that syndromes of insulin resistance (obesity, type 2 diabetes and the metabolic syndrome) are associated with an increased risk of pre-menopausal triple negative breast cancer, and with a worse prognosis in those with early stage triple negative breast cancer (36, 77, 101, 102). Our animal models of human triple negative breast cancer (MDA-MB-231 and LCC6) in the hyperinsulinaemia mice support the hypothesis that hyperinsulinaemia increases tumour growth and progression in triple negative breast cancers. In contrast to the NeuNT model, which is a transgenic model, driven by overexpression of activated Neu, the MDA-MB-231 and LCC6 cell lines do not have activating mutations in Neu or other tyrosine kinase receptors. Hyperinsulinaemia may lead to increased tumour growth in the MDA-MB-231 and

LCC6 models by activating the PI3K/Akt pathway which may promote tumor growth in synergy with other tumor promoting mutations. We have not yet demonstrated in vivo if hyperinsulinaemia promotes the growth of ER $\alpha$ -positive breast cancers, or if hyperinsulinaemia alters ER $\alpha$  expression in vivo.

The mechanism by which insulin could increase tumour growth in the *Neu-NT* and triple negative models model may be complex. Our results demonstrate that MTB/TAN/MKR<sup>+/+</sup> mice demonstrate higher levels of phosphorylated IR/IGF-IR than MTB/TAN control mice, suggesting that insulin is acting through its cognate receptor and/or the highly homologous IGF-IR to promote mammary tumour growth. In human breast cancer phosphorylated IR/IGF-IR has been reported to be a prognostic marker of poor outcome for breast cancer, regardless of subtype (90). Challenges exist with the reliability of quantifying IR / IGF-1R phosphorylation in clinical breast cancer specimens, due to the variability introduced in fixation times of tissues in surgical operating rooms and the rapid dephosphorylation of the receptors. Furthermore, immunohistochemistry cannot detect whether it is the insulin receptor or IGF-1R that is phosphorylated, using currently available antibodies. Total IR expression has also been quantified in clinical studies by immunohistochemistry, and in some studies has been associated with a worse prognosis in breast cancer (106). Increased RNA expression of the IR has previously reported to occur sporadically in 8.6% of breast cancer specimens (n=93), and in MDA-MB-231 cells (119). In addition, the oncogenes *Neu*, *Wnt1* and *Ret*, as well as loss of the tumour suppressor p53 have been found to amplify IR expression in breast cancers (49, 146). We have observed an increase in IR expression, relative to IGF-1R expression in human triple negative breast cancer cell lines that are ER $\alpha$ -negative with different oncogenic mutations. Furthermore, we have seen an increase in IR protein expression in tumours from hyperinsulinaemic mice, compared to WT mice. In our animal models, we consistently see an increase in c-myc protein expression. Therefore, in future studies we will examine the effects of hyperinsulinaemia on the growth of human ER $\alpha$ -positive (MCF7) breast xenografts. We will also further examine the role of insulin on regulating ER $\alpha$  expression, and the effect of inhibiting ER $\alpha$  on IR expression. We will examine if c-myc regulates IR expression, and if insulin increases expression of its own receptor through c-myc.

The ratio of IR isoform A (IR-A) to isoform B (IR-B) is also important in breast cancer, and recently a higher IR-A/IR-B ratio has been observed in the luminal B subtype of breast cancer, and in human breast cancers resistant to hormonal therapy (65, 71). We found that the non-tumourigenic MCF10A cell line had lower levels of the IR-A isoform compared to the tumourigenic cell lines, and in both the cancer cell lines and the human breast cancer cases the IR-A isoform was the predominant isoform. There are a number of splicing factors that regulate the splicing of various pre-mRNAs. We found that MBNL2 and SRSF3 consistently clustered with the IR isoforms in the breast cancer cases, and cancer cell lines. There is one previous study showing that the expression of MBNL2 correlates with IR splicing in a mouse model of colon cancer, but there are no published studies examining its significance in breast cancer (7). MBNL2 and SRSF3 have been shown in other cell lines to enhance exon 11 inclusion, and thus increase IR-B expression (68, 130). We plan to further investigate the importance of the IR isoforms and their splicing factors in the growth and metastasis of human breast cancers in the setting of hyperinsulinaemia.

A further complicating aspect of the link between endogenous hyperinsulinaemia and cancer progression, is that under conditions of hyperinsulinaemia, IGF binding proteins (IGFBP)-1 and -2 are repressed, which may lead to an increase in circulating “free” IGF-1 (27). In these studies we found that the IGF-1R protein expression is also increased in our tumour xenografts and orthografts from the hyperinsulinaemic mice, and administration of high doses of IGF-1 further promoted tumour growth in the setting of hyperinsulinaemia by activating the IGF-1R and IR, we believe through activating the hybrid receptors. We therefore used the LCC6 tumour cell line with a knockdown of the IR to determine if the major effect of insulin on tumour cell growth was through the IR or indirectly by increasing free IGF-1. We found that silencing the IR reduced the growth of the LCC6 tumours in the hyperinsulinaemic mice and the control mice, demonstrating that the IR plays a key role in tumour progression. However, as silencing the IR led to a reduction in tumour growth to a similar extent in the control and hyperinsulinaemic mice, these results suggest that while the IR is clearly an important receptor for tumour growth, hyperinsulinaemia may be driving tumour growth in addition by indirect mechanisms.

Although primary tumour size and growth is important in breast cancer, ultimately mortality from breast cancer is not from the primary tumour, but rather from tumour metastases. Hyperinsulinaemia, as shown in Figure 5, is associated with increased mortality from breast cancer and greater recurrence. Therefore, in these studies we also aimed to understand the role of hyperinsulinaemia in breast cancer metastasis. We found that hyperinsulinaemia led to an increase in breast cancer metastasis in three of our models (MDA-MB-231 xenografts, MTB/TAN tumours, and MVT1 orthotopic tumours). In all three models we found an increase in the protein expression of vimentin. Vimentin belongs to the intermediate filament (IF) family of proteins and has recently been shown to be an important marker of the EMT in epithelial cells, which normally express only cytokeratin-type IFs (129), Vimentin is not specific for EMT, and is also a marker of cancer-associated fibroblasts (138). Additionally, there is an interaction between the tumour cells and these cancer-associated fibroblasts that induces EMT in breast cancer cells (135). In breast cancer cells, vimentin expression correlates with increased migration and invasion (60, 85). In human breast cancer specimens, several studies have reported overexpression of vimentin as a marker of poor prognosis (84). These studies are the first to show that hyperinsulinaemia increased vimentin expression, and that in vivo orthotopic injection of tumour cells with vimentin knockdown decreased breast cancer metastasis in the setting of hyperinsulinaemia. In the transgenic model in these studies, the MTB/TAN model, the majority of the vimentin positive cells did not co-stain with Neu, meaning that the hyperinsulinaemic mice may have had a greater desmoplastic reaction to the tumours, leading to the infiltration of more cancer associated fibroblasts. Alternatively, or coincidentally, these vimentin positive cells could have been tumour cells that underwent EMT and lost Neu expression. In our orthotopic and xenotopic models, the tumour cells already expressed vimentin, prior to being injected into the mice, therefore insulin enhanced their vimentin expression. We did not examine whether the microenvironment around the tumours in orthotopic or xenograft tumours in the MKR mice were also associated with an increase in the infiltration of vimentin-positive cells. These results also reveal novel phosphorylation sites on vimentin, and a number of deamidation sites. Protein deamidation is associated with immune responses in other conditions such as celiac, but its role in cancer immunity has been not been well explored (38). Interestingly, vimentin and ATP synthase (that co-immunoprecipitated with

vimentin), are both recognised as autoantigens that trigger T cell responses in immune diseases (131, 137). Therefore, the interaction between vimentin and ATP synthase may be involved in mitochondrial ATP synthesis, or they may be autoantigens in the tumour that alter the T cell response. Post-translational modifications of vimentin are also known to alter the cytoskeletal function of the protein, but again this area of research has not been well explored in cancer (133). In our future studies we plan to determine how insulin regulates vimentin protein levels, to determine if insulin alters the novel phosphorylation sites identified on vimentin by LC/MS, if insulin alters vimentin deamidation, and if vimentin plays an important role in cancer progression by interacting with T lymphocytes or cancer associated fibroblasts.

Examining the role of the insulin analogues in breast cancer growth had important translational implications. Over 25% of adult patients with diabetes in the US take insulin therapy (103), and it is used by millions of people worldwide. In addition, using these insulin analogues allowed us to further explore the role of insulin receptor activation and breast cancer growth in vivo. As discussed above, insulin downregulates the expression of IGFBP's and therefore, may result in more free IGF-1, which may indirectly be the mechanism through which insulin leads to tumour progression. In the LCC6 tumours we found that silencing the IR did reduce tumour growth in vivo in the hyperinsulinaemic mice, demonstrating that the IR is the main mediator of insulin's effects in vivo. With the immunoprecipitation studies, we demonstrated that it is the IR, rather than the IGF-1R that is activated in the tumours in the MKR mice. Furthermore, we found that activating the IR, using the mitogenic insulin analogue AspB10 further increased IR phosphorylation in vivo, and increased MVT1 tumour growth. AspB10 has previously been shown to induce spontaneous mammary tumours in rats [17]. Some in vitro studies report increased IR phosphorylation after AspB10 stimulation [22], although others have reported that AspB10 stimulates cell proliferation by acting through the IR and IGF-1R [20]. These in vitro studies found significantly greater IGF-1R phosphorylation compared to human insulin when using concentrations of AspB10 ten times higher than those used in our studies [20]. At concentrations of 10nM, IGF-1R phosphorylation by AspB10 was comparable that seen in response to human insulin in MCF7 cells [20], findings consistent with those from 5nM insulin or AspB10 stimulation in mouse embryonic fibroblasts [19].

Differences between in vitro and in vivo potency of AspB10 have been previously described [35] and highlight the need for caution when interpreting the results of in vitro studies. In vivo studies have not previously demonstrated whether AspB10 exerts its mitogenic effects through the IR or IGF-1R [21, 25]. Understanding the mechanism through which AspB10 promotes tumour growth is important for the development of new insulin analogues to ensure they are not mitogenic. While AspB10 increases mammary tumour growth in the dose range used in our study, no increase in rodent tumour growth with similar doses of human insulin has been found; this may be due to differences in IR affinity or dissociation rates between human insulin and AspB10, as previously described by others in in vitro studies [22].

Using the long acting basal insulin analogues in current clinical use, we found that none promoted the growth of MVT1 tumours in the MKR mouse, when compared to human insulin or vehicle treatment. Furthermore, all of these analogues led to phosphorylation of the IR in vivo, rather than the IGF-1R that was only activated by IGF-1.

This is the first in vivo study examining the effects of a non-metabolizable form of insulin glargine on tumour growth and receptor phosphorylation. We found that in vivo, A21Gly,DiD-Arg does not have mitogenic effects over vehicle, or human insulin. In addition, treating animals with this non-metabolizable form of insulin glargine did not lead to activation of the IGF-1R in the tumours. Overall, these findings are reassuring, given the large number of patients with breast cancer who have Type 2 diabetes, and the high percent of patients with Type 2 diabetes who are treated with basal insulin analogues. Our findings showing the lack of mitogenicity with insulin glargine are consistent with the pre-marketing rodent insulin glargine carcinogenicity studies (136), and also with a prospective human study on insulin glargine demonstrating no increase in the incidence of breast or any cancers or cancer deaths in new users of insulin glargine (74).

However, previous pre-clinical carcinogenicity studies and also the human study were designed to study whether insulin glargine led to the development of spontaneous tumours rather than to the progression of established cancers. Insulin glargine has been shown in vitro to have mitogenic effects on specific cell lines that express high levels of the IGF-1R (88, 134). The lack of mitogenicity of



insulin glargine in vivo however, was believed be due to the rapid metabolism of glargine to its M1 metabolite (99, 134). This M1 metabolite has not demonstrated mitogenicity in previous in vitro studies on cancer cell lines and has no greater affinity for the IGF-1R than human insulin (134). Therefore, even after administration of high doses of insulin glargine, we found that glargine is metabolized into the M1 metabolite and did not lead to tumour progression.

More surprising is our finding that the non-metabolizable analogue A21Gly,DiD-Arg also did not promote tumour growth in vivo. Previous in vitro studies have found that A21,Gly,DiD-Arg has similar affinity for the IGF-1R as insulin glargine, with similar mitogenic potency to insulin glargine in SAOS-2 cells (147). This insulin analogue is not metabolized in vitro by the carboxypeptidases that metabolize insulin glargine, therefore retaining its greater affinity for the IGF-1R than human insulin in vivo. This compound allowed us to mimic, in our mouse model, the effects that insulin glargine may have in a tumour-bearing person with the postulated slow rate of metabolism of insulin glargine, and therefore greater exposure to higher circulating levels of the parent glargine than the M1 metabolite. In clinical studies some variability has been observed in the inter-individual rates of metabolism of insulin glargine into the M1 metabolite (13), These findings have called into question if circulating concentrations of the glargine parent compound could be reached to activate the IGF-1R in some patients on chronic high doses of insulin glargine. In SAOS-2 and MCF-7 cell lines, although the mitogenic potency of both insulin glargine and A21Gly,DiD-Arg is higher than human insulin and the M1 metabolite of glargine, they have significantly lower mitogenic potency compared to IGF-1 (147). Similarly, although the affinity of insulin glargine and A21Gly-DiD-Arg for the IGF-1R is significantly higher than human insulin, it remains substantially lower than IGF-1 (134, 147). Therefore, while in vitro these compounds have a higher affinity for the IGF-1R than human insulin, in vivo where systemic and local IGF-1 are present, their relatively higher affinity for the IGF-1R in vitro does not translate into in vivo IGF-1R phosphorylation, nor into increased mammary tumour growth. These findings again highlight the need for complimentary in vitro and in vivo studies in examining the role of insulin, insulin analogues and IGF's in tumour progression.

New insulin analogues, and new methods of insulin delivery continue to be developed and it is important to determine if these new analogues may promote

cancer cell growth in vitro and in vivo. Our understanding of the complex interactions between insulin, its analogues and the IR and IGF-1R is still evolving (58, 108). We have learned that certain amino acid modifications to human insulin lead to increased mitogenicity in vitro and in vivo, such as with AspB10 insulin (51, 110, 134) and other modifications change the affinity of insulin for the IR and IGF-1R (58, 88).

Overall, with the greater risk of breast cancer mortality in patients with Type 2 diabetes, we need to further understand the pathophysiology linking these conditions, and ideally find therapies that may provide benefit to both the metabolic and oncological conditions of the patient. The findings of this study are reassuring for patients and for those treating patients with breast cancer and insulin-requiring diabetes.

Our human study aims to translate our pre-clinical work into meaningful improvements in patient survival. We are focusing on the survival disparity between the Black and White women with breast cancer in the US, due to the coincidently high rates of obesity and insulin resistance in this population. We anticipate finding that insulin resistance and hyperinsulinaemia are associated with poor prognostic indices in Black and White women, and that these conditions are more prevalent in the Black population. We also anticipate finding the presence of the IR and IGF-1R in breast cancer tissue, we anticipate finding an increase in total IR, specifically the IR-A isoform in women with insulin resistance. In addition, we do expect to find an association between insulin resistance and the presence of increased IR signaling in the tumours. We also expect to find an association between the greater IR/IGF-1R signaling and poor breast cancer prognosis. We expect that the phosphatidylinositol 3-kinase (PI3-K)/Akt pathway, rather than the ERK1/2 pathway will be the main signaling pathway activated by the IR in breast cancers from hyperinsulinaemic patients. These results would be in keeping with our previous pre-clinical studies (44, 115).

There are certain limitations to this clinical study that we recognise. We ask patients to self-identify race. We are not conducting genetic tests to determine biologic racial categories due to budgetary constraints and the uncertain utility of ancestry information markers. This study is cross-sectional, not longitudinal. Our outcome variable, a pathology measure of poor prognosis breast cancer, is a

proxy of survival. We do not conduct a complete follow-up survey to ascertain recurrence because: 1) tumour size, nodal status, ER and Her2 status have been validated measures of prognosis in studies ascertaining survival and 2) given an expected 2 year recurrence rate of 12%, we would not have adequate power to revalidate these prognostic indices. This study will not assess the ability of endogenous hyperinsulinaemia to stimulate the development of new incident cancer, but rather its potential mechanistic link to cancer progression and mortality. As our primary focus is on the role of hyperinsulinaemia and insulin receptor signaling pathways, we do not include tests of chronic inflammation and adipose tissue factors. However, with the patients' consent, we will bank frozen serum to enable future studies on novel markers in obesity, insulin resistance and cancer.

A randomized controlled trial (RCT) trial testing metformin treatment for breast cancer in the adjuvant setting is currently underway (NCT01101438, <https://clinicaltrials.gov/ct2/show/NCT01101438?term=NCT01101438&rank=1> last accessed 5<sup>th</sup> October 2015). The driving hypothesis is that metformin reduces signaling through the PI3K/Akt signaling pathway, activates 5' adenosine monophosphate activated protein kinase (AMPK) which in turn, inhibits mammalian target of rapamycin (mTOR), a protein activated by the IR signaling pathway that helps control cell division and survival. However, the metformin trial will leave unanswered the relationship between insulin resistance, race and poor prognosis breast cancer for two key reasons: 1) typically, only 2.5% of patients recruited for clinical trials are Black and 2) based on their target accrual of 3,582, the metformin study will not have sufficient power to ascertain racial differences in the relationship between insulin resistance and poor prognosis breast cancer. In addition, women in this study are unselected for the presence of insulin resistance, or being tested for the presence of the organic cation transporters (OCTs) on their tumours that would allow metformin to enter the tumour.

Ultimately, the results of these studies have provided novel insights into the importance of hyperinsulinaemia and IR expression and activation in the progression of breast cancer. Through our ongoing clinical studies, we will advance our understanding of the role of hyperinsulinaemia, the insulin receptor and its isoforms in breast cancer progression. We will also examine how the IR isoforms are regulated in breast cancers, and their importance to cancer

progression. We will further explore the role of hyperinsulinaemia and IR signaling in regulating downstream proteins including vimentin and how these proteins may be interacting with the tumour microenvironment to induce a tumour promoting lymphocyte reaction. Developing a greater understanding of these aspects of the link between hyperinsulinaemia and cancer will allow us to identify the specific therapies that will improve the survival of women with obesity, diabetes, the metabolic syndrome and breast cancer.

## References

1. **Adams TD, Stroup AM, Gress RE, Adams KF, Calle EE, Smith SC, Halverson RC, Simper SC, Hopkins PN, and Hunt SC.** Cancer incidence and mortality after gastric bypass surgery. *Obesity* 17: 796-802, 2009.
2. **Agin A, Jeandidier N, Gasser F, Grucker D, and Sapin R.** Glargine blood biotransformation: in vitro appraisal with human insulin immunoassay. *Diabetes & metabolism* 33: 205-212, 2007.
3. **Agurs-Collins T, Adams-Campbell LL, Kim KS, and Cullen KJ.** Insulin-like growth factor-1 and breast cancer risk in postmenopausal African-American women. *Cancer detection and prevention* 24: 199-206, 2000.
4. **Ahern TP, Hankinson SE, Willett WC, Pollak MN, Eliassen AH, and Tamimi RM.** Plasma C-peptide, mammographic breast density, and risk of invasive breast cancer. *Cancer epidemiology, biomarkers & prevention : a publication of the American Association for Cancer Research, cosponsored by the American Society of Preventive Oncology* 22: 1786-1796, 2013.
5. **Albergaria A, Ricardo S, Milanezi F, Carneiro V, Amendoeira I, Vieira D, Cameselle-Teijeiro J, and Schmitt F.** Nottingham Prognostic Index in triple-negative breast cancer: a reliable prognostic tool? *BMC cancer* 11: 299, 2011.
6. **Alberti KG, Eckel RH, Grundy SM, Zimmet PZ, Cleeman JI, Donato KA, Fruchart JC, James WP, Loria CM, Smith SC, Jr., International Diabetes Federation Task Force on E, Prevention, National Heart L, Blood I, American Heart A, World Heart F, International Atherosclerosis S, and International Association for the Study of O.** Harmonizing the metabolic syndrome: a joint interim statement of the International Diabetes Federation Task Force on Epidemiology and Prevention; National Heart, Lung, and Blood Institute; American Heart Association; World Heart Federation; International Atherosclerosis Society; and International Association for the Study of Obesity. *Circulation* 120: 1640-1645, 2009.
7. **Andres SF, Simmons JG, Mah AT, Santoro MA, Van Landeghem L, and Lund PK.** Insulin receptor isoform switching in intestinal stem cells, progenitors, differentiated lineages and tumors: evidence that IR-B limits proliferation. *Journal of cell science* 126: 5645-5656, 2013.
8. **Ashwell SG, and Home PD.** Insulin glargine: the first clinically useful extended-action insulin analogue. *Expert opinion on pharmacotherapy* 2: 1891-1902, 2001.
9. **Atwood CS, Hovey RC, Glover JP, Chepko G, Ginsburg E, Robison WG, and Vonderhaar BK.** Progesterone induces side-branching of the ductal epithelium in the mammary glands of peripubertal mice. *The Journal of endocrinology* 167: 39-52, 2000.
10. **Ausk KJ, Boyko EJ, and Ioannou GN.** Insulin resistance predicts mortality in nondiabetic individuals in the U.S. *Diabetes care* 33: 1179-1185, 2010.
11. **Balslev I, Axelsson CK, Zedeler K, Rasmussen BB, Carstensen B, and Mouridsen HT.** The Nottingham Prognostic Index applied to 9,149 patients from the studies of the Danish Breast Cancer Cooperative Group (DBCG). *Breast cancer research and treatment* 32: 281-290, 1994.
12. **Barone BB, Yeh HC, Snyder CF, Peairs KS, Stein KB, Derr RL, Wolff AC, and Brancati FL.** Long-term all-cause mortality in cancer patients with

preexisting diabetes mellitus: a systematic review and meta-analysis. *JAMA : the journal of the American Medical Association* 300: 2754-2764, 2008.

13. **Bates T, Evans T, Lagord C, Monypenny I, Kearins O, and Lawrence G.** A population based study of variations in operation rates for breast cancer, of comorbidity and prognosis at diagnosis: failure to operate for early breast cancer in older women. *European journal of surgical oncology : the journal of the European Society of Surgical Oncology and the British Association of Surgical Oncology* 40: 1230-1236, 2014.

14. **Belfiore A, Frasca F, Pandini G, Sciacca L, and Vigneri R.** Insulin receptor isoforms and insulin receptor/insulin-like growth factor receptor hybrids in physiology and disease. *Endocrine reviews* 30: 586-623, 2009.

15. **Bell ET.** Carcinoma of the pancreas. I. A clinical and pathologic study of 609 necropsied cases. II. The relation of carcinoma of the pancreas to diabetes mellitus. *The American journal of pathology* 33: 499-523, 1957.

16. **Bendell JC, Rodon J, Burris HA, de Jonge M, Verweij J, Birlle D, Demanse D, De Buck SS, Ru QC, Peters M, Goldbrunner M, and Baselga J.** Phase I, dose-escalation study of BKM120, an oral pan-Class I PI3K inhibitor, in patients with advanced solid tumors. *Journal of clinical oncology : official journal of the American Society of Clinical Oncology* 30: 282-290, 2012.

17. **Bentov I, LeRoith D, and Werner H.** The WT1 Wilms' tumor suppressor gene: a novel target for insulin-like growth factor-I action. *Endocrinology* 144: 4276-4279, 2003.

18. **Bickell NA, Wang JJ, Oluwole S, Schrag D, Godfrey H, Hiotis K, Mendez J, and Guth AA.** Missed opportunities: racial disparities in adjuvant breast cancer treatment. *Journal of clinical oncology : official journal of the American Society of Clinical Oncology* 24: 1357-1362, 2006.

19. **Birks S, Peeters A, Backholer K, O'Brien P, and Brown W.** A systematic review of the impact of weight loss on cancer incidence and mortality. *Obesity reviews : an official journal of the International Association for the Study of Obesity* 13: 868-891, 2012.

20. **Bolli GB, Hahn AD, Schmidt R, Eisenblatter T, Dahmen R, Heise T, and Becker RH.** Plasma exposure to insulin glargine and its metabolites M1 and M2 after subcutaneous injection of therapeutic and suprathreshold doses of glargine in subjects with type 1 diabetes. *Diabetes care* 35: 2626-2630, 2012.

21. **Bonora E, Targher G, Alberiche M, Bonadonna RC, Saggiani F, Zenere MB, Monauni T, and Muggeo M.** Homeostasis model assessment closely mirrors the glucose clamp technique in the assessment of insulin sensitivity: studies in subjects with various degrees of glucose tolerance and insulin sensitivity. *Diabetes care* 23: 57-63, 2000.

22. **Bordeleau L, Yakubovich N, Dagenais GR, Rosenstock J, Probstfield J, Chang Yu P, Ryden LE, Pirags V, Spinaz GA, Birkeland KI, Ratner RE, Marin-Neto JA, Keltai M, Riddle MC, Bosch J, Yusuf S, Gerstein HC, and Investigators OT.** The association of basal insulin glargine and/or n-3 fatty acids with incident cancers in patients with dysglycemia. *Diabetes care* 37: 1360-1366, 2014.

23. **Borowsky AD, Namba R, Young LJ, Hunter KW, Hodgson JG, Tepper CG, McGoldrick ET, Muller WJ, Cardiff RD, and Gregg JP.** Syngeneic mouse mammary carcinoma cell lines: two closely related cell lines with divergent metastatic behavior. *Clin Exp Metastasis* 22: 47-59, 2005.

24. **Bruning JC, Michael MD, Winnay JN, Hayashi T, Horsch D, Accili D, Goodyear LJ, and Kahn CR.** A muscle-specific insulin receptor knockout exhibits

features of the metabolic syndrome of NIDDM without altering glucose tolerance. *Molecular cell* 2: 559-569, 1998.

25. **Bu W, Chen J, Morrison GD, Huang S, Creighton CJ, Huang J, Chamness GC, Hilsenbeck SG, Roop DR, Leavitt AD, and Li Y.** Keratin 6a marks mammary bipotential progenitor cells that can give rise to a unique tumor model resembling human normal-like breast cancer. *Oncogene* 30: 4399-4409, 2011.
26. **Caan BJ, Kwan ML, Hartzell G, Castillo A, Slattery ML, Sternfeld B, and Weltzien E.** Pre-diagnosis body mass index, post-diagnosis weight change, and prognosis among women with early stage breast cancer. *Cancer causes & control : CCC* 19: 1319-1328, 2008.
27. **Calle EE, and Kaaks R.** Overweight, obesity and cancer: epidemiological evidence and proposed mechanisms. *Nature reviews Cancer* 4: 579-591, 2004.
28. **Calle EE, Rodriguez C, Walker-Thurmond K, and Thun MJ.** Overweight, obesity, and mortality from cancer in a prospectively studied cohort of U.S. adults. *The New England journal of medicine* 348: 1625-1638, 2003.
29. **Calle EE, Thun MJ, Petrelli JM, Rodriguez C, and Heath CW, Jr.** Body-mass index and mortality in a prospective cohort of U.S. adults. *The New England journal of medicine* 341: 1097-1105, 1999.
30. **Campbell PT, Newton CC, Patel AV, Jacobs EJ, and Gapstur SM.** Diabetes and cause-specific mortality in a prospective cohort of one million U.S. adults. *Diabetes care* 35: 1835-1844, 2012.
31. **Chettouh H, Fartoux L, Aoudjehane L, Wendum D, Claperon A, Chretien Y, Rey C, Scatton O, Soubrane O, Conti F, Praz F, Housset C, Rosmorduc O, and Desbois-Mouthon C.** Mitogenic insulin receptor-A is overexpressed in human hepatocellular carcinoma due to EGFR-mediated dysregulation of RNA splicing factors. *Cancer research* 73: 3974-3986, 2013.
32. **Cho HS, Mason K, Ramyar KX, Stanley AM, Gabelli SB, Denney DW, Jr., and Leahy DJ.** Structure of the extracellular region of HER2 alone and in complex with the Herceptin Fab. *Nature* 421: 756-760, 2003.
33. **Christou NV, Lieberman M, Sampalis F, and Sampalis JS.** Bariatric surgery reduces cancer risk in morbidly obese patients. *Surgery for obesity and related diseases : official journal of the American Society for Bariatric Surgery* 4: 691-695, 2008.
34. **Cox ME, Gleave ME, Zakikhani M, Bell RH, Piura E, Vickers E, Cunningham M, Larsson O, Fazli L, and Pollak M.** Insulin receptor expression by human prostate cancers. *The Prostate* 69: 33-40, 2009.
35. **Cui X, Lazard Z, Zhang P, Hopp TA, and Lee AV.** Progesterone crosstalks with insulin-like growth factor signaling in breast cancer cells via induction of insulin receptor substrate-2. *Oncogene* 22: 6937-6941, 2003.
36. **Davis AA, and Kaklamani VG.** Metabolic syndrome and triple-negative breast cancer: a new paradigm. *International journal of breast cancer* 2012: 809291, 2012.
37. **Drejer K, Kruse V, Larsen UD, Hougaard P, Bjorn S, and Gammeltoft S.** Receptor binding and tyrosine kinase activation by insulin analogues with extreme affinities studied in human hepatoma HepG2 cells. *Diabetes* 40: 1488-1495, 1991.
38. **du Pre MF, and Sollid LM.** T-cell and B-cell immunity in celiac disease. *Best practice & research Clinical gastroenterology* 29: 413-423, 2015.
39. **Duggan C, Irwin ML, Xiao L, Henderson KD, Smith AW, Baumgartner RN, Baumgartner KB, Bernstein L, Ballard-Barbash R, and McTiernan A.** Associations of insulin resistance and adiponectin with mortality in women with

- breast cancer. *Journal of clinical oncology : official journal of the American Society of Clinical Oncology* 29: 32-39, 2011.
40. **Dunnwald LK, Rossing MA, and Li CI.** Hormone receptor status, tumor characteristics, and prognosis: a prospective cohort of breast cancer patients. *Breast cancer research : BCR* 9: R6, 2007.
  41. **Edge SB, and Compton CC.** The American Joint Committee on Cancer: the 7th edition of the AJCC cancer staging manual and the future of TNM. *Annals of surgical oncology* 17: 1471-1474, 2010.
  42. **Evans JM, Donnelly LA, Emslie-Smith AM, Alessi DR, and Morris AD.** Metformin and reduced risk of cancer in diabetic patients. *Bmj* 330: 1304-1305, 2005.
  43. **Evans M, Schumm-Draeger PM, Vora J, and King AB.** A review of modern insulin analogue pharmacokinetic and pharmacodynamic profiles in type 2 diabetes: improvements and limitations. *Diabetes, obesity & metabolism* 13: 677-684, 2011.
  44. **Ferguson RD, Novosyadlyy R, Fierz Y, Alikhani N, Sun H, Yakar S, and Leroith D.** Hyperinsulinemia enhances c-Myc-mediated mammary tumor development and advances metastatic progression to the lung in a mouse model of type 2 diabetes. *Breast Cancer Res* 14: R8, 2012.
  45. **Fernandez AM, Kim JK, Yakar S, Dupont J, Hernandez-Sanchez C, Castle AL, Filmore J, Shulman GI, and Le Roith D.** Functional inactivation of the IGF-I and insulin receptors in skeletal muscle causes type 2 diabetes. *Genes & development* 15: 1926-1934, 2001.
  46. **Fierz Y, Novosyadlyy R, Vijayakumar A, Yakar S, and LeRoith D.** Insulin-sensitizing therapy attenuates type 2 diabetes-mediated mammary tumor progression. *Diabetes* 59: 686-693, 2010.
  47. **Fortina P, and Surrey S.** Digital mRNA profiling. *Nature biotechnology* 26: 293-294, 2008.
  48. **Friberg E, Orsini N, Mantzoros CS, and Wolk A.** Diabetes mellitus and risk of endometrial cancer: a meta-analysis. *Diabetologia* 50: 1365-1374, 2007.
  49. **Frittitta L, Cerrato A, Sacco MG, Weidner N, Goldfine ID, and Vigneri R.** The insulin receptor content is increased in breast cancers initiated by three different oncogenes in transgenic mice. *Breast cancer research and treatment* 45: 141-147, 1997.
  50. **Galea MH, Blamey RW, Elston CE, and Ellis IO.** The Nottingham Prognostic Index in primary breast cancer. *Breast cancer research and treatment* 22: 207-219, 1992.
  51. **Gallagher EJ, Alikhani N, Tobin-Hess A, Blank J, Buffin NJ, Zelenko Z, Tennagels N, Werner U, and LeRoith D.** Insulin receptor phosphorylation by endogenous insulin or the insulin analog AspB10 promotes mammary tumor growth independent of the IGF-I receptor. *Diabetes* 62: 3553-3560, 2013.
  52. **Gallagher EJ, Fierz Y, Ferguson RD, and LeRoith D.** The pathway from diabetes and obesity to cancer, on the route to targeted therapy. *Endocrine practice : official journal of the American College of Endocrinology and the American Association of Clinical Endocrinologists* 16: 864-873, 2010.
  53. **Gallagher EJ, Fierz Y, Vijayakumar A, Haddad N, Yakar S, and LeRoith D.** Inhibiting PI3K reduces mammary tumor growth and induces hyperglycemia in a mouse model of insulin resistance and hyperinsulinemia. *Oncogene* 31: 3213-3222, 2012.
  54. **Galloway JA.** Insulin treatment for the early 80s: facts and questions about old and new insulins and their usage. *Diabetes care* 3: 615-622, 1980.



55. **Garrett TP, McKern NM, Lou M, Elleman TC, Adams TE, Lovrecz GO, Kofler M, Jorissen RN, Nice EC, Burgess AW, and Ward CW.** The crystal structure of a truncated ErbB2 ectodomain reveals an active conformation, poised to interact with other ErbB receptors. *Molecular cell* 11: 495-505, 2003.
56. **Gaudet MM, Carter BD, Patel AV, Teras LR, Jacobs EJ, and Gapstur SM.** Waist circumference, body mass index, and postmenopausal breast cancer incidence in the Cancer Prevention Study-II Nutrition Cohort. *Cancer causes & control* : CCC 25: 737-745, 2014.
57. **Gauger KJ, Bassa LM, Henchey EM, Wyman J, Ser-Dolansky J, Shimono A, and Schneider SS.** The effects of diet induced obesity on breast cancer associated pathways in mice deficient in SFRP1. *Molecular cancer* 13: 117, 2014.
58. **Gauguin L, Klaproth B, Sajid W, Andersen AS, McNeil KA, Forbes BE, and De Meyts P.** Structural basis for the lower affinity of the insulin-like growth factors for the insulin receptor. *The Journal of biological chemistry* 283: 2604-2613, 2008.
59. **Geiss GK, Bumgarner RE, Birditt B, Dahl T, Dowidar N, Dunaway DL, Fell HP, Ferree S, George RD, Grogan T, James JJ, Maysuria M, Mitton JD, Oliveri P, Osborn JL, Peng T, Ratcliffe AL, Webster PJ, Davidson EH, Hood L, and Dimitrov K.** Direct multiplexed measurement of gene expression with color-coded probe pairs. *Nature biotechnology* 26: 317-325, 2008.
60. **Gilles C, Polette M, Mestdagh M, Nawrocki-Raby B, Ruggeri P, Birembaut P, and Foidart JM.** Transactivation of vimentin by beta-catenin in human breast cancer cells. *Cancer research* 63: 2658-2664, 2003.
61. **Goodwin PJ, Ennis M, Bahl M, Fantus IG, Pritchard KI, Trudeau ME, Koo J, and Hood N.** High insulin levels in newly diagnosed breast cancer patients reflect underlying insulin resistance and are associated with components of the insulin resistance syndrome. *Breast cancer research and treatment* 114: 517-525, 2009.
62. **Guevara-Aguirre J, Balasubramanian P, Guevara-Aguirre M, Wei M, Madia F, Cheng CW, Hwang D, Martin-Montalvo A, Saavedra J, Ingles S, de Cabo R, Cohen P, and Longo VD.** Growth hormone receptor deficiency is associated with a major reduction in pro-aging signaling, cancer, and diabetes in humans. *Science translational medicine* 3: 70ra13, 2011.
63. **Hanahan D, and Weinberg RA.** Hallmarks of cancer: the next generation. *Cell* 144: 646-674, 2011.
64. **Hansen BF, Glendorf T, Hegelund AC, Lundby A, Lutzen A, Slaaby R, and Stidsen CE.** Molecular characterisation of long-acting insulin analogues in comparison with human insulin, IGF-1 and insulin X10. *PloS one* 7: e34274, 2012.
65. **Harrington SC, Weroha SJ, Reynolds C, Suman VJ, Lingle WL, and Haluska P.** Quantifying insulin receptor isoform expression in FFPE breast tumors. *Growth hormone & IGF research : official journal of the Growth Hormone Research Society and the International IGF Research Society* 22: 108-115, 2012.
66. **Harvie M, Hooper L, and Howell AH.** Central obesity and breast cancer risk: a systematic review. *Obesity reviews : an official journal of the International Association for the Study of Obesity* 4: 157-173, 2003.
67. **Hemkens LG, Grouven U, Bender R, Gunster C, Gutschmidt S, Selke GW, and Sawicki PT.** Risk of malignancies in patients with diabetes treated with human insulin or insulin analogues: a cohort study. *Diabetologia* 52: 1732-1744, 2009.

68. **Ho TH, Charlet BN, Poulos MG, Singh G, Swanson MS, and Cooper TA.** Muscleblind proteins regulate alternative splicing. *The EMBO journal* 23: 3103-3112, 2004.
69. **Homs J, and Luong D.** Symptoms and survival in patients with advanced disease. *Journal of palliative medicine* 10: 904-909, 2007.
70. **Hongisto V, Jernstrom S, Fey V, Mpindi JP, Kleivi Sahlberg K, Kallioniemi O, and Perala M.** High-throughput 3D screening reveals differences in drug sensitivities between culture models of JIMT1 breast cancer cells. *PloS one* 8: e77232, 2013.
71. **Huang J, Morehouse C, Streicher K, Higgs BW, Gao J, Czapiga M, Boutrin A, Zhu W, Brohawn P, Chang Y, Viner J, LaVallee T, Richman L, Jallal B, and Yao Y.** Altered expression of insulin receptor isoforms in breast cancer. *PloS one* 6: e26177, 2011.
72. **Huang Z, Willett WC, Colditz GA, Hunter DJ, Manson JE, Rosner B, Speizer FE, and Hankinson SE.** Waist circumference, waist:hip ratio, and risk of breast cancer in the Nurses' Health Study. *American journal of epidemiology* 150: 1316-1324, 1999.
73. **Hunt BR, Whitman S, and Hurlbert MS.** Increasing Black:White disparities in breast cancer mortality in the 50 largest cities in the United States. *Cancer epidemiology* 38: 118-123, 2014.
74. **Investigators OT, Gerstein HC, Bosch J, Dagenais GR, Diaz R, Jung H, Maggioni AP, Pogue J, Probstfield J, Ramachandran A, Riddle MC, Ryden LE, and Yusuf S.** Basal insulin and cardiovascular and other outcomes in dysglycemia. *The New England journal of medicine* 367: 319-328, 2012.
75. **Iqbal J, Ginsburg O, Rochon PA, Sun P, and Narod SA.** Differences in breast cancer stage at diagnosis and cancer-specific survival by race and ethnicity in the United States. *Jama* 313: 165-173, 2015.
76. **Irwin ML, Duggan C, Wang CY, Smith AW, McTiernan A, Baumgartner RN, Baumgartner KB, Bernstein L, and Ballard-Barbash R.** Fasting C-peptide levels and death resulting from all causes and breast cancer: the health, eating, activity, and lifestyle study. *Journal of clinical oncology : official journal of the American Society of Clinical Oncology* 29: 47-53, 2011.
77. **Jain R, Strickler HD, Fine E, and Sparano JA.** Clinical studies examining the impact of obesity on breast cancer risk and prognosis. *Journal of mammary gland biology and neoplasia* 18: 257-266, 2013.
78. **Johansson GS, and Arnqvist HJ.** Insulin and IGF-I action on insulin receptors, IGF-I receptors, and hybrid insulin/IGF-I receptors in vascular smooth muscle cells. *Am J Physiol Endocrinol Metab* 291: E1124-1130, 2006.
79. **Jonassen I, Havelund S, Hoeg-Jensen T, Steensgaard DB, Wahlund PO, and Ribel U.** Design of the novel protraction mechanism of insulin degludec, an ultra-long-acting basal insulin. *Pharmaceutical research* 29: 2104-2114, 2012.
80. **Kang S, Brange J, Burch A, Volund A, and Owens DR.** Absorption kinetics and action profiles of subcutaneously administered insulin analogues (AspB9GluB27, AspB10, AspB28) in healthy subjects. *Diabetes care* 14: 1057-1065, 1991.
81. **Kaplan SA.** The insulin receptor. *The Journal of pediatrics* 104: 327-336, 1984.
82. **Kim WG, Park JW, Willingham MC, and Cheng SY.** Diet-induced obesity increases tumor growth and promotes anaplastic change in thyroid cancer in a mouse model. *Endocrinology* 154: 2936-2947, 2013.
83. **Kitamura T, Kahn CR, and Accili D.** Insulin receptor knockout mice. *Annual review of physiology* 65: 313-332, 2003.

84. **Kokkinos MI, Wafai R, Wong MK, Newgreen DF, Thompson EW, and Waltham M.** Vimentin and epithelial-mesenchymal transition in human breast cancer--observations in vitro and in vivo. *Cells, tissues, organs* 185: 191-203, 2007.
85. **Korsching E, Packeisen J, Liedtke C, Hungermann D, Wulfiging P, van Diest PJ, Brandt B, Boecker W, and Buerger H.** The origin of vimentin expression in invasive breast cancer: epithelial-mesenchymal transition, myoepithelial histogenesis or histogenesis from progenitor cells with bilinear differentiation potential? *The Journal of pathology* 206: 451-457, 2005.
86. **Kroenke CH, Sweeney C, Kwan ML, Quesenberry CP, Weltzien EK, Habel LA, Castillo A, Bernard PS, Factor RE, Kushi LH, and Caan BJ.** Race and breast cancer survival by intrinsic subtype based on PAM50 gene expression. *Breast cancer research and treatment* 144: 689-699, 2014.
87. **Kurtzhals P.** Pharmacology of insulin detemir. *Endocrinology and metabolism clinics of North America* 36 Suppl 1: 14-20, 2007.
88. **Kurtzhals P, Schaffer L, Sorensen A, Kristensen C, Jonassen I, Schmid C, and Trub T.** Correlations of receptor binding and metabolic and mitogenic potencies of insulin analogs designed for clinical use. *Diabetes* 49: 999-1005, 2000.
89. **Larsson SC, Mantzoros CS, and Wolk A.** Diabetes mellitus and risk of breast cancer: a meta-analysis. *International journal of cancer Journal international du cancer* 121: 856-862, 2007.
90. **Law JH, Habibi G, Hu K, Masoudi H, Wang MY, Stratford AL, Park E, Gee JM, Finlay P, Jones HE, Nicholson RI, Carboni J, Gottardis M, Pollak M, and Dunn SE.** Phosphorylated insulin-like growth factor-I/insulin receptor is present in all breast cancer subtypes and is related to poor survival. *Cancer research* 68: 10238-10246, 2008.
91. **LeRoith D, Werner H, Neuenschwander S, Kalebic T, and Helman LJ.** The role of the insulin-like growth factor-I receptor in cancer. *Annals of the New York Academy of Sciences* 766: 402-408, 1995.
92. **Li HJ, Che XM, Zhao W, He SC, Zhang ZL, and Chen R.** Diet-induced obesity potentiates the growth of gastric cancer in mice. *Experimental and therapeutic medicine* 4: 615-620, 2012.
93. **Lipscombe LL, Chan WW, Yun L, Austin PC, Anderson GM, and Rochon PA.** Incidence of diabetes among postmenopausal breast cancer survivors. *Diabetologia* 56: 476-483, 2013.
94. **Liu H, Radisky DC, Yang D, Xu R, Radisky ES, Bissell MJ, and Bishop JM.** MYC suppresses cancer metastasis by direct transcriptional silencing of  $\alpha$ 5 and  $\beta$ 3 integrin subunits. *Nature cell biology* 14: 567-574, 2012.
95. **Liu J, Coady S, Carr JJ, Hoffmann U, Taylor HA, and Fox CS.** Differential associations of abdominal visceral, subcutaneous adipose tissue with cardiometabolic risk factors between African and European Americans. *Obesity* 22: 811-818, 2014.
96. **Liu Z, Brooks RS, Ciappio ED, Kim SJ, Crott JW, Bennett G, Greenberg AS, and Mason JB.** Diet-induced obesity elevates colonic TNF- $\alpha$  in mice and is accompanied by an activation of Wnt signaling: a mechanism for obesity-associated colorectal cancer. *The Journal of nutritional biochemistry* 23: 1207-1213, 2012.
97. **Ljung R, Talback M, Haglund B, Jonasson JM, Gudbjornsdottir S, and Steineck G.** Insulin glargine use and short-term incidence of breast cancer - a four-year population-based observation. *Acta oncologica* 51: 400-402, 2012.

98. **Lu Y, Zi X, Zhao Y, Mascarenhas D, and Pollak M.** Insulin-like growth factor-I receptor signaling and resistance to trastuzumab (Herceptin). *Journal of the National Cancer Institute* 93: 1852-1857, 2001.
99. **Lucidi P, Porcellati F, Candeloro P, Cioli P, Andreoli AM, Marzotti S, Schmidt R, Bolli GB, and Fanelli CG.** Glargine metabolism over 24 h following its subcutaneous injection in patients with type 2 diabetes mellitus: a dose-response study. *Nutrition, metabolism, and cardiovascular diseases : NMCD* 24: 709-716, 2014.
100. **Luijten M, Verhoef A, Dormans JA, Beems RB, Cremers HW, Nagelkerke NJ, Adlercreutz H, Penalvo JL, and Piersma AH.** Modulation of mammary tumor development in Tg.NK (MMTV/c-neu) mice by dietary fatty acids and life stage-specific exposure to phytoestrogens. *Reproductive toxicology* 23: 407-413, 2007.
101. **Ma FJ, Liu ZB, Qu L, Hao S, Liu GY, Wu J, and Shao ZM.** Impact of type 2 diabetes mellitus on the prognosis of early stage triple-negative breast cancer in People's Republic of China. *OncoTargets and therapy* 7: 2147-2154, 2014.
102. **Maiti B, Kundranda MN, Spiro TP, and Daw HA.** The association of metabolic syndrome with triple-negative breast cancer. *Breast cancer research and treatment* 121: 479-483, 2010.
103. **Mann DM, Woodward M, Ye F, Krousel-Wood M, and Muntner P.** Trends in medication use among US adults with diabetes mellitus: glycemic control at the expense of controlling cardiovascular risk factors. *Archives of internal medicine* 169: 1718-1720, 2009.
104. **Marques RG, Fontaine MJ, and Rogers J.** C-peptide: much more than a byproduct of insulin biosynthesis. *Pancreas* 29: 231-238, 2004.
105. **Marshall J.** Transwell((R)) invasion assays. *Methods Mol Biol* 769: 97-110, 2011.
106. **Mathieu MC, Clark GM, Allred DC, Goldfine ID, and Vigneri R.** Insulin receptor expression and clinical outcome in node-negative breast cancer. *Proceedings of the Association of American Physicians* 109: 565-571, 1997.
107. **Maynard GD.** A STATISTICAL STUDY IN CANCER DEATH-RATES *Biometrika* 7: 276-304, 1910.
108. **Menting JG, Whittaker J, Margetts MB, Whittaker LJ, Kong GK, Smith BJ, Watson CJ, Zakova L, Kletvikova E, Jiracek J, Chan SJ, Steiner DF, Dodson GG, Brzozowski AM, Weiss MA, Ward CW, and Lawrence MC.** How insulin engages its primary binding site on the insulin receptor. *Nature* 493: 241-245, 2013.
109. **Michels KB, Solomon CG, Hu FB, Rosner BA, Hankinson SE, Colditz GA, Manson JE, and Nurses' Health S.** Type 2 diabetes and subsequent incidence of breast cancer in the Nurses' Health Study. *Diabetes care* 26: 1752-1758, 2003.
110. **Milazzo G, Sciacca L, Papa V, Goldfine ID, and Vigneri R.** ASPB10 insulin induction of increased mitogenic responses and phenotypic changes in human breast epithelial cells: evidence for enhanced interactions with the insulin-like growth factor-I receptor. *Molecular carcinogenesis* 18: 19-25, 1997.
111. **Moody SE, Sarkisian CJ, Hahn KT, Gunther EJ, Pickup S, Dugan KD, Innocent N, Cardiff RD, Schnall MD, and Chodosh LA.** Conditional activation of Neu in the mammary epithelium of transgenic mice results in reversible pulmonary metastasis. *Cancer cell* 2: 451-461, 2002.
112. **Mosthaf L, Grako K, Dull TJ, Coussens L, Ullrich A, and McClain DA.** Functionally distinct insulin receptors generated by tissue-specific alternative splicing. *The EMBO journal* 9: 2409-2413, 1990.

113. **Mulligan AM, O'Malley FP, Ennis M, Fantus IG, and Goodwin PJ.** Insulin receptor is an independent predictor of a favorable outcome in early stage breast cancer. *Breast cancer research and treatment* 106: 39-47, 2007.
114. **Neville MC, Webb P, Ramanathan P, Mannino MP, Pecorini C, Monks J, Anderson SM, and MacLean P.** The insulin receptor plays an important role in secretory differentiation in the mammary gland. *American journal of physiology Endocrinology and metabolism* 305: E1103-1114, 2013.
115. **Novosyadlyy R, Lann DE, Vijayakumar A, Rowzee A, Lazzarino DA, Fierz Y, Carboni JM, Gottardis MM, Pennisi PA, Molinolo AA, Kurshan N, Mejia W, Santopietro S, Yakar S, Wood TL, and LeRoith D.** Insulin-mediated acceleration of breast cancer development and progression in a nonobese model of type 2 diabetes. *Cancer Res* 70: 741-751, 2010.
116. **Ohshiro K, Schwartz AM, Levine PH, and Kumar R.** Alternate estrogen receptors promote invasion of inflammatory breast cancer cells via non-genomic signaling. *PLoS one* 7: e30725, 2012.
117. **Olivo-Marston SE, Hursting SD, Perkins SN, Schetter A, Khan M, Croce C, Harris CC, and Lavigne J.** Effects of calorie restriction and diet-induced obesity on murine colon carcinogenesis, growth and inflammatory factors, and microRNA expression. *PLoS one* 9: e94765, 2014.
118. **Onitilo AA, Stankowski RV, Berg RL, Engel JM, Glurich I, Williams GM, and Doi SA.** Breast cancer incidence before and after diagnosis of type 2 diabetes mellitus in women: increased risk in the prediabetes phase. *European journal of cancer prevention : the official journal of the European Cancer Prevention Organisation* 23: 76-83, 2014.
119. **Papa V, Milazzo G, Goldfine ID, Waldman FM, and Vigneri R.** Sporadic amplification of the insulin receptor gene in human breast cancer. *Journal of endocrinological investigation* 20: 531-536, 1997.
120. **Parisi F, Gonzalez AM, Nadler Y, Camp RL, Rimm DL, Kluger HM, and Kluger Y.** Benefits of biomarker selection and clinico-pathological covariate inclusion in breast cancer prognostic models. *Breast cancer research : BCR* 12: R66, 2010.
121. **Parker ED, and Folsom AR.** Intentional weight loss and incidence of obesity-related cancers: the Iowa Women's Health Study. *International journal of obesity and related metabolic disorders : journal of the International Association for the Study of Obesity* 27: 1447-1452, 2003.
122. **Peairs KS, Barone BB, Snyder CF, Yeh HC, Stein KB, Derr RL, Brancati FL, and Wolff AC.** Diabetes mellitus and breast cancer outcomes: a systematic review and meta-analysis. *Journal of clinical oncology : official journal of the American Society of Clinical Oncology* 29: 40-46, 2011.
123. **Pei XF, Noble MS, Davoli MA, Rosfjord E, Tilli MT, Furth PA, Russell R, Johnson MD, and Dickson RB.** Explant-cell culture of primary mammary tumors from MMTV-c-Myc transgenic mice. *In vitro cellular & developmental biology Animal* 40: 14-21, 2004.
124. **Reaven GM.** Relationships among insulin resistance, type 2 diabetes, essential hypertension, and cardiovascular disease: similarities and differences. *Journal of clinical hypertension* 13: 238-243, 2011.
125. **Rehnan AG.** Insulin analogues and cancer risk: the emergence of second-generation studies. *Diabetologia* 55: 7-9, 2012.
126. **Rehnan AG, Tyson M, Egger M, Heller RF, and Zwaren M.** Body-mass index and incidence of cancer: a systematic review and meta-analysis of prospective observational studies. *Lancet* 371: 569-578, 2008.

127. **Ruiter R, Visser LE, van Herk-Sukel MP, Coebergh JW, Haak HR, Geelhoed-Duijvestijn PH, Straus SM, Herings RM, and Stricker BH.** Risk of cancer in patients on insulin glargine and other insulin analogues in comparison with those on human insulin: results from a large population-based follow-up study. *Diabetologia* 55: 51-62, 2012.
128. **Samani AA, Yakar S, LeRoith D, and Brodt P.** The role of the IGF system in cancer growth and metastasis: overview and recent insights. *Endocrine reviews* 28: 20-47, 2007.
129. **Satelli A, and Li S.** Vimentin in cancer and its potential as a molecular target for cancer therapy. *Cellular and molecular life sciences : CMLS* 68: 3033-3046, 2011.
130. **Sen S, Langiewicz M, Jumaa H, and Webster NJ.** Deletion of splicing factor SRSF3 in hepatocytes predisposes to hepatocellular carcinoma in mice. *Hepatology* 2014.
131. **Senecal JL, Oliver JM, and Rothfield N.** Anticytoskeletal autoantibodies in the connective tissue diseases. *Arthritis and rheumatism* 28: 889-898, 1985.
132. **Sjostrom L, Gummesson A, Sjostrom CD, Narbro K, Peltonen M, Wedel H, Bengtsson C, Bouchard C, Carlsson B, Dahlgren S, Jacobson P, Karason K, Karlsson J, Larsson B, Lindroos AK, Lonroth H, Naslund I, Olbers T, Stenlof K, Torgerson J, Carlsson LM, and Swedish Obese Subjects S.** Effects of bariatric surgery on cancer incidence in obese patients in Sweden (Swedish Obese Subjects Study): a prospective, controlled intervention trial. *The Lancet Oncology* 10: 653-662, 2009.
133. **Snider NT, and Omary MB.** Post-translational modifications of intermediate filament proteins: mechanisms and functions. *Nature reviews Molecular cell biology* 15: 163-177, 2014.
134. **Sommerfeld MR, Muller G, Tschank G, Seipke G, Habermann P, Kurrle R, and Tennagels N.** In vitro metabolic and mitogenic signaling of insulin glargine and its metabolites. *PloS one* 5: e9540, 2010.
135. **Soon PS, Kim E, Pon CK, Gill AJ, Moore K, Spillane AJ, Benn DE, and Baxter RC.** Breast cancer-associated fibroblasts induce epithelial-to-mesenchymal transition in breast cancer cells. *Endocrine-related cancer* 20: 1-12, 2013.
136. **Stammberger I, Bube A, Durchfeld-Meyer B, Donaubaue H, and Troschau G.** Evaluation of the carcinogenic potential of insulin glargine (LANTUS) in rats and mice. *International journal of toxicology* 21: 171-179, 2002.
137. **Stulik J, Hernychova L, Porkertova S, Pozler O, Tuckova L, Sanchez D, and Bures J.** Identification of new celiac disease autoantigens using proteomic analysis. *Proteomics* 3: 951-956, 2003.
138. **Sugimoto H, Mundel TM, Kieran MW, and Kalluri R.** Identification of fibroblast heterogeneity in the tumor microenvironment. *Cancer biology & therapy* 5: 1640-1646, 2006.
139. **Suissa S, Azoulay L, Dell'Aniello S, Evans M, Vora J, and Pollak M.** Long-term effects of insulin glargine on the risk of breast cancer. *Diabetologia* 54: 2254-2262, 2011.
140. **Verheus M, Peeters PH, Rinaldi S, Dossus L, Biessy C, Olsen A, Tjonneland A, Overvad K, Jeppesen M, Clavel-Chapelon F, Tehard B, Nagel G, Linseisen J, Boeing H, Lahmann PH, Arvaniti A, Psaltopoulou T, Trichopoulou A, Palli D, Tumino R, Panico S, Sacerdote C, Sieri S, van Gils CH, Bueno-de-Mesquita BH, Gonzalez CA, Ardanaz E, Larranaga N, Garcia CM, Navarro C, Quiros JR, Key T, Allen N, Bingham S, Khaw KT, Slimani N, Riboli E, and Kaaks R.** Serum C-peptide levels and breast cancer risk: results

- from the European Prospective Investigation into Cancer and Nutrition (EPIC). *International journal of cancer Journal international du cancer* 119: 659-667, 2006.
141. **Wagenknecht LE, Langefeld CD, Scherzinger AL, Norris JM, Haffner SM, Saad MF, and Bergman RN.** Insulin sensitivity, insulin secretion, and abdominal fat: the Insulin Resistance Atherosclerosis Study (IRAS) Family Study. *Diabetes* 52: 2490-2496, 2003.
  142. **Wagner KU, McAllister K, Ward T, Davis B, Wiseman R, and Hennighausen L.** Spatial and temporal expression of the Cre gene under the control of the MMTV-LTR in different lines of transgenic mice. *Transgenic research* 10: 545-553, 2001.
  143. **Wallace TM, Levy JC, and Matthews DR.** Use and abuse of HOMA modeling. *Diabetes care* 27: 1487-1495, 2004.
  144. **Warburg O, Wind F, and Negelein E.** The Metabolism of Tumors in the Body. *The Journal of general physiology* 8: 519-530, 1927.
  145. **Waxler SH, Tabar P, and Melcher LR.** Obesity and the time of appearance of spontaneous mammary carcinoma in C3H mice. *Cancer research* 13: 276-278, 1953.
  146. **Webster NJ, Resnik JL, Reichart DB, Strauss B, Haas M, and Seely BL.** Repression of the insulin receptor promoter by the tumor suppressor gene product p53: a possible mechanism for receptor overexpression in breast cancer. *Cancer research* 56: 2781-2788, 1996.
  147. **Werner U, Korn M, Schmidt R, Wendrich TM, and Tennagels N.** Metabolic effect and receptor signalling profile of a non-metabolisable insulin glargine analogue. *Archives of physiology and biochemistry* 120: 158-165, 2014.
  148. **Williamson DF, Pamuk E, Thun M, Flanders D, Byers T, and Heath C.** Prospective study of intentional weight loss and mortality in overweight white men aged 40-64 years. *American journal of epidemiology* 149: 491-503, 1999.
  149. **Wynder EL, Escher GC, and Mantel N.** An epidemiological investigation of cancer of the endometrium. *Cancer* 19: 489-520, 1966.
  150. **Xu W, Yang Z, and Lu N.** A new role for the PI3K/Akt signaling pathway in the epithelial-mesenchymal transition. *Cell adhesion & migration* 9: 317-324, 2015.
  151. **Yakar S, Leroith D, and Brodt P.** The role of the growth hormone/insulin-like growth factor axis in tumor growth and progression: Lessons from animal models. *Cytokine & growth factor reviews* 16: 407-420, 2005.
  152. **Yakar S, Pennisi P, Zhao H, Zhang Y, and LeRoith D.** Circulating IGF-1 and its role in cancer: lessons from the IGF-1 gene deletion (LID) mouse. *Novartis Foundation symposium* 262: 3-9; discussion 9-18, 265-268, 2004.
  153. **Yee D.** Insulin-like growth factor receptor inhibitors: baby or the bathwater? *Journal of the National Cancer Institute* 104: 975-981, 2012.
  154. **Zhao H, Dupont J, Yakar S, Karas M, and LeRoith D.** PTEN inhibits cell proliferation and induces apoptosis by downregulating cell surface IGF-IR expression in prostate cancer cells. *Oncogene* 23: 786-794, 2004.
  155. **Zhu QS, Rosenblatt K, Huang KL, Lahat G, Brobey R, Bolshakov S, Nguyen T, Ding Z, Belousov R, Bill K, Luo X, Lazar A, Dicker A, Mills GB, Hung MC, and Lev D.** Vimentin is a novel AKT1 target mediating motility and invasion. *Oncogene* 30: 457-470, 2011.
  156. **Zubeldia-Plazaola A, Ametller E, Mancino M, Prats de Puig M, Lopez-Plana A, Guzman F, Vinyals L, Pastor-Arroyo EM, Almendro V, Fuster G, and Gascon P.** Comparison of methods for the isolation of human breast epithelial and myoepithelial cells. *Frontiers in cell and developmental biology* 3: 32, 2015.

## Appendix I. Publications From the Work in This Thesis

### Published Papers

The work described in this thesis has been published in the following papers, attached to this thesis:

1. **Hyperinsulinemia promotes metastasis to the lung in a mouse model of Her2-mediated breast cancer.** *Ferguson RD, Gallagher EJ, Cohen D, Tobin-Hess A, Alikhani N, Novosyadlyy R, Haddad N, Yakar S, LeRoith D.* Endocrine Related Cancer. 2013 May 21;20(3):391-401. doi: 10.1530/ERC-12-0333. PMID: 23572162
2. **Insulin receptor phosphorylation by endogenous insulin or the insulin analog AspB10 promotes mammary tumor growth independent of the IGF-I receptor.** *Gallagher EJ, Alikhani N, Tobin-Hess A, Blank J, Buffin NJ, Zelenko Z, Tennagels N, Werner U, LeRoith D.* Diabetes. 2013 Oct;62(10):3553-60. doi: 10.2337/db13-0249. PMID: 23835331; PubMed Central PMCID: PMC3781483.
3. **Inhibiting PI3K reduces mammary tumor growth and induces hyperglycemia in a mouse model of insulin resistance and hyperinsulinemia.** *Gallagher EJ, Fierz Y, Vijayakumar A, Haddad N, Yakar S, LeRoith D.* Oncogene. 2012 Jul 5;31(27):3213-22. doi: 10.1038/onc.2011.495. PMID: 22037215; PubMed Central PMCID: PMC3275680.
4. **Metabolic syndrome and pre-diabetes contribute to racial disparities in breast cancer outcomes: hypothesis and proposed pathways.** *Gallagher EJ, LeRoith D, Franco R, Antoniou IM, Nayak A, Livaudais-Toman J, Bickell N.* Diabetes Metab Res Rev 2016; doi: 10.1022/dmrr.2795. PMID: 26896340.



# Hyperinsulinemia promotes metastasis to the lung in a mouse model of *Her2*-mediated breast cancer

Rosalyn D Ferguson, Emily J Gallagher, Dara Cohen, Aviva Tobin-Hess, Nyosha Alikhani, Ruslan Novosyadlyy, Nadine Haddad, Shoshana Yakar and Derek LeRoith

Division of Endocrinology, Diabetes and Bone Diseases, The Samuel Bronfman Department of Medicine, Mount Sinai School of Medicine, New York, New York 10029, USA

Correspondence should be addressed to D LeRoith

**Email**  
derek.leroith@mssm.edu

## Abstract

The *Her2* oncogene is expressed in ~25% of human breast cancers and is associated with metastatic progression and poor outcome. Epidemiological studies report that breast cancer incidence and mortality rates are higher in women with type 2 diabetes. Here, we use a mouse model of *Her2*-mediated breast cancer on a background of hyperinsulinemia to determine how elevated circulating insulin levels affect *Her2*-mediated primary tumor growth and lung metastasis. Hyperinsulinemic (MKR<sup>+/+</sup>) mice were crossed with doxycycline-inducible *Neu-NT* (MTB/TAN) mice to produce the MTB/TAN/MKR<sup>+/+</sup> mouse model. Both MTB/TAN and MTB/TAN/MKR<sup>+/+</sup> mice were administered doxycycline in drinking water to induce *Neu-NT* mammary tumor formation. In tumor tissues removed at 2, 4, and 6 weeks of *Neu-NT* overexpression, we observed increased tumor mass and higher phosphorylation of the insulin receptor/IGF1 receptor, suggesting that activation of these receptors in conditions of hyperinsulinemia could contribute to the increased growth of mammary tumors. After 12 weeks on doxycycline, although no further increase in tumor weight was observed in MTB/TAN/MKR<sup>+/+</sup> compared with MTB/TAN mice, the number of lung metastases was significantly higher in MTB/TAN/MKR<sup>+/+</sup> mice compared with controls (MTB/TAN/MKR<sup>+/+</sup> 16.41 ± 4.18 vs MTB/TAN 5.36 ± 2.72). In tumors at the 6-week time point, we observed an increase in vimentin, a cytoskeletal protein and marker of mesenchymal cells, associated with epithelial-to-mesenchymal transition and cancer-associated fibroblasts. We conclude that hyperinsulinemia in MTB/TAN/MKR<sup>+/+</sup> mice resulted in larger primary tumors, with more mesenchymal cells and therefore more aggressive tumors with more numerous pulmonary metastases.

## Key Words

- ▶ type 2 diabetes
- ▶ breast cancer

*Endocrine-Related Cancer*  
(2013) 20, 391–401

## Introduction

Over the last three decades, the relationship between type 2 diabetes and breast cancer has been evaluated by numerous epidemiological studies. Most of these support

a positive association between diabetes and breast cancer, with several recent meta-analyses suggesting that women with type 2 diabetes are at significantly greater risk of

developing, relapsing with, and dying from breast cancer than women who do not have diabetes (Larsson *et al.* 2007, Peairs *et al.* 2011, Boyle *et al.* 2012). The relationship between insulin, specifically, and breast cancer has been assessed by several epidemiological studies. Independent of all other confounding factors, hyperinsulinemia was reported to be a significant factor for incident breast cancer (Pisani 2008, Gunter *et al.* 2009), while another study reported an association between raised insulin levels and breast cancer metastasis and mortality (Goodwin *et al.* 2002). Both raised C-peptide (a marker of secreted insulin levels) and insulin resistance have been recently reported to be linked to breast cancer-specific death (Duggan *et al.* 2011, Irwin *et al.* 2011). High circulating insulin levels have also been associated with a risk of breast cancer recurrence (Formica *et al.* 2012). After breast tumor surgery, elevated insulin levels in the circulation have been reported to be associated with an adverse prognosis during the first 5 years after diagnosis (Goodwin *et al.* 2012). While epidemiological studies only suggest a link between hyperinsulinemia and accelerated tumor growth, some proof-of-concept experimental studies indicate that hyperinsulinemia indeed promotes tumor development (Fierz *et al.* 2010, Novosyadlyy *et al.* 2010).

In our previous studies, we have specifically focused on the impact of hyperinsulinemia on breast cancer progression using the MKR mouse model. Female MKR mice are insulin resistant and hyperinsulinemic while the remaining are nonobese and only mildly hyperglycemic. Using this hyperinsulinemic model, we have observed significantly increased growth of transgenic (PyVmt) and orthotopically induced mammary tumors and have demonstrated a mechanistic link between hyperinsulinemia and increased cancer progression through increased activation of the insulin receptor (IR)/IGF1 receptor (IGF1R) and the phosphatidylinositol 3-kinase (PI3-K)/Akt/mTOR pathway (Novosyadlyy *et al.* 2010).

In the clinical setting, the differential influence of type 2 diabetes and its complications on subtype-specific breast cancer warrants further investigation. Around 25% of breast cancers belong to the subtype characterized by amplification of the gene encoding human epidermal growth factor receptor 2 (Her2), which is associated with high risk of metastasis and poor outcome (Slamon *et al.* 1989, Seshadri *et al.* 1993). Recently, a retrospective study has evaluated the benefit of the antidiabetic treatments metformin and thiazolidinediones on women with type 2 diabetes and Her2+ breast cancer. Initial analysis of the study cohort revealed that type 2 diabetes was a significant predictor of reduced overall survival in women with

stage 2 or higher Her2+ breast cancer, independent of other confounding factors such as age, estrogen receptor (ER)/progesterone receptor (PR) expression, and BMI. Furthermore, the antidiabetic therapies significantly increased overall survival and significantly reduced the risk of Her2+ breast cancer-specific mortality (He *et al.* 2012). Although insulin levels in these patients were not reported, both metformin and thiazolidinediones are insulin sensitizers, suggesting that improvements in insulin resistance in type 2 diabetics could have an impact on Her2+ breast cancer progression.

Her2 (also known as ErbB2 or *Neu* in rodents) belongs to the epidermal growth factor receptor family of receptor tyrosine kinases (RTK), which includes Her1 (also known as EGFR or ErbB1), Her3 (or ErbB3), and Her4 (or ErbB4). Unlike the other family members, no specific ligand has been identified for Her2 and its activity is dependent on its dimerization with either ligand-activated EGFR or Her3. At high expression levels resulting from *ERBB2* amplification, homodimers are also activated (Harari & Yarden 2000, Yarden 2001). Despite the lack of kinase activity of Her3, dimers of Her2/Her3 constitute the most potent signaling combination of all EGFR family dimers (Pinkas-Kramarski *et al.* 1996, Holbro *et al.* 2003), and a prevention of Her2/Her3 heterodimerization provides a significant clinical benefit in patients with Her2+ breast cancer (Baselga & Swain 2010). Activation of Her2/Her3 dimers leads to upregulation of multiple downstream pathways including the canonical PI3-K/Akt/mTOR signaling cascade and the mitogen-activated protein kinase (MAPK) pathway (Jin & Esteva 2008). Importantly, these two pathways are also the principal signaling pathways involved in the growth-promoting effects of the activated IR/IGF1R in tumorigenesis. Indeed, Her2 also dimerizes with the IGF1R leading to the emergence of resistance to Her2 pharmacotherapies (Lu *et al.* 2001).

Transgenic mouse models of Her2 (*Neu*)-mediated mammary carcinogenesis include those with constitutive activation of wild-type *Neu* (*c-Neu*) or oncogenic (activated) *Neu* (*Neu-NT*) under control of the MMTV promoter. Both *c-Neu* and *Neu-NT* overexpression result in invasive mammary carcinomas with latency periods of around 7 and 3 months respectively (Ursini-Siegel *et al.* 2007). A conditionally activated model of mammary-specific *Neu-NT* has also been engineered by crossing MMTV-reverse tetracycline transactivator (rtTA) (MTB) transgenic mice with mice bearing the *TetO-Neu-NT* transgene (TAN) to generate MTB/TAN offspring (Moody *et al.* 2002). Tumor latency in this model is short, with development of multiple mammary tumors with 100%

penetration within a few weeks and further progression to spontaneous lung metastasis (Moody *et al.* 2002).

Given that in mammary tumors from *Neu-NT* transgenic mice, the PI3-K/Akt/mTOR signaling pathway should already be active, an interesting question that arises is whether the induction of systemic hyperinsulinemia in these mice could enhance *Neu-NT*-mediated tumor growth via IR/IGF1R activation. To address this issue, we crossed homozygous *MKR*<sup>+/+</sup> mice with MTB/TAN mice to yield MTB/TAN/*MKR*<sup>+/+</sup> offspring, thus generating hyperinsulinemic mice expressing a doxycycline-inducible *Neu-NT* transgene. When induced with doxycycline, MTB/TAN/*MKR*<sup>+/+</sup> mice develop early *Neu-NT*-mediated mammary gland hyperplastic changes more rapidly than controls and go on to develop larger mammary tumors. Furthermore, MTB/TAN/*MKR*<sup>+/+</sup> mice exhibit higher numbers of lung macrometastases, suggesting that chronic hyperinsulinemia can augment *Neu-NT*-mediated primary tumor growth as well as the progression to lung metastasis.

## Materials and methods

### Animal studies

Animal care and maintenance were provided by the Mount Sinai School of Medicine AAALAC Accredited Animal Facility. All procedures were approved by the Institutional Animal Care and Use Committee of the Mount Sinai School of Medicine according to the National Institute of Health Guidelines. All mice used in this study were on Friend Virus B (National Institute of health) (FVB/N) genetic background. Mice were housed four per cage in a clean mouse facility and fed a standard mouse chow (PicoLab Rodent Diet 20, 5053; LabDiet, Brentwood, MO, USA) *ad libitum* on a 12 h light:12 h darkness cycle. Plasma insulin levels were measured by the sensitive rat insulin RIA kit (Millipore, St Charles, MO, USA). An insulin tolerance test was performed on animals previously fasted for 4 h. Insulin (0.75 units/kg of body weight) was injected intraperitoneally and blood glucose values were measured immediately before and 15, 30, and 60 min after insulin injection. For induction of *Neu-NT*, mice were administered 1.5 mg/ml doxycycline (Sigma–Aldrich) in drinking water for the duration of the period of tumor growth from 2 weeks up to 12 weeks. Doxycycline water was changed twice per week. Mice were followed on a daily basis and body score conditions were recorded. To determine tumor mass, each animal was killed and mammary tumors from all thoracic and inguinal glands

were carefully dissected and weighed. For analysis of pulmonary metastases, mice were killed and lungs were inflated via the trachea with 10% formalin, removed, and examined for macrometastatic lesions.

### Mammary gland whole mount analysis

Inguinal mammary glands were removed, placed on a glass slide, and fixed for 4 h in Carnoy's fixative (60% ethanol (100%), 30% chloroform, and 10% glacial acetic acid). Glands were serially hydrated in 100, 95, 70, 50, and 30% ethanol for 15 min each, rinsed in water for 5 min, and stained overnight with carmine alum. Glands were then serially dehydrated in 30, 50, 70, 95, and 100% ethanol for 15 min each and cleared overnight in xylene. Glands were then covered by Mount-Quick mounting medium (Daido Sangyo, Tokyo, Japan), before a glass coverslip was placed on top. Photographs were carried out using a stereomicroscope (Zeiss, Thornwood, NY, USA) at 4× magnification. Quantification of the relative area of end buds was performed using Image J by measuring the mean end bud area of four random images at 4× objective taken from each whole mount.

### Histology and immunofluorescence

Lungs were fixed in 10% formalin before being embedded in paraffin and sectioned and stained using hematoxylin and eosin (H&E). For immunofluorescence studies, mammary tumors were cut in cross section at the time of killing, fixed in 10% formalin before being embedded in paraffin, and sectioned. Five-micron sections were deparaffinized, rehydrated, and subjected to antigen retrieval. Primary antibodies used were a rabbit polyclonal antibody to vimentin (Cell Signaling Technologies, Danvers, MA, USA) and a mouse MAB to Neu (Abcam, Cambridge, MA, USA). Secondary antibodies used were AlexaFluor-568-conjugated goat anti-rabbit IgG and Alexa-Fluor-488-conjugated goat anti-mouse IgG (Invitrogen, Molecular Probes, Eugene, OR, USA). Nuclei were counterstained with 0.2 µg/ml 4',6-diamidino-2-phenylindole (DAPI; Sigma–Aldrich).

### Western blotting

Tumor tissues were lysed in chilled lysis buffer (pH 7.4) containing 50 mM Tris, 150 mM NaCl, 1 mM EDTA, 1.25% CHAPS, 1 mM sodium orthovanadate, 10 mM sodium pyrophosphate, 8 mM B-glycerophosphate, and Complete Protease Inhibitor Cocktail tablet. Protein

concentration of samples was measured using the BCA protein assay kit (Thermo Scientific, Rockford, IL, USA). Protein samples were resuspended in  $3\times$  loading buffer containing DTT (Cell Signaling Technologies) and denatured by boiling for 5 min at  $96^{\circ}\text{C}$ . Samples were then subjected to SDS-PAGE (8 or 8–16% Tris–glycine gel; Life Technologies) and transferred to a nitrocellulose membrane. Membranes were probed with the appropriate primary antibodies: anti-phospho IR- $\beta^{(\text{Y1150/51})}$ /IGF1R $\beta^{(\text{Y1135/36})}$ , anti-phospho Akt $^{\text{Ser473}}$ , anti-total Akt, and anti-vimentin (Cell Signaling Technologies) and then reblotted with B-actin (Sigma–Aldrich) or anti-IR $\beta$  (Santa Cruz Biotechnology) before being incubated with secondary antibodies (LI-COR Biosciences, Lincoln, NE, USA) and being exposed to the LI-COR infrared detection system (LI-COR Biosciences).

### Statistical analysis

Statistical analyses were conducted using the Student's *t*-test. Results are expressed as means  $\pm$  S.E.M.

## Results

### MTB/TAN/MKR $^{+/+}$ mice express the same metabolic phenotype as the parental MKR $^{+/+}$ mouse strain

Transgenic MMTV-rtTA (MTB) and TetO-*Neu-NT* (TAN) mice were previously crossed to yield bitransgenic MTB/TAN offspring demonstrating doxycycline-dependent *Neu-NT* expression in luminal mammary epithelial cells and subsequent development of gross mammary tumors and pulmonary macrometastases (Moody *et al.* 2002). We crossed MTB/TAN with homozygous MKR mice to yield MTB/TAN/MKR $^{+/+}$  mice. Female MTB/TAN/MKR $^{+/+}$  mice showed the same metabolic abnormalities as the homozygous female MKR $^{+/+}$  mice (Novosyadlyy *et al.* 2010) namely lowered body weight, mild hyperglycemia, increased systemic insulin, and severe insulin resistance (Fig. 1A, B, C, and D).

### MTB/TAN/MKR $^{+/+}$ mice show augmented *Neu-NT*-induced abnormalities of the mammary gland at 8 weeks compared with MTB/TAN controls

Others have shown that doxycycline-induced *Neu-NT* expression results in noticeable hyperplastic abnormalities in the mouse mammary gland such as the presence of cellular masses along the length of ducts, as well as terminal end bud enlargement due to the presence of

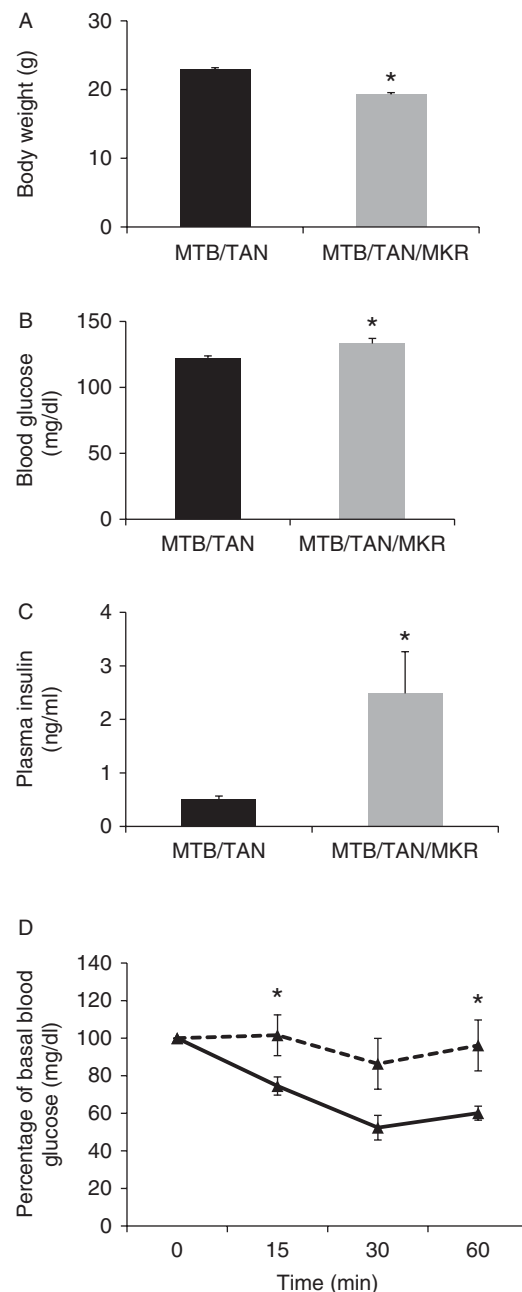


**Figure 1**

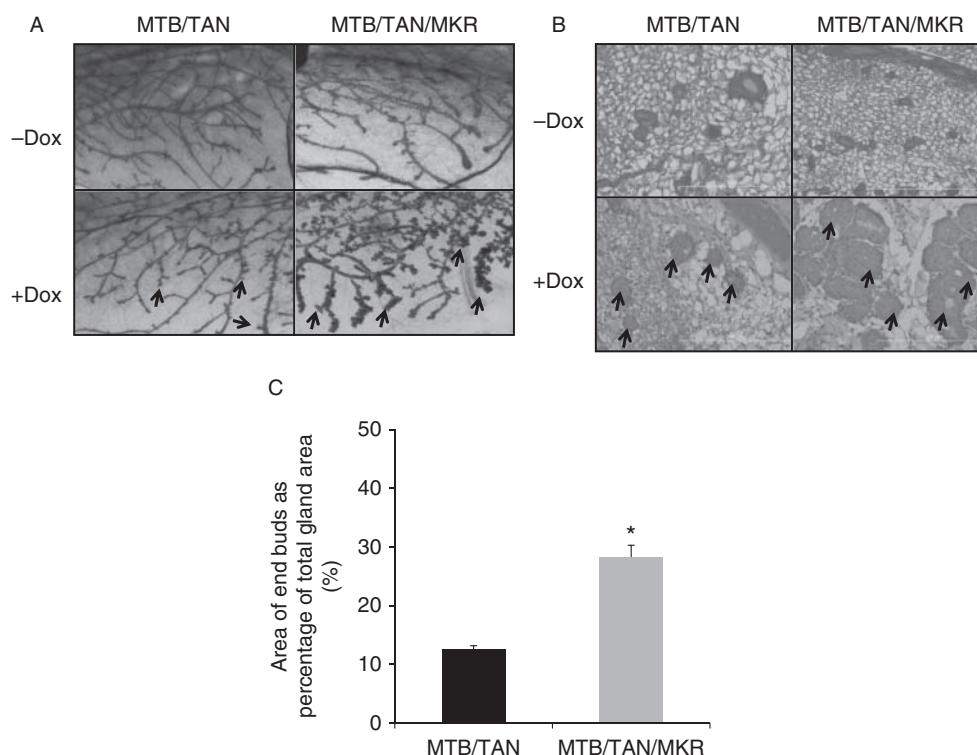
Metabolic characterization of the MTB/TAN/MKR $^{+/+}$  mouse model. (A) Body weight (MTB/TAN,  $n=14$ ; MTB/TAN/MKR $^{+/+}$ ,  $n=10$ ), (B) blood glucose (MTB/TAN,  $n=30$ ; MTB/TAN/MKR $^{+/+}$ ,  $n=22$ ), and (C) serum insulin (MTB/TAN,  $n=13$ ; MTB/TAN/MKR $^{+/+}$ ,  $n=20$ ) of MTB/TAN and MTB/TAN/MKR $^{+/+}$  mice at 8 weeks of age. (D) An insulin tolerance test was performed on fasted 8-week-old MTB/TAN/MKR $^{+/+}$  ( $n=5$ ) and MTB/TAN mice ( $n=5$ ) after i.p. injection of insulin (0.75 units/kg). Blood samples were obtained from the tail vein and glucose concentrations were determined at the indicated time points. Graphs represent mean values of each group, error bars represent the S.E.M. \* $P$  value  $< 0.05$ .

acinar-like structures (Moody *et al.* 2002). We investigated whether hyperinsulinemia would have an additive effect on these early *Neu-NT*-mediated hyperplastic abnormalities by induced *Neu-NT* expression for 3 days in 8-week-old MTB/TAN/MKR<sup>+/+</sup> and MTB/TAN mice, killing the animals and comparing mammary gland morphology by whole mount analysis. As MKR<sup>+/+</sup> mice have precocious mammary gland growth and differentiation compared with control mice at both 3 and 15 weeks (Novosyadlyy & LeRoith 2010), we also performed whole mount analysis and H&E staining of mammary glands from 8-week-old MTB/TAN/MKR<sup>+/+</sup> and MTB/TAN mice, which had not been administered doxycycline (Fig. 2A and B, upper panels). In MTB/TAN/MKR<sup>+/+</sup> mice, we found *Neu-NT*-mediated abnormalities to be enhanced compared with MTB/TAN controls, with larger cellular masses growing on ducts, greater terminal end bud enlargement, and precocious lobular development (Fig. 2A, lower panels and C). This finding was further confirmed by histological evaluation of H&E-stained

sections of the mammary gland (Fig. 2B, lower panels) where we observed advanced ductal hyperplasia in MTB/TAN/MKR<sup>+/+</sup> mice compared with MTB/TAN controls.

### ***Neu-NT*-induced mammary tumor burden is greater in MTB/TAN/MKR<sup>+/+</sup> mice than in MTB/TAN mice and is regulated through IR/IGF1R signaling pathways**

When doxycycline was administered for several weeks, MTB/TAN mice developed multiple invasive mammary adenocarcinomas with tumors arising in all inguinal and thoracic glands (Moody *et al.* 2002). We administered doxycycline to 8-week-old MTB/TAN and MTB/TAN/MKR<sup>+/+</sup> mice for 2, 4, 6, or 12 weeks. Mice were killed at each time point and the combined tumor weight from all inguinal and thoracic glands from each mouse was recorded. As shown in Fig. 3A, MTB/TAN/MKR<sup>+/+</sup> mice exhibited significantly higher total tumor mass than MTB/TAN controls at all time points with the exception of the 12-week time point, suggesting

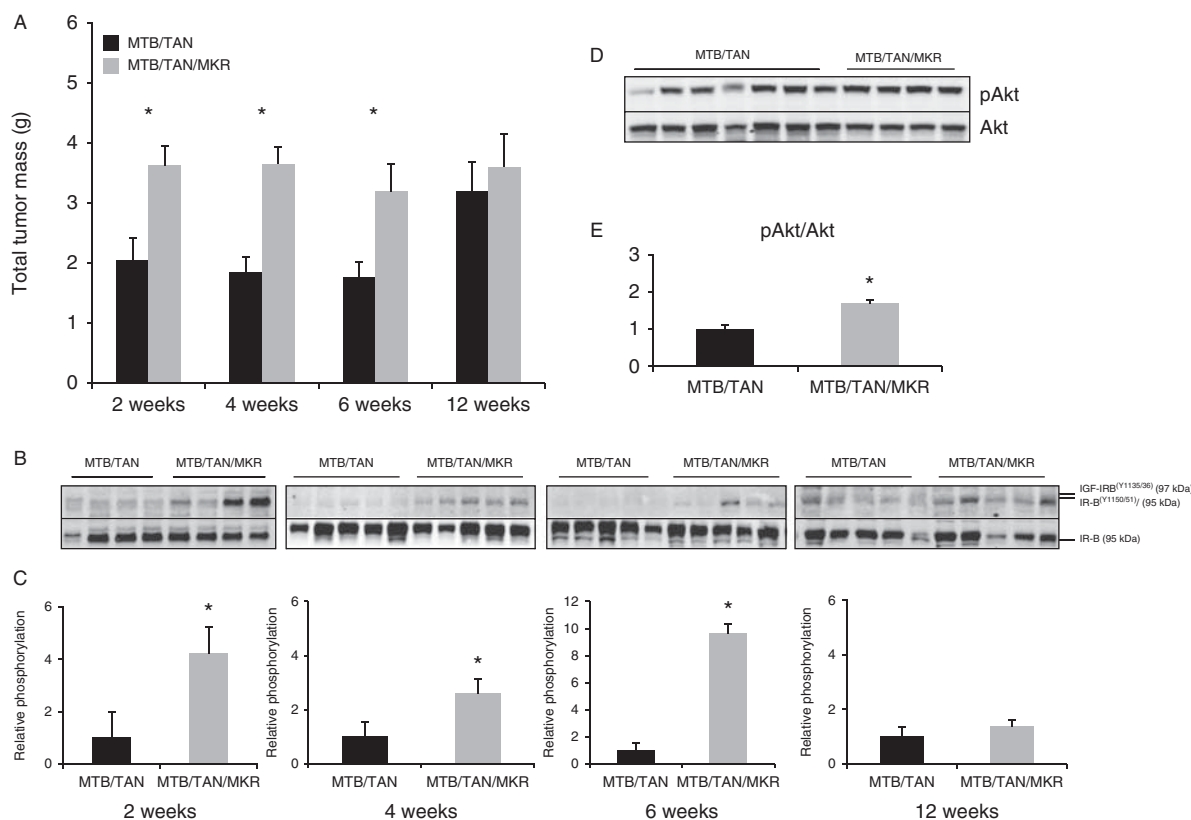


**Figure 2**

Effect of hyperinsulinemia on *Neu-NT*-mediated mammary gland hyperplasia. (A) Whole mount analysis of mammary glands obtained from 8-week-old female MTB/TAN and MTB/TAN/MKR<sup>+/+</sup> mice without doxycycline (–Dox) and after 3 days of doxycycline treatment (+Dox). (B) Histological analysis (H&E staining) of mammary glands after 3 days of doxycycline treatment. (C) Quantification of percentage area of mammary

gland whole mounts composed of end buds (MTB/TAN, *n*=3; MTB/TAN/MKR, *n*=3). Arrows, End buds (A) and ductal hyperplasia. (C) At least five animals per group were analyzed and the representative images are shown. Original magnification,  $\times 4$  (A) and  $\times 40$  (B). Graph represents mean for each group, error bars represent S.E.M. \**P* value < 0.05.



**Figure 3**

Tumor growth, IR $\beta$ /IGF1R $\beta$ , and Akt signaling are enhanced in tumors from MTB/TAN/MKR<sup>+/+</sup> mice compared with MTB/TAN controls. (A) MTB/TAN and MTB/TAN/MKR<sup>+/+</sup> mice were maintained on doxycycline for 2, 4, 6, or 12 weeks. Mice were killed and the combined tumor mass from all mammary glands was recorded. For the 2-week time point, MTB/TAN,  $n=11$ ; MTB/TAN/MKR<sup>+/+</sup>,  $n=4$ . For the 4-week time point, MTB/TAN,  $n=11$ ; MTB/TAN/MKR<sup>+/+</sup>,  $n=7$ . For the 6-week time point, MTB/TAN,  $n=16$ ; MTB/TAN/MKR<sup>+/+</sup>,  $n=6$ . For the 12-week time point, MTB/TAN,  $n=12$ ; MTB/TAN/MKR<sup>+/+</sup>,  $n=11$ . (B) Tumor tissue was subjected to western blot

analysis and probed with antibodies to phosphorylated IR $\beta$ (Y1150/51)/IGF1R $\beta$ (Y1135/36) and then reblotted with antibodies to IR $\beta$ . (D) Western blot analysis of tumor tissue from mice maintained on doxycycline for 2 weeks probed with antibodies to phosphorylated Akt<sup>Ser473</sup> and total Akt. Using densitometry, protein expression was quantified (C and E). Error bars represent S.E.M. \* $P<0.05$ . For the 2-week time point, western blot is representative of MTB/TAN,  $n=9$ ; MTB/TAN/MKR<sup>+/+</sup>,  $n=4$  samples. For 4- and 6-week time points, MTB/TAN,  $n=7$ ; MTB/TAN/MKR<sup>+/+</sup>,  $n=7$  samples. For 12-week time point MTB/TAN,  $n=10$ ; MTB/TAN/MKR<sup>+/+</sup>,  $n=10$ .

that hyperinsulinemia augments *Neu-NT*-driven mammary tumor growth. We extracted proteins from tumor tissues to examine whether IR/IGF1R activation was upregulated in MTB/TAN/MKR<sup>+/+</sup> mice compared with MTB/TAN controls. As shown in Fig. 3B and C, mammary tumor tissues from MTB/TAN/MKR<sup>+/+</sup> mice demonstrated higher levels of phosphorylated IR/IGF1R (IR $\beta$ /IGF1R $\beta$ ) after 2, 4, and 6 weeks of *Neu-NT* upregulation, suggesting that these receptors may be involved in mediating the additional tumor growth present in MTB/TAN/MKR<sup>+/+</sup> mice. In MTB/TAN/MKR<sup>+/+</sup> and MTB/TAN mice that had been administered doxycycline for a period of 12 weeks, we observed an increase in IR/IGF1R phosphorylation in mammary tissues of MTB/TAN/MKR<sup>+/+</sup> mice, which was not statistically significant (Fig. 3B and C). There was no significant difference in tumor weights after 12 weeks

of doxycycline administration, possibly due to tumors reaching their physiologically maximal size after this time period (Fig. 3A). We also compared activation of Akt, which lies downstream of both the IR/IGF1R and Her2 and found that at 2 weeks there was a significant upregulation of phosphorylated Akt in tumors from MTB/TAN/MKR<sup>+/+</sup> mice compared with MTB/TAN mice (Fig. 3D and E). At later stages of tumor development, levels of activation of Akt in the tumors appeared to be similar in the two groups.

#### ***Neu-NT*-induced spontaneous lung macrometastases are enhanced in MTB/TAN/MKR<sup>+/+</sup> mice after 12 weeks of tumor growth**

MTB/TAN mice were reported to harbor *Neu-NT*-dependent spontaneous lung macrometastases (Moody *et al.* 2002).

We removed the lungs of killed MTB/TAN/MKR<sup>+/+</sup> and MTB/TAN mice after 2, 4, 6, or 12 weeks of doxycycline-induced *Neu-NT* expression in mammary epithelium and recorded the numbers of visible macrometastases. We also examined H&E-stained sections of lung at all time points for both micrometastases and macrometastases. After 2, 4, or 6 weeks of *Neu* expression and mammary tumor growth, no visible macrometastases were observed in either MTB/TAN/MKR<sup>+/+</sup> or MTB/TAN mice. However, H&E staining revealed the presence of micrometastases in lungs of both groups of mice after 6 weeks of *Neu* expression (data not shown). Although there was a trend for the number of micrometastases to be increased in MTB/TAN/MKR<sup>+/+</sup> mice (0.3 micromets/lung section in MTB/TAN vs 0.8 micromets/lung section in MTB/TAN/MKR<sup>+/+</sup>), this did not reach statistical

significance. In contrast, after 12 weeks of *Neu* expression in mammary tissue, macrometastases could be clearly observed in the lungs, and these were significantly increased in MTB/TAN/MKR<sup>+/+</sup> compared with MTB/TAN mice (Fig. 4A and B), suggesting that hyperinsulinemia increases the metastatic potential of *Neu*-driven mammary carcinogenesis.

#### ***Neu-NT*-induced mammary tumors in MTB/TAN/MKR<sup>+/+</sup> mice express higher levels of vimentin**

To determine whether hyperinsulinemia enhances the progression of *Neu-NT*-mediated primary tumors to lung metastases, we analyzed tumor tissue for the expression of vimentin protein, a marker of mesenchymal cells. As shown in Fig. 5A and B, western blot analysis of tumor

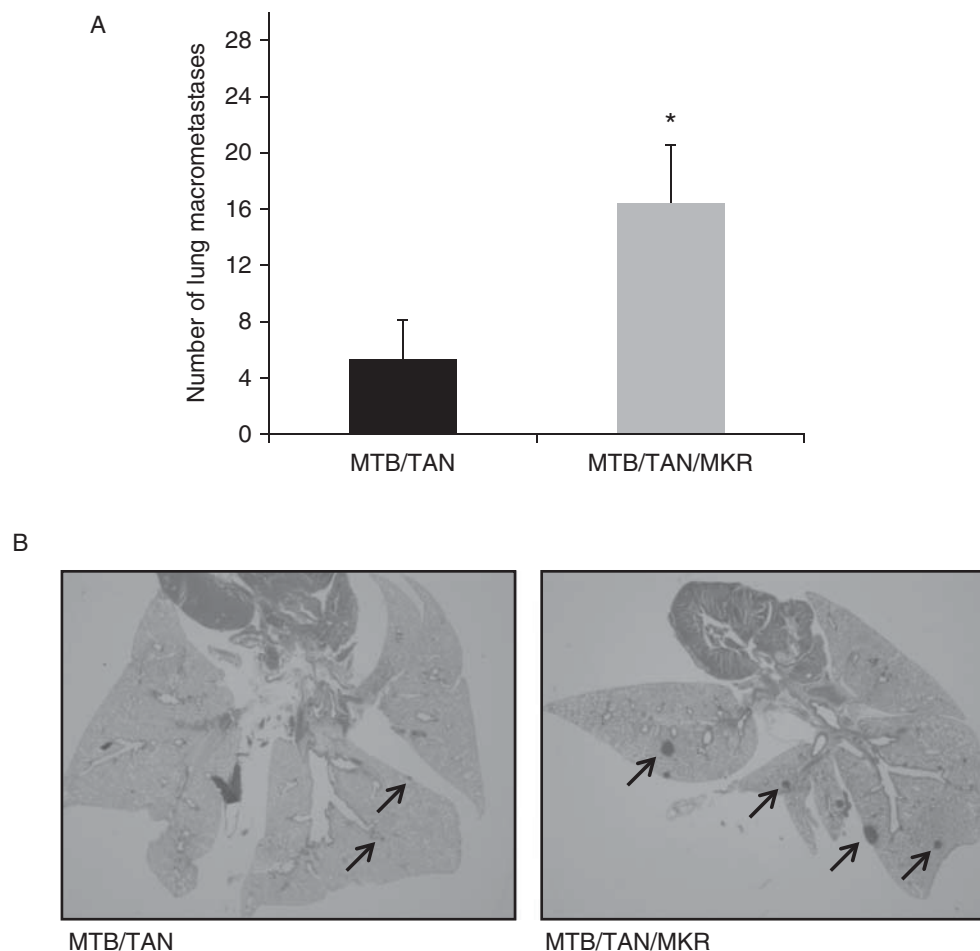


**Figure 4**

Metastatic progression is enhanced in MTB/TAN/MKR<sup>+/+</sup> mice. After 12 weeks on doxycycline, MTB/TAN and MTB/TAN/MKR<sup>+/+</sup> mice were killed, lungs were removed and inflated, and (A) number of lung macrometastases were recorded. Graph represents the mean for each group, error bars

represent S.E.M. \**P* value < 0.05. (B) Lungs were paraffin embedded, sectioned, and stained with H&E to reveal macrometastases. Original magnification 4×. Arrows indicate metastatic cells.

lysates demonstrated increased vimentin expression in tumors from 6-week-old MTB/TAN/MKR<sup>+/+</sup> mice compared with MTB/TAN mice. We additionally analyzed vimentin expression in 6-week tumor tissues by immunofluorescent staining of paraffin-embedded sections. As shown in Fig. 5B and C, vimentin levels as measured by immunofluorescence were significantly elevated, indicating that more mesenchymal cells were present in MTB/TAN/MKR<sup>+/+</sup> mice at this time point. The vimentin-positive cells generally did not stain positive for Neu, indicating that these were either cells that had undergone epithelial-to-mesenchymal transition (EMT) and lost Neu expression, or were cancer-associated fibroblasts. At 4 and 12 weeks of tumor development, we did not observe significant differences in vimentin expression (data not shown).

## Discussion

Epidemiological evidence suggests a causal relationship between type 2 diabetes and the incidence, recurrence, and mortality from breast cancer. Hyperinsulinemia has been identified as a specific factor that may drive breast cancer cell proliferation, but data on human patients that focus on how specific subtypes of breast cancer respond to elevated circulating insulin are limited. Overexpression of ErbB2/Her2 is responsible for around 25% of all human breast cancers and results in aggressive primary tumors, which commonly metastasize to the lungs. In this study, we have employed the MKR mouse model with a conditionally activated *Neu-NT* to represent this subtype of breast cancer. We have demonstrated for the first time

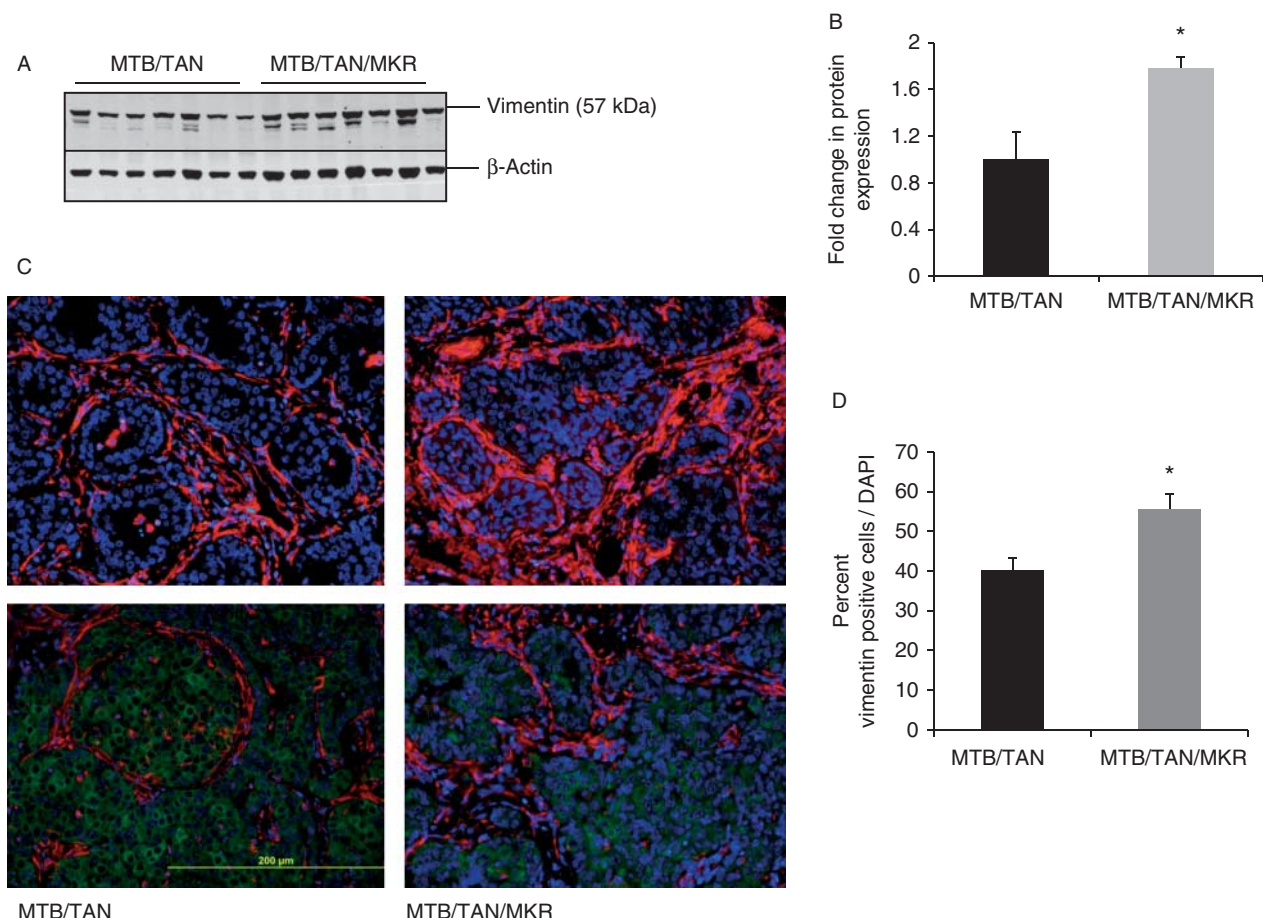


**Figure 5**

Vimentin expression is enhanced in MTB/TAN/MKR<sup>+/+</sup> mice. (A). After 6-weeks *Neu-NT* upregulation, mammary tumors were removed from MTB/TAN and MTB/TAN/MKR<sup>+/+</sup> mice, tumor lysates were subjected to western blot analysis, and probed with anti-vimentin antibodies. Using densitometry, protein expression was quantified (B). Tumor tissue was paraffin embedded, sectioned, and analyzed by immunofluorescence microscopy for the expression of vimentin (red) and Neu (green) proteins,

nuclei were stained with DAPI (blue) (C). Vimentin expression was analyzed using 'Image J' program to quantify expression of vimentin protein in 6-week tumors from MTB/TAN and MTB/TAN/MKR<sup>+/+</sup> mice (D). Photographs are representative of at least four mice from each group. Five high-power fields were photographed on every slide and each image was quantified. Original magnification 40×. Graphs represent the mean for each group, error bars represent s.e.m. \**P* value < 0.05.



in an animal model that hyperinsulinemia significantly affects the rate of *Neu-NT*-mediated mammary tumor development as well as the progression of breast cancer metastasis to the lungs.

Previously, we have employed the MKR mouse model to demonstrate that PyVmT-driven mammary gland hyperplasia at 3 and 15 weeks' postnatal development is more advanced under conditions of hyperinsulinemia (Novosyadlyy et al. 2010). Hyperplasia of the mammary gland has previously been shown to occur rapidly (3–4 days) after conditionally activated *Neu-NT* expression (Moody et al. 2002). In MTB/TAN/MKR<sup>+/+</sup> mice, we observed that in the presence of elevated insulin, mammary gland hyperplasia was more advanced after 3 days, suggesting that hyperinsulinemia can enhance the mitogenic effect of *Neu* oncogenic transformation on terminal end buds during mammary growth and development. The MMTV-c-*Neu* mouse model has been previously used to determine the effect of a high-fat diet (HFD) on mammary gland hyperplasia. Although this is a different model from ours, having a much longer tumor latency, it is interesting to note that either 5 or 10 weeks HFD treatment in FVB/N mice had no effect on mammary gland hyperplasia in MMTV-c-*Neu* mice compared with controls, suggesting that at very early stages of tumor development, insulin may have a more potent effect than dietary fat in promoting terminal end bud hyperplasia. In the same model, it was shown that an HFD based on corn oil resulted in a shorter tumor latency than an HFD based on fish oils, suggesting that at later stages of tumor development, fats may play a role in tumor development but individual dietary components have different effects (Luijten et al. 2007).

We found that chronic (2–6 weeks) elevations of *Neu-NT* led to significantly larger mammary tumors in MTB/TAN/MKR<sup>+/+</sup> mice compared with controls, suggesting that hyperinsulinemia enhances *Neu-NT*-mediated tumor formation and growth. This result is in agreement with our previous finding that orthotopic inoculation of three different mammary tumor cell lines (one over-expressing *Neu*) each resulted in larger tumor formation in MKR mice compared with controls (Novosyadlyy et al. 2010, Ferguson et al. 2012) and demonstrates that *Neu-NT*-mediated mammary tumor growth can be specifically enhanced by hyperinsulinemia. The mechanism by which insulin could increase tumor growth in the *Neu-NT* model may be complex. Our results demonstrate that MTB/TAN/MKR<sup>+/+</sup> mice demonstrate higher levels of phosphorylated IR/IGF1R than MTB/TAN control mice, suggesting that insulin is acting through its cognate

receptor and/or the highly homologous IGF1R to promote mammary tumor growth. In human breast cancer tissues, phosphorylated IR/IGF1R has been reported to be a prognostic marker of poor outcome for breast cancer, regardless of subtype (Law et al. 2008). The ratio of IR isoform A (IR-A) to isoform B (IR-B) is also important in breast cancer, and recently, a higher IR-A:IR-B ratio has been observed in the luminal B subtype of breast cancer (Huang et al. 2011). Breast cancer cells in culture have also been reported to express higher levels of the IR (Osborne et al. 1978) and proliferate directly in response to insulin (Bollig-Fischer et al. 2011). The signaling pathways activated by the *Neu-NT* tyrosine kinase significantly overlap with those of the IR/IGF1R and include the canonical PI3-K/Akt/mTOR and MAPK signaling pathways. It is thus possible that activation of the IR/IGF1R causes amplification of the canonical *Neu* signaling pathways, which could possibly lead to increased tumor cell proliferation and/or survival.

Under conditions of hyperinsulinemia, IGF binding proteins (IGFBP)-1 and -2 are repressed (Calle & Kaaks 2004), which may lead to an increase in circulating 'free' IGF1. In the MTB/TAN/MKR<sup>+/+</sup> mouse model, increased IGF1 levels at the level of the target tissue could lead to increased activation of the IGF1R, thus directly increasing tumor growth. The *Neu* RTK has no known ligand, depending on its activation upon dimerization with either ErbB3 or ErbB1 (Cho et al. 2003, Garrett et al. 2003). Interestingly, *Neu* also dimerizes with IGF1R, an occurrence that provides a significant source of resistance to *Her2*-mediated therapies in humans (Lu et al. 2001, 2004). Thus, in our MTB/TAN/MKR<sup>+/+</sup> mouse model, it is possible that elevations of either insulin or 'free' IGF1 could promote tumor growth through increased activation of *Neu*/IGF1R hybrids (Nahta et al. 2006).

Our finding of greater numbers of lung metastases in MTB/TAN/MKR<sup>+/+</sup> mice suggests that, as well as promoting primary tumor growth, insulin may also enhance primary tumor progression and/or circulating tumor cell survival in the lung. Our previous work has demonstrated that murine mammary tumor cell line Mvt1 is able to form more lung metastases in MKR mice as a result of whether an orthotopic cell inoculation or an intravenous injection (Ferguson et al. 2012). Evidence that the IR specifically is involved in either homing to or survival in the lung has come from a report by Zhang et al. (2010), who showed that shRNA knockdown of the IR in breast cancer cell line LCC6 resulted in reduced ability of these cells to form lung metastases following intravenous injection into nude mice. The EMT permits tumor cells to gain the plasticity

required to extravasate from the primary tumor site. During extravasation cells become increasingly mesenchymal in nature due to numerous changes in cytoskeletal scaffolding protein structures. Vimentin belongs to the intermediate filament (IF) family of proteins and has recently been shown to be an important marker of the EMT in epithelial cells that normally express only cytokeratin-type IFs (Zeisberg & Neilson 2009, Satelli & Li 2011). Vimentin is not specific for EMT and is also a marker of cancer-associated fibroblasts (Sugimoto et al. 2006). Additionally, recent studies have demonstrated that cancer-associated fibroblasts induce EMT in breast cancer cells (Soon et al. 2013). In breast cancer cells, vimentin expression has been shown to be correlated with increased migration and invasion (Gilles et al. 2003, Korsching et al. 2005), and in human breast cancer specimens, several studies have reported overexpression of vimentin as a marker of poor prognosis (Kokkinos et al. 2007). In this study, we observed elevated expression of vimentin as early as 6 weeks of Neu-NT upregulation. The majority of the vimentin-positive cells did not co-stain with Neu. This suggests the MTB/TAN/MKR<sup>+/+</sup> mice have a greater desmoplastic reaction to the tumors, with more numerous cancer-associated fibroblasts. Another explanation that we cannot exclude is that these vimentin-positive cells are tumor cells that have undergone EMT and have lost Neu expression. Our finding of hyperinsulinemia leading to greater lung metastasis could thus be due to an increase in the dissemination of tumor cells from the primary tumor associated with increase in the number of cancer-associated fibroblasts, or due to a direct effect of insulin on the tumors, inducing EMT. It is also possible that hyperinsulinemia may lead to greater cell survival, intravasation, and proliferation in lung tissue.

In summary, we have shown that hyperinsulinemia promotes advanced mammary gland hyperplasia, primary tumor growth, and lung metastasis in a Her2/Neu model of breast cancer. Further studies are required to determine whether, in promoting lung metastases, hyperinsulinemia enhances cell dissemination from the primary tumor, cell survival/adhesion in the lung, or both of these processes.

#### Declaration of interest

The authors declare that there is no conflict of interest that could be perceived as prejudicing the impartiality of the research reported.

#### Funding

This work was supported by the NIH/NCI (R01CA128798-01A3) and American Diabetes Association (1-13-B5-108).

#### Acknowledgements

The authors thank Lewis A Chodosh, MD, PhD (Perelman School of Medicine, University of Pennsylvania, PA, USA), for donating MMTV-MTB/TAN transgenic mice. They also thank Dr Archana Vijayakumar for performing animal insulin measurements.

#### References

- Baselga J & Swain SM 2010 CLEOPATRA: a phase III evaluation of pertuzumab and trastuzumab for HER2-positive metastatic breast cancer. *Clinical Breast Cancer* **10** 489–491. (doi:10.3816/CBC.2010.n.065)
- Bollig-Fischer A, Dewey TG & Ethier SP 2011 Oncogene activation induces metabolic transformation resulting in insulin-independence in human breast cancer cells. *PLoS ONE* **6** e17959. (doi:10.1371/journal.pone.0017959)
- Boyle P, Boniol M, Koechlin A, Robertson C, Valentini F, Coppens K, Fairley LL, Zheng T, Zhang Y, Pasterk M et al. 2012 Diabetes and breast cancer risk: a meta-analysis. *British Journal of Cancer* **107** 1608–1617. (doi:10.1038/bjc.2012.414)
- Calle EE & Kaaks R 2004 Overweight, obesity and cancer: epidemiological evidence and proposed mechanisms. *Nature Reviews. Cancer* **4** 579–591. (doi:10.1038/nrc1408)
- Cho HS, Mason K, Ramyar KX, Stanley AM, Gabelli SB, Denney DW, Jr & Leahy DJ 2003 Structure of the extracellular region of HER2 alone and in complex with the Herceptin Fab. *Nature* **421** 756–760. (doi:10.1038/nature01392)
- Duggan C, Irwin ML, Xiao L, Henderson KD, Smith AW, Baumgartner RN, Baumgartner KB, Bernstein L, Ballard-Barbash R & McTiernan A 2011 Associations of insulin resistance and adiponectin with mortality in women with breast cancer. *Journal of Clinical Oncology* **29** 32–39. (doi:10.1200/JCO.2009.26.4473)
- Ferguson RD, Novosyadlyy R, Fierz Y, Alikhani N, Sun H, Yakar S & Leroith D 2012 Hyperinsulinemia enhances c-Myc-mediated mammary tumor development and advances metastatic progression to the lung in a mouse model of type 2 diabetes. *Breast Cancer Research* **14** R8. (doi:10.1186/bcr3089)
- Fierz Y, Novosyadlyy R, Vijayakumar A, Yakar S & LeRoith D 2010 Insulin-sensitizing therapy attenuates type 2 diabetes-mediated mammary tumor progression. *Diabetes* **59** 686–693. (doi:10.2337/db09-1291)
- Formica V, Tesaro M, Cardillo C & Roselli M 2012 Insulinemia and the risk of breast cancer and its relapse. *Diabetes, Obesity & Metabolism* **14** 1073–1080.
- Garrett TP, McKern NM, Lou M, Elleman TC, Adams TE, Lovrecz GO, Kofler M, Jorissen RN, Nice EC, Burgess AW et al. 2003 The crystal structure of a truncated ErbB2 ectodomain reveals an active conformation, poised to interact with other ErbB receptors. *Molecular Cell* **11** 495–505. (doi:10.1016/S1097-2765(03)00048-0)
- Gilles C, Polette M, Mestdagt M, Nawrocki-Raby B, Ruggeri P, Birembaut P & Foidart JM 2003 Transactivation of vimentin by  $\beta$ -catenin in human breast cancer cells. *Cancer Research* **63** 2658–2664.
- Goodwin PJ, Ennis M, Pritchard KI, Trudeau ME, Koo J, Madarnas Y, Hartwick W, Hoffman B & Hood N 2002 Fasting insulin and outcome in early-stage breast cancer: results of a prospective cohort study. *Journal of Clinical Oncology* **20** 42–51. (doi:10.1200/JCO.20.1.42)
- Goodwin PJ, Ennis M, Pritchard KI, Trudeau ME, Koo J, Taylor SK & Hood N 2012 Insulin- and obesity-related variables in early-stage breast cancer: correlations and time course of prognostic associations. *Journal of Clinical Oncology* **30** 164–171. (doi:10.1200/JCO.2011.36.2723)
- Gunter MJ, Hoover DR, Yu H, Wassertheil-Smoller S, Rohan TE, Manson JE, Li J, Ho GY, Xue X, Anderson GL et al. 2009 Insulin, insulin-like growth factor-I, and risk of breast cancer in postmenopausal women. *Journal of the National Cancer Institute* **101** 48–60. (doi:10.1093/jnci/djn415)

- Harari D & Yarden Y 2000 Molecular mechanisms underlying ErbB2/HER2 action in breast cancer. *Oncogene* **19** 6102–6114. (doi:10.1038/sj.onc.1203973)
- He X, Esteva FJ, Ensor J, Hortobagyi GN, Lee MH & Yeung SC 2012 Metformin and thiazolidinediones are associated with improved breast cancer-specific survival of diabetic women with HER2+ breast cancer. *Annals of Oncology* **23** 1771–1780. (doi:10.1093/annonc/mdr534)
- Holbro T, Beerli RR, Maurer F, Koziczak M, Barbas CF, III & Hynes NE 2003 The ErbB2/ErbB3 heterodimer functions as an oncogenic unit: ErbB2 requires ErbB3 to drive breast tumor cell proliferation. *PNAS* **100** 8933–8938. (doi:10.1073/pnas.1537685100)
- Huang J, Morehouse C, Streicher K, Higgs BW, Gao J, Czapiga M, Boutrin A, Zhu W, Brohawn P, Chang Y et al. 2011 Altered expression of insulin receptor isoforms in breast cancer. *PLoS ONE* **6** e26177. (doi:10.1371/journal.pone.0026177)
- Irwin ML, Duggan C, Wang CY, Smith AW, McTiernan A, Baumgartner RN, Baumgartner KB, Bernstein L & Ballard-Barbash R 2011 Fasting C-peptide levels and death resulting from all causes and breast cancer: the health, eating, activity, and lifestyle study. *Journal of Clinical Oncology* **29** 47–53. (doi:10.1200/JCO.2010.28.4752)
- Jin Q & Esteva FJ 2008 Cross-talk between the ErbB/HER family and the type I insulin-like growth factor receptor signaling pathway in breast cancer. *Journal of Mammary Gland Biology and Neoplasia* **13** 485–498. (doi:10.1007/s10911-008-9107-3)
- Kokkinos MI, Wafai R, Wong MK, Newgreen DF, Thompson EW & Waltham M 2007 Vimentin and epithelial-mesenchymal transition in human breast cancer – observations *in vitro* and *in vivo*. *Cells, Tissues, Organs* **185** 191–203. (doi:10.1159/000101320)
- Korsching E, Packeisen J, Liedtke C, Hungermann D, Wulffing P, van Diest PJ, Brandt B, Boecker W & Buerger H 2005 The origin of vimentin expression in invasive breast cancer: epithelial-mesenchymal transition, myoepithelial histogenesis or histogenesis from progenitor cells with bilinear differentiation potential? *Journal of Pathology* **206** 451–457. (doi:10.1002/path.1797)
- Larsson SC, Mantzoros CS & Wolk A 2007 Diabetes mellitus and risk of breast cancer: a meta-analysis. *International Journal of Cancer* **121** 856–862. (doi:10.1002/ijc.22717)
- Law JH, Habibi G, Hu K, Masoudi H, Wang MY, Stratford AL, Park E, Gee JM, Finlay P, Jones HE et al. 2008 Phosphorylated insulin-like growth factor-I/insulin receptor is present in all breast cancer subtypes and is related to poor survival. *Cancer Research* **68** 10238–10246. (doi:10.1158/0008-5472.CAN-08-2755)
- Lu Y, Zi X, Zhao Y, Mascarenhas D & Pollak M 2001 Insulin-like growth factor-I receptor signaling and resistance to trastuzumab (Herceptin). *Journal of the National Cancer Institute* **93** 1852–1857. (doi:10.1093/jnci/93.24.1852)
- Lu D, Zhang H, Ludwig D, Persaud A, Jimenez X, Burtrum D, Balderes P, Liu M, Bohlens P, Witte L et al. 2004 Simultaneous blockade of both the epidermal growth factor receptor and the insulin-like growth factor receptor signaling pathways in cancer cells with a fully human recombinant bispecific antibody. *Journal of Biological Chemistry* **279** 2856–2865. (doi:10.1074/jbc.M310132200)
- Luijten M, Verhoef A, Dormans JA, Beems RB, Cremers HW, Nagelkerke NJ, Adlercreutz H, Penalvo JL & Piersma AH 2007 Modulation of mammary tumor development in Tg.NK (MMTV/c-neu) mice by dietary fatty acids and life stage-specific exposure to phytoestrogens. *Reproductive Toxicology* **23** 407–413. (doi:10.1016/j.reprotox.2006.12.001)
- Moody SE, Sarkisian CJ, Hahn KT, Gunther EJ, Pickup S, Dugan KD, Innocent N, Cardiff RD, Schnall MD & Chodosh LA 2002 Conditional activation of Neu in the mammary epithelium of transgenic mice results in reversible pulmonary metastasis. *Cancer Cell* **2** 451–461. (doi:10.1016/S1535-6108(02)00212-X)
- Nahta R, Yu D, Hung MC, Hortobagyi GN & Esteva FJ 2006 Mechanisms of disease: understanding resistance to HER2-targeted therapy in human breast cancer. *Nature Clinical Practice. Oncology* **3** 269–280. (doi:10.1038/ncponc0509)
- Novosyadlyy R & LeRoith D 2010 Hyperinsulinemia and type 2 diabetes: impact on cancer. *Cell Cycle* **9** 1449–1450. (doi:10.4161/cc.9.8.11512)
- Novosyadlyy R, Lann DE, Vijayakumar A, Rowzee A, Lazzarino DA, Fierz Y, Carboni JM, Gottardis MM, Pennisi PA, Molinolo AA et al. 2010 Insulin-mediated acceleration of breast cancer development and progression in a nonobese model of type 2 diabetes. *Cancer Research* **70** 741–751. (doi:10.1158/0008-5472.CAN-09-2141)
- Osborne CK, Monaco ME, Lippman ME & Kahn CR 1978 Correlation among insulin binding, degradation, and biological activity in human breast cancer cells in long-term tissue culture. *Cancer Research* **38** 94–102.
- Pearis KS, Barone BB, Snyder CF, Yeh HC, Stein KB, Derr RL, Brancati FL & Wolff AC 2011 Diabetes mellitus and breast cancer outcomes: a systematic review and meta-analysis. *Journal of Clinical Oncology* **29** 40–46. (doi:10.1200/JCO.2009.27.3011)
- Pinkas-Kramarski R, Shelly M, Glathe S, Ratzkin BJ & Yarden Y 1996 Neu differentiation factor/neuregulin isoforms activate distinct receptor combinations. *Journal of Biological Chemistry* **271** 19029–19032. (doi:10.1074/jbc.271.32.19029)
- Pisani P 2008 Hyper-insulinaemia and cancer, meta-analyses of epidemiological studies. *Archives of Physiology and Biochemistry* **114** 63–70. (doi:10.1080/13813450801954451)
- Satelli A & Li S 2011 Vimentin in cancer and its potential as a molecular target for cancer therapy. *Cellular and Molecular Life Sciences* **68** 3033–3046. (doi:10.1007/s00018-011-0735-1)
- Seshadri R, Fargira FA, Horsfall DJ, McCaul K, Setlur V & Kitchen P 1993 Clinical significance of HER-2/neu oncogene amplification in primary breast cancer. The South Australian Breast Cancer Study Group. *Journal of Clinical Oncology* **11** 1936–1942.
- Slamon DJ, Godolphin W, Jones LA, Holt JA, Wong SG, Keith DE, Levin WJ, Stuart SG, Udove J, Ullrich A et al. 1989 Studies of the HER-2/neu proto-oncogene in human breast and ovarian cancer. *Science* **244** 707–712. (doi:10.1126/science.2470152)
- Soon PS, Kim E, Pon CK, Gill AJ, Moore K, Spillane AJ, Benn DE & Baxter RC 2013 Breast cancer-associated fibroblasts induce epithelial-to-mesenchymal transition in breast cancer cells. *Endocrine-Related Cancer* **20** 1–12. (doi:10.1530/ERC-12-0227)
- Sugimoto H, Mundel TM, Kieran MW & Kalluri R 2006 Identification of fibroblast heterogeneity in the tumor microenvironment. *Cancer Biology & Therapy* **5** 1640–1646. (doi:10.4161/cbt.5.12.3354)
- Ursini-Siegel J, Schade B, Cardiff RD & Muller WJ 2007 Insights from transgenic mouse models of ERBB2-induced breast cancer. *Nature Reviews. Cancer* **7** 389–397. (doi:10.1038/nrc2127)
- Yarden Y 2001 Biology of HER2 and its importance in breast cancer. *Oncology* **61** (Suppl 2) 1–13. (doi:10.1159/000055396)
- Zeisberg M & Neilson EG 2009 Biomarkers for epithelial-mesenchymal transitions. *Journal of Clinical Investigation* **119** 1429–1437. (doi:10.1172/JCI36183)
- Zhang H, Fagan DH, Zeng X, Freeman KT, Sachdev D & Yee D 2010 Inhibition of cancer cell proliferation and metastasis by insulin receptor downregulation. *Oncogene* **29** 2517–2527. (doi:10.1038/onc.2010.17)

Received in final form 27 March 2013

Accepted 9 April 2013

Made available online as an Accepted Preprint

9 April 2013

# Insulin Receptor Phosphorylation by Endogenous Insulin or the Insulin Analog AspB10 Promotes Mammary Tumor Growth Independent of the IGF-I Receptor

Emily Jane Gallagher,<sup>1</sup> Nyosha Alikhani,<sup>1</sup> Aviva Tobin-Hess,<sup>1</sup> Jeffrey Blank,<sup>1</sup> Nicholas J. Buffin,<sup>1</sup> Zara Zelenko,<sup>1</sup> Norbert Tennagels,<sup>2</sup> Ulrich Werner,<sup>2</sup> and Derek LeRoith<sup>1</sup>

Endogenous hyperinsulinemia and insulin receptor (IR)/IGF-I receptor (IGF-IR) phosphorylation in tumors are associated with a worse prognosis in women with breast cancer. In vitro, insulin stimulation of the IR increases proliferation of breast cancer cells. However, in vivo studies demonstrating that IR activation increases tumor growth, independently of IGF-IR activation, are lacking. We hypothesized that endogenous hyperinsulinemia increases mammary tumor growth by directly activating the IR rather than the IGF-IR or hybrid receptors. We aimed to determine whether stimulating the IR with the insulin analog AspB10 could increase tumor growth independently of IGF-IR signaling. We induced orthotopic mammary tumors in control FVB/n and hyperinsulinemic MKR mice, and treated them with the insulin analog AspB10, recombinant human IGF-I, or vehicle. Tumors from mice with endogenous hyperinsulinemia were larger and had greater IR phosphorylation, but not IGF-IR phosphorylation, than those from control mice. Chronic AspB10 administration also increased tumor growth and IR (but not IGF-IR) phosphorylation in tumors. IGF-I led to activation of both the IGF-IR and IR and probably hybrid receptors. Our results demonstrate that IR phosphorylation increases tumor growth, independently of IGF-IR/hybrid receptor phosphorylation, and warrant consideration when developing therapeutics targeting the IGF-IR, but not the IR. *Diabetes* 62:3553–3560, 2013

Individuals with obesity, the metabolic syndrome (MetS), and type 2 diabetes (T2D) have increased breast cancer incidence and mortality (1–3). Endogenous hyperinsulinemia appears to be an important factor linking obesity, T2D, MetS, and breast cancer (4–6). The association between endogenous insulin concentration and breast cancer risk seems to be independent of obesity (6,7). In women without diabetes, with early-stage breast cancer, hyperinsulinemia is associated with a lower disease-free and overall survival (8).

It is hypothesized that hyperinsulinemia may increase tumor growth by direct and/or indirect mechanisms. Direct mechanisms involve insulin acting on the insulin receptor (IR) or IGF-I receptor (IGF-IR) on tumor cells, activating signaling pathways and tumor growth (9,10). Indirect mechanisms include hyperinsulinemia stimulating hepatic IGF-I synthesis, decreasing IGF binding protein-1 synthesis,

and thus increasing local IGF-I concentrations to act on the tumor (10,11). In vitro studies are unable to distinguish these potential direct and indirect effects. Studies have reported that increased IR expression in breast cancers is associated with decreased survival (12). The presence of phosphorylated IR/IGF-IR in the primary tumor is also associated with a worse prognosis (12). However, these studies have not been able to discriminate between IR and IGF-IR phosphorylation. Additionally, human studies provide associations, but not mechanistic links between hyperinsulinemia and breast cancer growth.

In vivo studies demonstrating that hyperinsulinemia increases tumor growth by acting directly on the tumor IR are lacking. We previously reported that, in an animal model, endogenous hyperinsulinemia increases mammary tumor growth by increasing phosphorylation of the IR/IGF-IR (9). We have shown that decreasing endogenous insulin levels and blocking the IR/IGF-IR using a tyrosine kinase inhibitor decreased tumor growth and metastases (9,13,14). However, we have not previously demonstrated that the greater tumor growth in these mice is a result of insulin acting directly on the IR, rather than through the IGF-IR (9). Previous studies of exogenous human insulin administration have not demonstrated an increase in mammary tumor growth in rodents (15,16). However, the insulin analog AspB10, a rapid-acting insulin analog, has been shown to increase mammary tumor development in rats (17,18). AspB10 binds the IR with greater affinity than human insulin and has a slower rate of dissociation from the IR in vitro, raising the possibility that activation of the IR is mediating its tumor-promoting effects (19–25).

We hypothesized that hyperinsulinemia increases mammary tumor growth through the direct effects on the IR. We also hypothesized that chronic activation of the IR in vivo is capable of promoting tumor growth independently of IGF-IR activation. For this study, we used the female MKR mouse, a nonobese mouse model of endogenous hyperinsulinemia (9). The female MKR mice demonstrate no hyperglycemia or dyslipidemia; have normal circulating levels of cytokines and IGF-I; and have no increase in leptin or decrease in adiponectin (9,13). Therefore, this animal model has allowed us to determine the effects of hyperinsulinemia in isolation from many of the other factors reported to contribute to breast cancer growth with obesity, T2D, and the MetS (10).

In this study, we found that in mice with endogenous hyperinsulinemia orthotopic mammary tumors had IR phosphorylation, but not IGF-IR phosphorylation. Additionally, we report that chronic stimulation of IR phosphorylation, without increased IGF-IR phosphorylation, enhanced mammary tumor growth in these models. Our findings indicate that, in the setting of endogenous hyperinsulinemia,

From the <sup>1</sup>Division of Endocrinology, Diabetes and Bone Diseases, Samuel Bronfman Department of Medicine, Icahn School of Medicine at Mount Sinai, New York, New York; and <sup>2</sup>R&D Diabetes Division, Sanofi-Aventis Deutschland, Frankfurt am Main, Germany.

Corresponding author: Derek LeRoith, derek.leroith@mssm.edu.

Received 12 February 2013 and accepted 21 June 2013.

DOI: 10.2337/db13-0249

© 2013 by the American Diabetes Association. Readers may use this article as long as the work is properly cited, the use is educational and not for profit, and the work is not altered. See <http://creativecommons.org/licenses/by-nc-nd/3.0/> for details.



insulin is directly driving tumor growth by acting on the IR, rather than through indirect effects mediated by IGF-I or the IGF-IR.

## RESEARCH DESIGN AND METHODS

**Animals.** Animal study protocols were approved by the Mount Sinai School of Medicine Institutional Animal Care and Use Committee. Mice were housed in The Mount Sinai School of Medicine Center for Comparative Medicine and Surgery, an Association for Assessment and Accreditation of Laboratory Animal Care International-accredited facility. Mice had a 12-h light/dark cycle, free access to mouse chow (Picolab rodent diet #5053; LabDiet, St. Louis, MO) and water. All mice were female, on the FVB/N background, and 8–12 weeks old. The MKR mice express a human dominant-negative IGF-IR expressed in skeletal muscle only that forms hybrids with the IR, leading to skeletal muscle insulin resistance, with subsequent whole-body insulin resistance (26). The generation and characteristics of the MKR mice have been previously described (9,26).

**In vitro studies.** The MVT1 murine mammary carcinoma cell line was derived from an explant tumor culture from MMTV-c-Myc/Vegf transgenic mice (27). Met1 murine mammary tumor cells were derived from MMTV-Polyoma virus middle T antigen (PyVmt) transgenic mice (28). Met1 and MVT1 cells were cultured as previously described (9,14). Cells were stimulated with PBS, 10 nmol/L insulin (Humulin R; Eli Lilly, Indianapolis, IN), AspB10 (provided by Sanofi-Aventis, Frankfurt am Main, Germany), or recombinant human IGF-I (rhIGF-I) (Ipsen, Brisbane, CA) for 10 min. After treatment, cells were lysed for protein extraction.

**Orthotopic tumor models.** Met-1 and MVT1 cells were prepared for injection as described previously (9,14). A total of 250,000 Met-1 cells or 100,000 MVT1 cells were inoculated into the fourth mammary fat pad of 8–10-week-old female virgin MKR and WT mice. Mice were treated with rhIGF-I (Ipsen, Brisbane, CA) (1 mg/kg, twice daily i.p.), AspB10 (12.5 IU/kg, twice daily s.c.; provided by Sanofi-Aventis, Frankfurt am Main, Germany), or PBS (vehicle). Tumor growth was measured in three dimensions using calipers. Tumor volume was calculated as follows:  $4/3 \times \pi \times r_1 \times r_2 \times r_3$  ( $r$  = radius). At the end of the study, mice were killed; tumors were removed and flash frozen in liquid nitrogen. Lungs were inflated and fixed with formalin; the number of surface macrometastases was quantified.

**Body weights, composition, blood glucose, insulin, and IGF-I measurement.** Body weights were measured weekly. Body composition analysis was performed using the EchoMRI 3-in-1 nuclear magnetic resonance system (Echo Medical Systems, Houston, TX), before tumor cell injection and at the end of treatment. Fed blood glucose measurements were performed on tail vein blood during tumor studies using a Bayer Contour Glucometer (Bayer Healthcare, Mishawaka, IN), prior to commencing treatment and weekly thereafter. Plasma insulin levels were measured at the end of the studies using the Sensitive Rat Insulin RIA kit (Millipore, St. Charles, MO). Serum IGF-I levels were measured by radioimmunoassay (ALPCO, Salem, NH).

**Insulin tolerance test.** MKR mice were fasted for 2 h prior to the insulin tolerance test, blood glucose was measured from the tail vein using a Bayer Contour Glucometer at time 0, immediately before PBS, human insulin (Humulin R; Eli Lilly, Indianapolis, IN), or AspB10 injection, and at 0.5, 1, 2, 4, 7, and 10 h after injection, at which time the mice were refed.

**Protein extraction, Western blot, and immunoprecipitation.** Protein extraction and Western blot analysis were performed as previously described (9,13). The following antibodies were used: anti-phospho-IGF-IR $\beta$ <sup>(Tyr1135/1136)</sup>/IR $\beta$ <sup>(Tyr1150/1151)</sup>, total IGF-IR $\beta$ , phospho<sup>(Ser473)</sup> and total Akt, phospho<sup>(Thr202/Tyr204)</sup>, and total p44/42 mitogen-activated protein kinase (Erk1/2) (Cell Signaling Technology, Danvers, MA), total IR $\beta$  and total IGF-IR $\beta$  (Santa Cruz Biotechnology, Santa Cruz, CA), and  $\beta$ -actin (Sigma-Aldrich, St. Louis, MO). Densitometric analysis was performed using ImageJ V1.44 software (National Institutes of Health). Immunoprecipitation of the IR $\beta$  and IGF-IR $\beta$  were performed using magnetic Dynabeads Protein G (Invitrogen Dynal, Oslo, Norway) as per the manufacturer's protocol, with the following modifications: 10  $\mu$ g anti-IR $\beta$  antibody or anti-IGF-IR $\beta$  was added to 1,000  $\mu$ g protein lysate, incubated with rotation overnight at 4°C; samples were incubated with the magnetic beads with rotation for 4 h at 4°C, after which they were washed with ice-cold Tris buffer (pH 7.4); and antigens were eluted using 3 $\times$  loading buffer supplemented with dithiothreitol, boiled at 96°C for 5 min, separated from the beads on a magnet (DynaMag; Invitrogen Dynal, Oslo, Norway), and loaded on an 8% Tris-Glycine gel (Novex; Life Technologies, Carlsbad, CA). The gel was probed for phospho-IGF-IR $\beta$ <sup>(Tyr1135/1136)</sup>/IR $\beta$ <sup>(Tyr1150/1151)</sup>, total IR $\beta$ , and total IGF-IR $\beta$ .

**Statistical analysis.** Differences between groups were calculated by the two-tailed Student *t* test when comparing two groups with equal variance and a one-way ANOVA with Holm-Sidak post hoc test when comparing more than

two groups, using the statistics software package SPSS Statistics (IBM, Armonk, NY). *P* values <0.05 were considered statistically significant.

## RESULTS

**Insulin and AspB10 led to IR phosphorylation, while IGF-I led to IGF-IR/hybrid receptor activation in vitro.** We first aimed to determine whether differences in IR and IGF-IR phosphorylation could be detected in two different murine tumor cell lines, with different oncogenes, in response to insulin, rhIGF-I, and the insulin analog AspB10. MVT1 and Met1 cells were stimulated with PBS or 10 nmol/L insulin, AspB10, or IGF-I for 10 min (Fig. 1A–D). Western blot analysis using the primary pIGF-IR $\beta$ <sup>(Tyr1135/1136)</sup>/pIR $\beta$ <sup>(Tyr1150/1151)</sup> antibody suggested that insulin and AspB10 stimulation led to IR $\beta$  phosphorylation, observed as a distinct band on the membrane at 95 kDa (Fig. 1A and B) (29). IGF-I stimulation led to phosphorylation of the IGF-IR $\beta$  at 97 kDa, as well as the IR $\beta$  at 95 kDa (Fig. 1A and B) (29). These findings suggested that in both MVT1 and Met1 cells, IGF-I-mediated phosphorylation of the IGF-IR $\beta$  and the IR $\beta$ , and probably the IR/IGF-IR hybrids. To confirm the Western blot findings, we performed immunoprecipitation of the IR $\beta$  and IGF-IR $\beta$  from the Met1 cell lysates. We found that insulin and AspB10 were indeed phosphorylating the IR $\beta$ , but not the IGF-IR $\beta$  (Fig. 1E–H), whereas IGF-I stimulation led to phosphorylation of the IGF-IR $\beta$  and probable IGF-IR/IR hybrids (Fig. 1E–H). Incidentally, we noted that AspB10 stimulation led to greater IR $\beta$  phosphorylation than insulin in Met1 cells (Fig. 1D). These results show that it is possible to distinguish differences in IR $\beta$  and IGF-IR $\beta$  phosphorylation in response to insulin, IGF-I, and AspB10 by Western blot as confirmed by immunoprecipitation in Met1 and MVT1 cell lines in vitro.

**Endogenous hyperinsulinemia and exogenous rhIGF-I increase the growth of Met1 and MVT1 tumors.** We have previously shown that MKR mice with endogenous hyperinsulinemia develop larger primary tumors and more metastases than WT mice using a variety of orthotopic and transgenic tumor models with different oncogenes (9,14). We aimed to determine whether endogenous hyperinsulinemia stimulated Met1 and MVT1 tumor growth by acting directly on the IR in vivo or by indirect mechanisms, namely through phosphorylation of the IGF-IR $\beta$ . To assess the effect of endogenous hyperinsulinemia on tumor growth and receptor phosphorylation, compared with rhIGF-I in vivo, we studied Met1 and MVT1 tumors from WT mice and MKR mice treated with rhIGF-I or vehicle. WT and MKR mice were orthotopically injected with 100,000 MVT1 or 250,000 Met1 tumor cells. Consistent with our previous studies, MKR mice developed larger MVT1 and Met1 tumors than WT mice (Fig. 2A and B). MVT1 and Met1 tumors were then induced in MKR mice, and when tumors were measurable, the MKR mice were divided into two groups with equal mean tumor size. From that time, rhIGF-I (1 mg/kg, twice daily i.p.) or vehicle was administered for 2 weeks. Serum IGF-I levels were measured 2 h after injection at the end of the study and were 2.6 times higher in the rhIGF-I-treated mice ( $806 \pm 59.05$  ng/mL) than vehicle-treated mice ( $302 \pm 8.75$  ng/mL, *P* < 0.05) (Fig. 2C). rhIGF-I-treated MKR mice developed significantly larger tumors than the vehicle-treated MKR mice (Fig. 2D and E). Repeated studies demonstrated a nonsignificant increase in the number of MVT1-derived pulmonary macrometastases in the rhIGF-I-treated group compared with the MKR vehicle-treated group (Fig. 2F). Western blot analysis of tumor

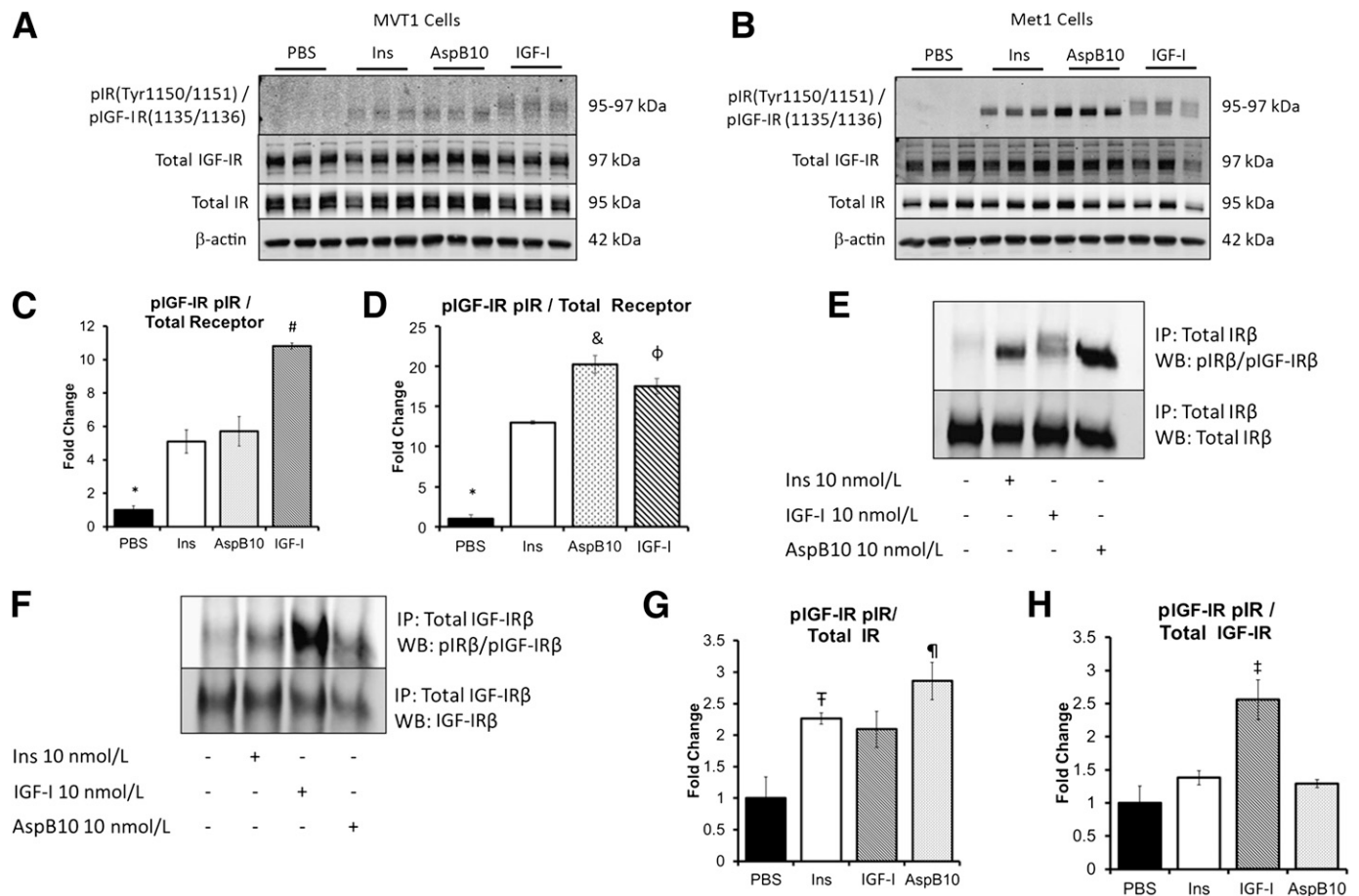


**FIG. 1.** Insulin and AspB10 led to IR phosphorylation but not IGF-IR phosphorylation in vitro. MVT1 and Met1 cells were stimulated with 10 nmol/L insulin (Ins), the insulin analog AspB10 (AspB10), rhIGF-I (IGF-I), or PBS. Western blot (WB) analysis of protein lysates (from MVT1 cells, **A**; from Met1 cells, **B**) and densitometry (from MVT1 cells, **C**; and from Met1 cells, **D**) demonstrated that insulin and AspB10 led to phosphorylation of the IR $\beta$ <sup>(Tyr 1150/1151)</sup> at 95 kDa, whereas IGF-I stimulation led to phosphorylation of the IGF-IR $\beta$ <sup>(Tyr 1135/1136)</sup> at 97 kDa and the IR $\beta$ <sup>(Tyr 1150/1151)</sup> at 95 kDa, most likely through hybrid receptor phosphorylation (**A** and **B**). Immunoprecipitation (IP) of the IR in Met1 cell lysates after in vitro stimulation with PBS, 10 nmol/L Ins, IGF-I, or AspB10 confirmed that insulin and AspB10 caused phosphorylation of the IR $\beta$ <sup>(Tyr 1150/1151)</sup>, whereas IGF-I led to IGF-IR $\beta$ <sup>(Tyr 1135/1136)</sup> and IR $\beta$ <sup>(Tyr 1150/1151)</sup> receptor phosphorylation, the latter likely through IR and hybrid receptor (**E** and **F**) with densitometry (**G** and **H**). Representative blots from experiments are shown. All experiments were performed two to three times. Bar graphs display means and SEM. \*PBS group significantly lower than all other groups,  $P < 0.05$ ; #IGF-I group significantly higher than all other groups,  $P < 0.05$ ; &AspB10 group significantly higher than human insulin group,  $P < 0.05$ ;  $\Phi$ IGF-I group significantly higher than human insulin group,  $P < 0.05$ ;  $\Phi$ human insulin group significantly greater than PBS,  $P < 0.05$ ;  $\Psi$ AspB10 significantly greater than PBS,  $P < 0.05$ ;  $\ddagger$ IGF-I group greater than PBS,  $P = 0.05$ . p, phosphorylated.

lysates demonstrated that rhIGF-I treatment led to phosphorylation of the IGF-IR $\beta$  at 97 kDa, and of IR $\beta$  at 95 kDa, in both Met1 and MVT1 tumors (Fig. 2*G* and *I*). In contrast, tumors from vehicle-treated MKR mice had only IR $\beta$  phosphorylation at 95 kDa (Fig. 2*G*–*I*). These results suggest that endogenous hyperinsulinemia increases mammary tumor growth by directly acting on the IR of the tumors and not by indirectly increasing IGF-IR phosphorylation. IGF-I in contrast leads to phosphorylation of the IGF-IR $\beta$  and IR $\beta$ , most likely through IGF-IR/IR hybrid receptors.

**Chronic administration of the insulin analog AspB10 increased Met1 and MVT1 tumor growth.** Our in vitro studies had shown that AspB10 increased IR $\beta$  phosphorylation in both Met1 and MVT1 cells, without increasing IGF-IR $\beta$  phosphorylation (Fig. 1*A*–*H*). Therefore, to investigate whether IR activation could truly increase tumor growth independently of IGF-IR activation, we used the insulin analog AspB10 to chronically activate the IR of the tumors in vivo. After orthotopic injection with MVT1 or Met1 tumor cells, mice were treated with AspB10 (12.5 IU/kg, twice daily s.c.) or vehicle for ~2 weeks after the tumors

became measurable. AspB10 treatment led to a significant increase in the size of both MVT1 and Met1 tumors (Fig. 3*A* and *B*). The increased average number of surface pulmonary macrometastases in the AspB10-treated group did not reach statistical significance (Fig. 3*C*). AspB10 treatment significantly increased plasma insulin concentrations to  $70.2 \pm 21.2$   $\mu$ g/L, compared with vehicle-treated mice ( $1.08 \pm 0.3$   $\mu$ g/L,  $P < 0.05$ ), when measured 2 h after insulin or vehicle injection. An insulin tolerance test revealed that AspB10 (12.5 units/kg s.c.) led to a reduction in blood glucose levels, similar to those for human insulin, from 30 min to 4 h after injection that reached a nadir ( $43.9 \pm 6.1\%$  baseline) 2 h after injection (Fig. 3*D*). No differences in body weight were observed between the AspB10- and vehicle-treated groups before or after 2 weeks of treatment (Fig. 3*E*). Although overall body weight was not different between the treatment groups, both vehicle- and AspB10-treated mice showed a relative loss of lean mass and a relative gain in fat mass; however, the change in lean and fat mass did not differ between the vehicle- and AspB10-treated groups (Fig. 3*F* and *G*).

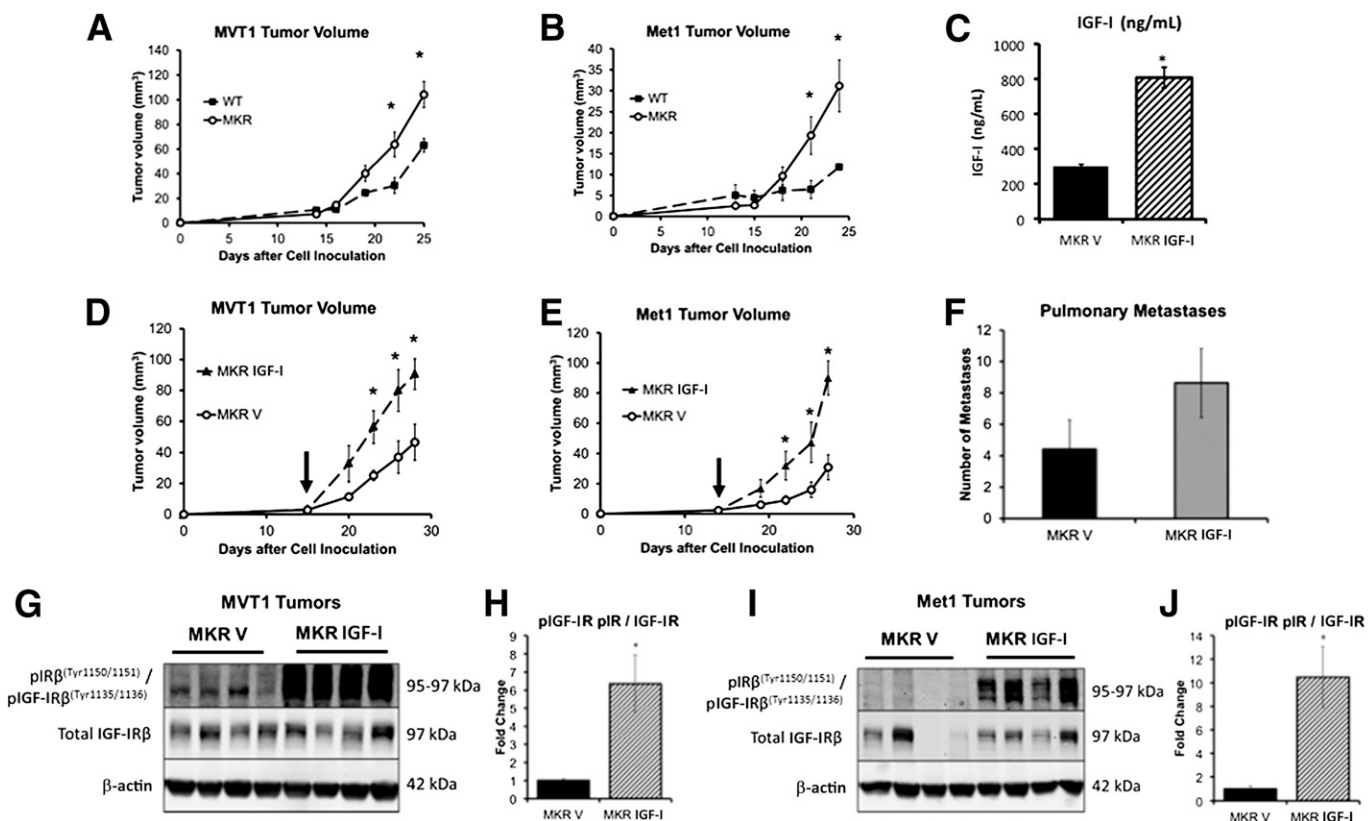


**FIG. 2.** IGF-I increased orthotopic MVT1 and Met1 tumor growth in the hyperinsulinemic MKR mice by increasing IGF-IR phosphorylation. WT and MKR mice were injected with tumor cells on Day 0. MKR mice developed larger MVT1 and Met1 tumors than WT mice (A and B). MVT1 and Met1 tumor cells were orthotopically injected into MKR mice, mice were divided into two groups with equal mean tumor size, and mice were administered either rhIGF-I or vehicle (vertical arrow indicates time when treatment began). Administration of rhIGF-I led to a further stimulation in tumor growth, over endogenous hyperinsulinemia (D and E). Serum IGF-I concentration in the rhIGF-I treatment group was 2.6 times that of the control group (C). The greater mean number of pulmonary macrometastases in the mice treated with rhIGF-I did not reach statistical significance, compared with vehicle-treated MKR mice (F). Western blot analysis of tumor lysates demonstrated that MKR mice with endogenous hyperinsulinemia (MKR V) show IR $\beta$  phosphorylation at 95 kDa, and rhIGF-I treatment led to increased IGF-IR $\beta$  and IR $\beta$  or hybrid receptor phosphorylation in MVT1 and Met1 tumors (G–J). Representative images from three repeated experiments of tumor volume and Western blots are displayed. The graphs represent the average for each group; error bars indicate SEM (A–F, H, and I). Statistical analysis was performed using a two-tailed *t* test; \*indicates statistically significant differences (*P* < 0.05) between the groups. *n* = 8–11 mice per group. p, phosphorylated.

**Endogenous hyperinsulinemia and AspB10 increased mammary tumor growth by directly activating the IR, but not the IGF-IR.** To ascertain whether AspB10 stimulated tumor growth in vivo by acting directly on the IR, we examined IR $\beta$  and IGF-IR $\beta$  phosphorylation in Met1 and MVT1 tumors after 2 weeks of AspB10 or vehicle treatment. Western blot analysis of the tumor lysates revealed that AspB10 treatment led to phosphorylation of the IR $\beta$ , but not the IGF-IR $\beta$ , in both MVT1 and Met1 tumors (Fig. 4A–D). To confirm these findings, the tumor lysates of MVT1 and Met1 tumors from WT mice, vehicle-treated MKR mice, IGF-I-treated MKR mice, and AspB10-treated MKR mice were subjected to immunoprecipitation of the IR $\beta$  and the IGF-IR $\beta$ , and were immunoblotted for the phosphorylated IGF-IR $\beta$ /IR $\beta$ . Tumors from vehicle-treated MKR mice demonstrated  $1.38 \pm 0.17$ -fold increased phosphorylation of the IR $\beta$  compared with tumors from WT mice (Fig. 4E), but no increase in IGF-IR $\beta$  phosphorylation was seen in the vehicle-treated MKR mice (Fig. 4F). Similarly, by immunoprecipitation AspB10 treatment led to  $1.81 \pm 0.17$ -fold increased phosphorylation of the IR $\beta$  compared with WT mice (Fig. 4E), but not the IGF-IR $\beta$  (Fig. 4F). In contrast, rhIGF-I administration led to phosphorylation of both the IGF-IR $\beta$  and IR $\beta$  (Fig. 4E and F). Taken together, these data demonstrate that

endogenous hyperinsulinemia directly increases tumor growth by acting on the IR of the tumors, but not the IGF-IR and that stimulating the IR, independently of the IGF-IR, further exacerbates tumor growth.

**AspB10-induced IR phosphorylation and rhIGF-I-induced IGF-IR/hybrid receptor phosphorylation led to increased Akt phosphorylation in tumors.** In order to examine whether differences in receptor activation in vivo led to differences in downstream signaling, we examined Akt and Erk1/2 phosphorylation in the two tumor types from mice treated with AspB10 or IGF-I. Despite the differences in receptor phosphorylation resulting from AspB10 and rhIGF-I administration, increased Akt phosphorylation was observed in MVT1 tumors after treatment with both AspB10 and rhIGF-I (Fig. 5A–D), although a greater fold change was observed in the rhIGF-I-treated group. In Met1 tumors, a 2.5-fold increase in Akt phosphorylation after rhIGF-I treatment (*P* < 0.05) and a 15% increase after AspB10 treatment, which did not reach statistical significance, were observed. No increase in Erk1/2 phosphorylation was found in MVT1 or Met1 tumors after either rhIGF-I or AspB10 treatment (Fig. 5A and B). These results show that, in tumors with certain oncogenes, despite differences in IR and IGF-IR activation, both rhIGF-I and AspB10 led to activation of the Akt signaling, rather than mitogen-activated protein kinase signaling.

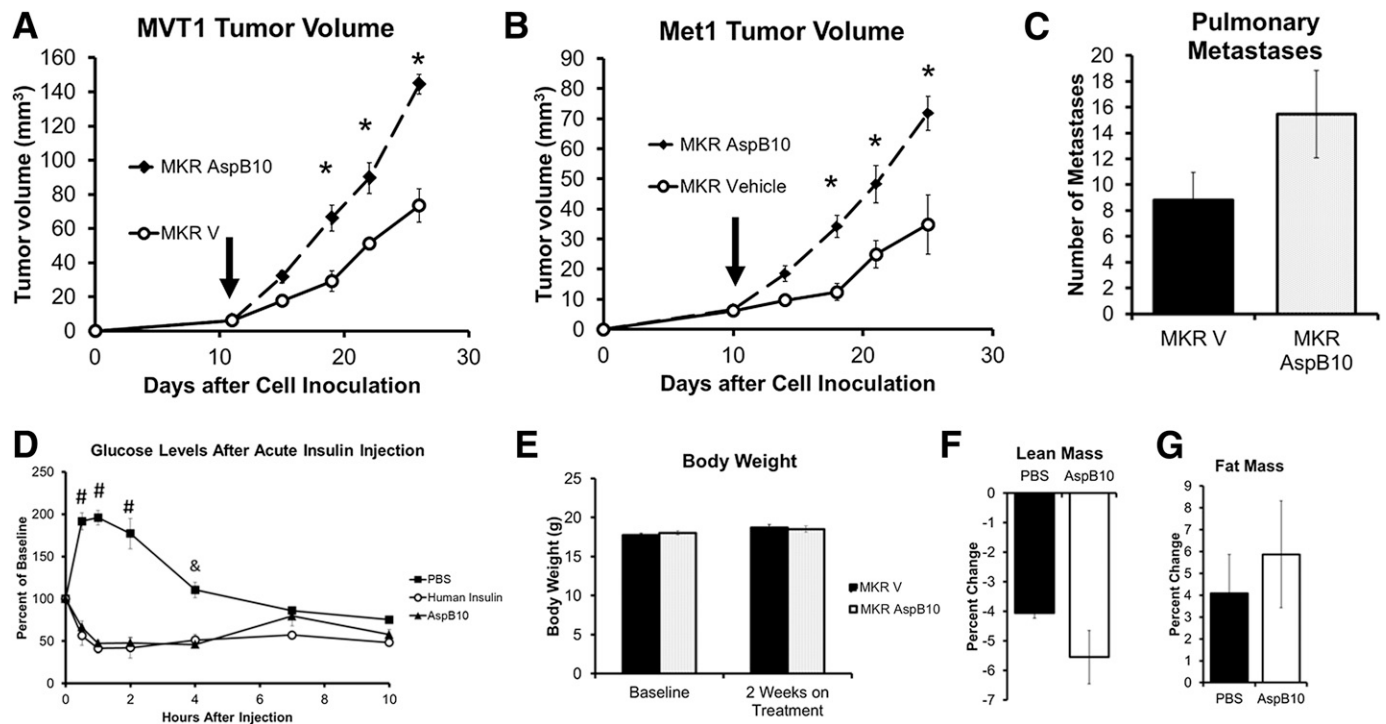


**FIG. 3.** Chronic activation of the IR by the insulin analog AspB10 increased orthotopic Met1 and MVT1 tumor growth. MKR mice were injected with MVT1 or Met1 tumor cells on Day 0. Treatment was started with AspB10 (12.5 IU/kg, twice daily s.c.) or vehicle, indicated by vertical arrow (A and B). AspB10 led to increased growth of both MVT1 and Met1 tumors (A and B). The number of pulmonary macrometastases showed a nonsignificant increase in the AspB10-treated group (C). An insulin tolerance test was performed with AspB10 (12.5 IU/kg s.c.), regular human insulin (12.5 IU/kg s.c.), and PBS (vehicle). Blood glucose was measured at 0.5, 1, 2, 4, 7, and 10 h after injection (D). Statistical analysis was performed using a one-way ANOVA for comparing more than two groups: # $P < 0.05$  between PBS and AspB10 and human insulin groups; & $P < 0.05$  between PBS- and AspB10-treated groups;  $n = 4$  per group. #PBS group was significantly greater than other groups,  $P < 0.05$ ; &PBS group was significantly higher than AspB10 group,  $P < 0.05$ . No change in body weight (E) or difference in relative lean or fat mass (F and G) was observed after 2 weeks of AspB10 administration. Graphs are representative of two studies. All graphs show the mean for each group, and error bars represent the SEM. Statistical analysis was performed using two-tailed  $t$  test. \* $P < 0.05$  between groups.  $n = 9$ –11 mice per group. MKR V, MKR mice with endogenous hyperinsulinemia.

## DISCUSSION

In this study, we aimed to establish whether endogenous hyperinsulinemia increases mammary tumor growth by directly acting on the IR, rather than through direct or indirect activation of the IGF-IR (9). Additionally, we aimed to determine whether chronic stimulation of the IR increased mammary tumor growth in the absence of IGF-IR phosphorylation. Our results demonstrate that endogenous hyperinsulinemia increases mammary tumor growth by acting directly on the IR. We observed no increase in IGF-IR phosphorylation in tumors from mice with endogenous hyperinsulinemia. Furthermore, we demonstrate that chronic stimulation of the IR, without IGF-IR activation, is capable of driving orthotopic mammary tumor growth in vivo.

Our findings add to the understanding of the link among obesity, T2D, the MetS, and breast cancer. Chronic endogenous hyperinsulinemia has been reported as a major factor linking these conditions (4,6–8,10). Our previous studies have demonstrated that MKR mice with endogenous hyperinsulinemia develop increased transgenic and orthotopic mammary tumor growth and metastases, with increased IGF-IR $\beta$ /IR $\beta$  phosphorylation, compared with tumors from WT mice (9,14). Lowering insulin levels or blocking IGF-IR $\beta$ /IR $\beta$  phosphorylation reduced tumor growth (9,13,14). It has been a matter of debate whether endogenous hyperinsulinemia in vivo has direct effects on the breast cancer IR, or whether endogenous hyperinsulinemia increases tumor growth by increasing the availability of local IGF-I to bind to and activate the IGF-IR. Our findings

are important, because in women with hyperinsulinemia, increased activation of the IR, rather than the IGF-IR, may be responsible for promoting tumor growth. Increased IR signaling may also be responsible for the increase in breast cancer risk and mortality in women with T2D, the MetS, and obesity, conditions associated with insulin resistance and hyperinsulinemia.

Our study is the first study demonstrating that IR activation, independent of IGF-IR activation, increases tumor growth in vivo.

Previous in vitro studies on breast cancer cell lines have shown that insulin stimulation increases IR phosphorylation and cell proliferation (14,30,31), suggesting that a direct effect of insulin on the IR is responsible for increasing tumor growth. Studies in human cancers have not been able to distinguish between IR and IGF-IR phosphorylation in breast cancer specimens (12). Although there are correlations between high levels of IR expression in human breast cancer specimens and poor prognosis, these studies have not shown that IR signaling increases breast cancer growth (12). Our findings are consistent with the studies by Zhang et al. (32), who reported that knocking down the IR in tumor cell lines reduced tumor growth and metastasis in vivo. It has been reported that IR signaling compensates when IGF-IR is downregulated in breast cancer cell lines (33). Establishing that IR activation is capable of driving tumor growth is important, because cancer therapies targeting the IGF-IR have been less effective than expected, possibly because of compensatory IR signaling



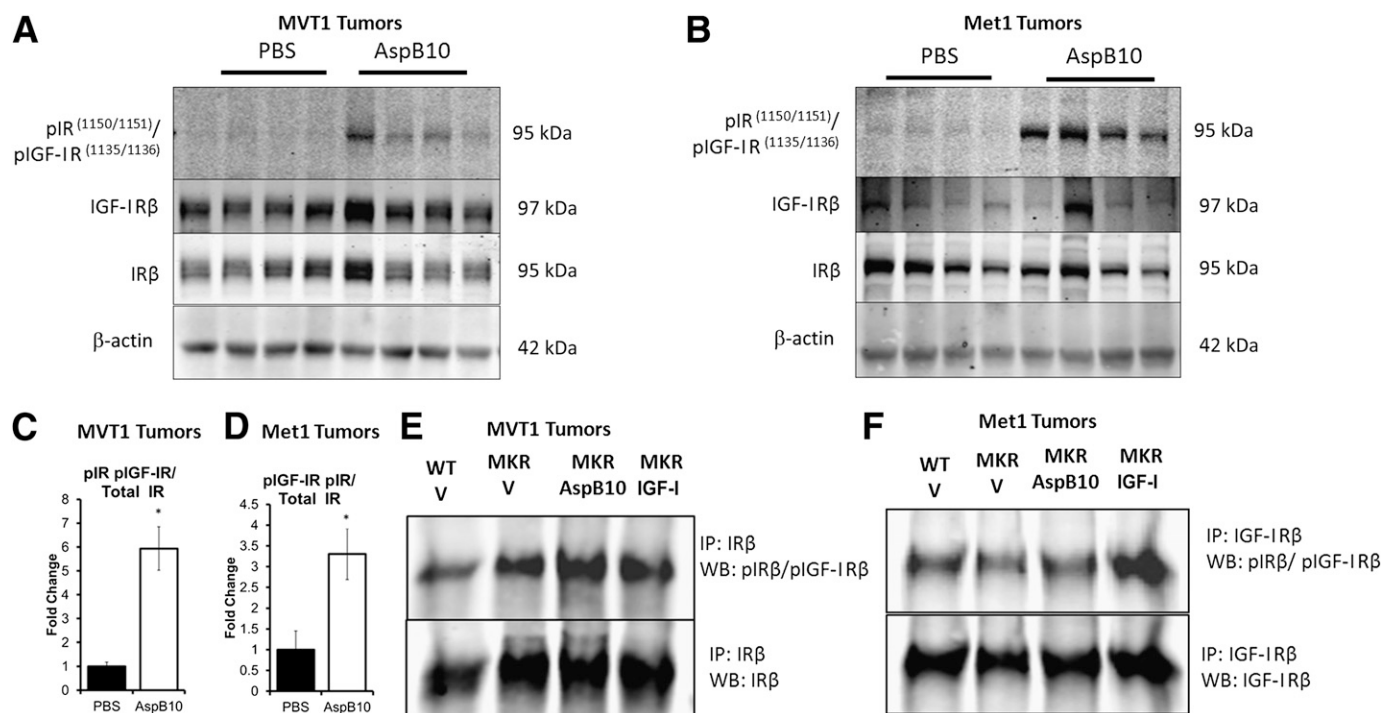


**FIG. 4.** Endogenous hyperinsulinemia and AspB10 treatment led to increased IR phosphorylation in MVT1 and Met1 tumors. Western blot (WB) analysis (representative blots, *A* and *B*) revealed that chronic AspB10 treatment led to increased IRβ phosphorylation at 95 kDa (*C* and *D*). Immunoprecipitation (IP) of the IRβ (representative blot, *E*) and IGF-IRβ (representative blot, *F*) was performed on MVT1 and Met1 tumor protein lysates. They were immunoblotted for the phosphorylated IGF-IRβ/IRβ. Endogenous hyperinsulinemia (MKR V) and chronic AspB10 administration (MKR AspB10) led to increased IR phosphorylation (*E*). rhIGF-I administration led to increased IGF-IRβ and IRβ phosphorylation (*E* and *F*). Graphs show the mean for each group, and error bars represent the SEM. Statistical analysis was performed using two-tailed *t* test. \**P* value < 0.05 between groups. *n* = 9–11 mice per group. p, phosphorylated; MKR V, MKR mice with endogenous hyperinsulinemia.

(34). Additionally, we found that rhIGF-I administration led to phosphorylation of the IGF-IR, IR, and probably hybrid receptors, as previously reported in in vitro studies (30). Therefore, it appears plausible that the IR is capable of driving tumor growth if the IGF-IR is selectively inhibited.

We used the insulin analog AspB10 to determine whether increased activation of the IR is capable of driving tumor growth, because it has previously been shown to induce spontaneous mammary tumors in rats (17) and our in vitro studies demonstrated increased IR phosphorylation after AspB10 stimulation. Some in vitro studies have reported increased IR phosphorylation after AspB10 stimulation (22), although others have reported that AspB10 stimulates cell proliferation by acting through the IR and IGF-IR (20). These in vitro studies found significantly greater IGF-IR phosphorylation compared with human insulin when using concentrations of AspB10 that were 10 times higher than those used in our studies (20). At concentrations of 10 nmol/L, IGF-IR phosphorylation was comparable to that seen in response to human insulin in MCF7 cells (20), findings consistent those from 5 nmol/L insulin or AspB10 stimulation in mouse embryonic fibroblasts (19). Differences between in vitro and in vivo potency of AspB10 have been previously described (35) and highlight the need for caution when interpreting the results of in vitro studies. In vivo studies have not previously demonstrated whether AspB10 exerts its mitogenic effects through the IR or IGF-IR (21,25). Understanding the mechanism through which AspB10 promotes tumor growth is important for the development of new insulin analogs to ensure they are not mitogenic. While AspB10 increases mammary tumor growth in the dose range used in our

study, no increase in rodent tumor growth with similar doses of human insulin has been found; this may be due to differences in IR affinity or dissociation rates between human insulin and AspB10, as previously described by others in in vitro studies (22).

Consistent with the findings of previous studies (19,21), we found increased phosphorylation of Akt in the MVT1 and Met1 tumors from hyperinsulinemic MKR mice after chronic treatment with AspB10 and rhIGF-I. Erk1/2 phosphorylation was not increased after treatment with AspB10 or IGF-I in either Met1 or MVT1 tumors. Previous studies have reported increased Erk1/2 phosphorylation in myoblasts and cardiomyocytes in response to AspB10 (36), and in multiple cell lines in response to rhIGF-I. Our previous studies found no increase in Erk1/2 phosphorylation in MVT1 tumors in the setting of endogenous hyperinsulinemia, and no increase in Erk phosphorylation in response to insulin in vitro (14). Our in vitro studies found that MVT1 cells (expressing the *c-myc/vegf* oncogene) have constitutively active Erk. While Erk phosphorylation is known to lead to increased *c-myc* expression, some recent studies report feedback interactions between *c-myc* and Erk in different cell types, although the mechanism through which this feedback may occur in MVT1 cells has not been elucidated (37–40).

Our previous studies have demonstrated that the MKR mice develop more numerous pulmonary metastases after orthotopic and intravenous tumor cell injection (14). Additionally, rhIGF-I increased metastases from colon cancer orthografts in our previous studies (41).

In this study, the difference in the number of metastases seen after treatment with rhIGF-I or AspB10 showed an

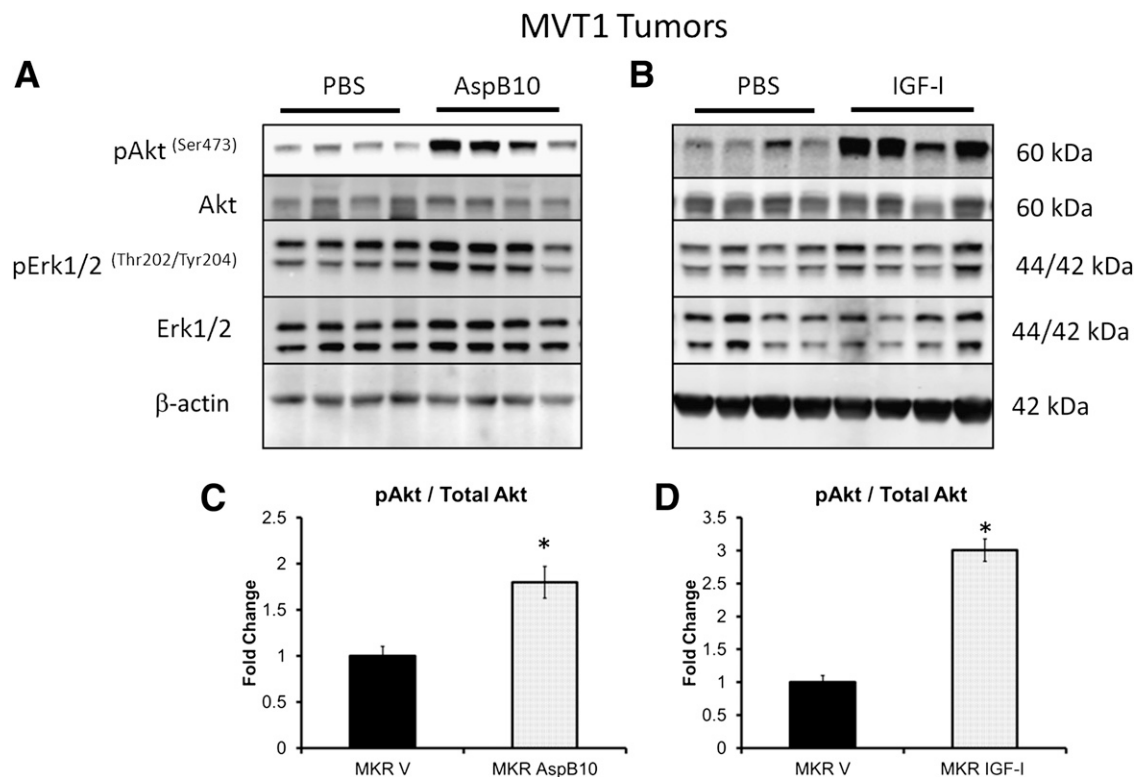


**FIG. 5.** Chronic administration of IGF-I and AspB10 led to increased phosphorylation of Akt, but no change in Erk1/2 phosphorylation. Western blot analysis of MVT1 tumor lysates at the end of the treatment periods with rhIGF-I and AspB10 revealed that rhIGF-I and AspB10 treatment led to increased Akt phosphorylation and no change in Erk1/2 phosphorylation (A–D). Graphs are representative of two studies for AspB10 treatment and three studies for rhIGF-I treatment. All graphs show the mean for each group, and error bars represent the SEM. Statistical analysis was performed using two-tailed *t* test. \**P* < 0.05 between groups. *n* = 9–11 mice per group. p, phosphorylated; MKR V, MKR mice with endogenous hyperinsulinemia.

increase that did not reach statistical significance; however, our study was underpowered to detect a difference in the number of pulmonary metastases.

We did not address the issue of which IR isoform is driving tumor growth in the setting of hyperinsulinemia or AspB10 administration. Two isoforms of the IR exist: IR-A, in which exon 11 is spliced; and IR-B, which contains exon 11 (42). IR-A is preferentially expressed in fetal tissues and certain tumors (42). Different signaling pathways may be activated by insulin stimulation of IR-A and IR-B in different tissue (43–45). Furthermore, activation of IR-A by different ligands (insulin or IGF-II) leads to the differential signaling effects (42). Many breast cancers express higher levels of IR-A than IR-B, and therefore increased binding of insulin to IR-A is hypothesized to drive tumor growth and resistance to chemotherapeutic agents (44,46). It was hypothesized that AspB10 has a higher affinity for IR-A than IR-B, but recent studies demonstrate that AspB10 has a similar affinity for IR-A and IR-B (19). In the same study, in cells expressing the IR-A isoform, AspB10 led to more cell transformation than human insulin (19). Therefore, the transformational effects of AspB10 may be more pronounced in mammary tumors where the IR-A:IR-B ratio is increased. Future *in vivo* studies should establish whether activation of IR-A or IR-B signaling is responsible for increasing tumor growth.

Overall, the MKR mouse has provided us a unique opportunity to study the effects of endogenous hyperinsulinemia on mammary tumor growth in the absence of other confounding factors. The results of our study show that in the setting of endogenous hyperinsulinemia, insulin causes IR, but not IGF-IR, phosphorylation. Our study

demonstrates for the first time, that direct stimulation of the IR, without IGF-IR activation, increases orthotopic mammary tumor growth. Therefore, in women with endogenous hyperinsulinemia, stimulation of the IR in breast tumors may increase tumor growth and metastases. This finding is an important consideration for the development of tailored treatments for women with obesity, T2D, the MetS, or endogenous hyperinsulinemia who develop breast cancer.

#### ACKNOWLEDGMENTS

This research was funded by a grant from Sanofi-Aventis, and supported by American Diabetes Association Grant 1-13-B5-108 to D.L.R. N.T. and U.W. are employees of Sanofi-Aventis. D.L.R. is a consultant for Sanofi. No other potential conflicts of interest relevant to this article were reported.

E.J.G. contributed to experimental design and the writing of the manuscript. N.A. performed the *in vivo* experiments. A.T.-H., J.B., N.J.B., and Z.Z. performed *in vivo* and *in vitro* experiments. N.T. and U.W. contributed to experimental design and writing the manuscript. D.L.R. contributed to experimental design, manuscript writing, and editing. E.J.G. and D.L.R. are the guarantors of this work and, as such, had full access to all the data in the study and take responsibility for the integrity of the data and the accuracy of the data analysis.

#### REFERENCES

1. Calle EE, Rodriguez C, Walker-Thurmond K, Thun MJ. Overweight, obesity, and mortality from cancer in a prospectively studied cohort of U.S. adults. *N Engl J Med* 2003;348:1625–1638

2. Campbell PT, Newton CC, Patel AV, Jacobs EJ, Gapstur SM. Diabetes and cause-specific mortality in a prospective cohort of one million U.S. adults. *Diabetes Care* 2012;35:1835–1844
3. Esposito K, Chiodini P, Colao A, Lenzi A, Giugliano D. Metabolic syndrome and risk of cancer: a systematic review and meta-analysis. *Diabetes Care* 2012;35:2402–2411
4. Lipscombe LL, Goodwin PJ, Zinman B, McLaughlin JR, Hux JE. Increased prevalence of prior breast cancer in women with newly diagnosed diabetes. *Breast Cancer Res Treat* 2006;98:303–309
5. Gunter MJ, Hoover DR, Yu H, et al. Insulin, insulin-like growth factor-I, and risk of breast cancer in postmenopausal women. *J Natl Cancer Inst* 2009;101:48–60
6. Del Giudice ME, Fantus IG, Ezzat S, McKeown-Eyssen G, Page D, Goodwin PJ. Insulin and related factors in premenopausal breast cancer risk. *Breast Cancer Res Treat* 1998;47:111–120
7. Kabat GC, Kim M, Caan BJ, et al. Repeated measures of serum glucose and insulin in relation to postmenopausal breast cancer. *Int J Cancer* 2009;125:2704–2710
8. Goodwin PJ, Ennis M, Pritchard KI, et al. Fasting insulin and outcome in early-stage breast cancer: results of a prospective cohort study. *J Clin Oncol* 2002;20:42–51
9. Novosyadlyy R, Lann DE, Vijayakumar A, et al. Insulin-mediated acceleration of breast cancer development and progression in a nonobese model of type 2 diabetes. *Cancer Res* 2010;70:741–751
10. Rose DP, Vona-Davis L. The cellular and molecular mechanisms by which insulin influences breast cancer risk and progression. *Endocr Relat Cancer* 2012;19:R225–R241
11. Gonullu G, Ersoy C, Ersoy A, et al. Relation between insulin resistance and serum concentrations of IL-6 and TNF-alpha in overweight or obese women with early stage breast cancer. *Cytokine* 2005;31:264–269
12. Law JH, Habibi G, Hu K, et al. Phosphorylated insulin-like growth factor-I/insulin receptor is present in all breast cancer subtypes and is related to poor survival. *Cancer Res* 2008;68:10238–10246
13. Fierz Y, Novosyadlyy R, Vijayakumar A, Yakar S, LeRoith D. Insulin-sensitizing therapy attenuates type 2 diabetes-mediated mammary tumor progression. *Diabetes* 2010;59:686–693
14. Ferguson RD, Novosyadlyy R, Fierz Y, et al. Hyperinsulinemia enhances c-Myc-mediated mammary tumor development and advances metastatic progression to the lung in a mouse model of type 2 diabetes. *Breast Cancer Res* 2012;14:R8
15. Lu S, Lee WM, Archer MC. Insulin does not promote rat mammary carcinogenesis. *Carcinogenesis* 1998;19:699–702
16. Stammberger I, Bube A, Durchfeld-Meyer B, Donaubaue H, Troschau G. Evaluation of the carcinogenic potential of insulin glargine (LANTUS) in rats and mice. *Int J Toxicol* 2002;21:171–179
17. Dideriksen L, Jorgensen L, Drejer K. Carcinogenic effect of the human insulin analogue B10 Asp in female rats (Abstract). *Diabetologia* 1992;35:A3
18. Hansen BF, Kurtzhals P, Jensen AB, Dejgaard A, Russell-Jones D. Insulin X10 revisited: a super-mitogenic insulin analogue. *Diabetologia* 2011;54:2226–2231
19. Sciacca L, Cassarino MF, Genua M, et al. Insulin analogues differently activate insulin receptor isoforms and post-receptor signalling. *Diabetologia* 2010;53:1743–1753
20. Milazzo G, Sciacca L, Papa V, Goldfine ID, Vigneri R. ASPB10 insulin induction of increased mitogenic responses and phenotypic changes in human breast epithelial cells: evidence for enhanced interactions with the insulin-like growth factor-I receptor. *Mol Carcinog* 1997;18:19–25
21. Oleksiewicz MB, Bonnesen C, Hegelund AC, et al. Comparison of intracellular signalling by insulin and the hypermitogenic AspB10 analogue in MCF-7 breast adenocarcinoma cells. *J Appl Toxicol* 2011;31:329–341
22. Kurtzhals P, Schäffer L, Sørensen A, et al. Correlations of receptor binding and metabolic and mitogenic potencies of insulin analogs designed for clinical use. *Diabetes* 2000;49:999–1005
23. Sommerfeld MR, Müller G, Tschank G, et al. In vitro metabolic and mitogenic signaling of insulin glargine and its metabolites. *PLoS One* 2010;5:e9540
24. Glendorf T, Knudsen L, Stidsen CE, et al. Systematic evaluation of the metabolic to mitogenic potency ratio for B10-substituted insulin analogues. *PLoS One* 2012;7:e29198
25. Hamel FG, Siford GL, Fawcett J, Chance RE, Frank BH, Duckworth WC. Differences in the cellular processing of AspB10 human insulin compared with human insulin and LysB28ProB29 human insulin. *Metabolism* 1999;48:611–617
26. Fernández AM, Kim JK, Yakar S, et al. Functional inactivation of the IGF-I and insulin receptors in skeletal muscle causes type 2 diabetes. *Genes Dev* 2001;15:1926–1934
27. Pei XF, Noble MS, Davoli MA, et al. Explant-cell culture of primary mammary tumors from MMTV-c-Myc transgenic mice. *In Vitro Cell Dev Biol Anim* 2004;40:14–21
28. Borowsky AD, Namba R, Young LJ, et al. Syngeneic mouse mammary carcinoma cell lines: two closely related cell lines with divergent metastatic behavior. *Clin Exp Metastasis* 2005;22:47–59
29. Johansson GS, Arnqvist HJ. Insulin and IGF-I action on insulin receptors, IGF-I receptors, and hybrid insulin/IGF-I receptors in vascular smooth muscle cells. *Am J Physiol Endocrinol Metab* 2006;291:E1124–E1130
30. Pandini G, Vigneri R, Costantino A, et al. Insulin and insulin-like growth factor-I (IGF-I) receptor overexpression in breast cancers leads to insulin/IGF-I hybrid receptor overexpression: evidence for a second mechanism of IGF-I signaling. *Clin Cancer Res* 1999;5:1935–1944
31. Osborne CK, Bolan G, Monaco ME, Lippman ME. Hormone responsive human breast cancer in long-term tissue culture: effect of insulin. *Proc Natl Acad Sci USA* 1976;73:4536–4540
32. Zhang H, Fagan DH, Zeng X, Freeman KT, Sachdev D, Yee D. Inhibition of cancer cell proliferation and metastasis by insulin receptor down-regulation. *Oncogene* 2010;29:2517–2527
33. Zhang H, Pelzer AM, Kiang DT, Yee D. Down-regulation of type I insulin-like growth factor receptor increases sensitivity of breast cancer cells to insulin. *Cancer Res* 2007;67:391–397
34. Yee D. Insulin-like growth factor receptor inhibitors: baby or the bathwater? *J Natl Cancer Inst* 2012;104:975–981
35. Völund A, Brange J, Drejer K, et al. In vitro and in vivo potency of insulin analogues designed for clinical use. *Diabet Med* 1991;8:839–847
36. Rakatzi I, Ramrath S, Ledwig D, et al. A novel insulin analog with unique properties: LysB3, GluB29 insulin induces prominent activation of insulin receptor substrate 2, but marginal phosphorylation of insulin receptor substrate 1. *Diabetes* 2003;52:2227–2238
37. Qiao D, Meyer K, Friedl A. Glypican-1 stimulates Skp2 autoinduction loop and G1/S transition in endothelial cells. *J Biol Chem* 2012;287:5898–5909
38. Velpula KK, Dasari VR, Tsung AJ, Dinh DH, Rao JS. Transcriptional repression of Mad-Max complex by human umbilical cord blood stem cells downregulates extracellular signal-regulated kinase in glioblastoma. *Stem Cells Dev* 2012;21:1779–1793
39. Marshall GM, Liu PY, Gherardi S, et al. SIRT1 promotes N-Myc oncogenesis through a positive feedback loop involving the effects of MKP3 and ERK on N-Myc protein stability. *PLoS Genet* 2011;7:e1002135
40. Lin CJ, Cencic R, Mills JR, Robert F, Pelletier J. c-Myc and eIF4F are components of a feedforward loop that links transcription and translation. *Cancer Res* 2008;68:5326–5334
41. Wu Y, Yakar S, Zhao L, Hennighausen L, LeRoith D. Circulating insulin-like growth factor-I levels regulate colon cancer growth and metastasis. *Cancer Res* 2002;62:1030–1035
42. Frasca F, Pandini G, Scalia P, et al. Insulin receptor isoform A, a newly recognized, high-affinity insulin-like growth factor II receptor in fetal and cancer cells. *Mol Cell Biol* 1999;19:3278–3288
43. Sciacca L, Prisco M, Wu A, Belfiore A, Vigneri R, Baserga R. Signaling differences from the A and B isoforms of the insulin receptor (IR) in 32D cells in the presence or absence of IR substrate-1. *Endocrinology* 2003;144:2650–2658
44. Kalla Singh S, Brito C, Tan QW, De León M, De León D. Differential expression and signaling activation of insulin receptor isoforms A and B: a link between breast cancer and diabetes. *Growth Factors* 2011;29:278–289
45. Leibiger B, Leibiger IB, Moede T, et al. Selective insulin signaling through A and B insulin receptors regulates transcription of insulin and glucokinase genes in pancreatic beta cells. *Mol Cell* 2001;7:559–570
46. Harrington SC, Werooha SJ, Reynolds C, Suman VJ, Lingle WL, Haluska P. Quantifying insulin receptor isoform expression in FFPE breast tumors. *Growth Horm IGF Res* 2012;22:108–115

## ORIGINAL ARTICLE

# Inhibiting PI3K reduces mammary tumor growth and induces hyperglycemia in a mouse model of insulin resistance and hyperinsulinemia

EJ Gallagher<sup>1</sup>, Y Fierz<sup>1</sup>, A Vijayakumar, N Haddad, S Yakar and D LeRoith

Division of Endocrinology, Diabetes and Bone Disease, Mount Sinai School of Medicine, New York, NY, USA

Women with type 2 diabetes mellitus (T2DM) are at a greater risk of developing and dying from breast cancer than women without T2DM. Insulin resistance and hyperinsulinemia underlie the pathogenesis of T2DM. In the MKR mouse model of insulin resistance, we have previously shown increased activation of the phosphatidylinositol 3-kinase (PI3K)/Akt/mTOR pathway in association with accelerated mammary tumor growth. In this study, we demonstrate that inhibiting PI3K with the oral pan-class I PI3K inhibitor, NVP-BKM120 reduced the growth of Met-1 and MCNeuA mammary tumor orthografts in the MKR mouse. NVP-BKM120 treatment decreased phosphorylation of Akt and S6 ribosomal protein (S6rp); no change in Erk1/2 phosphorylation was seen. Hyperglycemia, hypertriglyceridemia and greater hyperinsulinemia developed in the MKR mice treated with NVP-BKM120. We previously reported reduced tumor growth using intraperitoneal rapamycin in the MKR mouse, with the development of hyperglycemia and hypertriglyceridemia. Therefore, we examined whether the oral PI3K/mTOR inhibitor NVP-BEZ235 augmented the tumor suppressing effects of PI3K inhibition. We also investigated the effect of targeted PI3K/mTOR inhibition on PI3K/Akt/mTOR and Erk1/2 signaling, and the potential effects on glycemia. NVP-BEZ235 suppressed the growth of Met-1 and MCNeuA tumor orthografts, and decreased Akt and S6rp phosphorylation, despite increased Erk1/2 phosphorylation in Met-1 orthografts of MKR mice. Less marked hyperglycemia and hyperinsulinemia developed with NVP-BEZ235 than NVP-BKM120. Overall, the results of this study demonstrated that inhibiting PI3K/Akt/mTOR signaling with the oral agents NVP-BKM120 and NVP-BEZ235 decreased mammary tumor growth in the hyperinsulinemic MKR mouse. Inhibiting PI3K alone led to more severe metabolic derangement than inhibiting both PI3K and mTOR. Therefore, PI3K may be an important target for the treatment of breast cancer in women with insulin resistance. Monitoring for hyperglycemia and dyslipidemia should be considered when using these agents in humans, given the metabolic changes detected in this study.

Oncogene (2012) 31, 3213–3222; doi:10.1038/onc.2011.495; published online 31 October 2011

**Keywords:** insulin resistance; diabetes; breast cancer; PI3K inhibitor

## Introduction

Women with type 2 diabetes mellitus (T2DM) and the metabolic syndrome (a syndrome of insulin resistance and hyperinsulinemia) are at a greater risk of developing and dying from breast cancer than women without these conditions (Agnoli *et al.*, 2010; Patterson *et al.*, 2010; Peairs *et al.*, 2011). Even in the absence of T2DM or the metabolic syndrome, having a fasting insulin level that lies in the upper quartile of the normal population range has been reported to increase the risk of breast cancer recurrence and death, in women with early stage breast cancer (Goodwin *et al.*, 2002). In human breast cancer, insulin receptor (IR) content is frequently increased (Papa *et al.*, 1990), and therefore in the setting of insulin resistance and hyperinsulinemia, activation of the IR and its downstream signaling pathways may promote breast cancer growth. In our previous studies, we have employed the female MKR mouse to investigate the mechanisms underlying the link between hyperinsulinemia and breast cancer. The female MKR mouse has significant insulin resistance and hyperinsulinemia with mild glucose intolerance (Novosyadlyy *et al.*, 2010). Our previous studies have demonstrated that female MKR mice develop larger mammary tumors than wild type (WT) mice. The IR/insulin-like growth factor-1 receptor/phosphatidylinositol 3-kinase (PI3K)/Akt/mTOR pathway was the main signaling pathway that demonstrated increased activation in tumors from the MKR mice (Novosyadlyy *et al.*, 2010).

The PI3K/Akt/mTOR signaling pathway and its activation by IR $\beta$ /IGF-IR $\beta$  phosphorylation has recently received intense investigation with the emergence of resistance to current chemotherapeutic agents, and the identification of mutations that lead to dysregulation of this pathway (Junttila *et al.*, 2009; Creighton *et al.*, 2010; López-Knowles *et al.*, 2010). PI3K consists of two subunits, a p110 catalytic subunit and its regulatory p85 subunit. After receptor phosphorylation, binding of adaptor proteins, such as insulin receptor substrate-1, to the p85 subunit releases the p110 catalytic subunit from

Correspondence: Professor D LeRoith, Division of Endocrinology, Diabetes and Bone Disease, Mount Sinai School of Medicine, Box 1055, One Gustave L Levy Place, New York, NY 10029, USA. E-mail: Derek.Leroith@mssm.edu

<sup>1</sup>These authors contributed equally to this work.

Received 1 July 2011; revised 1 September 2011; accepted 23 September 2011; published online 31 October 2011

its inhibitory regulation and allows for the phosphorylation of phosphatidylinositol-4,5-bisphosphate to generate phosphatidylinositol-3,4,5-triphosphate. Phosphatidylinositol-3,4,5-triphosphate phosphorylates Akt leading to the activation of a plethora of signaling molecules. Multiple gene mutations can increase signaling through the PI3K/Akt/mTOR pathway in breast cancers, for example, loss of activity of the tumor suppressor gene phosphatase and tensin homolog deleted on chromosome ten, amino-acid substitutions in PI3KCA (encoding the p110 $\alpha$  catalytic subunit of PI3K), overexpression of human epidermal growth factor receptor-2 (HER-2) and mutations in Akt. In cell lines, increased PI3K signaling has been shown to confer resistance to the monoclonal antibody trastuzumab that is directed against HER-2, and is used to treat HER-2 receptor-positive breast cancers in women (O'Brien *et al.*, 2010). Additionally, in estrogen receptor (ER)-positive breast cancer cells, PI3K activity is associated with decreased expression of ER and ER target genes. This decreased ER expression in ER-positive tumors is associated with resistance to hormonal therapy (Creighton *et al.*, 2010). Therefore, insulin resistance and endogenous hyperinsulinemia, leading to increased activation of the PI3K signaling pathway, may result in resistance to HER-2 and ER targeted therapy, and so may be an important therapeutic target in individuals with breast cancer who have increased insulin levels, the metabolic syndrome or T2DM.

However, two particular concerns have arisen with regard to inhibiting the PI3K/Akt/mTOR pathway. First, that inhibition of PI3K signaling in HER-2-overexpressing tumors will lead to a compensatory increase in Erk1/2 signaling, as was recently described with the PI3K inhibitors, GDC-0941 and PIK-90 in cell lines and the dual PI3K/mTOR inhibitor, BEZ235 in xenografts inoculated into mice (Serra *et al.*, 2011). Second, that inhibiting PI3K may result in significant hyperglycemia. We have previously demonstrated that inhibiting mTOR with rapamycin led to increased glucose and triglyceride levels in MKR mice, but did not lead to a further increase in the already elevated plasma insulin levels and did not affect Ser<sup>473</sup> phosphorylation of Akt in tumors (Fierz *et al.*, 2010). PI3K inhibition would be expected to lead to different metabolic effects than rapamycin because of the effects of PI3K inhibition on the phosphorylation of Akt and on atypical isoforms of protein kinase C  $\zeta$ . Both Akt and atypical isoforms of protein kinase C  $\zeta$  are important for insulin-mediated glucose uptake in muscle and adipose tissue by glucose transporter 4 (GLUT4) (Kohn *et al.*, 1996; Liu *et al.*, 2006).

Therefore, we aimed to examine the effect of inhibiting PI3K on tumor progression and metabolic parameters in a mouse model of hyperinsulinemia. In this study we inhibited PI3K with the oral pan-class I inhibitor of PI3K, NVP-BKM120, and evaluated the growth of mammary tumor orthografts in the hyperinsulinemic MKR mouse. We examined the PI3K/Akt/mTOR signaling pathway to determine whether this inhibitor could adequately block signaling in tumors

from the MKR mouse, where the activity of this pathway is known to be increased. We also studied the phosphorylation of Erk1/2 to determine whether inhibition of PI3K led to a compensatory increase in Erk1/2 signaling in the MKR mouse. Additionally, we examined the effects of inhibiting PI3K on metabolic parameters, including glucose, insulin and triglyceride levels. Finally, in view of our previous study demonstrating that inhibiting mTOR with rapamycin led to hyperglycemia in the MKR mouse, but reduced tumor growth (Fierz *et al.*, 2010), we were interested to know whether inhibiting both PI3K and mTOR with the targeted dual inhibitor, NVP-BEZ235 would lead to an additional suppression of tumor growth, and whether it would affect insulin and glucose levels in the MKR mouse. We also aimed to discover whether the dual PI3K/mTOR inhibitor would lead to a compensatory increase in Erk1/2 signaling in this model, similar to the results from animal models without insulin resistance (Serra *et al.*, 2011).

## Results

### *Inhibiting PI3K reduces tumor growth in the MKR mouse*

The MKR mouse is a nonobese animal model of type 2 diabetes. The female MKR mouse has marked hyperinsulinemia, but only mild dysglycemia. We have previously demonstrated that after orthotopic inoculation of Met-1 and MCNeuA cells into the fourth mammary fat pad, MKR mice develop larger tumors than WT mice (Novosyadlyy *et al.*, 2010). Met-1 mammary tumor cells were initially derived from MMTV-Polyoma Virus middle T antigen transgenic mice (Borowsky *et al.*, 2005) and MCNeuA mammary tumor cells were derived from MMTV-Neu transgenic mice, the rodent equivalent of the human ErbB2 or HER-2 gene (Campbell *et al.*, 2002). Met-1 cells have a high proliferation rate and have a mesenchymal phenotype. MCNeuA cells have an epithelial phenotype and have a low proliferation rate.

We orthotopically inoculated MKR mice and WT mice with Met-1 and MCNeuA cells, as previously described (Novosyadlyy *et al.*, 2010). Cells were injected 1 week apart, to allow for the lower proliferation rate of the MCNeuA cells. At 2 weeks after injection of the Met-1 cells and 3 weeks after injection of MCNeuA cells, the MKR and WT mice were divided into two treatment groups that were matched for respective tumor size (Figures 1a and c). Mice were treated with NVP-BKM120 (50 mg/kg) by oral gavage, or the same volume of the vehicle. Treatment continued for 2 weeks with interval measurement of tumor growth over that time and measurement of tumor weight at the end of the study. The volumes of both Met-1 and MCNeuA tumors were significantly lower in the MKR mice treated with NVP-BKM120, compared with the MKR vehicle-treated group (Figures 1a and c). Similarly, the weights of MCNeuA and Met-1 tumors were significantly reduced in the MKR group treated with



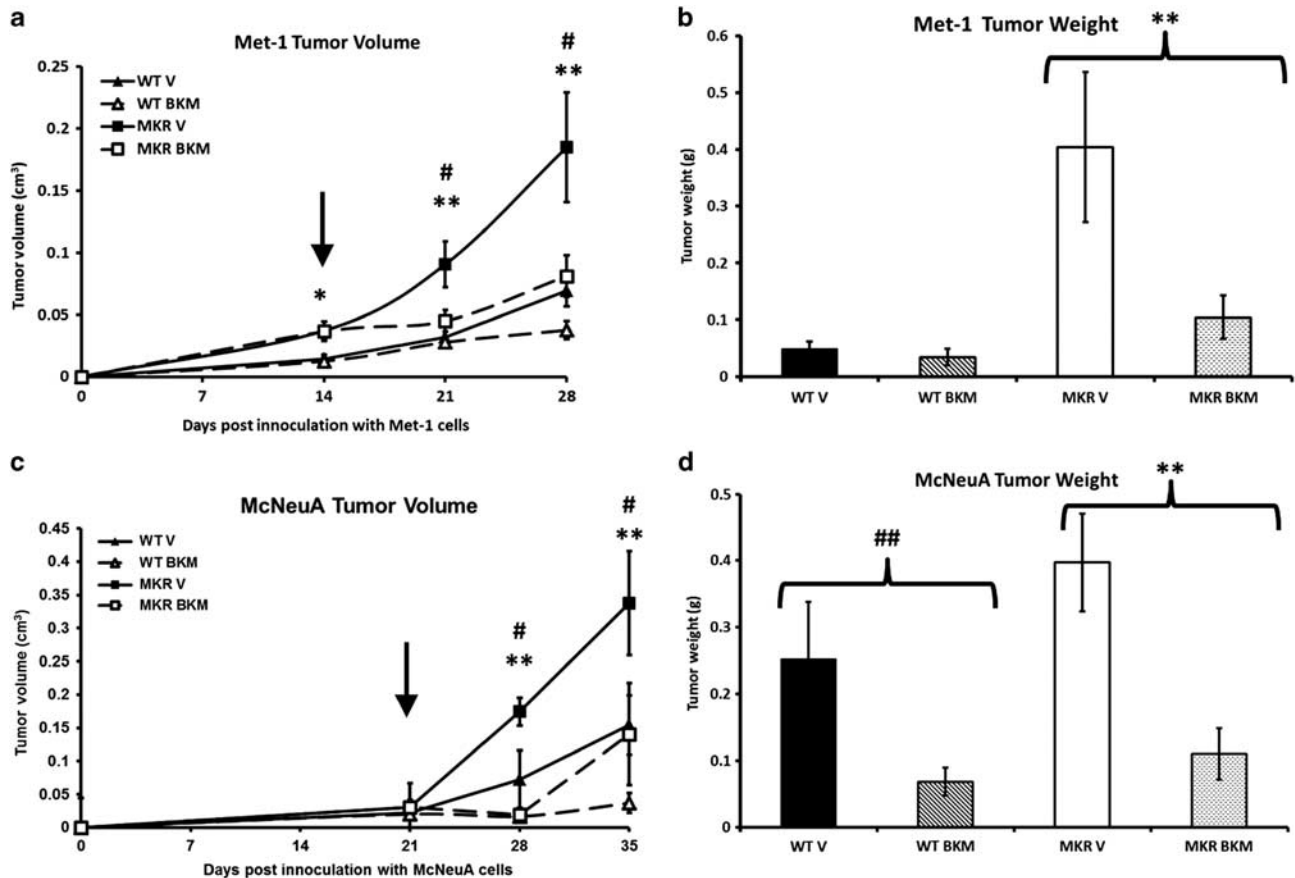


**Figure 1** Treatment with NVP-BKM120 reduced the accelerated tumor growth in the MKR mice. (a, c): Met-1 cells ( $0.5 \times 10^6$ ) and MCNeuA cells ( $1 \times 10^6$ ) were injected into the fourth mammary fat pad of 8–10-weeks old virgin WT and MKR mice on day 0. Treatment with NVP-BKM120 (BKM) or vehicle (V) began 2 weeks after Met-1 cell injection and 3 weeks after MCNeuA cell injection (arrows). Tumor volume was measured during the 2 weeks of treatment with NVP-BKM120 or vehicle. (b, d): Tumor weight was measured at necropsy. All data are expressed as mean  $\pm$  s.e.m. \* $P < 0.05$  between WT and MKR groups. \*\* $P < 0.05$  between MKR NVP-BKM120 and MKR vehicle groups. # $P < 0.05$  between the MKR vehicle group and the WT vehicle group. ## $P < 0.05$  between the WT NVP-BKM120 and WT vehicle-treated groups.  $n = 8$ –9 mice per group.

NVP-BKM120, and the MCNeuA tumor weights were also significantly reduced in the WT group (Figures 1b and d). Therefore, in the insulin resistant, hyperinsulinemic mouse, inhibiting PI3K with NVP-BKM120 decreases the growth of mammary tumors known to have increased activation of the PI3K/Akt/mTOR signaling pathway.

#### Blocking PI3K signaling with NVP-BKM120 reduces tumor growth by inhibition of Akt signaling in the MKR mouse

Our previous studies have demonstrated an increase in phosphorylation of  $\text{IR}\beta^{\text{(Tyr1150/1151)}}$ /IGF- $\text{IR}\beta^{\text{(Tyr1135/1136)}}$  and  $\text{Akt}^{\text{(Ser473)}}$  in Met-1 and MCNeuA tumors inoculated into MKR mice, compared with those injected into WT FVB/N mice (Novosyadlyy et al., 2010). No change was seen in phosphorylation of  $\text{Akt}^{\text{(Ser473)}}$  in response to treatment with the mTOR inhibitor rapamycin (Fierz et al., 2010). In this study, we again observed a statistically significant increase in  $\text{Akt}^{\text{(Ser473)}}$  phosphorylation in the MKR vehicle-treated group compared with the WT vehicle-treated groups (Figures 2a and b,

this difference is not marked with an asterisk on the densitometry 2C and 2E). Inhibiting PI3K resulted in decreased phosphorylation of  $\text{Akt}^{\text{(Ser473)}}$  in both WT and MKR mice, along with decreased phosphorylation of S6 ribosomal protein ( $\text{S6rp}^{\text{(Ser235/236)}}$ ) (Figures 2a–f). No change in  $\text{Erk1/2}^{\text{(Thr202/204)}}$  phosphorylation was seen in either WT or MKR mice treated with NVP-BKM120 (Figures 2g–j). Overall, NVP-BKM120 successfully reduces phosphorylation of Akt and S6rp in tumors from the MKR mouse that is known to have increased activation of Akt signaling. No change in Erk1/2 signaling was seen after treatment with NVP-BKM120 in either cell type in MKR or WT mice.

#### Inhibiting PI3K led to reduced proliferation in Met-1 tumor orthografts in MKR mice

We have previously demonstrated increased proliferation in the Met-1 tumors in MKR mice by evaluation of protein extracts for proliferating cell nuclear antigen on western blot (Fierz et al., 2010). To examine whether this increase in S phase growth was inhibited with NVP-BKM120, the mice were injected with 5-bromo-2'-

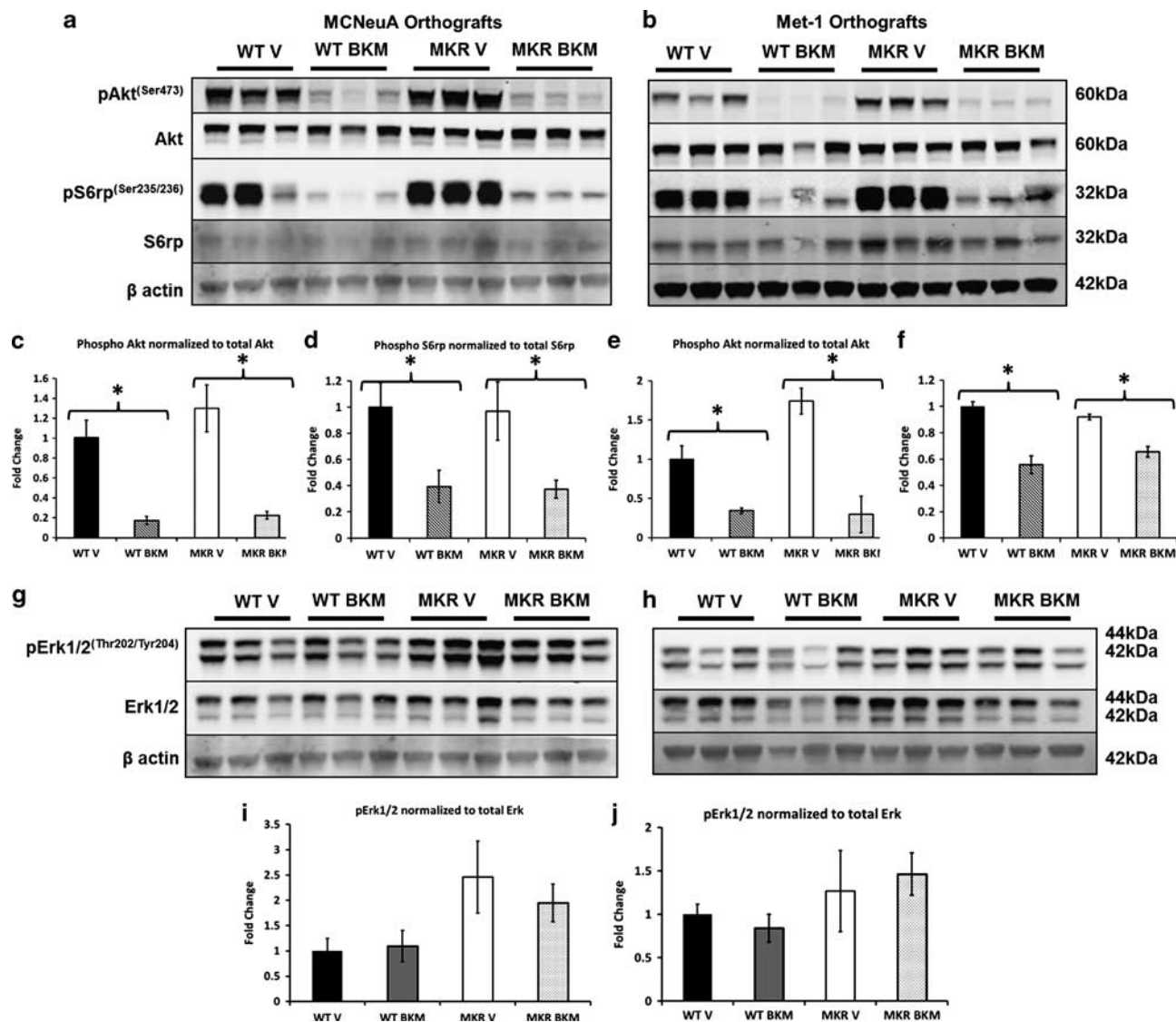


**Figure 2** Treatment with NVP-BKM120 reduced serine phosphorylation of Akt and S6rp in MCNeuA and Met-1 tumors treated with NVP-BKM120. Protein extracts from MCNeuA and Met-1 tumors from WT and MKR mice were size fractionated and immunoblotted against phospho<sup>(Ser473)</sup> and total Akt, phospho<sup>(Ser235/236)</sup> and total S6rp, and phospho<sup>(Thr202/Tyr204)</sup> and total Erk1/2 (**a, b, g, h**). Representative western blot analyses are displayed for MCNeuA tumors (**a, g**) and Met-1 tumors (**b, h**). **c–f, i, j** display the densitometric analyses of phosphorylated Akt normalized to total Akt, phosphorylated S6rp normalized to total S6rp levels and phosphorylated Erk1/2 normalized to total Erk1/2 for MCNeuA and Met-1 tumors. Data in (**c–f, i, j**) are presented as a fold change in the mean ( $\pm$  s.e.m.) of each group compared with the WT vehicle-treated group. \* $P < 0.05$  between groups. BKM, NVP-BKM120 treated; V, vehicle treated.

deoxyuridine (BrdU) 2 h before tumor tissue collection. The percent of cells that stained positive for BrdU in the Met-1 tumors was evaluated by immunofluorescence. We found a significantly higher percent of BrdU-positive cells in the vehicle-treated MKR mice ( $9.9 \pm 0.76\%$ ), compared with vehicle-treated WT mice ( $7.8 \pm 0.35\%$ ) (Figure 3a). Treatment of the MKR mice with NVP-BKM120 led to a significantly lower percent of BrdU-positive cells ( $5.8 \pm 1.13\%$ ), compared with vehicle-treated MKR mice ( $P = 0.001$ ). The percent of BrdU-positive cells in the Met-1 tumors from the MKR mice treated with NVP-BKM120 was comparable to the percent of BrdU-positive cells in the WT NVP-BKM120-treated group ( $5.8 \pm 0.63\%$ ).

Therefore, in the MKR mice, inhibiting PI3K with NVP-BKM120 attenuated the increased cellular proliferation in Met-1 tumors from the MKR mice (Figure 3b). Western blot analysis of apoptosis, using the antibody to the anti-apoptotic protein Bcl-2 revealed decreased levels of Bcl-2 when normalized to  $\beta$  actin, in the MKR vehicle-treated group, compared with the MKR NVP-BKM120-treated group (data not shown).

#### Mice treated with NVP-BKM120 developed metabolic derangements

Before treatment, MKR mice had mildly elevated blood glucose levels ( $10.6 \pm 0.5$  mmol/l), compared with WT mice

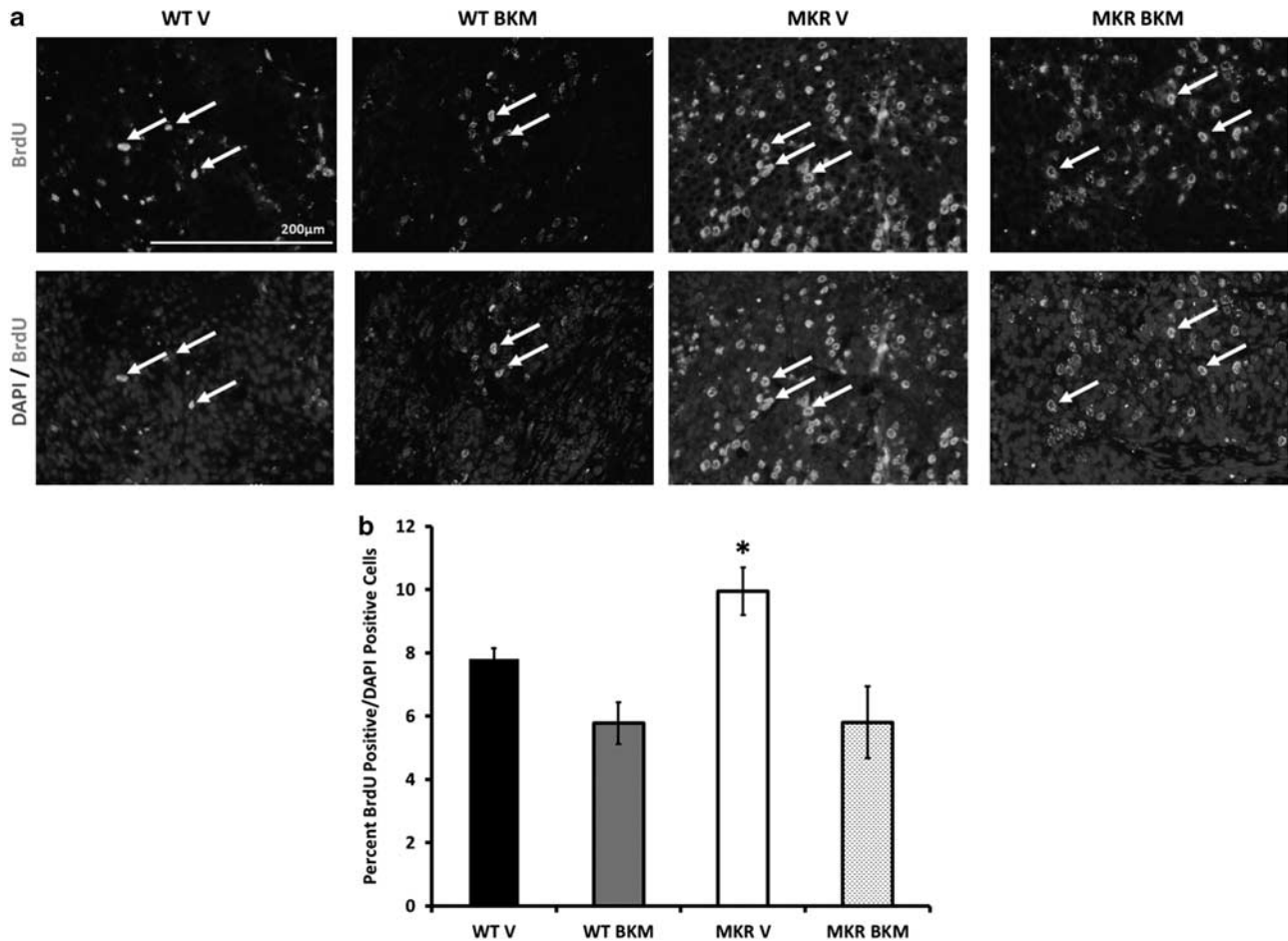


**Figure 3** NVP-BKM120 reduces the increased proliferation of Met-1 cell orthografts in MKR mice. Assessment of proliferation of Met-1 orthografts by BrdU incorporation, after intraperitoneal injection of BrdU (10  $\mu$ l/g body weight) and detection by immunofluorescence (mouse monoclonal antibody against BrdU, secondary antibody AlexaFluor 488-conjugated goat anti-mouse IgG (green) and nuclear counterstaining with DAPI (blue)). (a): Representative 40  $\times$  objective images of BrdU-positive Met-1 tumors (top row) and composite images of DAPI- and BrdU-positive Met-1 tumors (bottom row). White arrows point to BrdU-positive cells. (b): Quantitative analysis representing the percent of BrdU-positive cells to total number of DAPI-positive cells, expressed as means  $\pm$  s.e.m. \* $P$  < 0.05 between MKR vehicle-treated group and all other groups ( $n$  = 2–3 mice per group, with six 40  $\times$  fields per mouse). BKM, NVP-BKM120 treated; V, vehicle treated. A full colour version of this figure is available at the *Oncogene* journal online.

(7.2  $\pm$  0.2 mmol/l) (Figure 4a). Following 2 weeks of treatment, significant hyperglycemia developed in the WT and MKR groups treated with NVP-BKM120 (Figure 4), and was demonstrated during the glucose tolerance test (Figure 4b). Plasma insulin levels revealed that WT and MKR mice treated with NVP-BKM120 had significant hyperinsulinemia, compared with the vehicle-treated mice, with the levels for the WT mice increasing at an  $\sim$ seven fold and for MKR mice rising > ten fold (Figure 4c). Triglyceride levels also increased in the MKR mice treated with NVP-BKM120 to a modest (1.5-fold increase) but significant degree, although no increase was seen in the WT mice (Figure 4d).

#### Comparison of PI3K inhibition alone with the PI3K and mTOR dual inhibitor NVP-BEZ235

We were interested to discover the effects of inhibiting both PI3K and mTOR on the tumor growth and glucose control in the MKR mice. Our previous studies had

demonstrated that the mTOR inhibitor rapamycin reduced tumor growth, but increased glucose levels in the MKR mice, whereas our current study demonstrated that inhibiting PI3K with NVP-BKM120 also reduced tumor growth, but led to more severe hyperglycemia and hyperinsulinemia than rapamycin. We therefore speculated that inhibiting both PI3K and mTOR could have a synergistic effect on the reduction in tumor growth. Analogous to the study with NVP-BKM120, we inoculated the fourth mammary fat pad of WT and MKR mice with Met-1 and MCNeuA cells, and divided them into treatment groups, with the dual PI3K/mTOR inhibitor NVP-BEZ235 (40 mg tosylate salt/kg body weight) or the vehicle (10% NMP: 90% PEG300), by daily gavage for 2 weeks. Before treatment began, the groups were matched for tumor size, and serial measurements were taken during the study to calculate the tumor volume. At the end of the study tumor weights were also recorded. Proteins from the MCNeuA and Met-1 tumors were isolated, as previously described



and again phosphorylation of the Akt, S6rp and Erk1/2 were examined relative to their total protein levels.

The volumes of both MCNeuA and Met-1 tumors were again significantly decreased in the MKR mice treated with the dual PI3K/mTOR inhibitor NVP-BEZ235 (Figures 5a and b); tumor weight was not significantly different in the treatment groups, as there was a wide distribution in the tumor weights because of variable areas of necrosis (Figures 5c and d). Analysis of tumor proteins revealed a significant decrease in phosphorylation of Akt and S6rp in the MKR and WT NVP-BEZ235-treated group, compared with the vehicle-treated groups (Figures 5e–g and i). In contrast to the PI3K inhibitor NVP-BKM120, an increased Erk1/2 phosphorylation was seen in the Met-1

tumors from MKR mice treated with NVP-BEZ235, when compared with those treated with the vehicle (Figure 5j). Glucose intolerance and hyperinsulinemia developed in the MKR mice treated with NVP-BEZ235 (Figures 6a and b), but the degree of glucose intolerance and hyperinsulinemia was not as great as with NVP-BKM120 treatment. No significant hyperinsulinemia developed in the WT group treated with NVP-BEZ235, compared with controls (Figure 6b).

## Discussion

Our results demonstrate that in the MKR mouse model of insulin resistance, inhibiting PI3K with NVP-

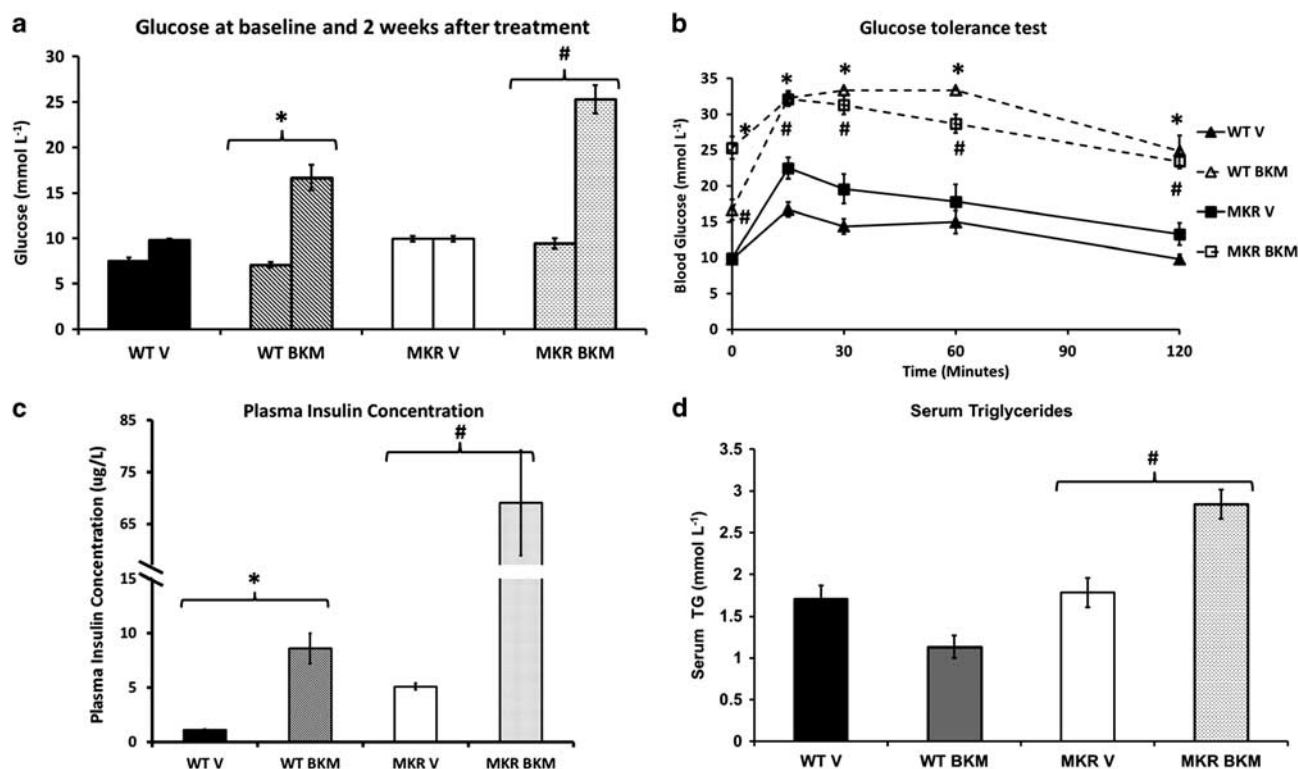
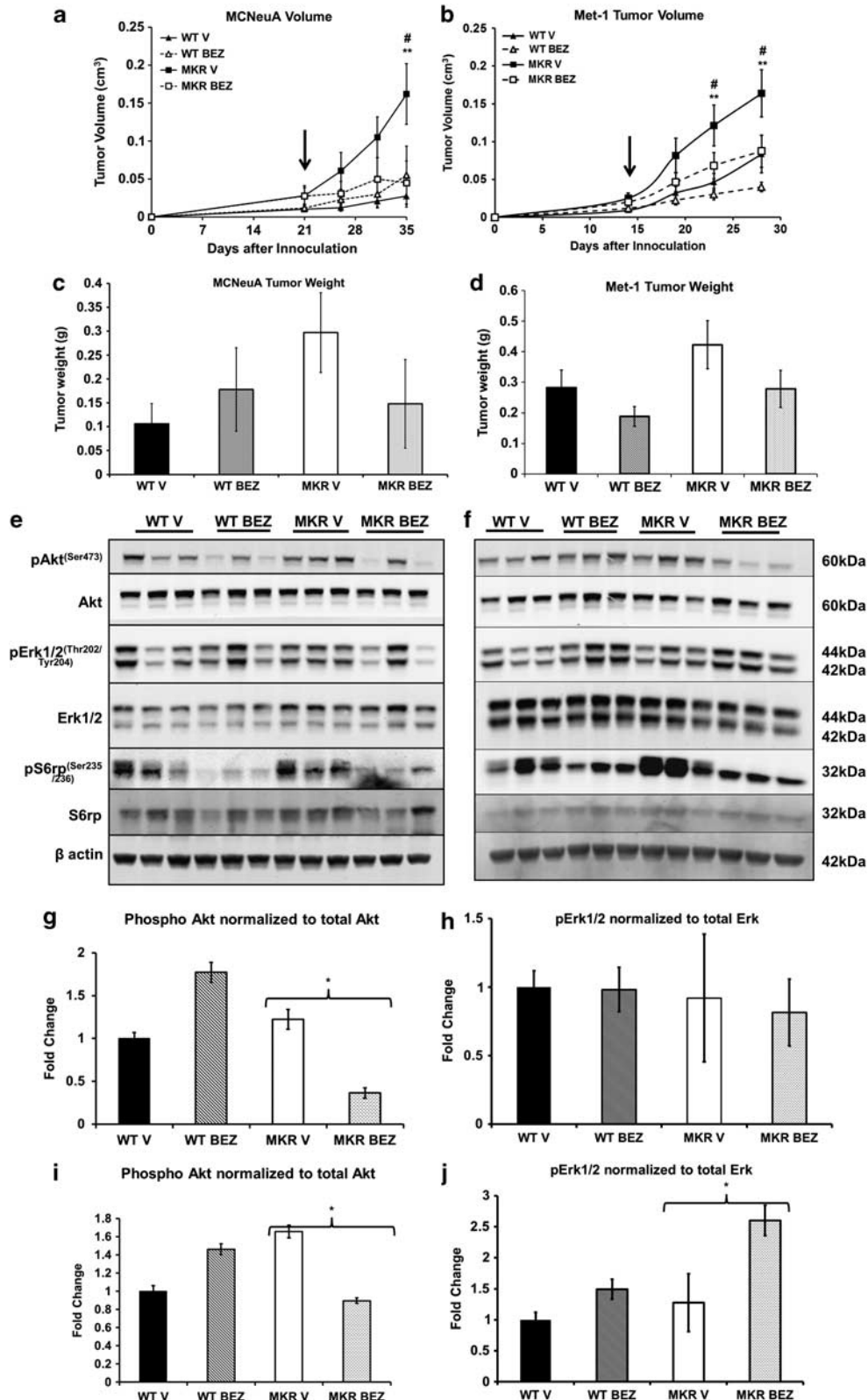


**Figure 4** NVP-BKM120 treatment led to hyperglycemia, hypertriglyceridemia and exacerbated hyperinsulinemia in MKR mice. (a): Mean random glucose levels at the start of treatment with NVP-BKM120 or vehicle and after 2 weeks of treatment. (b): Results of the 1.5 g/kg glucose tolerance test. Glucose was injected at time 0 and glucose measurements were taken at 0, 15, 30, 60 and 120 min. (c): Plasma insulin concentrations of the WT and MKR mice after 2 weeks of treatment with NVP-BKM120 or vehicle. The y-axis is broken at the parallel lines and the bar for the MKR BKM group is broken at the same point to aid visualization of the WT groups. (d): Serum triglyceride concentration in WT and MKR mice after 2 weeks of treatment with NVP-BKM120 or vehicle. All data are presented as the mean  $\pm$  s.e.m., \* $P < 0.05$  between the WT NVP-BKM120 treated mice and WT vehicle group. # $P < 0.05$  between MKR NVP-BKM120-treated mice and MKR vehicle-treated group. BKM, NVP-BKM120 treated; TG, serum triglyceride; V, vehicle treated.

**Figure 5** NVP-BEZ235 treatment reduced tumor volume in the MKR treated group, and decreased Akt<sup>(Ser473)</sup> and S6rp<sup>(Ser235/236)</sup> phosphorylation. (a, b): MCNeuA cells and Met-1 cells were injected into the fourth mammary fat pad as outlined in the methods section and Figure 1. NVP-BEZ235 (BEZ) and vehicle (V) treatment began 2 weeks after Met-1 injection and 3 weeks after MCNeuA injection (arrows). (a, b): Tumor volumes were measured during the 2 weeks of treatment. \* $P \leq 0.05$  between MKR NVP-BEZ235 and vehicle treated groups. \*\* $P < 0.05$  between MKR NVP-BKM120 and MKR vehicle groups. No.  $P < 0.05$  between MKR vehicle group and WT vehicle group. ## $P < 0.05$  between WT NVP-BKM120 and WT vehicle treated group. (c, d) Tumor weight was measured at the end of the study. (e, f) Representative western blots demonstrating protein extracts from MCNeuA and Met-1 tumors from WT and MKR mice treated with V and BEZ. (g–i): Densitometric analysis for MCNeuA and Met-1 tumors of the relative phosphorylation of Akt to total Akt and phosphorylation of Erk1/2 to total Erk1/2. Results are displayed as mean  $\pm$  s.e.m. and are presented as a fold change compared with the WT vehicle treated group. \* $P < 0.05$  between groups.

BKM120 decreased the growth of tumor orthografts known to have increased activation of the PI3K/Akt/mTOR pathway in the hyperinsulinemic mouse. In the MKR mouse, inhibiting PI3K alone reduced Akt

phosphorylation and did not lead to a compensatory increase in Erk1/2 signaling. In contrast to our study of rapamycin, inhibiting both PI3K and mTOR led to a reduction in Akt phosphorylation as well as a decrease



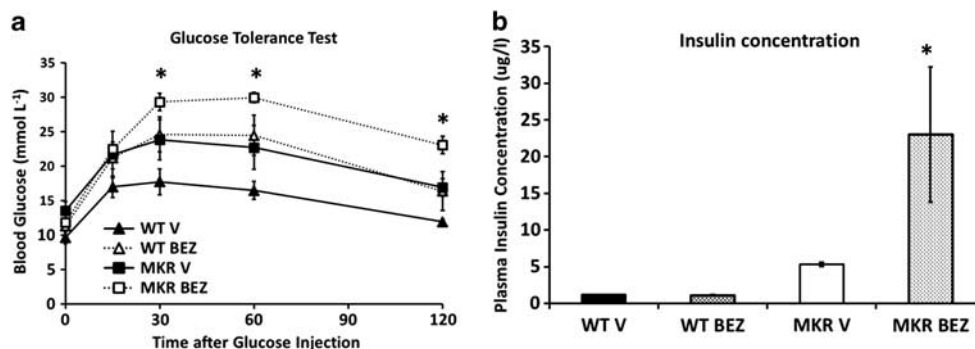


**Figure 6** Metabolic investigations demonstrated worsening glucose tolerance and hyperinsulinemia in the MKR mice treated with NVP-BEZ235. (a): Results of the 1.5 g/kg glucose tolerance test. Glucose was injected at time 0 and glucose measurements were taken at 0, 15, 30, 60 and 120 min. \* $P < 0.05$  between glucose levels of the MKR NVP-BEZ235 treated mice compared with MKR vehicle treated group. (b): Plasma insulin concentrations of the WT and MKR mice after 2 weeks of treatment with NVP-BEZ235 or vehicle. \* $P < 0.05$  between the MKR NVP-BEZ235 treated mice and MKR vehicle treated group and WT groups. Results are expressed as mean  $\pm$  s.e.m. V, vehicle treated, BEZ, NVP-BEZ235 treated.

in S6rp phosphorylation; however, increased activation of Erk1/2 signaling in Met-1 tumors from the MKR mouse treated with NVP-BEZ235 was seen. These results are partially consistent with the findings of other groups who reported that inhibition of PI3K alone (with GDC-0941 and PIK90), or in combination with mTOR (NVP-BEZ235) led to a compensatory increase in Erk1/2 signaling in tumor xenografts (Serra *et al.*, 2011). Notably, the PI3K inhibitors used were different as were the cell lines and animal models, all of which could account for different findings regarding Erk1/2 phosphorylation.

Other studies, in addition to ours, have reported that inhibiting PI3K results in no change, or in some cases, a reduction in Erk1/2 signaling (Wells *et al.*, 2007). As well as differences in cellular characteristics, different pharmacological agents possess varying activity against the different class 1A p110 isoforms of PI3K. Although in breast cancer, the PI3KCA gene that encodes for the p110 $\alpha$  is the most commonly mutated of the three class 1A isoforms (p110 $\alpha$ , p110 $\beta$  and p110 $\delta$ ), evidence from other cell lines show that inhibiting two of these three isoforms is insufficient to inhibit cell proliferation and survival (Foukas *et al.*, 2010). Therefore, PI3K inhibitors that preferentially target p110 $\alpha$  (GDC-0941 and PIK90) may not be as effective at preventing cellular proliferation and cell cycle progression as pan class 1A inhibitors, such as NVP-BKM120 and XL147.

The more pronounced glucose and insulin derangements in the WT and MKR mice treated with the PI3K inhibitor NVP-BKM120, may be the result of more pronounced PI3K and Akt inhibition with this compound than with the dual PI3K/mTOR inhibitor NVP-BEZ235. Our protein analysis demonstrated that the inhibition of Akt phosphorylation with NVP-BEZ235 was less marked than with the PI3K inhibitor NVP-BKM120. Similar findings regarding Akt phosphorylation have previously been reported, and other studies have demonstrated an increase in Akt phosphorylation at lower doses of NVP-BEZ235 (Serra *et al.*, 2008, 2011). At low concentrations, NVP-BEZ235 predominantly inhibits mTORC1 activity, whereas at

higher concentrations it inhibits PI3K and mTORC1/2. Therefore, in our study, the disproportionately greater suppression of S6rp phosphorylation, compared with Akt phosphorylation in NVP-BEZ235-treated tumors, may be the result of the different inhibitory concentration of NVP-BEZ235 on mTOR and Akt.

Insulin signaling is important for glucose uptake into skeletal muscle and adipose tissue by the glucose transporter GLUT4. Previous studies have demonstrated that inhibiting PI3K with wortmannin and LY294002 prevents the translocation of GLUT4 to the cell surface and glucose uptake into cells. Akt and atypical protein kinase C  $\zeta$  are important downstream targets of PI3K that mediate this glucose uptake (Liu *et al.*, 2006). Inhibitors of Akt have also been reported to cause hyperglycemia by GLUT4-dependent and independent mechanisms (Tan *et al.*, 2010). Only very low levels of Akt appear to be necessary to maintain GLUT4 function in certain cells, suggesting alternative unknown mechanisms are also in play (Tan *et al.*, 2010). The difference in Akt inhibition between NVP-BKM120 compared with NVP-BEZ235 may partly explain the more dramatic hyperglycemia that was observed with NVP-BKM120. Some studies using PI3K inhibitors have not reported dramatic hyperglycemia, an affect that may be related to the p110 isoform of PI3K that is inhibited: a pan class 1A inhibitor may lead to more severe glucose derangement than a selective p110 $\alpha$  inhibitor, although the roles that the different p110 isoforms play in the metabolic effects of insulin remain to be determined (Jia *et al.*, 2008; Sopasakis *et al.*, 2010).

In addition to more severe hyperglycemia, we noted more dramatic hyperinsulinemia with the PI3K inhibitor compared with the dual PI3K/mTOR inhibitor, which caused greater hyperinsulinemia than rapamycin (Fierz *et al.*, 2010). Inhibition of PI3K and Akt will directly lead to insulin resistance by preventing signal transduction through this pathway. Inhibiting mTOR in addition to PI3K may in fact improve insulin sensitivity, as the mTOR/S6 Kinase pathway causes serine phosphorylation of insulin receptor substrate-1, which

attenuates signaling. Therefore, inhibiting mTOR/S6 Kinase activity may reduce some of the insulin resistance caused by PI3K inhibition by relieving the inhibition of serine phosphorylation of insulin receptor substrate-1, allowing tyrosine phosphorylation of insulin receptor substrate-1 and activation of the insulin signaling pathway (Um *et al.*, 2006).

In conclusion, our study demonstrates that PI3K inhibitors reduce tumor growth in an animal model of insulin resistance and hyperinsulinemia. These results may be particularly relevant in individuals with insulin resistance, the metabolic syndrome and T2DM, who may have dysregulation of the PI3K pathway in breast cancer, as demonstrated in our mouse model. In our model, we demonstrate that with pan class 1 PI3K inhibition, there is no increase in activation of Erk1/2 signaling. Our data demonstrates a similar reduction in tumor growth with the dual PI3K/mTOR inhibitor and PI3K inhibition alone. However, dual inhibition of PI3K and mTOR importantly led to less severe hyperglycemia and hyperinsulinemia, which may be due to either less potent inhibition of Akt by NVP-BEZ235 or due to a reduction in insulin resistance by inhibiting mTOR. Based on the results of our study and other similar studies, many questions regarding the role of PI3K in tumor growth and metabolism have emerged. Future studies are needed to address the roles of hyperinsulinemia and diabetes in breast cancer mortality in women (Peairs *et al.*, 2011). Understanding more about the specific p110 isoforms in tumor growth and metabolism is necessary so that targeted therapy can lead to maximal tumor inhibition with minimal adverse metabolic consequences. This is particularly important as the PI3K/Akt/mTOR signaling pathway may be an important target in hyperinsulinemic women with breast cancer.

## Materials and methods

### Animals

The mice used in this study were all on the FVB/N background. WT FVB/N mice and MKR mice that have been characterized previously were used (Fernandez *et al.*, 2001; Novosyadlyy *et al.*, 2010). The mice were kept on a 12-h light/dark cycle, had free access to a standard mouse chow (Picolab rodent diet 5053; LabDiet, St Louis, MO, USA) and fresh water *ad libitum*. The Mount Sinai School of Medicine AAALAC-accredited animal facility provided animal care and maintenance.

### Orthotopic tumor models

Met-1 mammary tumor cells were initially derived from MMTV-Polyoma Virus middle T antigen (FVB/N) transgenic mice (Borowsky *et al.*, 2005), and MCNeuA mammary tumor cells were derived from MMTV-Neu (FVB/N) transgenic mice, the rodent equivalent of the human ERBB2 gene (Campbell *et al.*, 2002). Cell culture, preparation and injection were performed as described previously (Fierz *et al.*, 2010; Novosyadlyy *et al.*, 2010). Tumor cells were inoculated into the fourth mammary fat pad of 8–10-week-old female virgin homozygous MKR and WT FVB/N mice. Two weeks after

Met-1 cell and 3 weeks after MCNeuA cell inoculation, tumors were matched according to size between groups, and mice were treated with either the pan-class I PI3K inhibitor NVP-BKM120 (50 mg/kg body weight per day by oral gavage) dissolved in 1-methyl-2-pyrrolidone (NMP, Sigma-Aldrich, St Louis, MO, USA) and PEG300 (Sigma-Aldrich) to a ratio of 10% NMP: 90% PEG300, or the vehicle (10% NMP: 90% PEG 300). Similarly, treatment with the dual PI3K and mTOR inhibitor, NVP-BEZ235 (40 mg tosylate salt/kg body weight per day by oral gavage) dissolved in NMP and mixed in PEG300 (10% NMP: 90% PEG300) or vehicle (10% NMP: 90% PEG300), began 2 and 3 weeks after Met-1 and MCNeuA inoculation, respectively. Treatment continued in all groups for 14 days. Before and during treatment, tumor growth was measured in three dimensions (cranio-caudal, transverse and antero-posterior) using calipers. Tumor volume was calculated by the formula:  $\frac{4}{3} \times \pi \times r_1 \times r_2 \times r_3$  ( $r$  = radius). At the end of the study, mice were sacrificed, and tumors were removed and weighed. NVP-BKM120 and NVP-BEZ235 were obtained free of charge through material transfer agreements with Novartis Pharma (Basel, Switzerland).

### Protein extraction and western blot analysis

Protein extraction and western blot analysis were performed as previously described (Fierz *et al.*, 2010; Novosyadlyy *et al.*, 2010). Phospho<sup>(Ser235/236)</sup> and total S6rp, phospho<sup>(Ser473)</sup> and total Akt, phospho<sup>(Thr202/Tyr204)</sup> and total p44/42 MAPK (Erk1/2) and Bcl-2 were purchased from Cell Signaling Technology (Danvers, MA, USA). The anti- $\beta$ -actin antibody was purchased from Sigma-Aldrich. Densitometric analysis was performed using ImageJ V1.44 software (National Institutes of Health, Bethesda, MD, USA).

### Immunofluorescence

To quantify BrdU incorporation (as detected by immunofluorescence), MKR and WT FVB/N mice were injected intraperitoneally with BrdU (Sigma-Aldrich) at 10  $\mu$ l/g of body weight, 2 h before killing of mice. Glands were fixed in 4% paraformaldehyde and embedded in paraffin. Sections were deparaffinized, rehydrated and subjected to antigen retrieval, as previously described (Cannata *et al.*, 2010). A mouse monoclonal antibody against BrdU (IIB5; 1:250; Santa Cruz Biotechnology, Santa Cruz, CA, USA) was used. Immunofluorescence staining was detected by incubation with secondary AlexaFluor 488-conjugated (green) goat anti-mouse IgG (1:500; Invitrogen, Eugene, OR, USA) for 2 h. Nuclei were counterstained with (4',6-diamidino-2-phenylindole) DAPI (0.2  $\mu$ g/ml; Sigma-Aldrich). At least twelve individual  $\times$  40 objective fields per group were captured for counting BrdU-positive cells. The total number of DAPI-positive cells and BrdU-positive cells were counted and recorded. Results were expressed as the percent of BrdU/DAPI staining cells (Arpino *et al.*, 2007).

### Metabolic assays

Blood glucose levels were checked weekly with an automated glucometer (Bayer Contour, Mishawaka, IN, USA). Plasma insulin levels were measured by ELISA (Mercodia AB, Upsala, Sweden). A glucose tolerance test was performed after 8 h of fasting using a glucose bolus of 1.5 g/kg body weight administered by intraperitoneal injection. Blood glucose was measured from the tail vein immediately before (time 0) and 15, 30, 60 and 120 min after glucose injection. Serum triglycerides were assayed by the triglycerides reagent set and manufacturers specifications (Pointe Scientific, Canton, MI, USA).



### Statistical analysis

Results are expressed as the mean  $\pm$  s.e.m. Statistical analyses were performed using the ANOVA (analysis of variance) followed by a Fisher's test. A *P*-value of  $<0.05$  was used to define statistical significance.

### Conflict of interest

The authors declare no conflict of interest.

### References

- Agnoli C, Berrino F, Abagnato CA, Muti P, Panico S, Crosignani P *et al.* (2010). Metabolic syndrome and postmenopausal breast cancer in the ORDET cohort: a nested case-control study. *Nutr Metab Cardiovasc Dis* **20**: 41–48.
- Arpino G, Gutierrez C, Weiss H, Rimawi M, Massarweb S, Bharwani L *et al.* (2007). Treatment of human epidermal growth factor receptor 2-overexpressing breast cancer xenografts with multiagent-targeted therapy. *JNCI* **99**: 694–705.
- Borowsky AD, Namba R, Young LJ, Hunter KW, Hodgson JG, Tepper CG *et al.* (2005). Syngeneic mouse mammary carcinoma cell lines: two closely related cell lines with divergent metastatic behavior. *Clin Exp Metastasis* **22**: 47–59.
- Campbell MJ, Wollish WS, Lobo M, Esserman LJ. (2002). Epithelial and fibroblast cell lines derived from a spontaneous mammary carcinoma in a MMTV/neu transgenic mouse. *In vitro Cell Dev Biol Anim* **38**: 326–333.
- Cannata D, Lann D, Wu Y, Elis S, Sun H, Yakar S *et al.* (2010). Elevated circulatory IGF-I promotes mammary gland development and proliferation. *Endocrinology* **151**: 5751–5761.
- Creighton CJ, Fu X, Hennessy B, Casa AJ, Zhang Y, Gonzalez-Angulo AM *et al.* (2010). Proteomic and transcriptomic profiling reveals a link between the PI3K pathway and lower estrogen receptor (ER) levels and activity in ER+ breast cancer. *Breast Cancer Res* **12**: R40.
- Fernandez AM, Kim JK, Yakar S, Dupont J, Hernandez-Sanchez C, Castle AL *et al.* (2001). Functional inactivation of the IGF-I and insulin receptors in skeletal muscle causes type 2 diabetes. *Genes Dev* **15**: 1926–1934.
- Fierz Y, Novosyadlyy R, Vijayakumar A, Yakar S, LeRoith D. (2010). Mammalian target of rapamycin inhibition abrogates insulin-mediated mammary tumor progression in type 2 diabetes. *Endocr Relat Cancer* **17**: 941–951.
- Foukas LC, Berejeno IM, Gray A, Khwaja A, Vanhaesebroeck B. (2010). Activity of any class 1A PI3K isoform can sustain cell proliferation and survival. *Proc Natl Acad Science* **107**: 11381–11386.
- Goodwin PJ, Ennis M, Pritchard KI, Trudeau ME, Koo J, Madarnas Y *et al.* (2002). Fasting insulin and outcome in early-stage breast cancer: results of a prospective cohort study. *J Clin Oncol* **20**: 42–51.
- Jia S, Liu Z, Zhang S, Liu P, Zhang L, Lee SH *et al.* (2008). Essential roles of PI(3)K-p110beta in cell growth, metabolism and tumorigenesis. *Nature* **454**: 776–779.
- Junttila TT, Akita RW, Parsons K, Fields C, Lewis Phillips GD, Friedman LS *et al.* (2009). Ligand-independent HER2/HER3/PI3K complex is disrupted by trastuzumab and is effectively inhibited by the PI3K inhibitor GDC-0941. *Cancer Cell* **15**: 429–440.
- Kohn AD, Summers SA, Birnbaum MJ, Roth RA. (1996). Expression of a constitutively active Akt Ser/Thr kinase in 3T3-L1 adipocytes stimulates glucose uptake and glucose transporter 4 translocation. *J Biol Chem* **271**: 31372–31378.
- Liu LZ, Zhao HL, Zuo J, Ho SK, Chan JC, Meng Y *et al.* (2006). Protein kinase C $\zeta$  mediates insulin-induced glucose transport through actin remodeling in L6 muscle cells. *Mol Biol Cell* **17**: 2322–2330.
- López-Knowles E, O'Toole SA, McNeil CM, Millar EK, Qiu MR, Crea P *et al.* (2010). PI3K pathway activation in breast cancer is associated with the basal-like phenotype and cancer-specific mortality. *Int J Cancer* **126**: 1121–1131.
- Novosyadlyy R, Lann DE, Vijayakumar A, Rowzee A, Lazzarino DA, Fierz Y *et al.* (2010). Insulin-mediated acceleration of breast cancer development and progression in a nonobese model of type 2 diabetes. *Cancer Res* **70**: 741–751.
- O'Brien NA, Browne BC, Chow L, Wang Y, Ginther C, Arboleda J *et al.* (2010). Activated phosphoinositide 3-kinase/AKT signaling confers resistance to trastuzumab but not lapatinib. *Mol Cancer Ther* **9**: 1489–1502.
- Papa V, Pezzino V, Costantino A, Belfiore A, Giuffrida D, Frittitta L *et al.* (1990). Elevated insulin receptor content in human breast cancer. *J Clin Invest* **86**: 1503–1510.
- Patterson RE, Flatt SW, Saquib N, Rock CL, Caan BJ, Parker BA *et al.* (2010). Medical comorbidities predict mortality in women with a history of early stage breast cancer. *Breast Cancer Res Treat* **122**: 859–865.
- Peairs KS, Barone BB, Snyder CF, Yeh HC, Stein KB, Derr RL *et al.* (2011). Diabetes mellitus and breast cancer outcomes: a systematic review and meta-analysis. *J Clin Oncol* **29**: 40–46.
- Serra V, Markman B, Scatriti M, Eichorn PJ, Valero V, Guzman M *et al.* (2008). NVP-BEZ235, a dual PI3K/mTOR inhibitor, prevents PI3K signaling and inhibits the growth of cancer cells with activating PI3K mutations. *Cancer Res* **68**: 8022–8030.
- Serra V, Scaltriti M, Prudkin L, Eichhorn PJ, Ibrahim YH, Chandarlapaty S *et al.* (2011). PI3K inhibition results in enhanced HER signaling and acquired ERK dependency in HER2-overexpressing breast cancer. *Oncogene* **30**: 2547–2557.
- Sopasakis VR, Liu P, Suzuki R, Kondo T, Winnay J, Tran TT *et al.* (2010). Specific roles of the p110alpha isoform of phosphatidylinositol 3-kinase in hepatic insulin signaling and metabolic regulation. *Cell Metab* **11**: 220–230.
- Tan SX, Ng Y, James DE. (2010). Akt inhibitors reduce glucose uptake independently of their effects on Akt. *Biochem J* **432**: 191–197.
- Um SH, D'Alessio D, Thoma G. (2006). Nutrient overload, insulin resistance and ribosomal protein S6 kinase 1, S6K1. *Cell Metab* **3**: 393–402.
- Wells V, Downward J, Malluci L. (2007). Functional inhibition of PI3K by the betaGBP molecule suppresses Ras-MAPK signaling to block cell proliferation. *Oncogene* **26**: 7709–7714.

### Acknowledgements

DLR received a mentor award from the American Diabetes Association. This work was funded by National Cancer Institute grant R01-5R01-CA128799. YF received grants from the Swiss National Science Foundation [PBBSB-120851 and PBBSB3-120851] and the Novartis Foundation, the Roche Research Foundation and the Oncosuisse Foundation. NVP-BKM120 and NVP-BEZ235 were supplied by Novartis Pharma (Basel, Switzerland) free of charge.

**Title: Metabolic syndrome and pre-diabetes contribute to racial disparities in breast cancer outcomes: Hypothesis and Proposed Pathways.**

Authors: Emily J Gallagher<sup>1</sup>, Derek LeRoith<sup>1</sup>, Rebeca Franco<sup>2</sup>, Irini Markella Antoniou<sup>1</sup>, Anupma Nayak<sup>3</sup>, Jennifer Livaudais-Toman<sup>2</sup>, Nina Bickell<sup>2</sup>.

**Affiliations:**

1. Icahn School of Medicine at Mount Sinai, Division of Endocrinology, Diabetes and Bone Disease, Department of Medicine, One Gustave L. Levy Place, Box 1055, New York, NY 10029
2. Icahn School of Medicine at Mount Sinai, Department of Population Health Science and Policy, Department of Medicine, One Gustave L. Levy Place, Box 1077, New York, NY 10029.
3. Icahn School of Medicine at Mount Sinai, Dubin Breast Cancer Center, Department of Pathology, One Gustave L. Levy Place, 1176 Fifth Avenue, , New York, NY 10029.

**Short Title: Metabolic syndrome in cancer disparities**

**Corresponding Author:**

Emily J Gallagher

**Address:**

Division of Endocrinology, Diabetes and Bone Disease,  
Department of Medicine,  
One Gustave L. Levy Place,  
Box 1055  
New York, NY 10029, USA

**Telephone:** 212-241-1500

**Fax:** 212-241-4218

**Email Addresses:**

Emily Gallagher: [Emily.gallagher@mssm.edu](mailto:Emily.gallagher@mssm.edu);

Derek LeRoith: [Derek.LeRoith@mssm.edu](mailto:Derek.LeRoith@mssm.edu)

Rebeca Franco: [Rebeca.Franco@mountsinai.org](mailto:Rebeca.Franco@mountsinai.org)

Jennifer Livaudais-Toman: [Jennifer.Toman@ucsf.edu](mailto:Jennifer.Toman@ucsf.edu)

Irini Markella Antoniou: [irinimarkella.antoniou@mssm.edu](mailto:irinimarkella.antoniou@mssm.edu)

Anupma Nayak: [anupma.nayak@mountsinai.org](mailto:anupma.nayak@mountsinai.org)

Nina Bickell: [Nina.Bickell@mssm.edu](mailto:Nina.Bickell@mssm.edu)

This article has been accepted for publication and undergone full peer review but has not been through the copyediting, typesetting, pagination and proofreading process, which may lead to differences between this version and the Version of Record. Please cite this article as doi: 10.1002/dmrr.2795

## **Abstract**

### **Background:**

Women with obesity and Type 2 diabetes (T2D) are at greater risk of dying from breast cancer than women without these conditions. Obesity and T2D are associated with insulin resistance and endogenous hyperinsulinemia, and are more common in Black women. There is increasing disparity in breast cancer mortality between Black and White women in the U.S. We hypothesize that insulin resistance and endogenous hyperinsulinemia in Black women with breast cancer contribute to their greater breast cancer mortality and are associated with increased insulin receptor signaling in tumors.

### **Methods:**

We will recruit 350 Black women and 936 White women with newly diagnosed breast cancer. We will determine the presence or absence of the metabolic syndrome / pre-diabetes, and insulin resistance by measuring body mass index (BMI), waist circumference, lipids, blood pressure, glucose, insulin-like growth factor binding protein 1 and insulin. Breast cancer prognosis will be determined by a Nottingham Prognostic Index (NPI), with poor prognosis being defined as NPI >4.4. Tumor insulin receptor signaling will be determined by immunohistochemistry. Insulin receptor subtype expression will be measured using Nanostring. Analysis of these factors will determine whether endogenous hyperinsulinemia is associated with a worse prognosis in Black women than White women, and increased tumor insulin receptor signaling.

### **Conclusions**

The results of this study will determine if the metabolic syndrome and pre-diabetes contribute to racial disparities in breast cancer mortality. It may provide the basis for targeting systemic insulin resistance and/or tumor insulin receptor signaling to reduce racial disparities in breast cancer mortality.

**Key Words:** Diabetes, Metabolic Syndrome, Breast Cancer, Racial Disparities, Insulin Resistance, Insulin Receptor

## Background

The Cancer Prevention Study II found that overweight and obese women had an increased relative risk of breast cancer mortality compared to women of normal weight, defined by body mass index (BMI) [8]. Similarly, women with Type 2 diabetes also have greater breast cancer mortality than non-diabetic women [6, 9]. Further, individuals with the metabolic syndrome, a syndrome associated with abdominal obesity, impaired glucose tolerance, hypertension and dyslipidemia, also have worse breast cancer outcomes [13]. Previous human studies have found that women with insulin resistance and endogenous hyperinsulinemia have a worse prognosis when diagnosed with early stage breast cancer [16]. Furthermore, animal models have also found that hyperinsulinemia is associated with an increase in primary breast cancer growth and metastasis [17, 18]. Chronically elevated insulin levels may lead to activation of the IR, which is expressed on many cancer cells.

The Health, Eating, Activity and Lifestyle (HEAL) study found that Black women with breast cancer had higher insulin resistance scores than White women when measured by the homeostasis model assessment-estimated insulin resistance (HOMA-IR) [19]. The prevalence of insulin resistance and endogenous hyperinsulinemia is greater in Black than White women in the U.S.; however the studies examining circulating insulin levels and breast cancer incidence and recurrence have largely been performed in White populations. Increased IR expression in pathological breast cancer tissues and increased phosphorylation of the IR/ IGF-1R has been associated with a worse prognosis in some studies [20]. Certain breast cancer cell lines derived from Black women express higher levels of the IR [21], but it is unknown whether there is higher IR expression in pathological specimens from Black women compared to White women. Therefore, it is important to understand whether endogenous hyperinsulinemia and IR signaling are key factors contributing to the racial disparity in breast cancer mortality between Black and White women. If insulin resistance and hyperinsulinemia are important factors, then strategies to improve the metabolic health of these women and reduce endogenous hyperinsulinemia or the use of adjuvant therapies to target hyperinsulinemia and the IR signaling pathway may improve survival.

Breast cancer is the second leading cause of cancer death in women in the U.S. [1]. Although breast cancer mortality has been declining overall, there is an increasing disparity in the mortality



between Black and White women [2]. A number of biologic and socio-economic factors may contribute to greater mortality in Black women with breast cancer [3]. Mortality in breast cancer is primarily predicted by the characteristics of the cancer, including stage at presentation, and histological findings including hormone receptor (estrogen receptor (ER) and progesterone receptor (PR)) and HER2 status [4, 5]. Patient characteristics including advanced age at the time of diagnosis, overweight or obesity and the presence of co-morbidities, including diabetes, also impact survival [6-9]. Traditional breast cancer risk factors as well as access to breast cancer screening and treatment contribute to some of the survival disparities, but do not provide a complete explanation [10, 11]. Compared to White women with breast cancer, Black women are more likely to have tumor characteristics associated with poor prognosis (as summarized in Figure 1), including more advanced stage at presentation and ER and PR negative cancers[10]. In addition, there are greater rates of obesity and Type 2 diabetes in the Black population, compared with the White population [12]. Until we understand why Black women with breast cancer have a worse prognosis than White women, we will not be able to improve the prognosis of Black women and prolong their survival.

In this study we aim to determine whether metabolic factors associated with obesity, the metabolic syndrome and Type 2 diabetes are more common in Black women with newly diagnosed breast cancer than White women, and whether these metabolic abnormalities are associated with tumor characteristics associated with a poor prognosis and with increased IR and IGF-1R expression and signaling in the tumors.

#### **Methods / Design:**

This study was approved by the Institutional Review Board of the Icahn School of Medicine at Mount Sinai.

#### *Patient Accrual*

Women over the age of 21 years with newly diagnosed breast cancer will be eligible for the study. Women who self-identify as Black or White race will be recruited. Individuals who identify as Hispanic Black will be included, as prognostic differences between non-Hispanic and Hispanic Black women have not been definitively described. However, we will exclude those who identify as

Hispanic White, as this group is more likely to have ER/PR negative tumors than non-Hispanic White women (26% vs 19%, respectively) and would potentially attenuate the association between hormone receptor status and race.

At each participating site, all women over the age of 21 years with a primary diagnosis of breast cancer will be identified and consented prior to their surgery. Patients' demographic characteristics, access to care, factors affecting breast cancer prognosis, overall health status and prognosis and factors affecting insulin resistance will be assessed using a validated questionnaire. Women who have undergone bariatric surgery for weight loss, organ transplantation, have Type 1 diabetes or medically treated Type 2 diabetes, have been taking oral glucocorticoid treatment within two weeks of blood draw and tumor resection, have taken neoadjuvant therapies, have end stage renal disease or hepatic cirrhosis, or are receiving neoadjuvant therapy will be excluded as these conditions can affect insulin levels. The study design is summarized in Figure 2.

#### *Anthropometric Data*

Participant's height and weight will be recorded using a stadiometer that will be used throughout the study. Body mass index (BMI) will be calculated from weight (kg)/height<sup>2</sup> (m<sup>2</sup>). Waist circumference will be measured at the umbilical level and blood pressure will be recorded using standard National Health and Nutrition Examination Study (NHANES) procedures. Waist circumference and blood pressure along with the fasting preserved blood glucose and lipid measurements will be used to define the metabolic syndrome as described in the Laboratory Measurements section.

#### *Laboratory Measurements*

Blood will be drawn after an overnight fast for preserved plasma glucose, serum lipids (total cholesterol, low density lipoprotein (LDL) cholesterol, high-density (HDL) cholesterol, triglycerides (TG)), hemoglobin A1c (HbA1c), serum insulin, C-peptide, IGF-1, insulin-like growth factor binding protein-1 (IGFBP-1). Insulin resistance will be calculated from the HOMA-IR ([fasting plasma glucose (mg/dL) x fasting serum insulin (uU/ml)]/405) [22], a widely used and validated measure of insulin resistance [23]. Insulin resistance is defined as a HOMA-IR >2.8, the upper quartile of insulin resistance in the U.S. population, reported by the NHANES [24]. We will assess the presence of the

metabolic syndrome, defined by the 2009 International Diabetes Federation (IDF), National Heart, Lung and Blood Institute (NHLBI), American Heart Association (AHA), World Heart Federation (WHF), International Atherosclerosis Society (IAS) and International Association for the Study of Obesity (IASO) joint position statement, as the presence of 3 or more of the following features: waist circumference  $\geq 88$ cm; triglycerides (TG)  $\geq 150$ mg/dL; high density lipoprotein (HDL) cholesterol  $< 50$ mg/dL; systolic blood pressure  $\geq 130$ mmHg or diastolic blood pressure  $\geq 85$ mmHg; fasting glucose  $\geq 100$ mg/dL or the use of medication to treat elevated TG, low HDL or blood pressure [25].

#### *Determining Prognosis*

The final pathology report will be obtained which contains the tumor size, histological grade, nodal status, ER, PR and HER2/Neu status. Where available, Oncotype Dx reports will be recorded. Pathological data is used to calculate the Nottingham Prognostic Index (NPI). The NPI score is calculated as  $[0.2 \times \text{tumor size(cm)} + \text{lymph-node stage (1, node negative; 2, 1-3 positive lymph nodes; 3, } \geq 4 \text{ positive lymph nodes)} + \text{histological grade (1, well differentiated; 2, moderately differentiated; 3, poorly differentiated)}]$  [26]. The NPI has maximal prognostic benefit in ER positive, early stage disease, as it measures the intrinsic biological features of a tumor and its probability of metastasizing [27]. Tumor grade will be defined by the Nottingham combined histological grade (NCHG), as recommended by the American Joint Committee on Cancer (AJCC) [5]. Based on a recent U.S. study that dichotomized NPI at 4.4 (poor prognosis  $> 4.4$  and good prognosis  $\leq 4.4$ ) and showed significant differences in biomarkers (e.g., hormone receptor, Her2) in these groups [28, 29], we will define good prognosis as those women with an NPI score of  $\leq 4.4$ , and poor prognosis as an NPI score  $> 4.4$ . The improved NPI (iNPI) has been suggested to be an even stronger predictor of prognosis than the NPI. The iNPI is calculated by adding 1 point to the NPI for HER2 positivity and subtracting 1 point for PR positivity, with a score of  $> 5.4$  signifying a poor prognosis [30]. Therefore, we will determine whether insulin resistance is associated with a poor prognosis, defined primarily by NPI  $> 4.4$ , and secondarily by iNPI. Because the NPI and iNPI components ER/PR and HER2 status are proven to predict breast cancer survival, these indices will be used as proxy measures of survival to assess the relationship of insulin resistance, metabolic factors and tumor insulin receptors and signaling pathway on poor cancer prognosis.

### *Immunohistochemical Analysis of Formalin Fixed Paraffin Embedded Tissue Sections*

All recruitment sites will fix tissue specimens in 10% formalin for 48-72 hours before processing and embedding in paraffin. 5µm thick sections will be obtained for each patient's tumor paraffin block that was used by the hospital's pathology department to determine tumor ER/PR/HER2 status to maximize the sample's tumor tissue. Immunohistochemistry staining will be performed using previously described methods to detect the presence of the total IRβ, IGF-1Rβ, phosphorylation Akt(Ser473) and phosphorylation of ERK1/2(Thr202/Tyr204) in the tumor. Staining will be assessed by an Olympus AX70 microscope and automated CellSens imaging analysis software (Olympus, Center Valley, PA, USA) to determine the percent of positive cells in tumor regions of the slide and the intensity of staining, with random samples also assessed by an investigator, blinded to the clinical information of the patient from whom the sample was obtained. The prevalence of IRβ and IGF-1Rβ positive cells, the prevalence of the phosphorylated receptors (pIGF-1R/pIR), Akt phosphorylation (pAkt) and Erk1/2 phosphorylation (pErk1/2) between the two breast cancer prognosis groups will be assessed. For these intracellular markers, the Allred staining system will be used. The Allred score involves assessment of the proportion of positive stained cells and the intensity of staining. The proportion of positive stained cells is rated as 0 = no cells stained positive, 1 = between 0% and 1% stained positive, 2 = between 1% and 10% stained positive, 3 = between 10% and 30% stained positive, 4 = between 33% and 66% stained positive and 5 = between 66% and 100% stained positive. The intensity score is made based on the average intensity of staining, with 0 = negative, 1 = weak, 2 = intermediate and 3 = strong. The intensity score and proportion score will be added together to obtain the Allred score. A score of 0 or 2 will be interpreted as negative [31, 32].

### *RNA Isolation and Gene Expression Analysis*

Four 5µm sections will be cut from formalin fixed paraffin embedded blocks and RNA will be isolated from the samples using the RNeasy FFPE Kit (Qiagen, Valencia, CA), as per the manufacturer's protocol. RNA concentrations will be measured using the Nanodrop ND-1000 (Thermo Scientific, Wilmington, DE). A Custom CodeSet of genes has been designed and generated by Nanostring Technologies (Seattle, WA) to examine the expression of Insulin Receptor (IR) and the Insulin Receptor Isoforms, IR-A and IR-B, in addition to related splicing factors and the proliferation

gene Ki67. 150ng of RNA from each sample is subjected to gene expression analysis using Nanostring nCounter at the Mount Sinai qPCR Core Facility. The results will be normalized and analyzed using the nSolver Analysis Software 2.5. Differences in the expression of IR and the expression ratio of IR-A and IR-B will be compared between the White and African American patients, and correlated with laboratory and anthropometric measurements of obesity, the metabolic syndrome, insulin resistance and pre-diabetes.

#### *Outcomes and Statistical Analysis*

We will use the NPI rather than cancer stage at presentation to determine prognosis at the time of tumor resection, as the NPI is less affected by health care access than tumor stage and has been validated in several different countries [33, 28, 34]. To ensure the NPI is accurately portraying recurrence risk, we will conduct a small validation study in Year 4 of the study as the majority of early recurrences occur within the first two years of initial treatment [35]. We will call women recruited in Year 2 to ascertain and compare rates of recurrence between women with  $NPI > 4.4$  vs.  $NPI \leq 4.4$ . We will calculate percent agreement, kappa, sensitivity and specificity measures comparing NPI to recurrence in this sample.

Descriptive analyses will be performed to profile Black and White women separately including examination of proportions, means, and medians, as well as estimates of variability including standard errors, ranges, and confidence intervals. Continuous data distributions will be evaluated for appropriateness of scale, and transformations will be used where appropriate. For each racial group, we will compute appropriate summary statistics for women who have good prognosis ( $NPI \leq 4.4$ ;  $iNPI \leq 5.4$ ) and poor prognosis ( $NPI > 4.4$ ;  $iNPI > 5.4$ ). For each population (White and Black), we will compare good and poor prognosis patients with respect to age at diagnosis, year of diagnosis, income, education, access to care, stage at diagnosis family history of breast cancer, smoking status, BMI, waist circumference, blood pressure, lipid profile, medications, use of estrogen, fasting serum insulin, plasma glucose, HbA1c, C-peptide, IGFBP-1, tumor  $IR\beta$ , tumor  $IGF-1R\beta$ , pAkt, pErk.

Bivariate associations between high endogenous insulin levels and the presence of metabolic syndrome and obesity in each racial group will be explored to determine whether the association

between insulin resistance and tumor prognosis for each racial group is mediated by any of these factors. As lack of access to medical care and lower SES are well known to be associated with poor prognosis in breast cancer, due to later stage at diagnosis, different treatment and follow up, we will assess the relationship between preventative screening receipt, access to care and the NPI.

Multivariable analyses for each racial group will be performed to examine the association between insulin resistance ( $\text{HOMA-IR} > 2.8$ ) and poor tumor prognosis ( $\text{NPI} > 4.4$ ) using logistic regression, adjusting for potential confounding factors and assessing mediating factors for each group. Logistic regression will be used to model a binary outcome (poor/good prognosis) and covariates that are significantly associated with insulin resistance and poor prognosis in the sample will be included in the models, as well as those demonstrated in the literature to be strong confounders or mediators. Using the Wald test to identify significant interaction by race (significance level  $p < 0.05$ ), we will determine whether the association between insulin resistance and poor tumor prognosis differs significantly across racial groups. Further, we will assess whether the association between tumor IR and IGF-1R, pAkt and pERK1/2 correlate with tumor prognosis, and whether the degree of insulin resistance (HOMA-IR), serum insulin concentration, and poor tumor prognosis differ significantly between racial groups. In exploratory analyses, we will also further stratify our analyses according to measures of metabolic syndrome to determine whether the associations between IR expression and tumor prognosis for each racial group are mediated by any of these factors.

#### *Power Analysis*

This study is powered to detect a significant interaction by race of the association between insulin resistance (HOMA-IR) and poor prognosis breast cancer ( $\text{NPI} > 4.4$ ). Power calculations considered the following factors: the national U.S. prevalence of  $\text{HOMA-IR} > 2.8$  among healthy, non-diabetic women is 23% in White women, and 33% in Black women; the prevalence of poor prognosis breast cancer, defined as  $\text{NPI} > 4.4$ , in a large, racially and ethnically diverse Health Maintenance Organization (HMO) population of breast cancer patients is 33% in White women and 44% in Black women (unpublished data from Kaiser Permanente Northern California). The power calculation was based on the NPI rather than the iNPI because there is validating data for the NPI. Based on the power

analysis, 936 White women and 350 Black women would need to be recruited over 4 years to detect a significant interaction between insulin resistance and poor prognosis in breast cancer by race.

A prior study examining the relationship between insulin resistance and mortality among a sample of predominantly White women with breast cancer found a hazard ratio=1.6 among women with HOMA-IR scores >2.7 [36]. With a sample size of 936 White women, we will have adequate power to detect a main effect OR>1.6 in White women. As research involving other types of chronic disease has identified differential effect sizes by race, with ratios >1.5 comparing effect sizes between Black and White populations, our study is powered to be able to detect a ratio of similar magnitude ( $\geq 1.5$ ) comparing the strength of association between insulin resistance and poor prognosis breast cancer between Black and White women. Under the specified assumptions, this study will have >80% power to detect a significant interaction ratio of  $\geq 1.5$ , comparing the effect size in Black women to the effect size in White women (Type I error =0.05). It is also powered ( $\geq 80\%$ ) to detect an interaction of this magnitude under several alternative scenarios, given a variety of different prevalences of insulin resistance (range: 10-50%) and a variety of distributions of poor prognosis (range: 20-50%) for White and Black women.

## **Discussion**

The linked epidemics of obesity and diabetes mellitus that disparately affect Black women, coupled by Black women's greater mortality from breast cancer require exploration of possible mechanistic links. How do obesity, the metabolic syndrome, pre-diabetes, insulin resistance, hyperinsulinemia and insulin signaling in tumors result in more aggressive, poorer prognostic breast cancers? This study anticipates finding that insulin resistance and hyperinsulinemia are associated with poor prognostic indices in Black and White women with these conditions more prevalent in the Black population. We also anticipate finding the presence of the IR and IGF-1R in breast cancer tissue, but do not necessarily expect to see any association between the presence of these receptors and the presence of systemic insulin resistance. Rather, we expect to find a racial difference in ratio of IR-A to IR-B, related to the severity of hyperinsulinemia and insulin resistance, and the prognostic index of the cancer, as other have reported increased IR-A to IR-B ratio in subtypes of breast cancer with a worse prognosis [37, 38]. In contrast to those studies, we expect to find an association between insulin



resistance and the presence of increased IR signaling in the tumors. We expect that the phosphatidylinositol 3-kinase (PI3-K)/Akt pathway, rather than the ERK1/2 pathway will be the main signaling pathway activated by the IR in breast cancers from hyperinsulinemic patients. These results would be in keeping with our previous pre-clinical studies [17, 18]. In addition, we anticipate that there will be differences in the expression of IR-A / IR-B ratios, that will be associated with increased insulin resistance and breast cancer with a worse prognostic index.

There are certain limitations to our study that we recognize. In this proposal, we treat race as more of a biologic than a social construct. We ask patients to self-identify race. We are not conducting genetic tests to determine biologic racial categories due to budgetary constraints and the uncertain utility of ancestry information markers. This study is cross-sectional, not longitudinal though we will assess recurrence rates in an early recruited subgroup of women who will have had up to two years time to develop a recurrence. Our outcome variable, a pathology measure of poor prognosis breast cancer, is a proxy of survival. We do not conduct a complete follow-up survey to ascertain recurrence because: 1) tumor size, nodal status, ER and Her2 status have been validated measures of prognosis in studies ascertaining survival and 2) given an expected 2 year recurrence rate of 12%, we would not have adequate power to revalidate these prognostic indices.

This study will not assess the ability of endogenous hyperinsulinemia to stimulate the development of new incident cancer, but rather its potential mechanistic link to cancer progression and mortality. As our primary focus is on the role of hyperinsulinemia and insulin receptor signaling pathways, we do not include tests of chronic inflammation and adipose tissue factors. However, with the patients' consent, we will bank frozen serum to enable future studies on novel markers in obesity, insulin resistance and cancer.

The novel aspect of this study is that it will explore whether insulin resistance, endogenous hyperinsulinemia and IR signaling differ across racial groups, and whether insulin resistance and increased signaling through the IR in breast cancer cells can explain the differences in the breast cancer prognosis in White and Black women. Results may lead to strategies or treatments to reduce the disparity between these groups. Overall, understanding in which patients insulin resistance, hyperinsulinemia and the insulin signaling pathway is important for tumor growth would allow for



targeted therapy in this group and could reconcile the disparities in breast cancer mortality between White and Black women.

A randomized controlled trial (RCT) trial testing metformin treatment for breast cancer in the adjuvant setting is currently underway (NCT01101438, <https://clinicaltrials.gov/ct2/show/NCT01101438> last accessed 4<sup>th</sup> April 2015). The driving hypothesis is that metformin reduces signaling through the PI3K/Akt signaling pathway, activates 5' adenosine monophosphate activated protein kinase (AMPK) which in turn, inhibits mammalian target of rapamycin (mTOR), a protein activated by the IR signaling pathway that helps control cell division and survival. However, the metformin trial will leave unanswered the relationship between insulin resistance, race and poor prognosis breast cancer for two key reasons: 1) typically, only 2.5% of patients recruited for clinical trials are Black and 2) based on their target accrual of 3,582, the metformin study will not have sufficient power to ascertain racial differences in the relationship between insulin resistance and poor prognosis breast cancer. In addition, women recruited for the study will have already completed primary cancer treatments which are known to affect insulin resistance. Furthermore, patients who end up in RCTs are highly selected and may not be representative of breast cancer patients in the community.

Ultimately, if we discover in humans that hyperinsulinemia and the IR signaling pathway are of importance in breast cancer prognosis, then in the future, examining breast cancer specimens for activation of the IR signaling pathway would allow for the use of therapy targeting this pathway in patients who are refractory to current treatment.

## **Conclusions**

This study is the first specifically designed to address the role of obesity, the metabolic syndrome, pre-diabetes, and concomitant insulin resistance and hyperinsulinemia in racial disparities in breast cancer prognosis with adequate power to detect an interaction by race of the effect of insulin resistance on breast cancer prognosis. If insulin resistance and hyperinsulinemia can explain the differences in prognosis between Black and White women (beyond any differences in SES, access to medical care and other known risk factors for breast cancer survival), then therapies that decrease insulin resistance and block IR signaling may be used to reduce disparities in breast cancer survival.

## List of Abbreviations

BMI: Body Mass Index, ER: Estrogen Receptor, Erk: Extracellular signal-regulated kinase, HbA1c: Hemoglobin A1c, HER2: Human epidermal growth factor receptor 2, HOMA-IR: Homeostasis model assessment of insulin resistance, ICD-9: International Classification of Diseases 9, IGF-1: Insulin-like growth factor 1, IGF-1R: Insulin-like growth factor 1 receptor, IGFBP-1: Insulin -like growth factor binding protein-1, iNPI: Improved Nottingham Prognostic Index, IR: Insulin Receptor, mTOR: mammalian target of rapamycin, NHANES: National Health and Nutrition Examination Study, NPI: Nottingham Prognostic Index, PR: Progesterone Receptor, T2D: Type 2 diabetes

## Competing Interests

The authors declare that they have no competing interests

## Acknowledgements

Funding for this project is provided to N.B and D.L.R. by the NIH /NCI 5R01 CA171558, in addition to funding to D.L.R by NIH/NCI 2R01CA128799, and to E.J.G by NIH/NCI 1K08CA190770.

## Author Contributions

All authors contributed to the design of the study, preparation, editing and review of the manuscript.

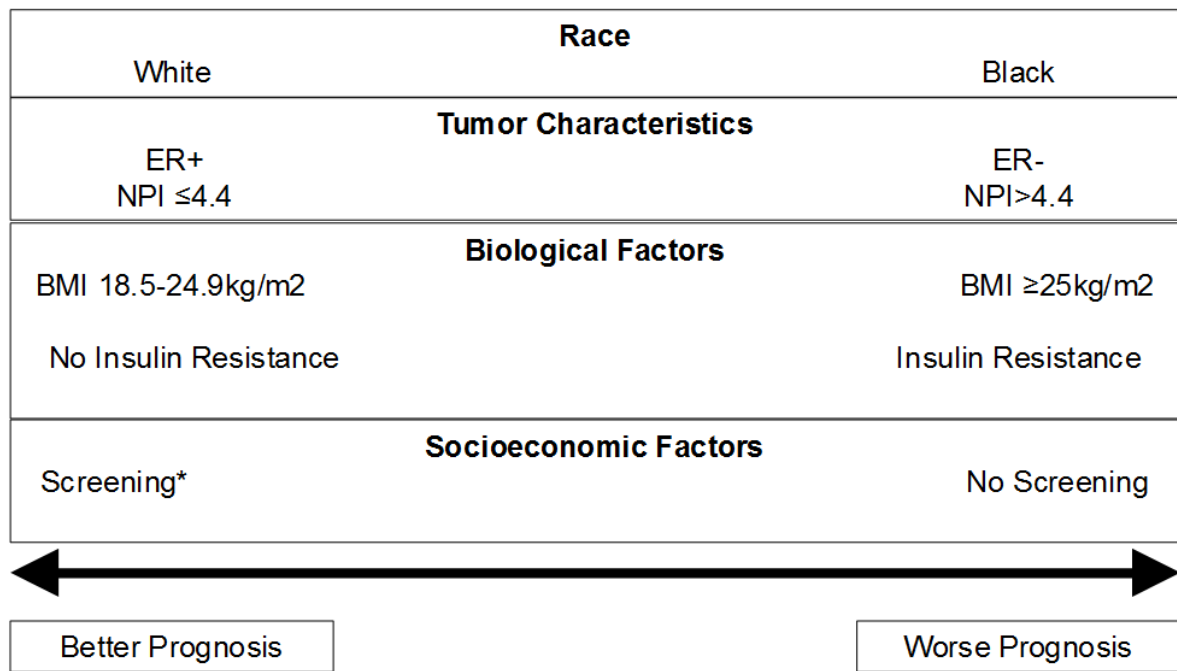
## References

1. Siegel RL, Miller KD, Jemal A. Cancer statistics, 2015. *CA: a cancer journal for clinicians*. 2015;65(1):5-29. doi:10.3322/caac.21254.
2. Hunt BR, Whitman S, Hurlbert MS. Increasing Black:White disparities in breast cancer mortality in the 50 largest cities in the United States. *Cancer epidemiology*. 2014;38(2):118-23. doi:10.1016/j.canep.2013.09.009.
3. Bickell NA, Wang JJ, Oluwole S, Schrag D, Godfrey H, Hiotis K et al. Missed opportunities: racial disparities in adjuvant breast cancer treatment. *Journal of clinical oncology : official journal of the American Society of Clinical Oncology*. 2006;24(9):1357-62. doi:10.1200/JCO.2005.04.5799.

4. Dunnwald LK, Rossing MA, Li CI. Hormone receptor status, tumor characteristics, and prognosis: a prospective cohort of breast cancer patients. *Breast cancer research : BCR*. 2007;9(1):R6. doi:10.1186/bcr1639.
5. Edge SB, Compton CC. The American Joint Committee on Cancer: the 7th edition of the AJCC cancer staging manual and the future of TNM. *Annals of surgical oncology*. 2010;17(6):1471-4. doi:10.1245/s10434-010-0985-4.
6. Barone BB, Yeh HC, Snyder CF, Peairs KS, Stein KB, Derr RL et al. Long-term all-cause mortality in cancer patients with preexisting diabetes mellitus: a systematic review and meta-analysis. *Jama*. 2008;300(23):2754-64. doi:10.1001/jama.2008.824.
7. Caan BJ, Kwan ML, Hartzell G, Castillo A, Slattery ML, Sternfeld B et al. Pre-diagnosis body mass index, post-diagnosis weight change, and prognosis among women with early stage breast cancer. *Cancer causes & control : CCC*. 2008;19(10):1319-28. doi:10.1007/s10552-008-9203-0.
8. Calle EE, Rodriguez C, Walker-Thurmond K, Thun MJ. Overweight, obesity, and mortality from cancer in a prospectively studied cohort of U.S. adults. *The New England journal of medicine*. 2003;348(17):1625-38. doi:10.1056/NEJMoa021423.
9. Peairs KS, Barone BB, Snyder CF, Yeh HC, Stein KB, Derr RL et al. Diabetes mellitus and breast cancer outcomes: a systematic review and meta-analysis. *Journal of clinical oncology : official journal of the American Society of Clinical Oncology*. 2011;29(1):40-6. doi:10.1200/JCO.2009.27.3011.
10. Iqbal J, Ginsburg O, Rochon PA, Sun P, Narod SA. Differences in breast cancer stage at diagnosis and cancer-specific survival by race and ethnicity in the United States. *Jama*. 2015;313(2):165-73. doi:10.1001/jama.2014.17322.
11. Kroenke CH, Sweeney C, Kwan ML, Quesenberry CP, Weltzien EK, Habel LA et al. Race and breast cancer survival by intrinsic subtype based on PAM50 gene expression. *Breast cancer research and treatment*. 2014;144(3):689-99. doi:10.1007/s10549-014-2899-5.
12. Liu J, Coady S, Carr JJ, Hoffmann U, Taylor HA, Fox CS. Differential associations of abdominal visceral, subcutaneous adipose tissue with cardiometabolic risk factors between African and European Americans. *Obesity*. 2014;22(3):811-8. doi:10.1002/oby.20307.
13. Calip GS, Malone KE, Gralow JR, Stergachis A, Hubbard RA, Boudreau DM. Metabolic syndrome and outcomes following early-stage breast cancer. *Breast cancer research and treatment*. 2014;148(2):363-77. doi:10.1007/s10549-014-3157-6.
14. Reaven GM. Banting lecture 1988. Role of insulin resistance in human disease. *Diabetes*. 1988;37(12):1595-607.
15. McLaughlin T, Allison G, Abbasi F, Lamendola C, Reaven G. Prevalence of insulin resistance and associated cardiovascular disease risk factors among normal weight, overweight, and obese individuals. *Metabolism: clinical and experimental*. 2004;53(4):495-9.
16. Goodwin PJ, Ennis M, Pritchard KI, Trudeau ME, Koo J, Madarnas Y et al. Fasting insulin and outcome in early-stage breast cancer: results of a prospective cohort study. *Journal of clinical oncology : official journal of the American Society of Clinical Oncology*. 2002;20(1):42-51.
17. Ferguson RD, Novosyadlyy R, Fierz Y, Alikhani N, Sun H, Yakar S et al. Hyperinsulinemia enhances c-Myc-mediated mammary tumor development and advances metastatic progression to the lung in a mouse model of type 2 diabetes. *Breast cancer research : BCR*. 2012;14(1):R8. doi:10.1186/bcr3089.
18. Novosyadlyy R, Lann DE, Vijayakumar A, Rowzee A, Lazzarino DA, Fierz Y et al. Insulin-mediated acceleration of breast cancer development and progression in a nonobese model of type 2 diabetes. *Cancer research*. 2010;70(2):741-51. doi:10.1158/0008-5472.CAN-09-2141.
19. Irwin ML, Duggan C, Wang CY, Smith AW, McTiernan A, Baumgartner RN et al. Fasting C-peptide levels and death resulting from all causes and breast cancer: the health, eating, activity, and lifestyle study. *Journal of clinical oncology : official journal of the American Society of Clinical Oncology*. 2011;29(1):47-53. doi:10.1200/JCO.2010.28.4752.

20. Law JH, Habibi G, Hu K, Masoudi H, Wang MY, Stratford AL et al. Phosphorylated insulin-like growth factor-i/insulin receptor is present in all breast cancer subtypes and is related to poor survival. *Cancer research*. 2008;68(24):10238-46. doi:10.1158/0008-5472.CAN-08-2755.
21. Agurs-Collins T, Adams-Campbell LL, Kim KS, Cullen KJ. Insulin-like growth factor-1 and breast cancer risk in postmenopausal African-American women. *Cancer detection and prevention*. 2000;24(3):199-206.
22. Wallace TM, Levy JC, Matthews DR. Use and abuse of HOMA modeling. *Diabetes care*. 2004;27(6):1487-95.
23. Bonora E, Targher G, Alberiche M, Bonadonna RC, Saggiani F, Zenere MB et al. Homeostasis model assessment closely mirrors the glucose clamp technique in the assessment of insulin sensitivity: studies in subjects with various degrees of glucose tolerance and insulin sensitivity. *Diabetes care*. 2000;23(1):57-63.
24. Ausk KJ, Boyko EJ, Ioannou GN. Insulin resistance predicts mortality in nondiabetic individuals in the U.S. *Diabetes care*. 2010;33(6):1179-85. doi:10.2337/dc09-2110.
25. Alberti KG, Eckel RH, Grundy SM, Zimmet PZ, Cleeman JI, Donato KA et al. Harmonizing the metabolic syndrome: a joint interim statement of the International Diabetes Federation Task Force on Epidemiology and Prevention; National Heart, Lung, and Blood Institute; American Heart Association; World Heart Federation; International Atherosclerosis Society; and International Association for the Study of Obesity. *Circulation*. 2009;120(16):1640-5. doi:10.1161/CIRCULATIONAHA.109.192644.
26. Galea MH, Blamey RW, Elston CE, Ellis IO. The Nottingham Prognostic Index in primary breast cancer. *Breast cancer research and treatment*. 1992;22(3):207-19.
27. Rakha EA, Reis-Filho JS, Baehner F, Dabbs DJ, Decker T, Eusebi V et al. Breast cancer prognostic classification in the molecular era: the role of histological grade. *Breast cancer research : BCR*. 2010;12(4):207. doi:10.1186/bcr2607.
28. Balslev I, Axelsson CK, Zedeler K, Rasmussen BB, Carstensen B, Mouridsen HT. The Nottingham Prognostic Index applied to 9,149 patients from the studies of the Danish Breast Cancer Cooperative Group (DBCG). *Breast cancer research and treatment*. 1994;32(3):281-90.
29. Parisi F, Gonzalez AM, Nadler Y, Camp RL, Rimm DL, Kluger HM et al. Benefits of biomarker selection and clinico-pathological covariate inclusion in breast cancer prognostic models. *Breast cancer research : BCR*. 2010;12(5):R66. doi:10.1186/bcr2633.
30. Van Belle V, Van Calster B, Brouckaert O, Vanden Bempt I, Pintens S, Harvey V et al. Qualitative assessment of the progesterone receptor and HER2 improves the Nottingham Prognostic Index up to 5 years after breast cancer diagnosis. *Journal of clinical oncology : official journal of the American Society of Clinical Oncology*. 2010;28(27):4129-34. doi:10.1200/JCO.2009.26.4200.
31. Henriksen KL, Rasmussen BB, Lykkesfeldt AE, Moller S, Ejlersen B, Mouridsen HT. Semi-quantitative scoring of potentially predictive markers for endocrine treatment of breast cancer: a comparison between whole sections and tissue microarrays. *Journal of clinical pathology*. 2007;60(4):397-404. doi:10.1136/jcp.2005.034447.
32. Allred DC, Harvey JM, Berardo M, Clark GM. Prognostic and predictive factors in breast cancer by immunohistochemical analysis. *Modern pathology : an official journal of the United States and Canadian Academy of Pathology, Inc.* 1998;11(2):155-68.
33. Bates T, Evans T, Lagord C, Monypenny I, Kearins O, Lawrence G. A population based study of variations in operation rates for breast cancer, of comorbidity and prognosis at diagnosis: failure to operate for early breast cancer in older women. *European journal of surgical oncology : the journal of the European Society of Surgical Oncology and the British Association of Surgical Oncology*. 2014;40(10):1230-6. doi:10.1016/j.ejso.2014.06.001.
34. Albergaria A, Ricardo S, Milanezi F, Carneiro V, Amendoeira I, Vieira D et al. Nottingham Prognostic Index in triple-negative breast cancer: a reliable prognostic tool? *BMC cancer*. 2011;11:299. doi:10.1186/1471-2407-11-299.

35. Saphner T, Tormey DC, Gray R. Annual hazard rates of recurrence for breast cancer after primary therapy. *Journal of clinical oncology : official journal of the American Society of Clinical Oncology*. 1996;14(10):2738-46.
36. Duggan C, Irwin ML, Xiao L, Henderson KD, Smith AW, Baumgartner RN et al. Associations of insulin resistance and adiponectin with mortality in women with breast cancer. *Journal of clinical oncology : official journal of the American Society of Clinical Oncology*. 2011;29(1):32-9. doi:10.1200/JCO.2009.26.4473.
37. Harrington SC, Weroha SJ, Reynolds C, Suman VJ, Lingle WL, Haluska P. Quantifying insulin receptor isoform expression in FFPE breast tumors. *Growth hormone & IGF research : official journal of the Growth Hormone Research Society and the International IGF Research Society*. 2012;22(3-4):108-15. doi:10.1016/j.ghir.2012.04.001.
38. Kalla Singh S, Brito C, Tan QW, De Leon M, De Leon D. Differential expression and signaling activation of insulin receptor isoforms A and B: A link between breast cancer and diabetes. *Growth factors*. 2011;29(6):278-89. doi:10.3109/08977194.2011.616200.



\* Screening consistent with US Preventive Task Force national guidelines

Figure 1.

Clinical and Biological Factors Potentially Contributing to the Racial Disparities in Breast Cancer Prognosis in Black and White Women.

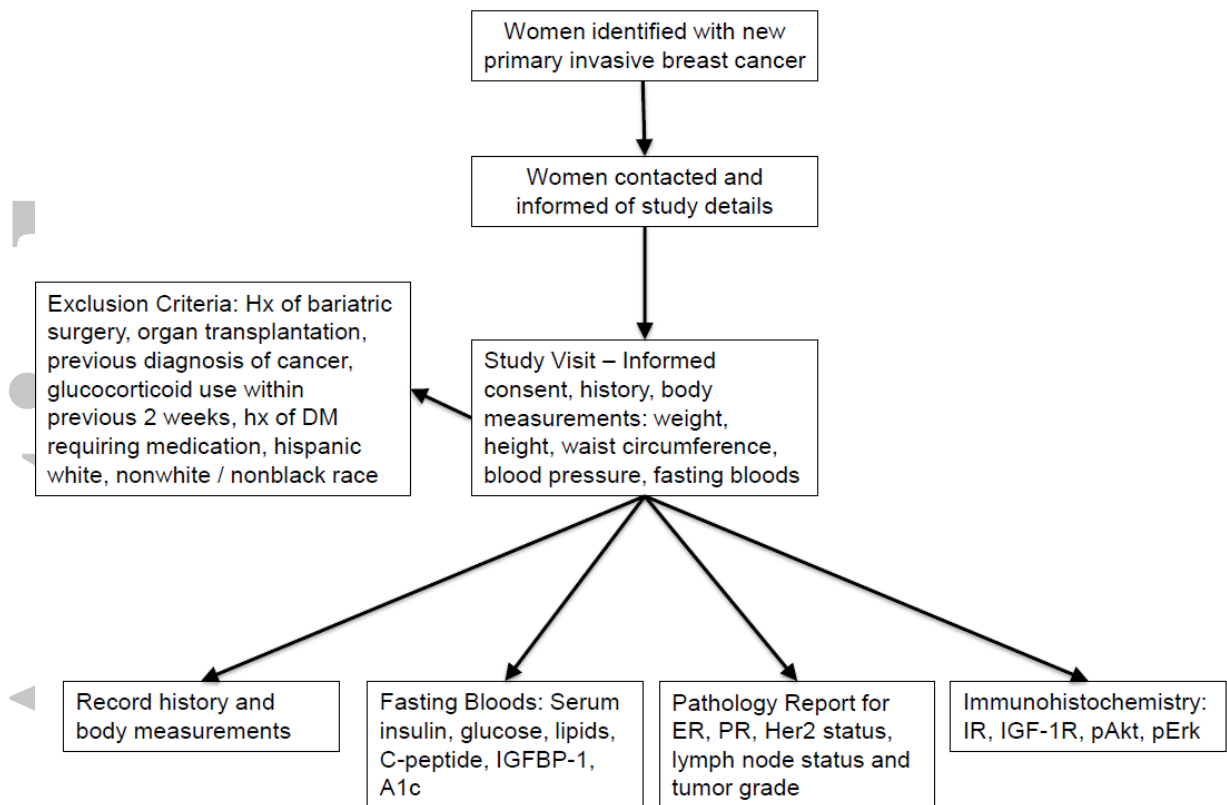


Figure 2.  
Schematic of the study design.



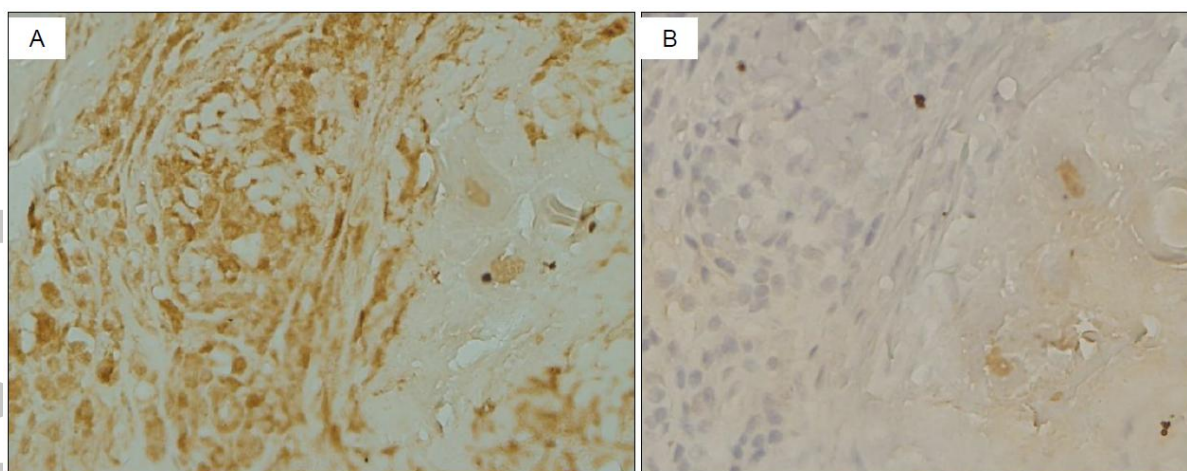


Figure 3.

### Insulin Receptor Expression in Breast Cancer

Representative image of immunohistochemical staining for the insulin receptor in invasive human breast cancer. Panel A demonstrates positive membrane staining, Panel B is the negative control for the same panel. Images were photographed at 40X objective.



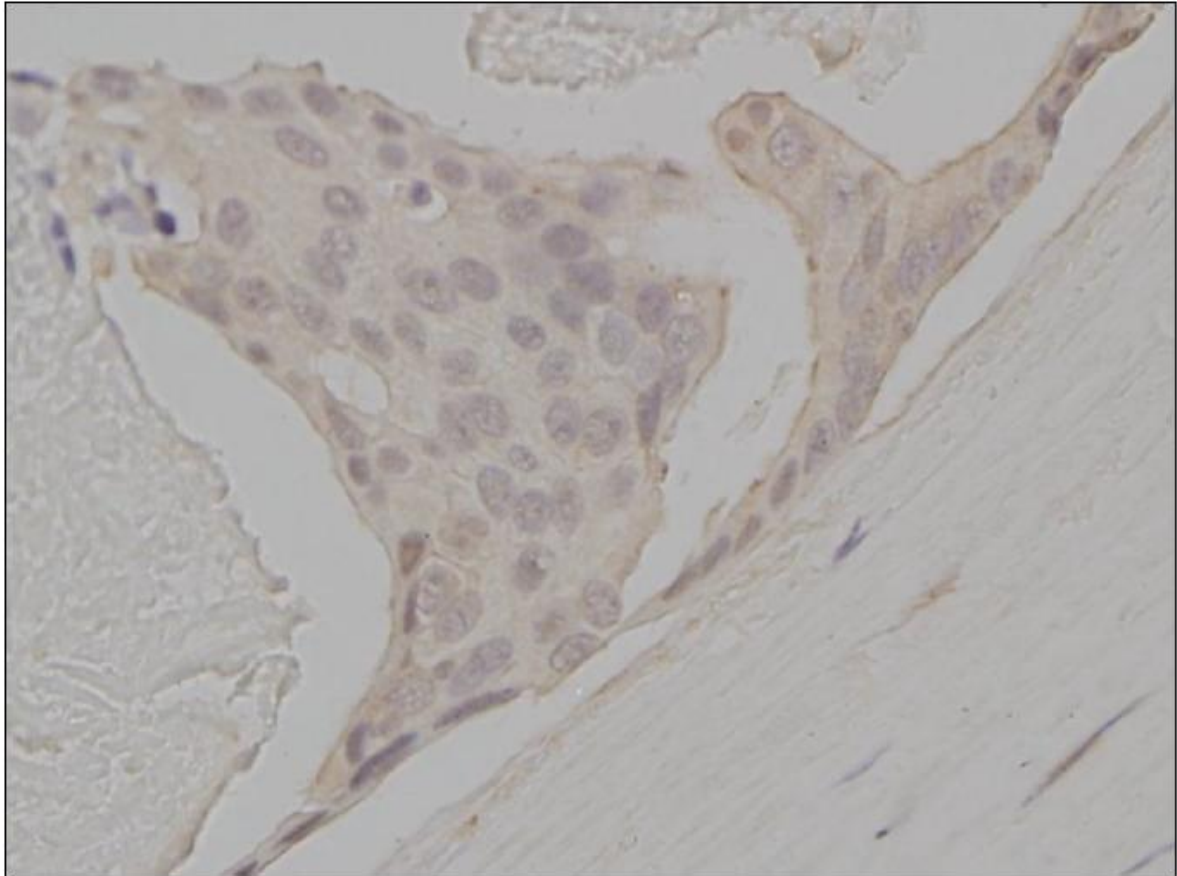


Figure 4.

Akt phosphorylation in Breast Cancer

Representative image of cytoplasmic pAkt staining of human breast cancer specimen. Image was photographed at 40X objective.

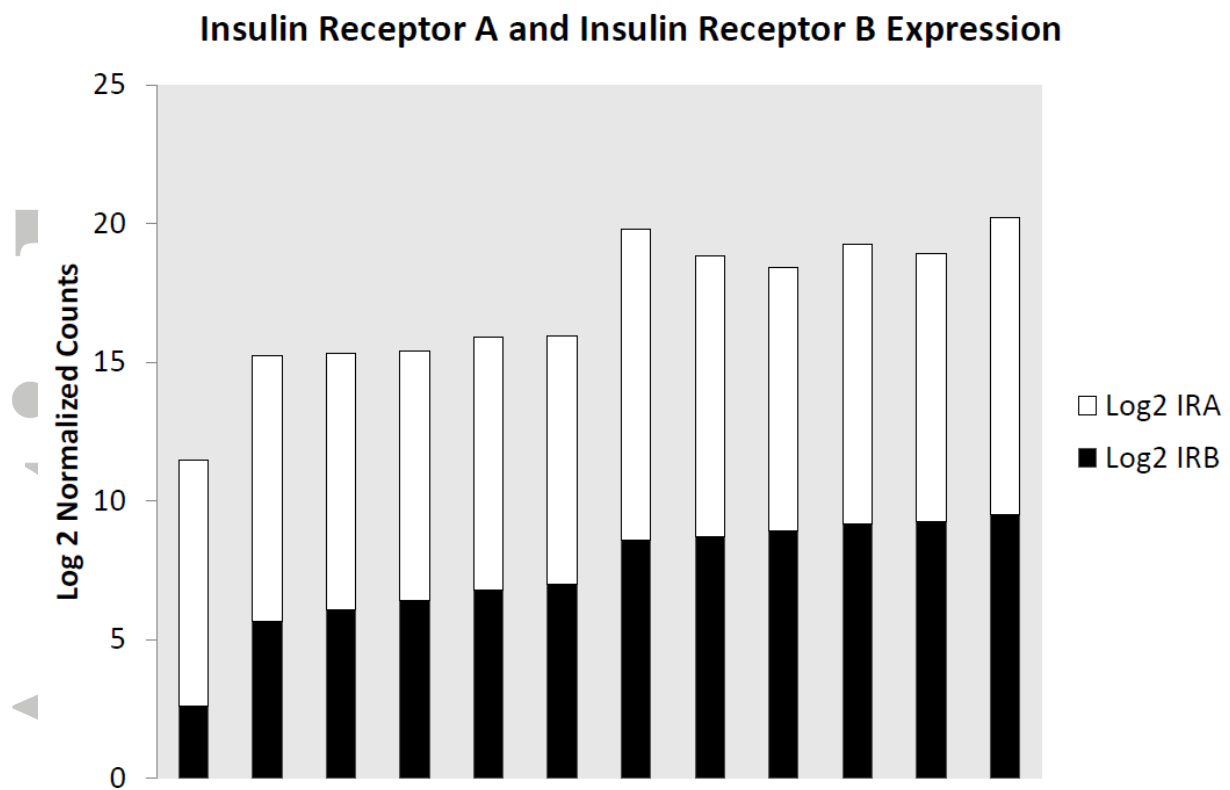


Figure 5.

Gene Expression analysis of Insulin Receptor Isoform A and B.

Insulin Receptor isoform A and B gene expression as determined by Nanostring nCounter analysis in initial 12 patient samples demonstrating the variation in IR-A and IR-B ratios between patients.